Astrofisica Nucleare e Subnucleare

Radiation Processes

Basic Radiation Concepts

Much of what we need to understand radiation processes in X-ray and γ-ray astronomy can be derived using classical electrodynamics and central to that development is the physics of the radiation of accelerated charged particles. The central relation is the *radiation loss rate of an accelerated charged particle* in the non-relativistic limit

$$-\left(\frac{\mathrm{d}E}{\mathrm{d}t}\right)_{\mathrm{rad}} = \frac{|\ddot{\boldsymbol{p}}|^2}{6\pi\varepsilon_0 c^3} = \frac{q^2|\ddot{\boldsymbol{r}}|^2}{6\pi\varepsilon_0 c^3}. \tag{1}$$

$\boldsymbol{p} = q\boldsymbol{r}$ is the *dipole moment* of the accelerated electron with respect to some origin. This formula is very closely related to the radiation rate of a dipole radio antenna and so is often referred to as the radiation loss rate for *dipole radiation*. Note that I will use *SI units* in all the derivations, although it will be necessary to convert the results into the conventional units used in X-ray and γ-ray astronomy when they are confronted with observations. Thus, I will normally use metres, kilograms, teslas and so on.

The radiation of an accelerated charged particle (5)

To find the total radiation rate, we integrate over all solid angles, that is, we integrate over θ with respect to the direction of the acceleration. Integrating over solid angle means integrating over $\mathrm{d}\Omega = 2\pi \sin\theta \, \mathrm{d}\theta$ and so

$$-\left(\frac{\mathrm{d}E}{\mathrm{d}t}\right)_{\mathrm{rad}} = \int_0^{\pi} \frac{|\ddot{\boldsymbol{p}}|^2 \sin^2\theta}{16\pi^2 \varepsilon_0 c^3} \, 2\pi \sin\theta \, \mathrm{d}\theta. \tag{8}$$

We find the key result

$$\boxed{-\left(\frac{\mathrm{d}E}{\mathrm{d}t}\right)_{\mathrm{rad}} = \frac{|\ddot{\boldsymbol{p}}|^2}{6\pi\varepsilon_0 c^3} = \frac{q^2 |\ddot{\boldsymbol{r}}|^2}{6\pi\varepsilon_0 c^3}.} \tag{9}$$

This result is sometimes called *Larmor's formula* – precisely the same result comes out of the full theory. These formulae embody the three essential properties of the radiation of an accelerated charged particle.

Example - Thomson Scattering

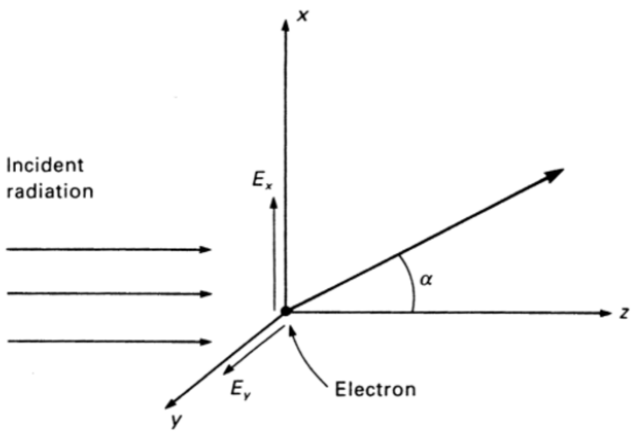

Thomson scattering is the scattering of electromagnetic waves by free electrons in the classical limit. Thomson first published the formula for the *Thomson cross-section* in 1906 in connection with the scattering of X-rays.
We seek the formula describing the scattering of a beam of radiation incident upon a stationary electron. We assume that the beam of incident radiation propagates in the positive z-direction. Without loss of generality, we arrange the geometry of the scattering so that the scattering angle α lies in the $x - z$ plane. In the case of unpolarised radiation, we resolve the electric field strength into components of equal intensity in the $\boldsymbol{i}_x$ and $\boldsymbol{i}_y$ directions.

Thomson Scattering

The electric fields experienced by the electron in the x and y directions, $E_x = E_{x0}\,\mathrm{exp}(\mathrm{i}\omega t)$ and $E_y = E_{y0}\,\mathrm{exp}(\mathrm{i}\omega t)$ respectively, cause the electron to oscillate and the accelerations in these directions are:

$$\ddot{r}_x = eE_x/m_\mathrm{e} \quad \ddot{r}_y = eE_y/m_\mathrm{e}. \tag{10}$$

We can therefore enter these accelerations into the radiation formula (9) which shows the angular dependance of the emitted radiation upon the polar angle θ. Let us treat the x-acceleration first. In this case, we can use the formula (9) directly with the substitution $\alpha = \pi/2 - \theta$. Therefore, the intensity of radiation scattered through angle θ into the solid angle $\mathrm{d}\Omega$ is

$$-\left(\frac{\mathrm{d}E}{\mathrm{d}t}\right)_x \mathrm{d}\Omega = \frac{e^2|\ddot{r}_x|^2 \sin^2\theta}{16\pi^2\varepsilon_0 c^3}\,\mathrm{d}\Omega = \frac{e^4|E_x|^2}{16\pi^2 m_\mathrm{e}^2 \varepsilon_0 c^3}\cos^2\alpha\,\mathrm{d}\Omega. \tag{11}$$

Thomson Scattering

We have to take time averages of E_x^2 and we find that $\overline{E_x^2} = E_{x0}^2/2$, where E_{x0} is the maximum field strength of the wave. We sum over all waves contributing to the E_x-component of radiation and express the result in terms of the incident energy per unit area upon the electron. The latter is given by Poynting's theorem, $\boldsymbol{S}_x = (\boldsymbol{E} \times \boldsymbol{H}) = c\varepsilon_0 E_x^2 \boldsymbol{i}_z$. Again, we take time averages and find that the contribution to the intensity in the direction α from the x-component of the acceleration is $S_x = \sum_i c\varepsilon_0 E_{x0}^2/2$. Therefore

$$-\left(\frac{\mathrm{d}E}{\mathrm{d}t}\right)_x \mathrm{d}\Omega = \frac{e^4 \cos^2\alpha}{16\pi^2 m_\mathrm{e}^2 \varepsilon_0 c^3} \sum_i \overline{E_x^2}\, \mathrm{d}\Omega = \frac{e^4 \cos^2\alpha}{16\pi^2 m_\mathrm{e}^2 \varepsilon_0^2 c^4} S_x \,\mathrm{d}\Omega. \qquad (12)$$

Thomson Scattering

Now let us look at the scattering of the E_y-component of the incident field. From the geometry of the previous diagram, it can be seen that the radiation in the $x - z$ plane from the acceleration of the electron in the y-direction corresponds to scattering at $\theta = 90°$ and so the scattered intensity in the α-direction is

$$-\left(\frac{\mathrm{d}E}{\mathrm{d}t}\right)_y \mathrm{d}\Omega = \frac{e^4}{16\pi^2 m_\mathrm{e}^2 \varepsilon_0^2 c^4} S_y \,\mathrm{d}\Omega. \tag{13}$$

The total scattered radiation into $\mathrm{d}\Omega$ is the sum of these components (notice that we add the intensities of the two independent field components).

$$-\left(\frac{\mathrm{d}E}{\mathrm{d}t}\right) \mathrm{d}\Omega = \frac{e^4}{16\pi^2 m_\mathrm{e}^2 \varepsilon_0^2 c^4}(1 + \cos^2\alpha)\frac{S}{2}\,\mathrm{d}\Omega \tag{14}$$

where $S = S_x + S_y$ and $S_x = S_y$ for unpolarised radiation. We now express the scattered intensity in terms of a differential scattering cross-section $\mathrm{d}\sigma_\mathrm{T}$ in the following way. We define the scattered intensity in direction α by the following relation

$$\frac{\mathrm{d}\sigma_\mathrm{T}(\alpha)}{\mathrm{d}\Omega} = \frac{\text{energy radiated per unit time per unit solid angle}}{\text{incident energy per unit time per unit area}}\,. \tag{15}$$

Thomson Scattering

Since the total incident energy is S, the differential cross-section for Thomson scattering is

$$\mathrm{d}\sigma_{\mathrm{T}}(\alpha) = \frac{e^4}{16\pi^2\varepsilon_0^2 m_{\mathrm{e}}^2 c^4} \frac{(1+\cos^2\alpha)}{2}\,\mathrm{d}\Omega. \quad (16)$$

In terms of the *classical electron radius* $r_{\mathrm{e}} = e^2/4\pi\varepsilon_0 m_{\mathrm{e}} c^2$, this can be expressed

$$\mathrm{d}\sigma_{\mathrm{T}} = \frac{r_{\mathrm{e}}^2}{2}(1+\cos^2\alpha)\,\mathrm{d}\Omega. \quad (17)$$

To find the total cross-section, we integrate over all angles α,

$$\sigma_{\mathrm{T}} = \int_0^{\pi} \frac{r_{\mathrm{e}}^2}{2}(1+\cos^2\alpha)\,2\pi\sin\alpha\,\mathrm{d}\alpha = \frac{8\pi}{3} r_{\mathrm{e}}^2 = \frac{e^4}{6\pi\varepsilon_0^2 m_{\mathrm{e}}^2 c^4}. \quad (18)$$

$$\boxed{\sigma_{\mathrm{T}} = 6.653 \times 10^{-29}\,\mathrm{m}^2.} \quad (19)$$

This is Thomson's famous result for the total cross-section for scattering by stationary free electrons and is justly referred to as the *Thomson cross-section*.

Thomson Scattering

- The scattering is symmetric with respect to the scattering of angle α. Thus as much radiation is scattered backwards as forwards.

- Another useful calculation is the scattering cross-section for 100% polarised emission. We can work this out by integrating the scattered intensity (11) over all angles.

$$-\left(\frac{\mathrm{d}E}{\mathrm{d}t}\right)_x = \frac{e^2|\ddot{\boldsymbol{r}}_x|^2}{16\pi^2\varepsilon_0 c^3}\int \sin^2\theta\, 2\pi\sin\theta\,\mathrm{d}\theta = \left(\frac{e^4}{6\pi\varepsilon_0^2 m_\mathrm{e}^2 c^4}\right) S_x. \tag{20}$$

We find the same total cross-section for scattering as before because it does not matter how the electron is forced to oscillate. The only important quantity is the total intensity incident upon it and it does not matter how anisotropic the radiation is. This result can be written in terms to the energy density of radiation u_rad in which the electron is located,

$$u_\mathrm{rad} = \sum_i u_i = \sum_i S_i/c, \tag{21}$$

and hence

$$-(\mathrm{d}E/\mathrm{d}t) = \sigma_\mathrm{T} c u_\mathrm{rad}. \tag{22}$$

- Thomson scattering is one of the most important processes which impedes the escape of photons from any region. We write down the expression for the energy scattered by the electron in terms of the number density N of photons of frequency ν so that

$$-\frac{\mathrm{d}(Nh\nu)}{\mathrm{d}t} = \sigma_{\mathrm{T}} c N h\nu. \tag{23}$$

There is no change of energy of the photons in the scattering process and so, if there are N_{e} electrons per unit volume, the number density of photons decreases exponentially with distance

$$\begin{aligned} -\frac{\mathrm{d}N}{\mathrm{d}t} &= \sigma_{\mathrm{T}} c N_{\mathrm{e}} N \qquad -\frac{\mathrm{d}N}{\mathrm{d}x} = \sigma_{\mathrm{T}} N_{\mathrm{e}} N \\ N &= N_0 \exp\left(-\int \sigma_{\mathrm{T}} N_{\mathrm{e}}\,\mathrm{d}x\right). \end{aligned} \tag{24}$$

Thus, the *optical depth* of the medium to Thomson scattering is

$$\tau = \int \sigma_{\mathrm{T}} N_{\mathrm{e}}\,\mathrm{d}x. \tag{25}$$

- In this process, the photons are scattered in random directions and so they perform a random walk, each step corresponding to the *mean free path* λ_{T} of the photon through the electron gas where $\lambda_{\mathrm{T}} = (\sigma_{\mathrm{T}} N_{\mathrm{e}})^{-1}$.

Inverse Compton Scattering

Comptonisation is a vast subject. *Inverse Compton scattering* involves the scattering of low energy photons to high energies by ultrarelativistic electrons so that the photons gain and the electrons lose energy. The process is called *inverse* because the electrons lose energy rather than the photons, the opposite of the standard Compton effect. We will treat the case in which the energy of the photon in the centre of momentum frame of the interaction is much less that $m_e c^2$, and consequently the Thomson scattering cross-section can be used to describe the probability of scattering.

Many of the most important results can be worked out using simple physical arguments, as for example in Blumenthal and Gould (1970) and Rybicki and Lightman (1979).

Inverse Compton Scattering

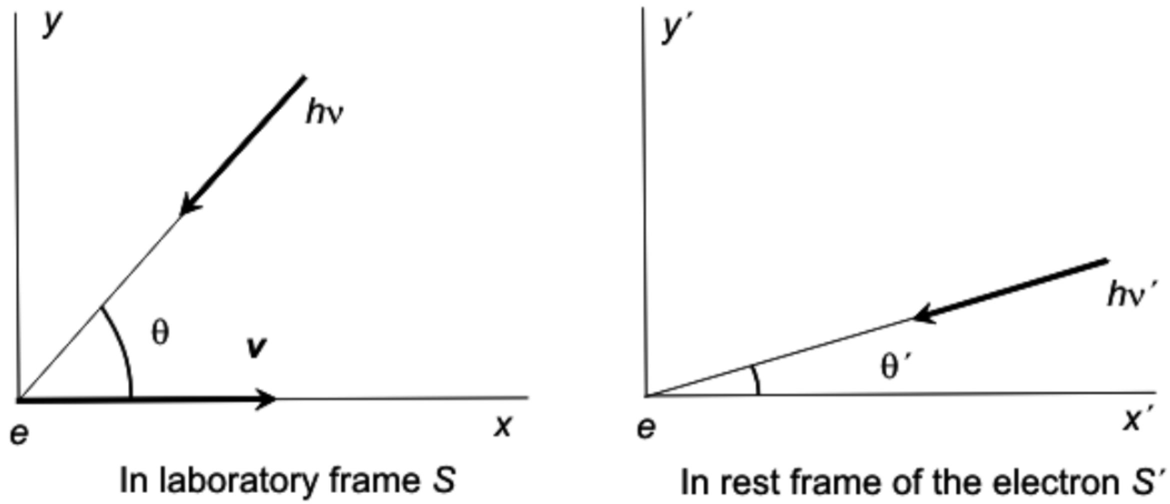

Consider a collision between a photon and a relativistic electron as seen in the laboratory frame of reference S and in the rest frame of the electron S′. Since $\hbar\omega' \ll m_e c^2$ in S′, the centre of momentum frame is very closely that of the relativistic electron. If the energy of the photon is $\hbar\omega$ and the angle of incidence θ in S, its energy in the frame S′ is

$$\hbar\omega' = \gamma\hbar\omega[1 + (v/c)\cos\theta] \tag{1}$$

according to the standard relativistic Doppler shift formula.

Inverse Compton Scattering

Similarly, the angle of incidence θ' in the frame S$'$ is related to θ by the formulae

$$\sin\theta' = \frac{\sin\theta}{\gamma[1 + (v/c)\cos\theta]} \quad ; \quad \cos\theta' = \frac{\cos\theta + v/c}{1 + (v/c)\cos\theta}. \tag{2}$$

Now, provided $\hbar\omega' \ll m_{\rm e}c^2$, the Compton interaction in the rest frame of the electron is simply Thomson scattering and hence the energy loss rate of the electron in S$'$ is just the rate at which energy is reradiated by the electron.

According to the analysis of Thomson scattering, the loss rate is

$$-({\rm d}E/{\rm d}t)' = \sigma_{\rm T} c U'_{\rm rad}, \tag{3}$$

where $U'_{\rm rad}$ is the energy density of radiation in the rest frame of the electron. As discussed in that section, it is of no importance whether or not the radiation is isotropic. The free electron oscillates in response to any incident radiation field. Our strategy is therefore to work out $U'_{\rm rad}$ in the frame of the electron S$'$ and then to use (3) to work out $({\rm d}E/{\rm d}t)'$. Because ${\rm d}E/{\rm d}t$ is an invariant between inertial frames, this is also the loss rate $({\rm d}E/{\rm d}t)$ in the observer's frame S.

Working out U'_{rad} in S′

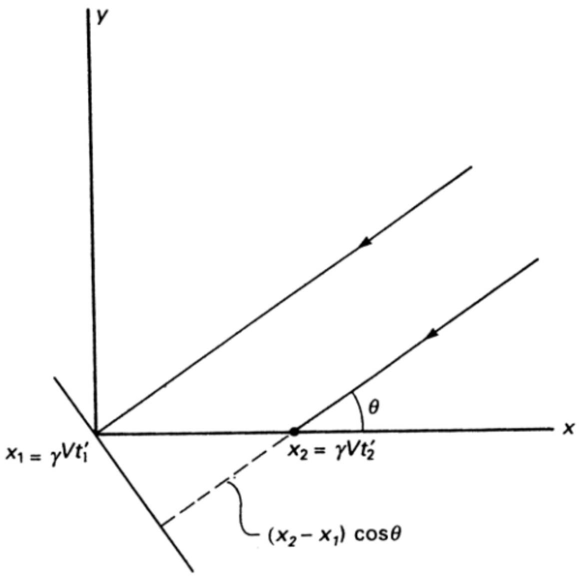

In S, the electron moves from x_1 to x_2 in the time interval t_1 to t_2. These are transformed into S′ by the standard Lorentz transformation

Suppose the number density of photons in a beam of radiation incident at angle θ to the x-axis is N. Then, the energy density of these photons in S is $N\hbar\omega$. The flux density of photons incident upon an electron stationary in S is $U_{\mathrm{rad}}c = N\hbar\omega c$.

Now let us work out the flux density of this beam in the frame of reference of the electron S′. We need two things, the energy of each photon in S′ and the rate of arrival of these photons at the electron in S′. The first of these is given by (3). The second factor requires a little bit of care, although the answer is obvious in the end. The beam of photons incident at angle θ in S arrives at an angle θ' in S′ according to the aberration formulae (2).

Working out U'_{rad} in S′

We are interested in the rate of arrival of photons at the origin of S′ and so let us consider two photons which arrive there at times t'_1 and t'_2. The coordinates of these events in S are

$$[x_1, 0, 0, t_1] = [\gamma V t'_1, 0, 0, \gamma t'_1] \quad \text{and} \quad [x_2, 0, 0, t_2] = [\gamma V t'_2, 0, 0, \gamma t'_2] \tag{4}$$

respectively. This calculation makes the important point that the photons in the beam are propagated along parallel but separate trajectories in S

From the geometry of the figure, it is apparent that the time difference when the photons arrive at a plane perpendicular to their direction of propagation in S is

$$\Delta t = t_2 + \frac{(x_2 - x_1)}{c} \cos\theta - t_1 = (t'_2 - t'_1)\gamma[1 + (v/c)\cos\theta], \tag{5}$$

that is, the time interval between the arrival of photons from the direction θ is shorter by a factor $\gamma[1 + (v/c)\cos\theta]$ in S′ than it is in S.

Working out $U'_{\rm rad}$ in S′

Thus, the rate of arrival of photons, and correspondingly their number density, is greater by this factor $\gamma[1 + (v/c)\cos\theta]$ in S′ as compared with S. This is exactly the same factor by which the energy of the photon has increased (3). On reflection, we should not be surprised by this result because these are two different aspects of the same relativistic transformation between the frames S and S′, in one case the frequency interval and, in the other, the time interval.

Thus, as observed in S′, the energy density of the beam is therefore

$$U'_{\rm rad} = [\gamma(1 + (v/c)\cos\theta)]^2\, U_{\rm rad}. \tag{6}$$

Now, this energy density is associated with the photons incident at angle θ in the frame S and consequently arrives within solid angle $2\pi \sin\theta\, d\theta$ in S. We assume that the radiation field in S is isotropic and therefore we can now work out the total energy density seen by the electron in S′ by integrating over solid angle in S, that is,

$$U'_{\rm rad} = U_{\rm rad} \int_0^{\pi} \gamma^2[1 + (v/c)\cos\theta]^2\, \tfrac{1}{2}\sin\theta\, d\theta. \tag{7}$$

The Inverse Compton Energy Loss Rate

Integrating, we find

$$U'_{\rm rad} = \tfrac{4}{3} U_{\rm rad}(\gamma^2 - \tfrac{1}{4}). \tag{8}$$

Therefore, substituting into (3), we find

$$({\rm d}E/{\rm d}t)' = ({\rm d}E/{\rm d}t) = \tfrac{4}{3}\sigma_{\rm T} c U_{\rm rad}(\gamma^2 - \tfrac{1}{4}). \tag{9}$$

Now, this is the energy gained by the photon field due to the scattering of the low energy photons. We have therefore to subtract the energy of these photons to find the total energy gain to the photon field in S. The rate at which energy is removed from the low energy photon field is $\sigma_{\rm T} c U_{\rm rad}$ and therefore, subtracting, we find

$${\rm d}E/{\rm d}t = \tfrac{4}{3}\sigma_{\rm T} c U_{\rm rad}(\gamma^2 - \tfrac{1}{4}) - \sigma_{\rm T} c U_{\rm rad} = \tfrac{4}{3}\sigma_{\rm T} c U_{\rm rad}(\gamma^2 - 1). \tag{10}$$

We now use the identity $(\gamma^2 - 1) = (v^2/c^2)\gamma^2$ to write the loss rate in its final form

$$\boxed{{\rm d}E/{\rm d}t = \tfrac{4}{3}\sigma_{\rm T} c U_{\rm rad}\left(\frac{v^2}{c^2}\right)\gamma^2.} \tag{11}$$

Synchrotron Radiation and Inverse Compton Losses

This is the remarkably elegant result we have been seeking. It is exact so long as $\gamma\hbar\omega \ll m_e c^2$.

Notice the remarkable similarity between the expressions for the loss rates by synchrotron radiation and by inverse Compton scattering, even down to the factor of $\frac{4}{3}$ in front of the two expressions.

$$-\left(\frac{\mathrm{d}E}{\mathrm{d}t}\right)_{\mathrm{IC}} = \frac{4}{3}\sigma_{\mathrm{T}} c U_{\mathrm{rad}} \left(\frac{v^2}{c^2}\right)\gamma^2 \qquad -\left(\frac{\mathrm{d}E}{\mathrm{d}t}\right)_{\mathrm{sync}} = \frac{4}{3}\sigma_{\mathrm{T}} c U_{\mathrm{mag}} \left(\frac{v}{c}\right)^2\gamma^2 \tag{12}$$

This is not an accident. The reason for the similarity is that, in both cases, the electron is accelerated by the electric field which it observes in its instantaneous rest-frame. The electron does not really care about the origin of the electric field. In the case of synchrotron radiation, the constant accelerating electric field is associated with the motion of the electron through the magnetic field $\boldsymbol{B}$, $\boldsymbol{E}' = \boldsymbol{v} \times \boldsymbol{B}$, and, in the case of inverse Compton scattering, it is the sum of all the electric fields of the incident waves.

The Spectrum of Inverse Compton Radiation

The next calculation is the determination of the spectrum of the scattered radiation. This can be found by performing two successive Lorentz transformations, first transforming the photon distribution into the frame S′ and then transforming the scattered radiation back into the laboratory frame of reference S. This is not a trivial calculation, but the exact result is given by Blumenthal and Gould (1970) for an incident isotropic photon field at a single frequency ν_0. They show that the spectral emissivity $I(\nu)$ may be written

$$I(\nu)\,\mathrm{d}\nu = \frac{3\sigma_{\mathrm{T}} c}{16\gamma^4}\frac{N(\nu_0)}{\nu_0^2}\nu\left[2\nu \ln\left(\frac{\nu}{4\gamma^2\nu_0}\right) + \nu + 4\gamma^2\nu_0 - \frac{\nu^2}{2\gamma^2\nu_0}\right]\mathrm{d}\nu, \qquad (13)$$

where the radiation field is assumed to be monochromatic with frequency ν_0; $N(\nu_0)$ is the number density of photons. At low frequencies, the term in square brackets in (13) is a constant and hence the scattered radiation has the form $I(\nu) \propto \nu$.

The Spectrum of Inverse Compton Radiation

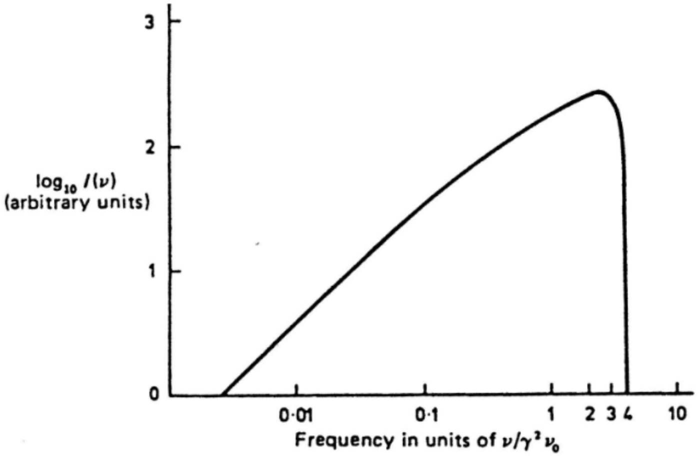

It is an easy calculation to show that the maximum energy which the photon can acquire corresponds to a head-on collision in which the photon is sent back along its original path. The maximum energy of the photon is

$$(\hbar\omega)_{\mathrm{max}} = \hbar\omega\gamma^2(1 + v/c)^2 \approx 4\gamma^2\hbar\omega_0. \quad (14)$$

Another interesting result comes out of the formula for the total energy loss rate of the electron (11). The number of photons scattered per unit time is $\sigma_{\mathrm{T}} c U_{\mathrm{rad}}/\hbar\omega_0$ and hence the average energy of the scattered photons is

$$\hbar\omega = \tfrac{4}{3}\gamma^2(v/c)^2\hbar\omega_0 \approx \tfrac{4}{3}\gamma^2\hbar\omega_0. \quad (15)$$

This result gives substance to the hand-waving argument that the photon gains one factor of γ in transforming into S′ and then gains another on transforming back to S.

Inverse Compton Radiation

The general result that the frequency of the scattered photons is $\nu \approx \gamma^2 \nu_0$ is of profound importance in high energy astrophysics. We know that there are electrons with Lorentz factors $\gamma \sim 100 - 1000$ in various types of astronomical source and consequently they scatter any low energy photons to very much higher energies. Consider the scattering of radio, infrared and optical photons scattered by electrons with $\gamma = 1000$.

Waveband	*Frequency (Hz)* ν_0	*Scattered Frequency (Hz) and Waveband*
Radio	10^9	10^{15} = UV
Far-infrared	3×10^{12}	3×10^{18} = X-rays
Optical	4×10^{14}	$4 \times 10^{21} \equiv 1.6$MeV = γ-rays

Thus, inverse Compton scattering is a means of creating very high energy photons indeed. It also becomes an inevitable drain of energy for high energy electrons whenever they pass through a region in which there is a large energy density of photons.

Emission of a Distribution of Electron Energies

When these formulae are used in astrophysical calculations, it is necessary to integrate over both the spectrum of the incident radiation and the spectrum of the relativistic electrons. The enthusiast is urged to consult the excellent review paper by Blumenthal and Gould (1970). Some of the results are, however, immediately apparent from the close analogy between the inverse Compton scattering and synchrotron radiation processes. For example,the spectrum of the inverse Compton scattering of photons of energy $h\nu$ by a power-law distribution of electron energies

$$\mathrm{d}N \propto E^{-p}\,\mathrm{d}E. \tag{16}$$

results in an intensity spectrum of the scattered radiation of the form

$$I(\nu) \propto \nu^{-(p-1)/2}, \tag{17}$$

Application to Double Radio Sources

The ratio of the total amount of energy liberated by synchrotron radiation and by inverse Compton scattering by the same distribution of electrons is

$$\frac{(\mathrm{d}E/\mathrm{d}t)_{\mathrm{sync}}}{(\mathrm{d}E/\mathrm{d}t)_{\mathrm{IC}}} = \frac{\int I_\nu \,\mathrm{d}\nu \ (\text{radio})}{\int I_X \,\mathrm{d}\nu_X \ (\text{X-ray})} = \frac{B^2/2\mu_0}{U_{\mathrm{rad}}}, \tag{18}$$

where U_{rad} is the energy density of radiation and B the magnetic flux density in the source region. Thus, if we measure the radio and X-ray flux densities from a source region and we know U_{rad}, we can find the magnetic flux density in the source. This type of phenomenon has been sought for in the hot spots and the extended structures of double radio sources. In the latter case, it is likely that the dominant source of low energy photons is the Cosmic Microwave Background Radiation.

Synchro-Compton Radiation and the Inverse Compton Catastrophe

Inverse Compton scattering is likely to be an important source of X-rays and γ-rays, for example, in the intense extragalactic γ-ray sources. Wherever there are large number densities of soft photons, the presence of ultrarelativistic electrons must result in the production of high energy photons, X-rays and γ-rays. The case of special interest in this chapter is that in which the same relativistic electrons which are the source of the soft photons are also responsible for scattering these photons to X-ray and γ-ray energies – this is the process known as *synchro-Compton Radiation*. One case of special importance is that in which the number density of low energy photons is so great that most of the energy of the electrons is lost by synchro-Compton radiation rather then by synchotron radiation. This line of reasoning leads to what is known as the *inverse Compton catastrophe*.

Ultra-High Energy γ-ray Sources

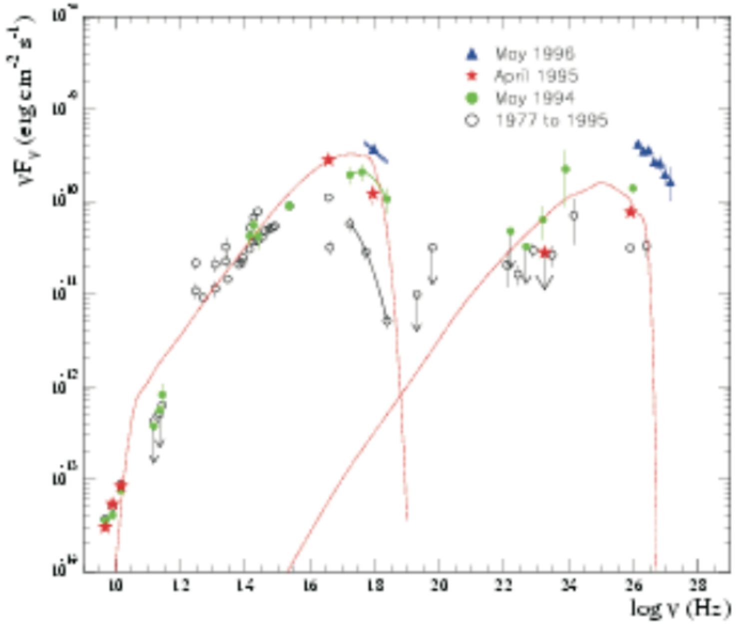

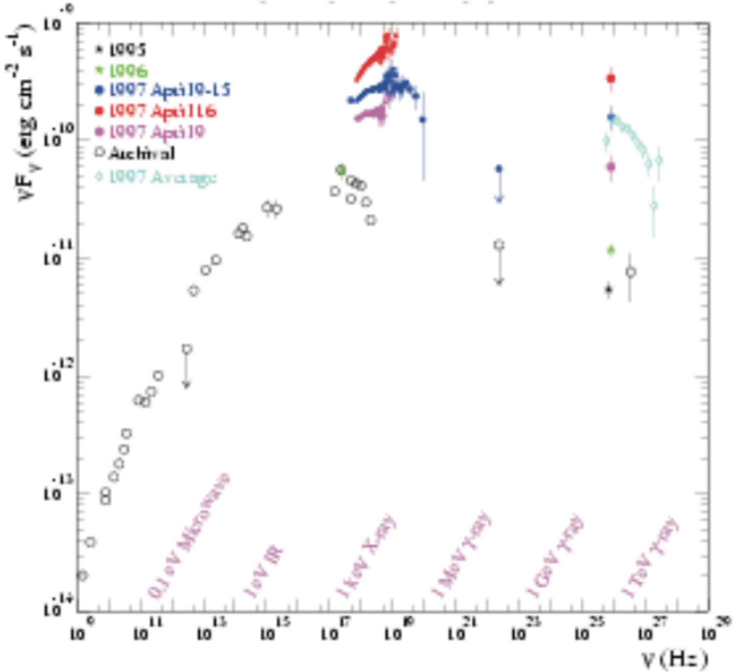

In the extreme γ-ray sources Markarian 421 and 501, it is very likely that some form of inverse Compton radiation is occurring, quite possible via the Synchro-Compton mechanism. These γ-ray sources are quite enormously luminous and variable. It is therefore likely that relativistic motions have to be involved to explain their luminosities and variability.

Astrofisica Nucleare e Subnucleare

Astrofisica al GeV

Exercise #6

- Find the web sites of AGILE and Fermi/LAT
- Check the status of future gamma-ray detectors (CALET, DAMPE, Gamma-400(?), HERD)

Photon Interactions

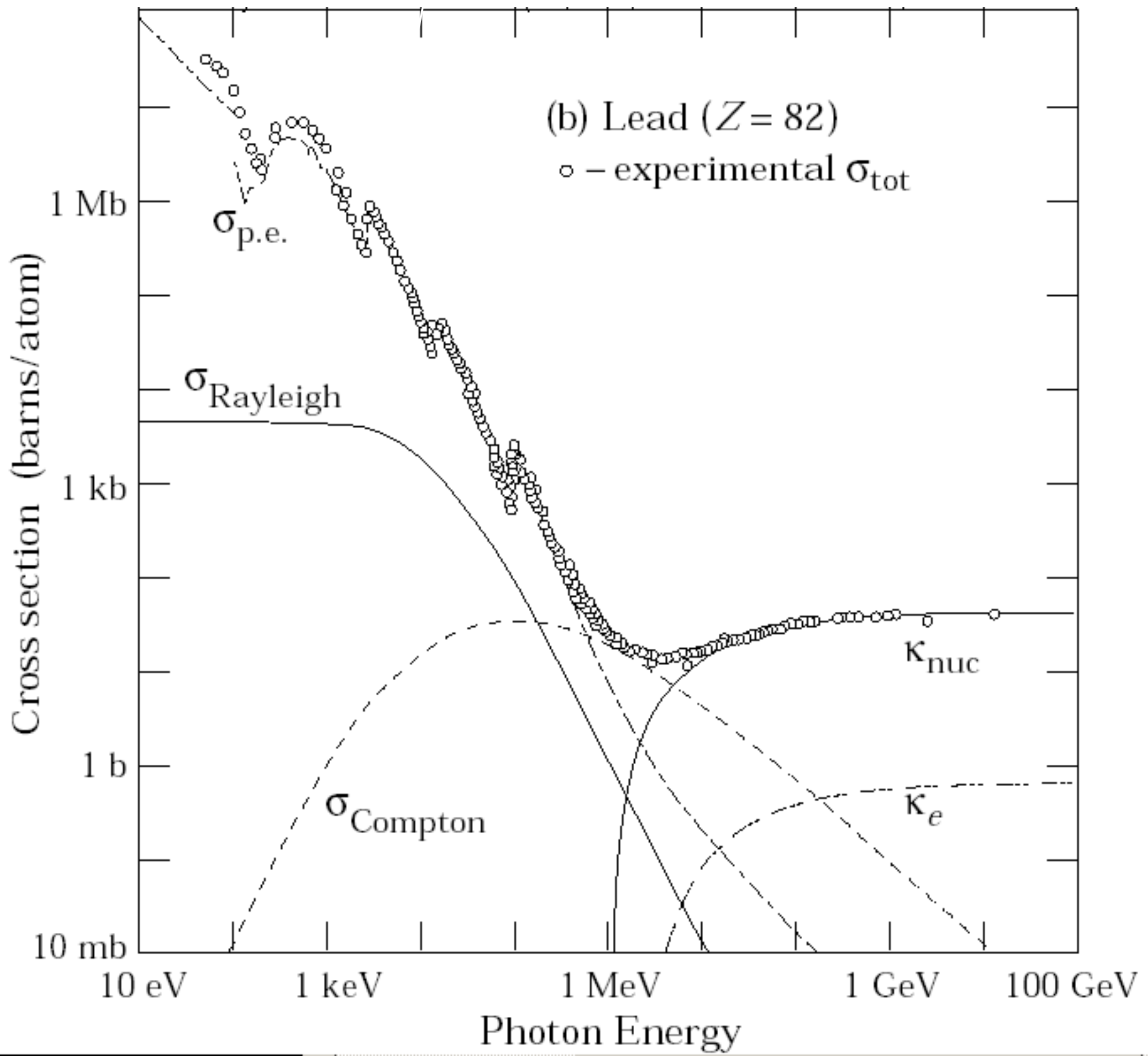

Detector Project

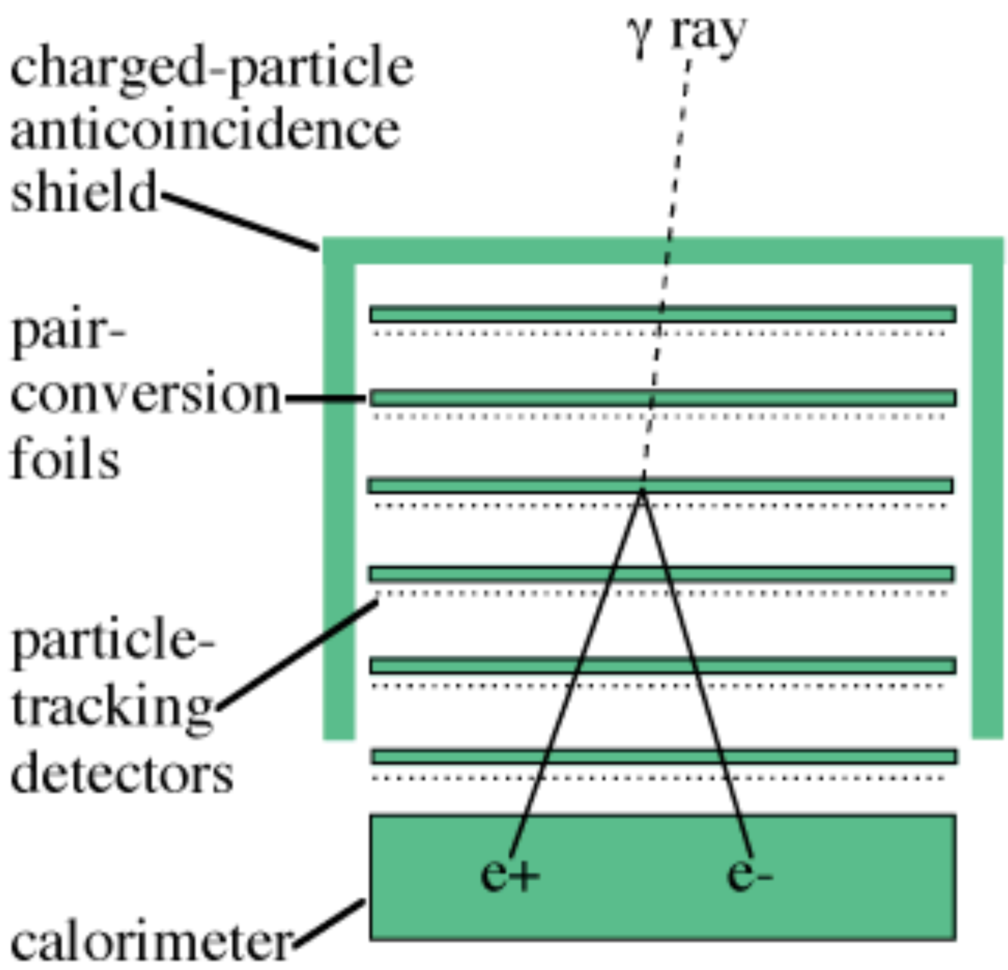

Gamma-ray astrophysics above 100 MeV

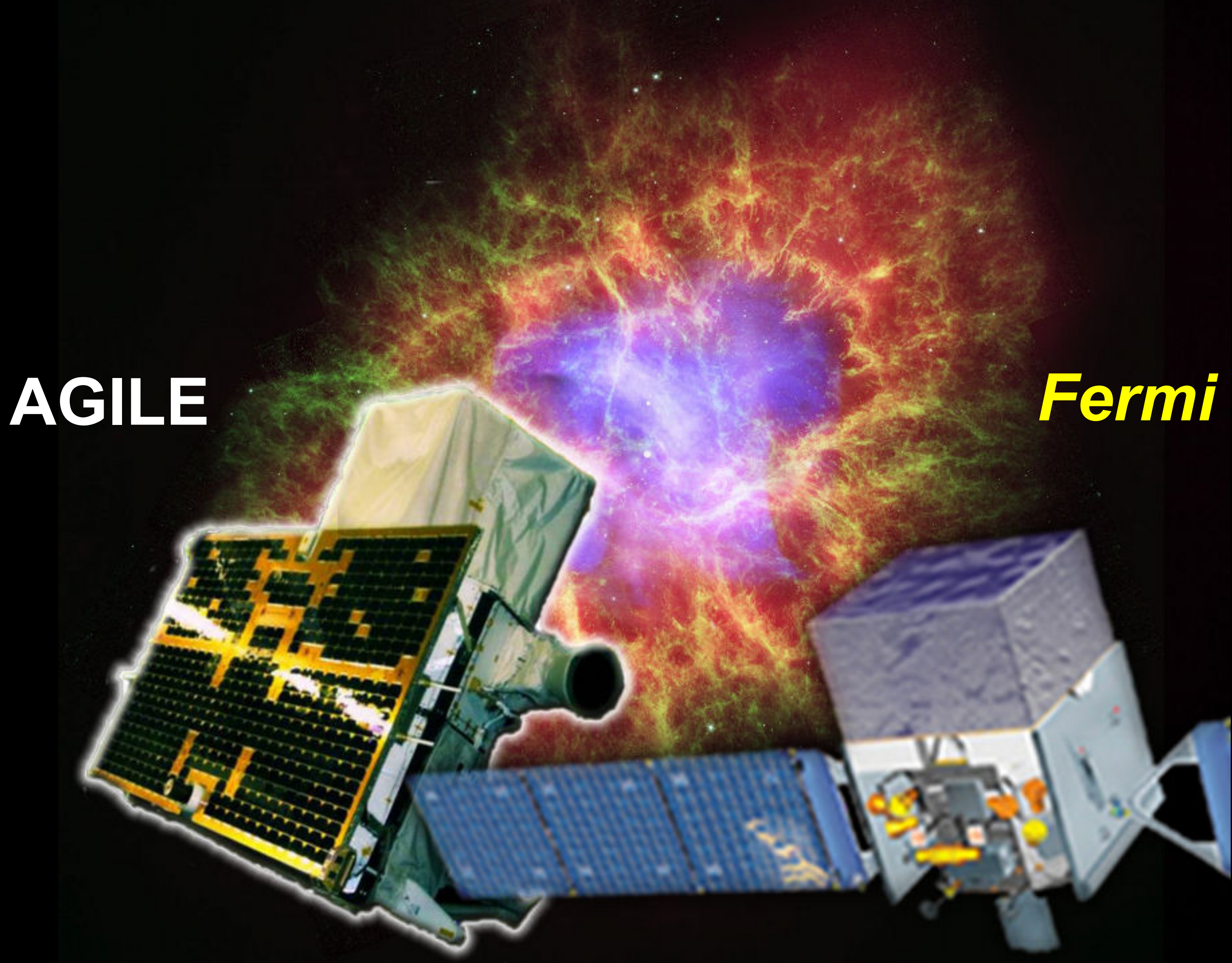

Picture of the day, Feb. 28, 2011, NASA-HEASARC

HE Gamma-ray Astrophysics
The EGRET legacy

EGRET

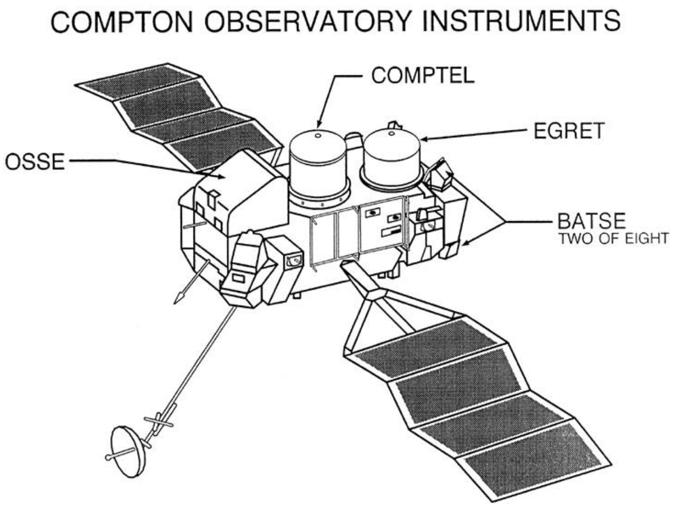

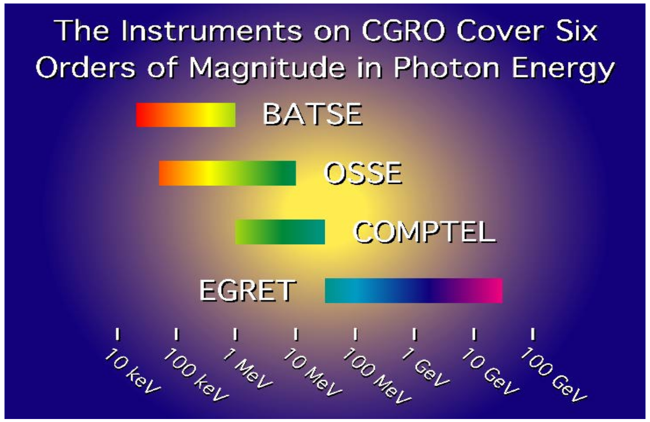

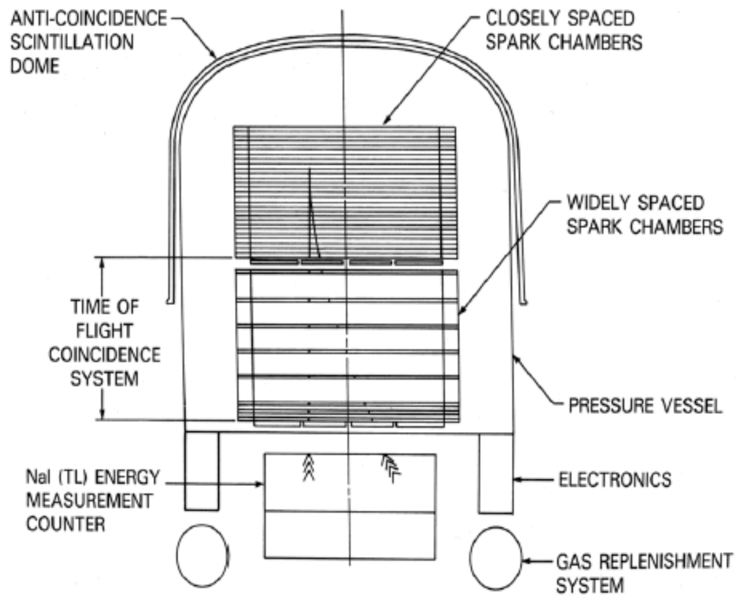

EGRET

- 1991-2000
- 30 MeV - 30 GeV
- AGN, GRB, Unidentified Sources, Diffuse Bkg

The HE sky from EGRET

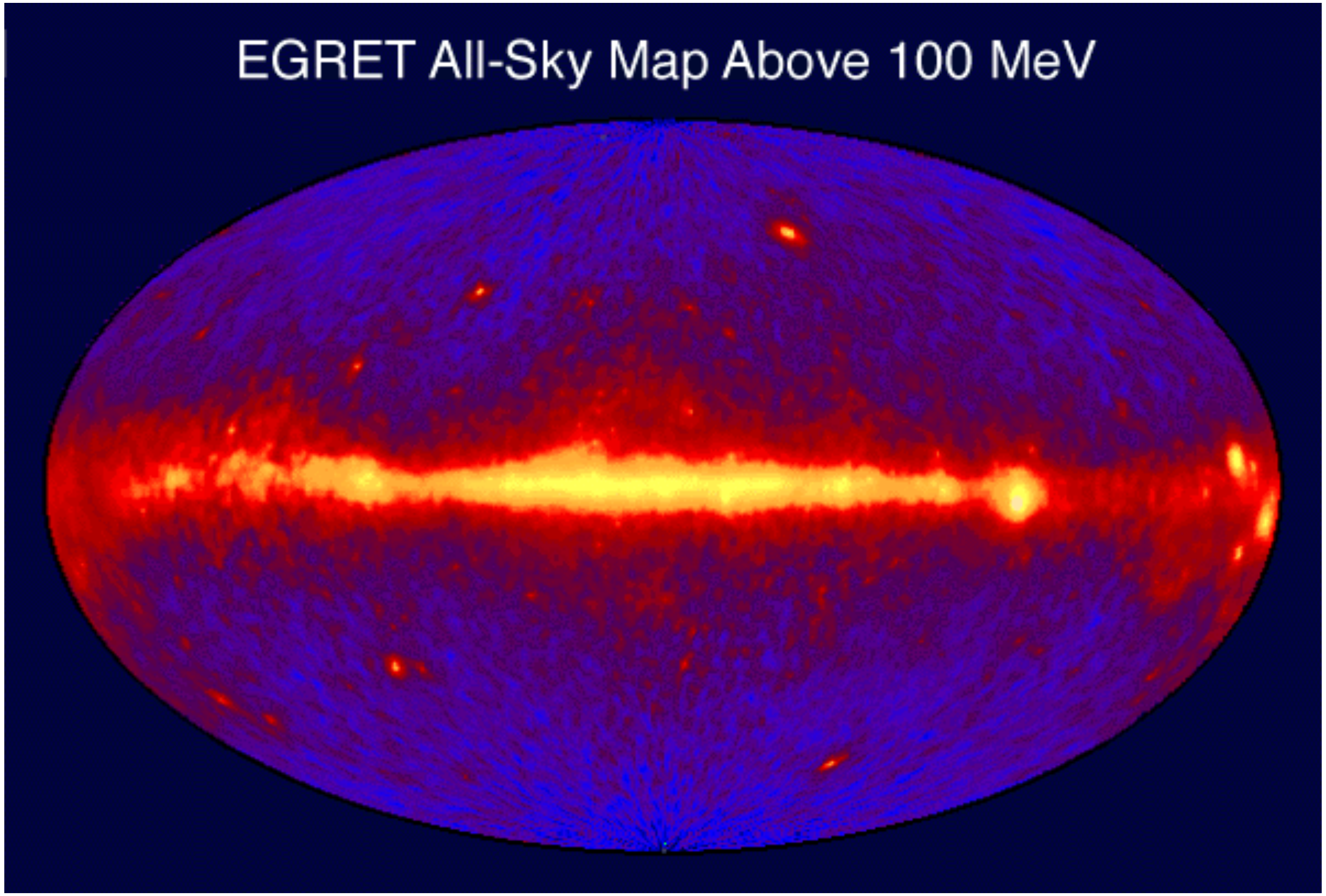

Analysis Topics

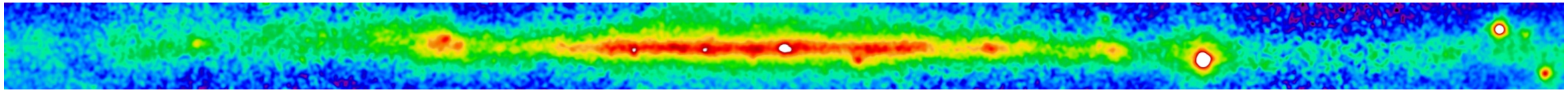

EGRET >300 MeV

- First a word about interstellar gamma-ray emission:
- Brightest at low latitudes, but detectable over the whole sky
- >60% of EGRET celestial gamma rays
- It fundamentally affects the approach to the analysis

Data Analysis

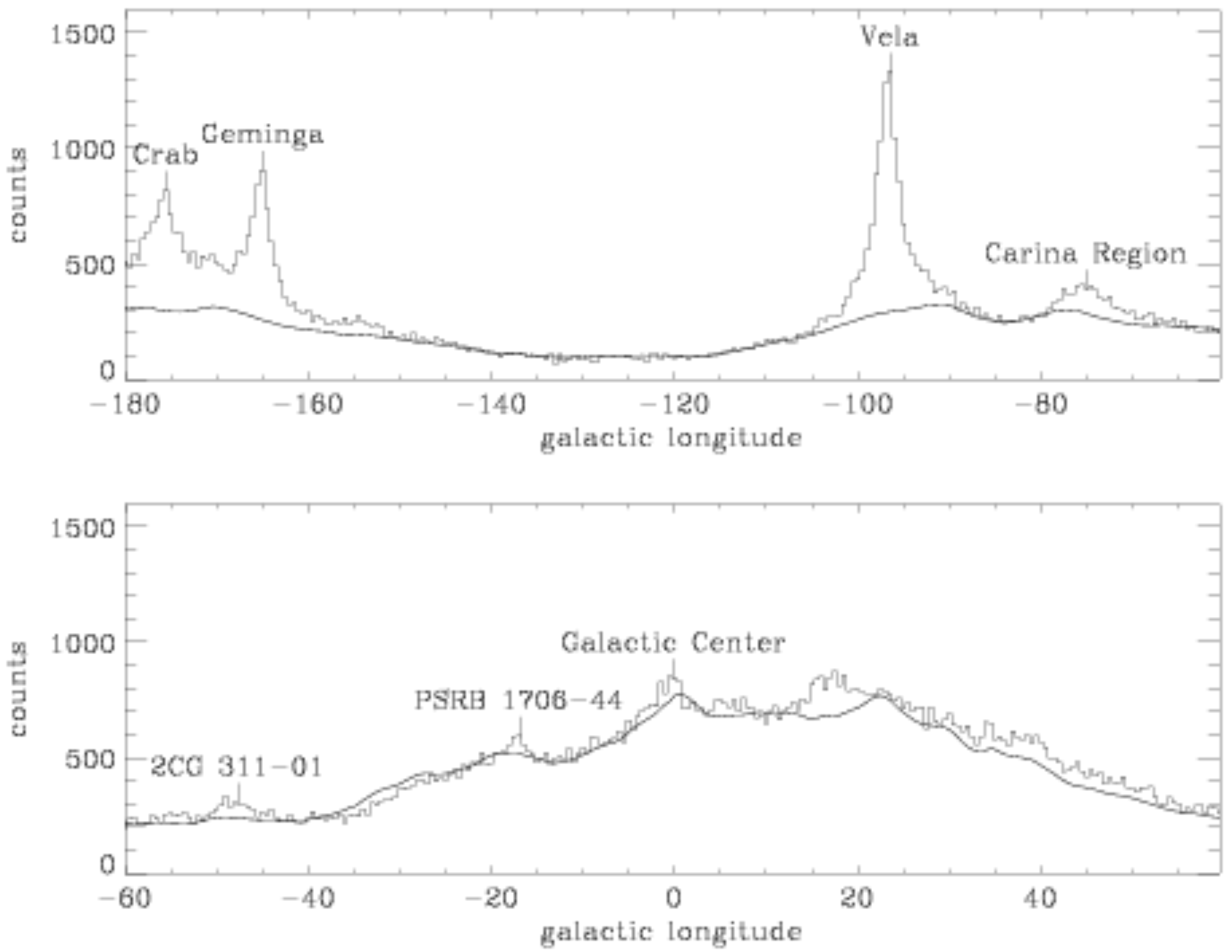

EGRET Gamma-ray Sources

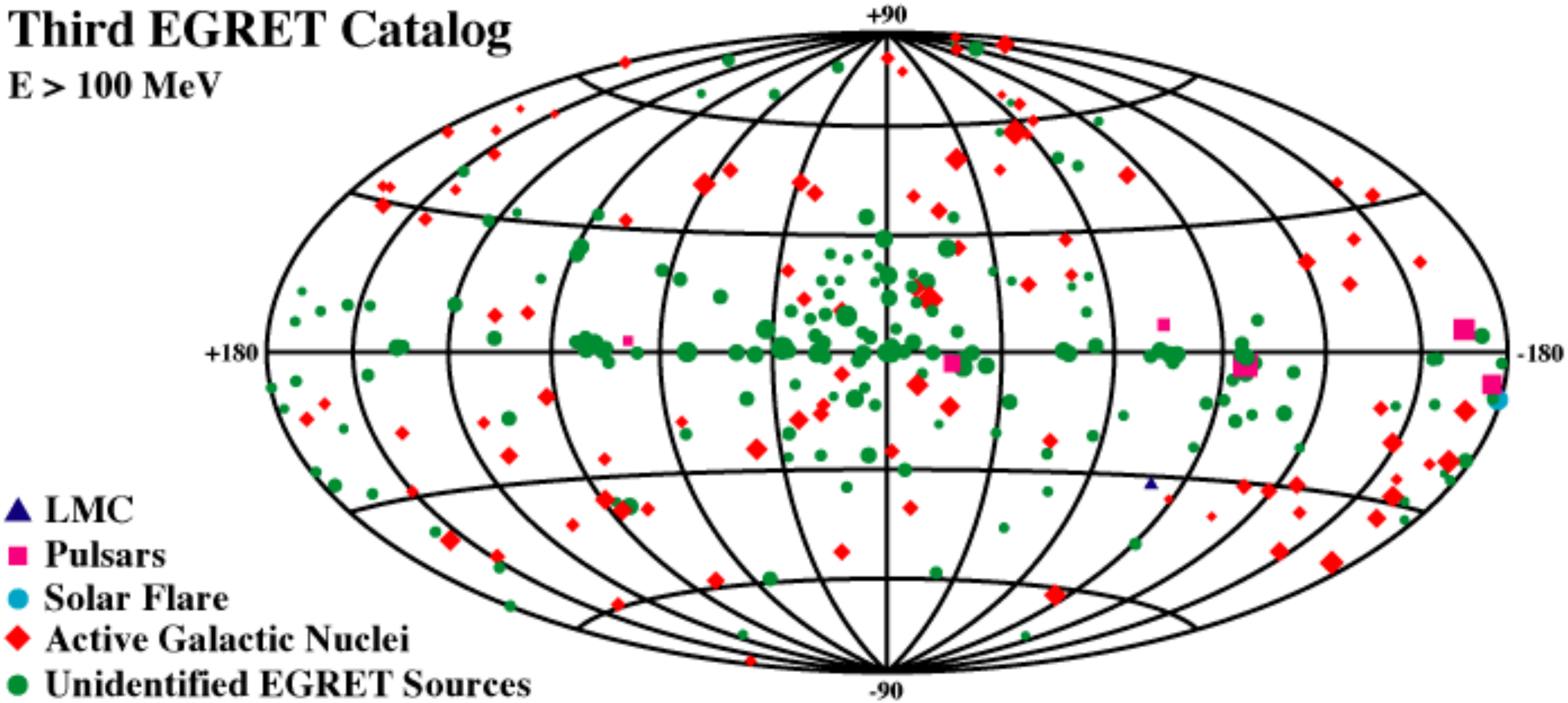

Challenge # 1

- Need simultaneous multiwavelength data to study variability and emission processes

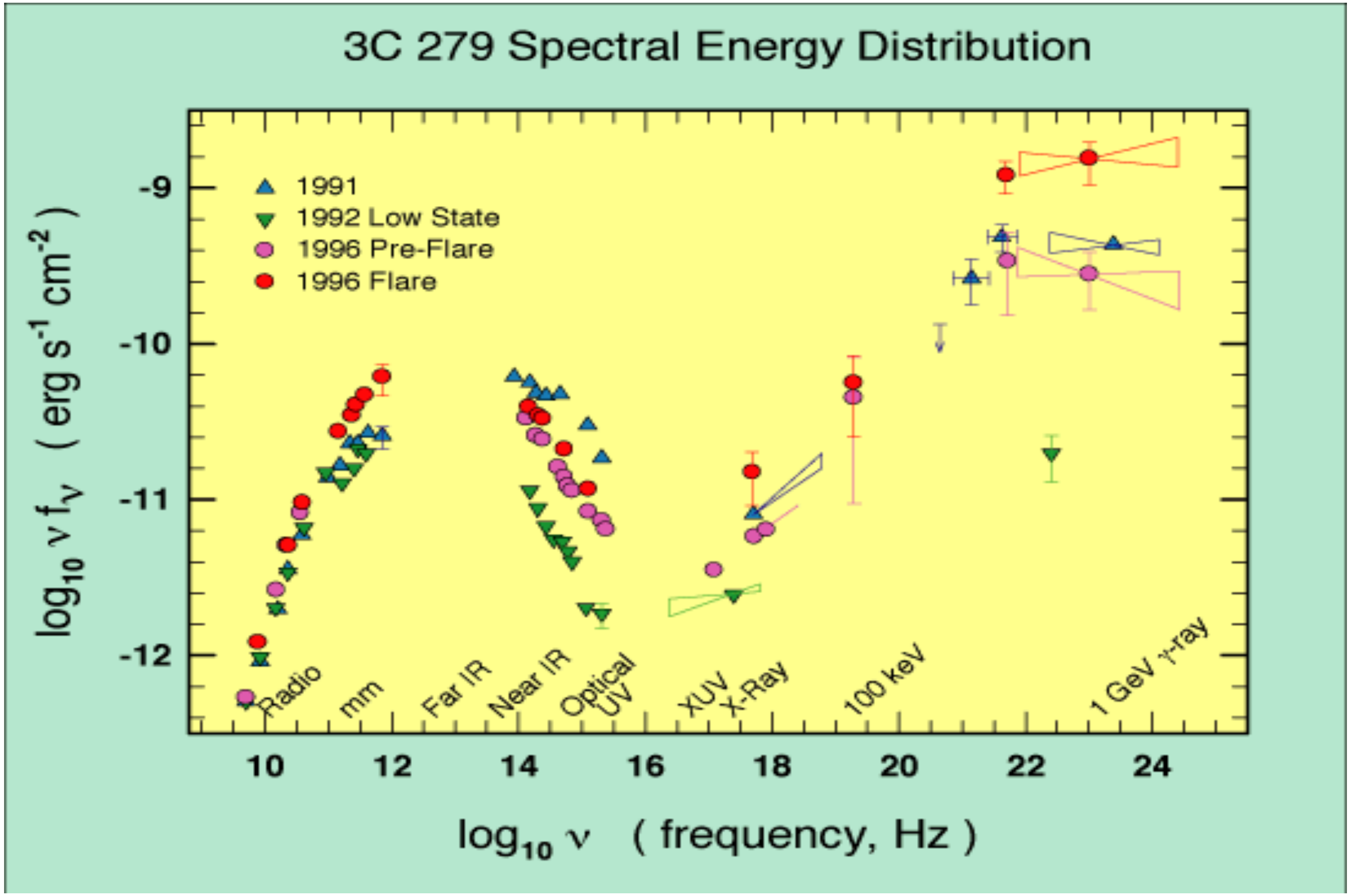

Active Galactic Nuclei

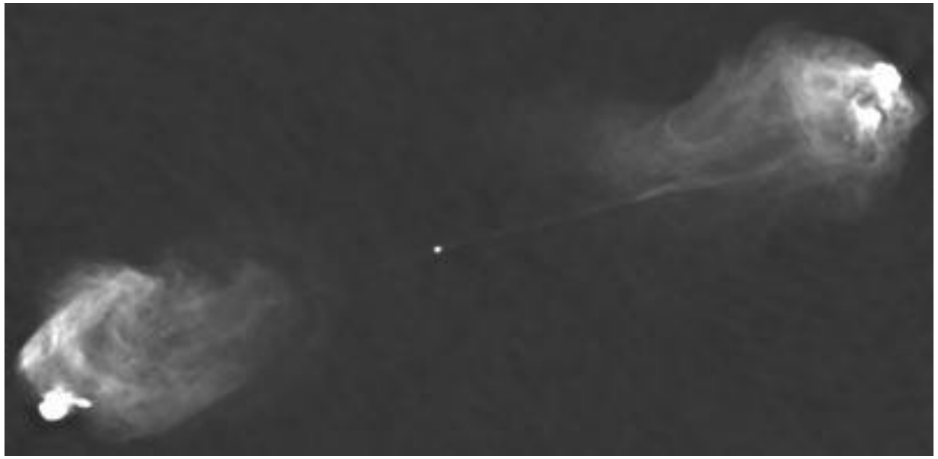

Radio

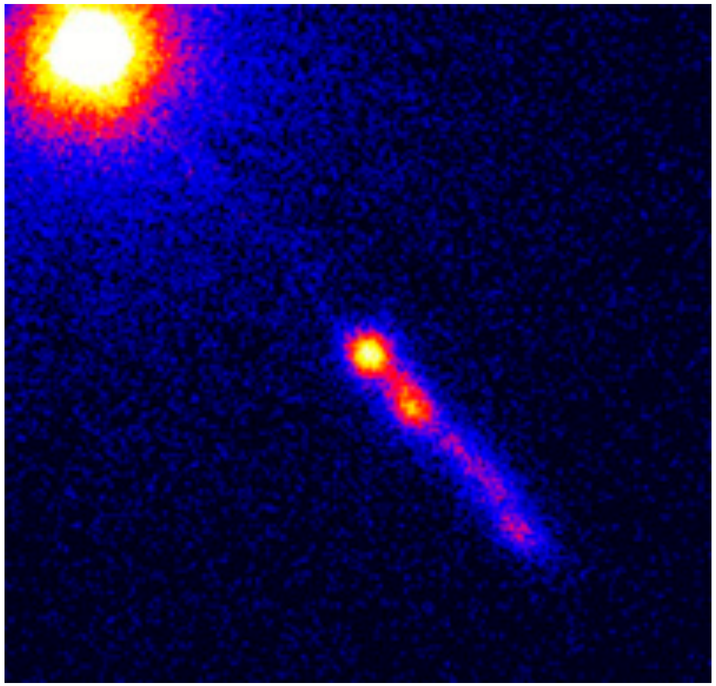

X-ray

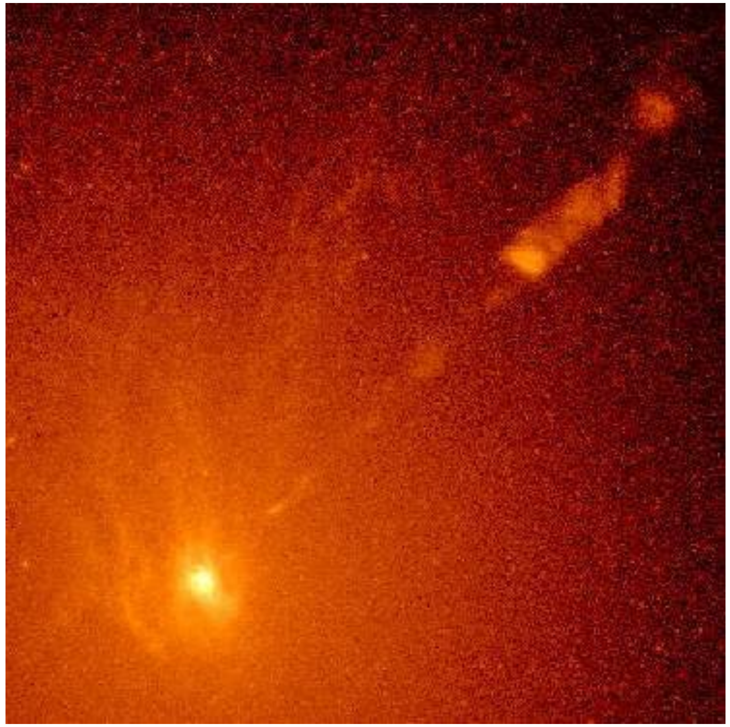

Optical

Active Galactic Nuclei

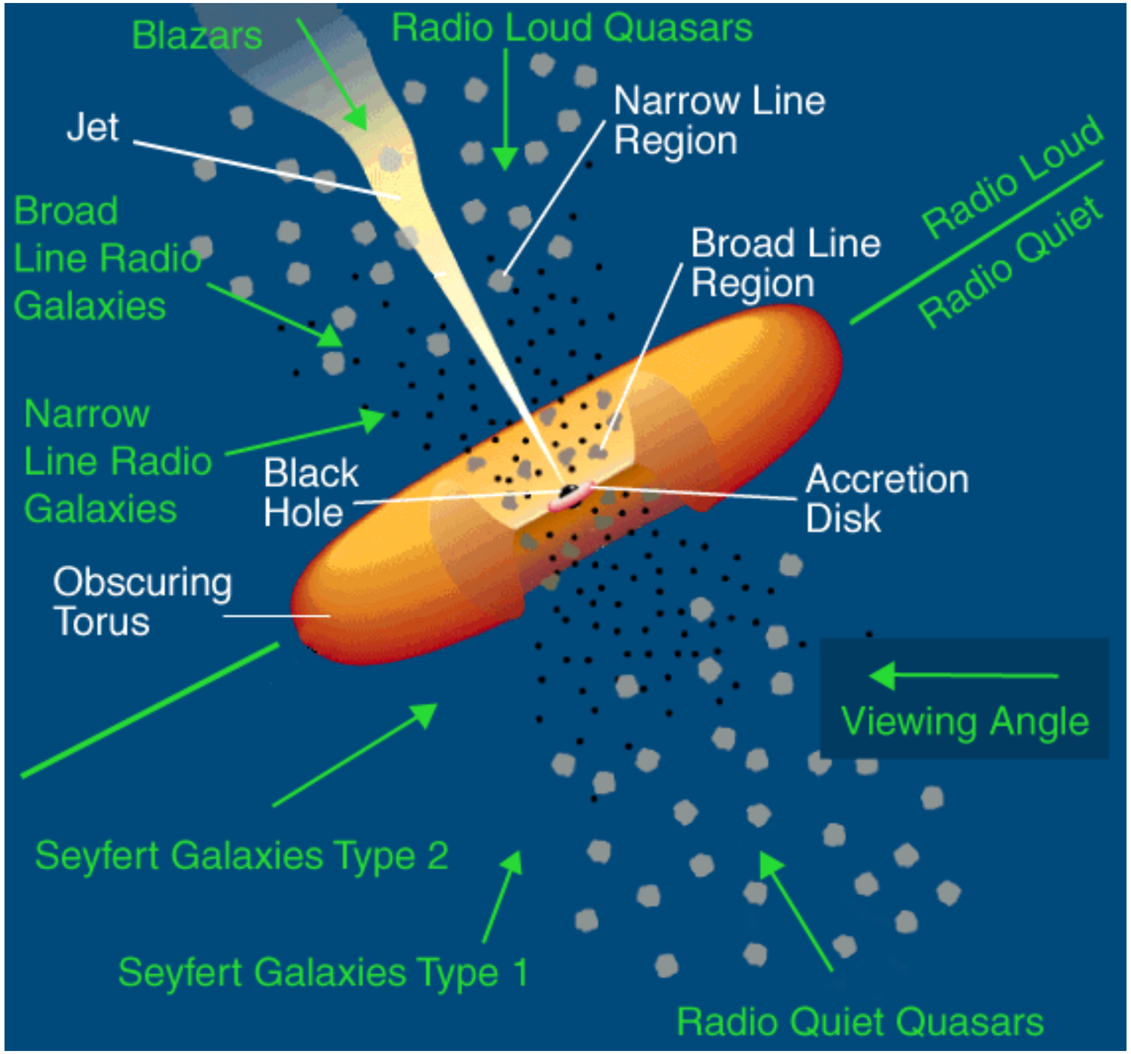

Models of AGN Gamma-ray Production

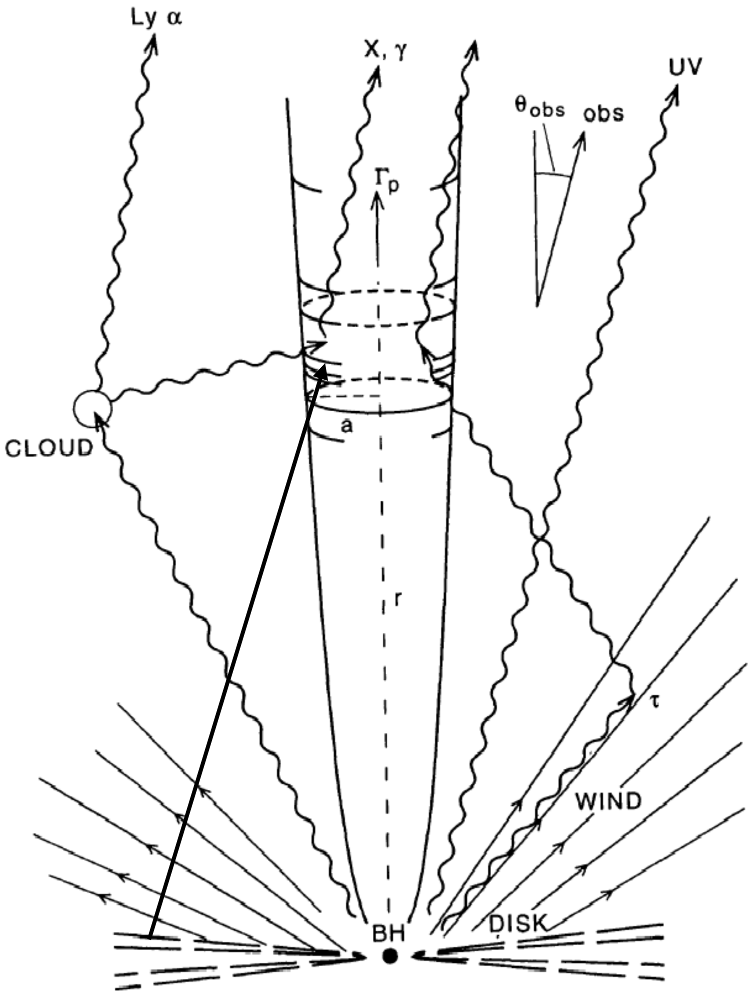

(from Sikora, Begelman, and Rees (1994))

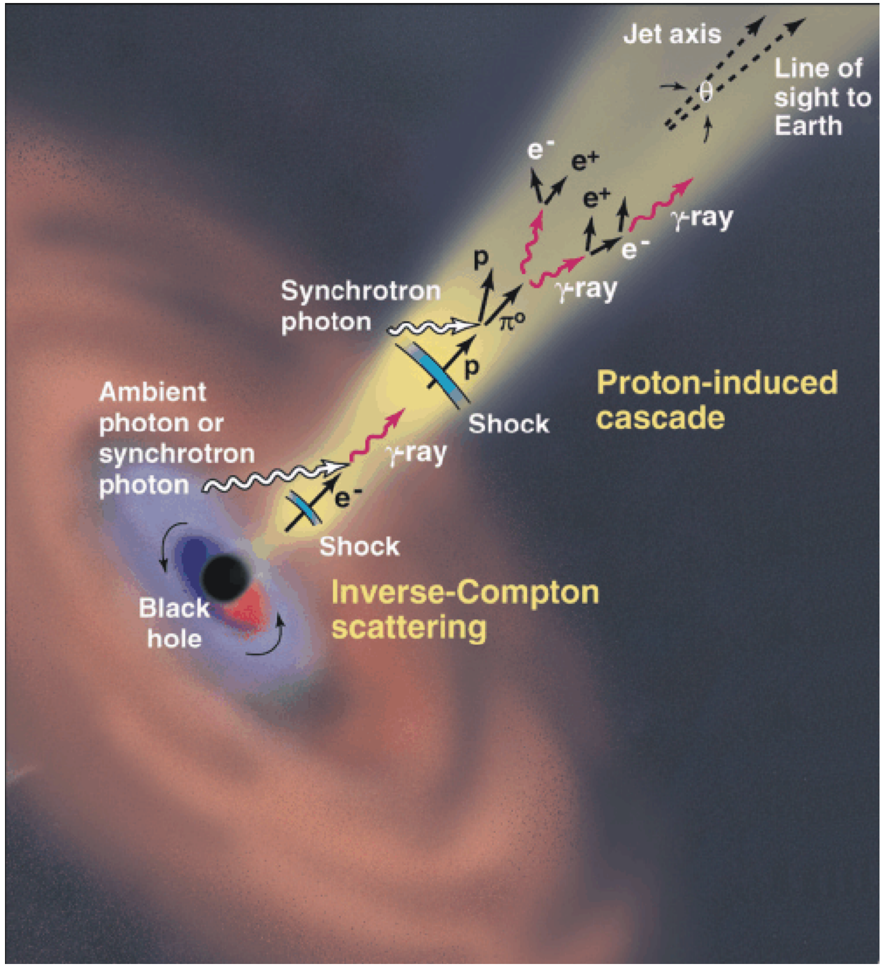

(credit:J. Buckley)

Active Galactic Nuclei

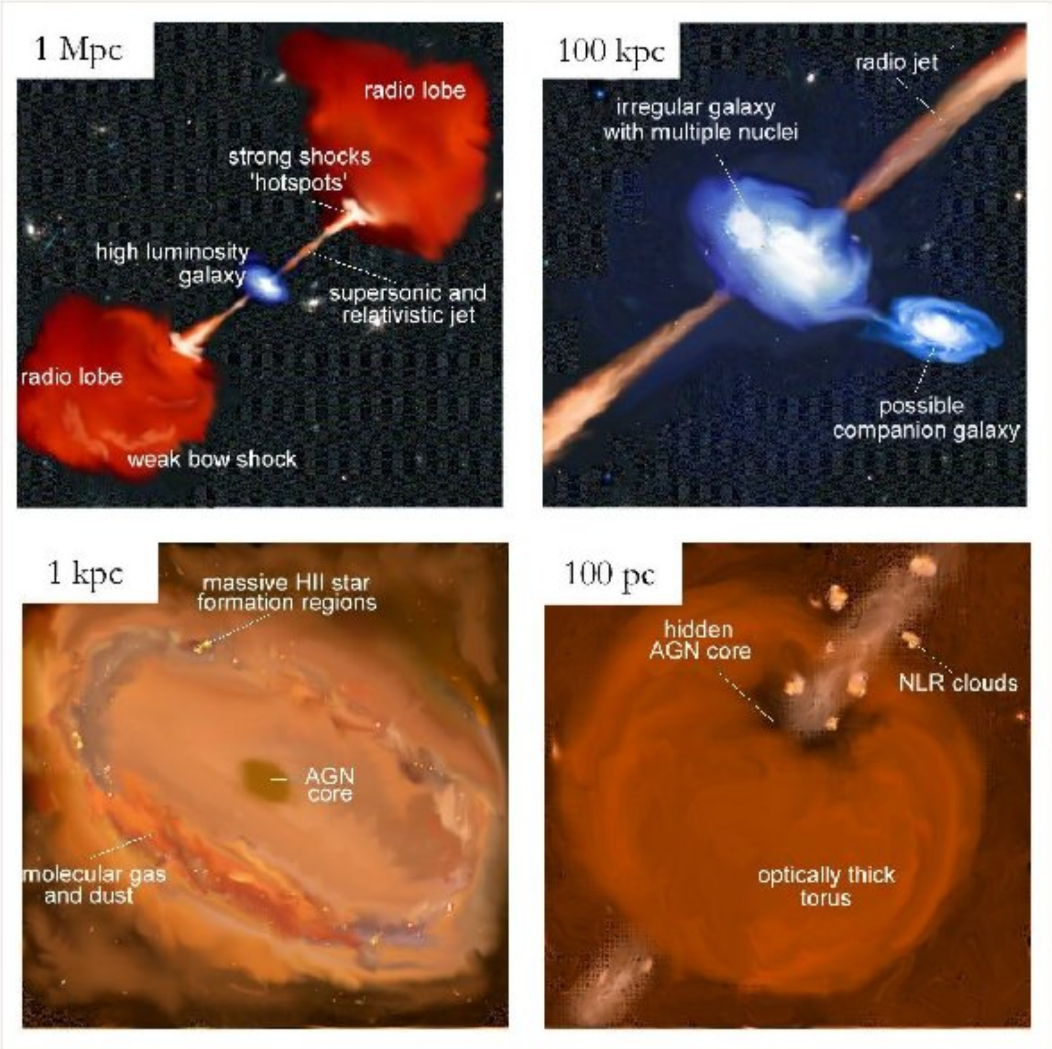

Artistic picture by S.Ciprini

Active Galactic Nuclei

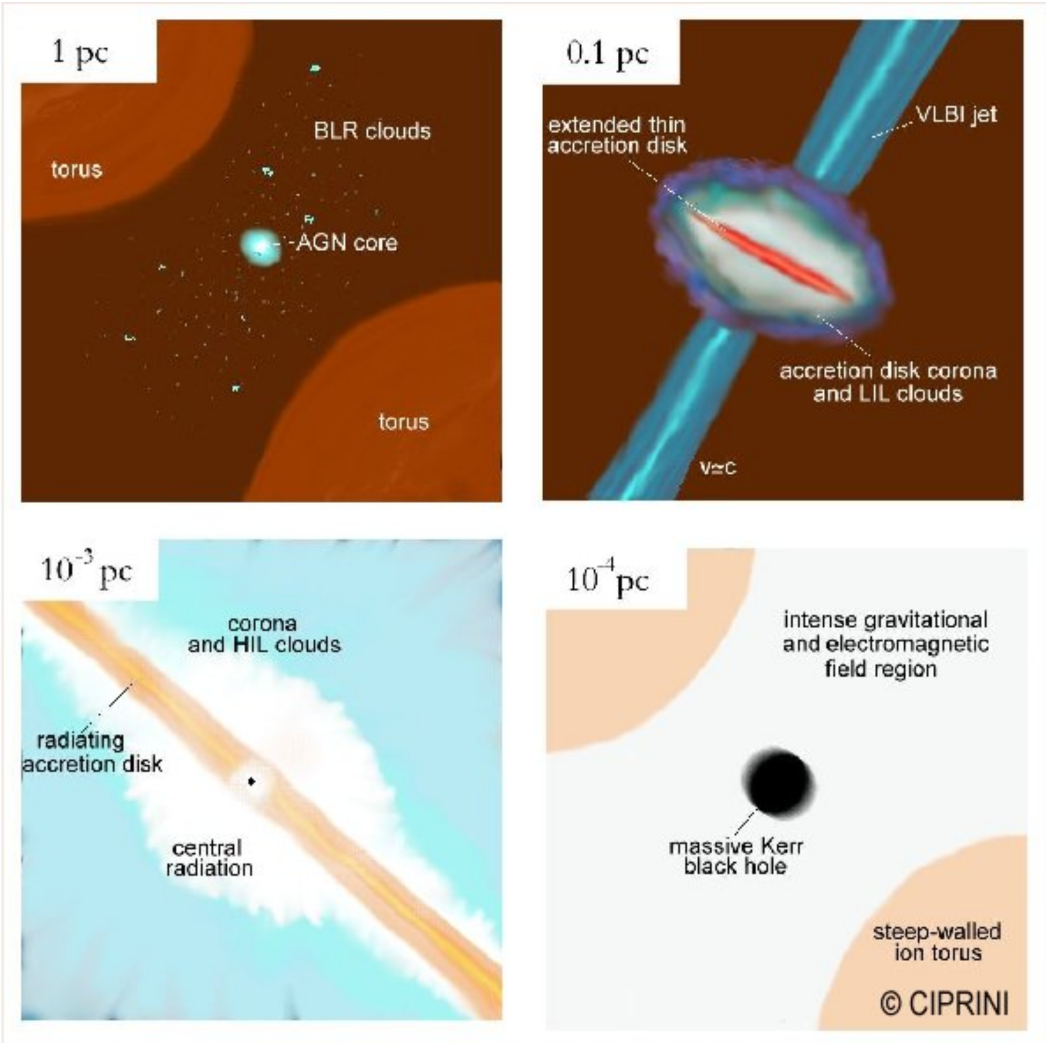

Artistic picture by S.Ciprini

M87 scales…

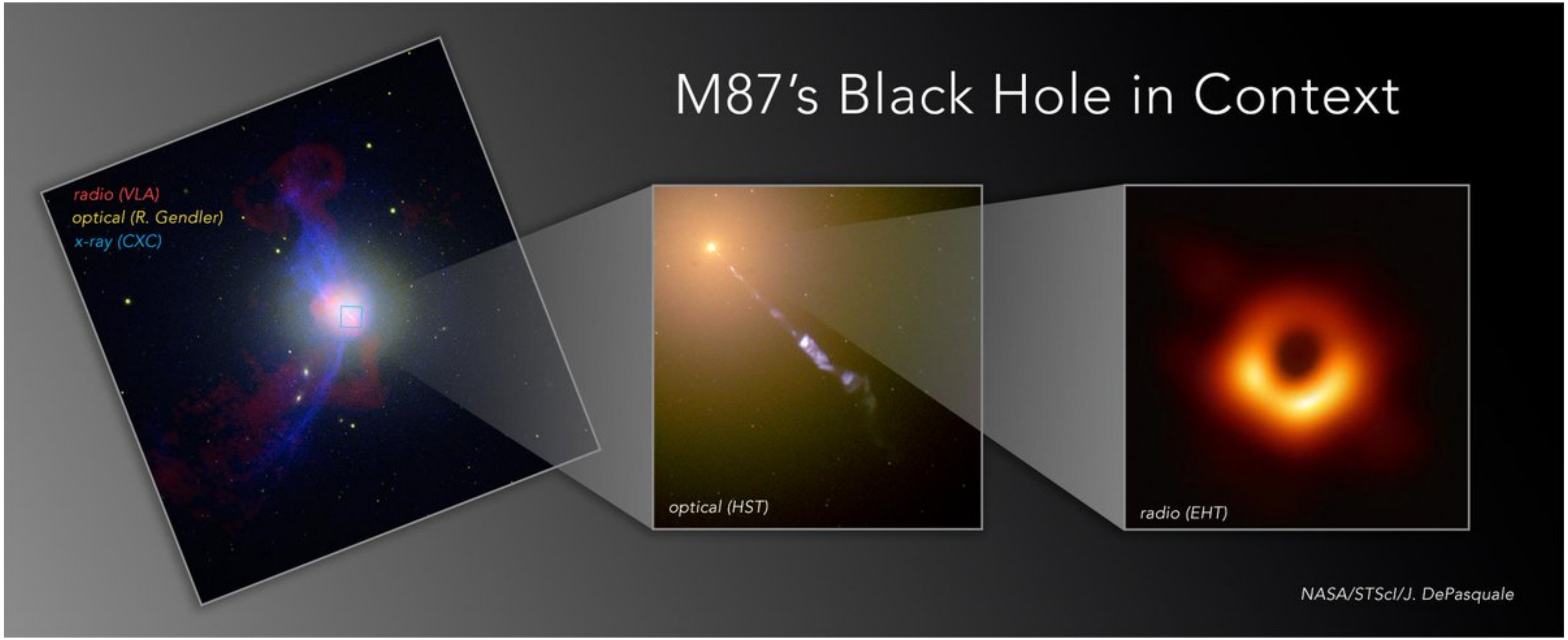
M87's Black Hole in Context
radio (VLA)
optical (R. Gendler)
x-ray (CXC)
optical (HST)
radio (EHT)
NASA/STScI/J. DePasquale

M87 scales…

radio “bubbles”

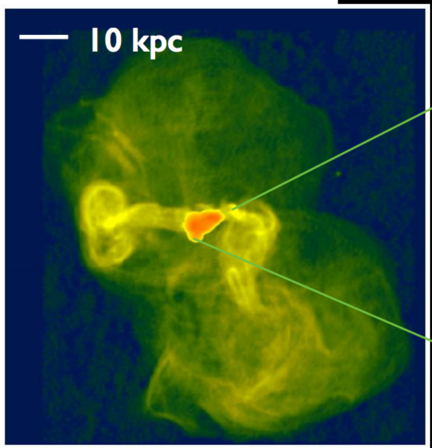

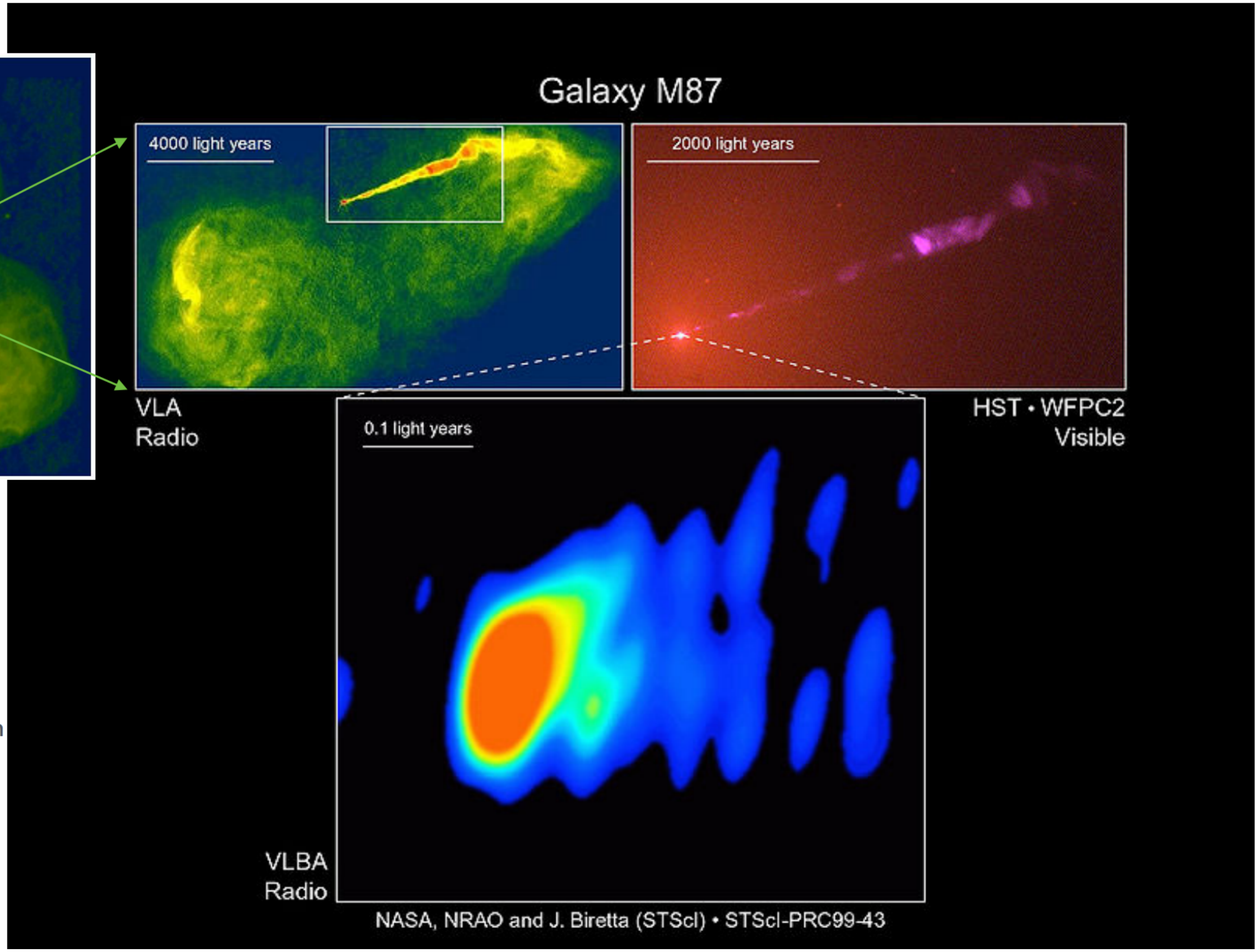

M87:

FR I radio galaxy

d~16 Mpc

$M_{BH}=(3\text{-}6)\times10^9\ M_{sun}$

M87 scales…

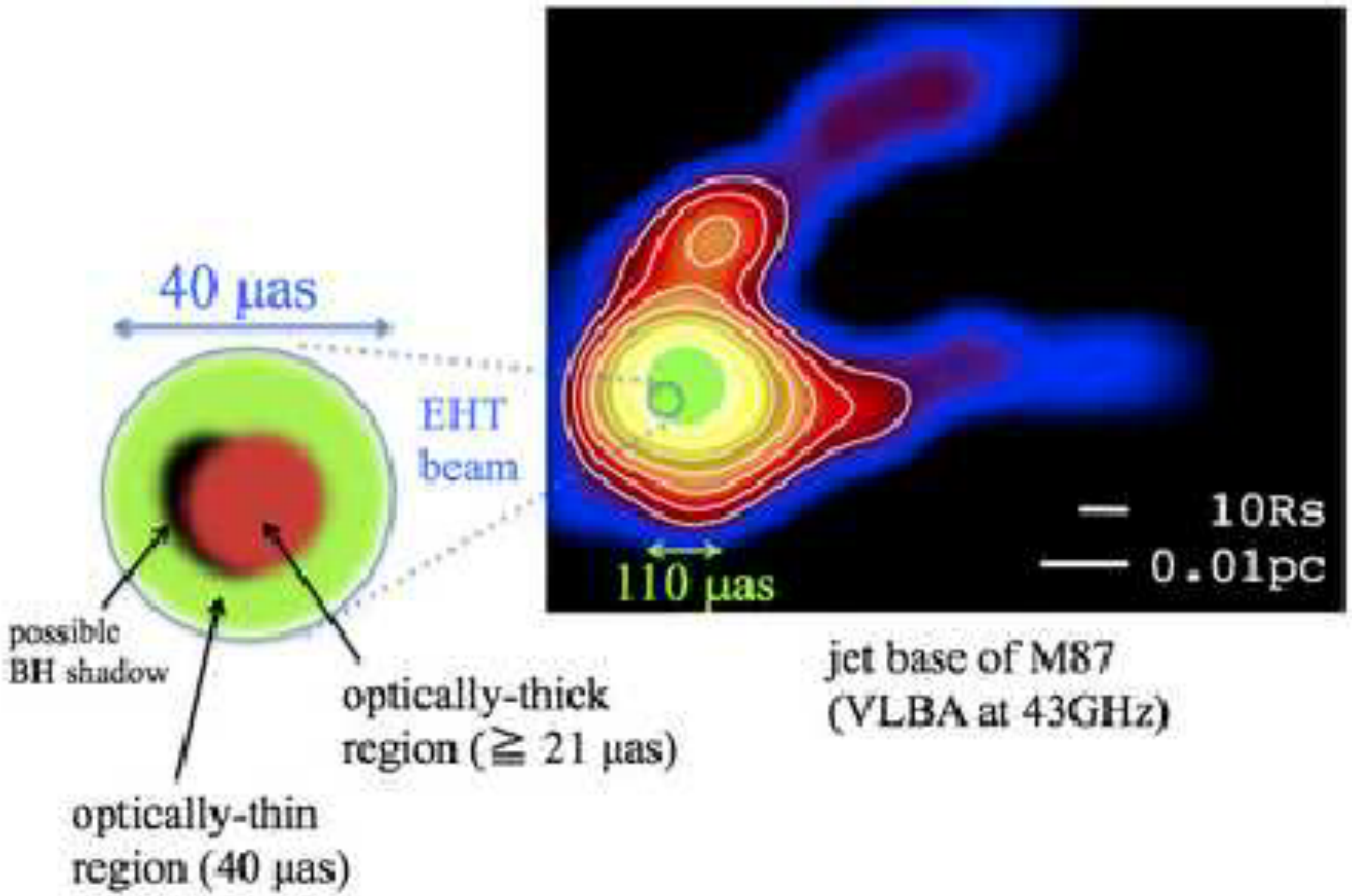

40 μas
EHT
beam
possible
BH shadow
optically-thin
region (40 μas)
optically-thick
region (≧ 21 μas)
10Rs
0.01pc
110 μas
jet base of M87
(VLBA at 43GHz)

AGN and the Extragalactic Background Light (EBL)

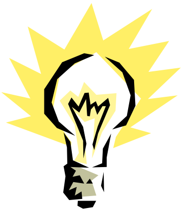

Look for roll-offs in blazar spectra due to attenuation:

(Stecker, De Jager & Salamon; Madau & Phinney; Macminn & Primack)

the start: A.I. Nikishov, Sov. Phys. JETP 14 (1962) 393.

If $\gamma\gamma$ c.m. energy > $2m_e$, pair creation will attenuate flux. For a flux of γ -rays with energy, E, this cross-section is maximized when the partner, ε, is

$$\epsilon \sim \frac{1}{3}\left(\frac{1TeV}{E}\right)eV$$

For 10 GeV- 100 GeV γ - rays, this corresponds to a partner photon energy in the optical - UV range. Density is sensitive to time of galaxy formation.

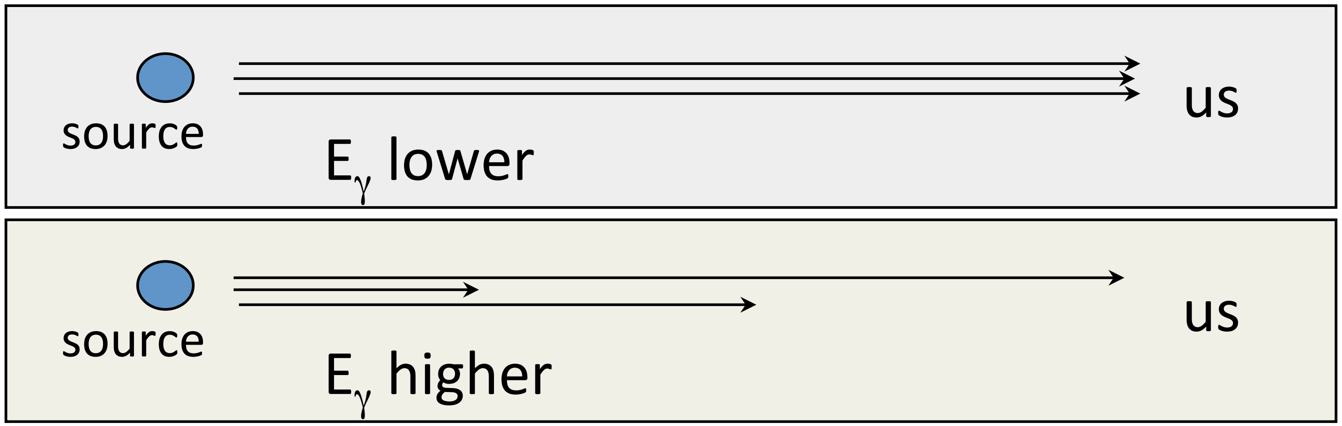

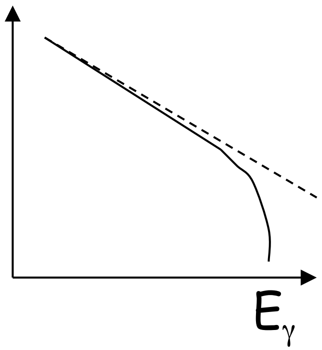

Challenge # 2

- Need more exposure and optimal timing (and radio monitoring) to discover more gamma-ray PSRs.

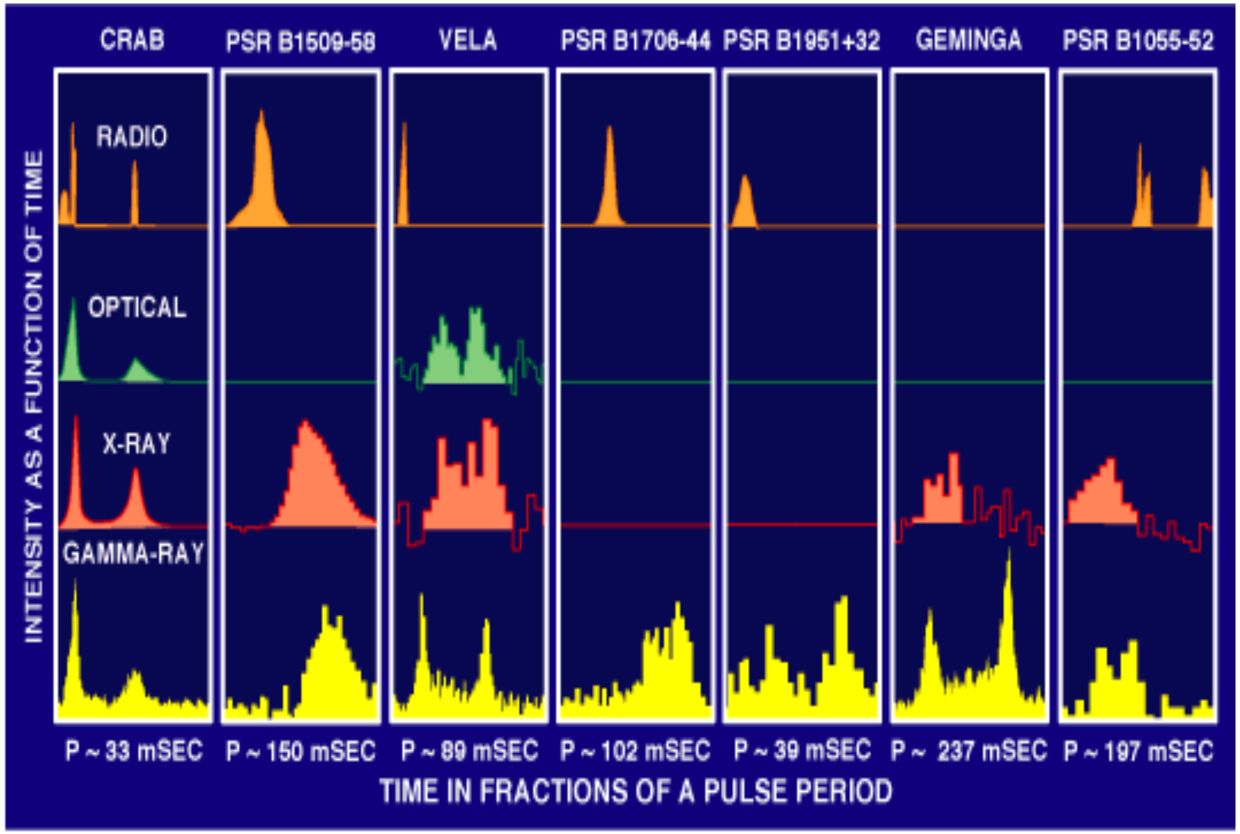

Pulsars

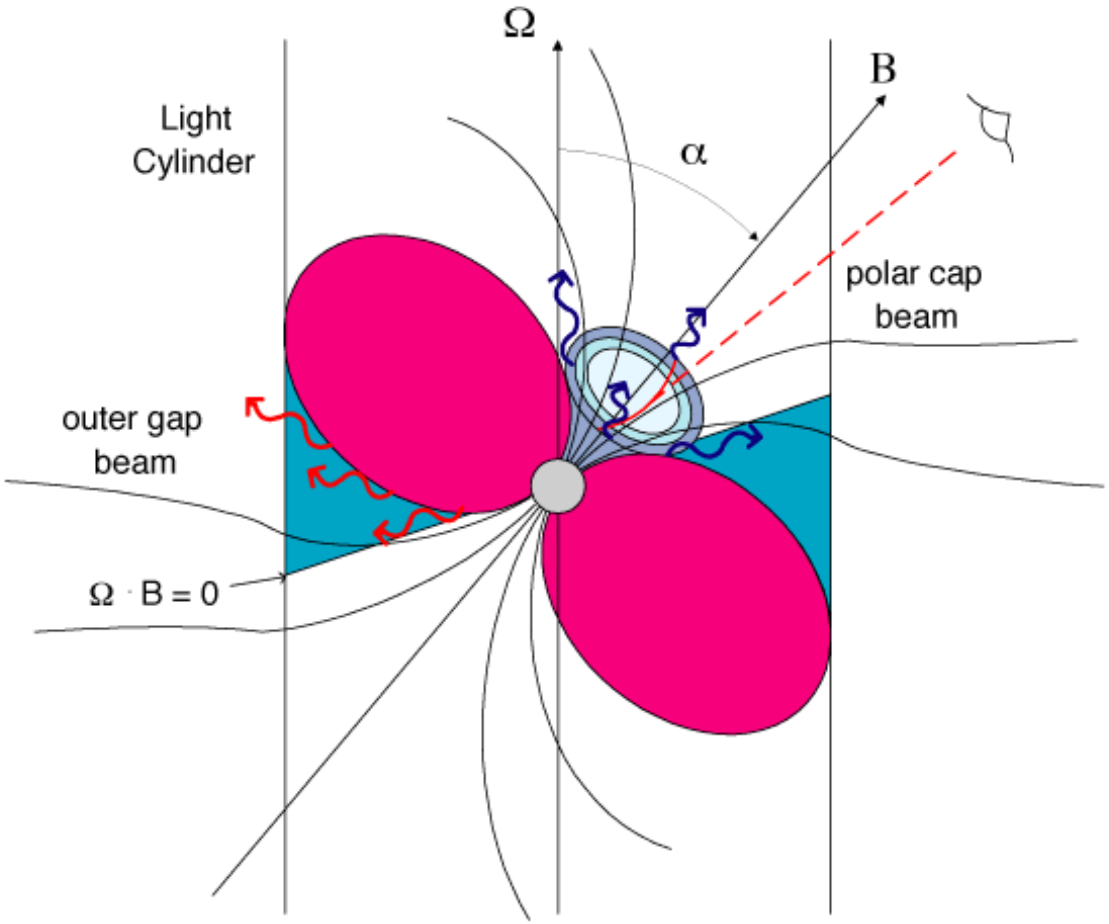

Challenge # 3

- Need fast timing for gamma-ray detection (improving EGRET deadtime, 100 msec → 100 microsec or less).

Prompt Emission (GRB 930131)

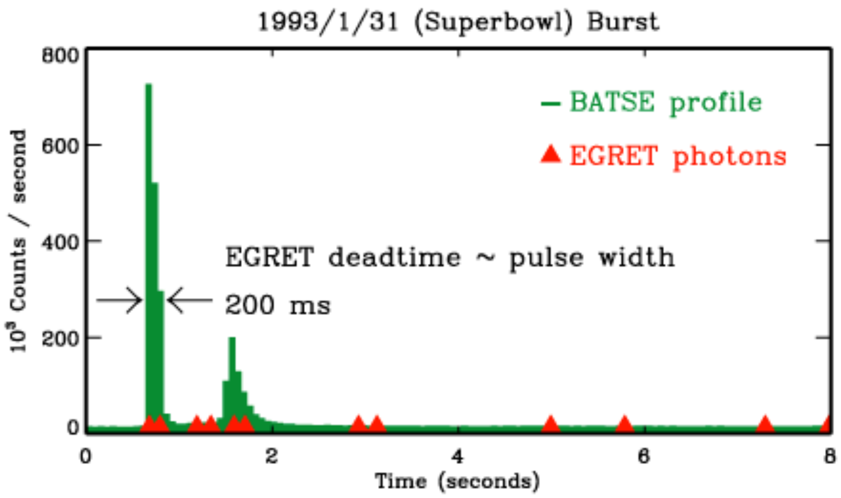

Delayed Emission (GRB 940217)

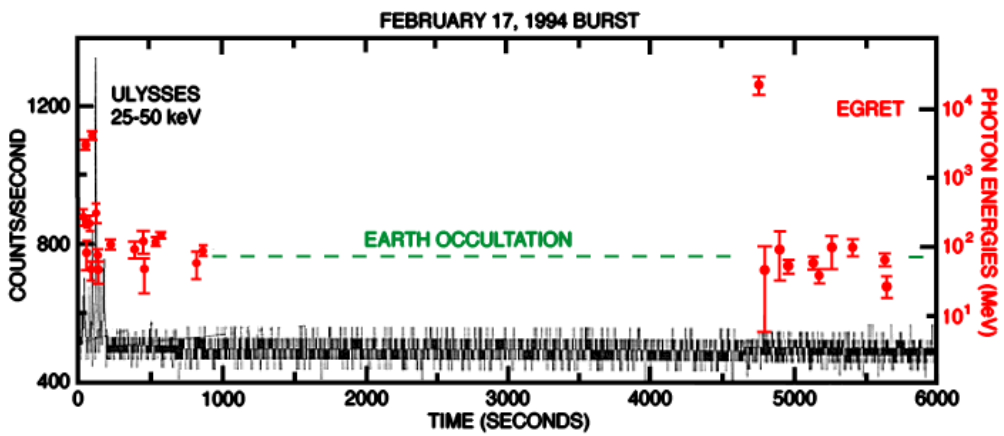

Solar flares

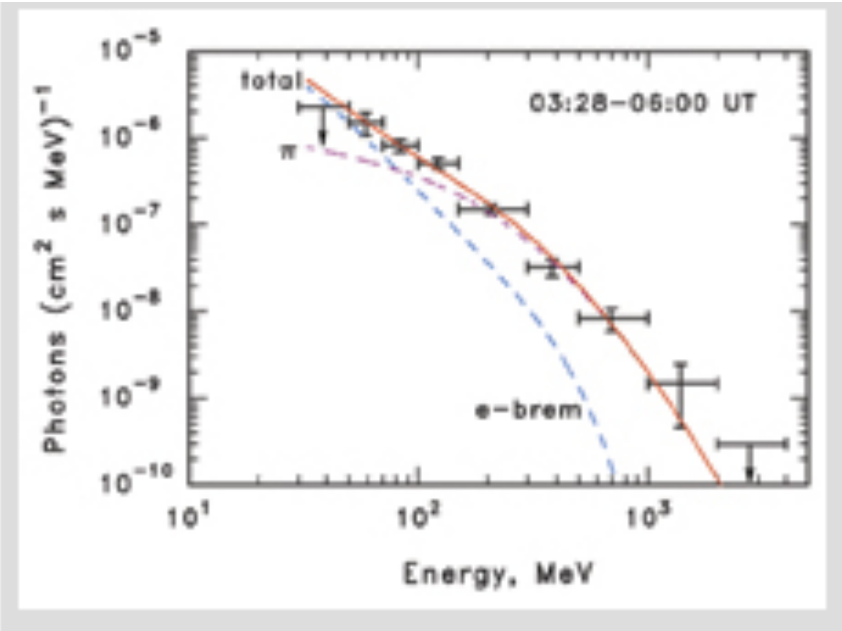

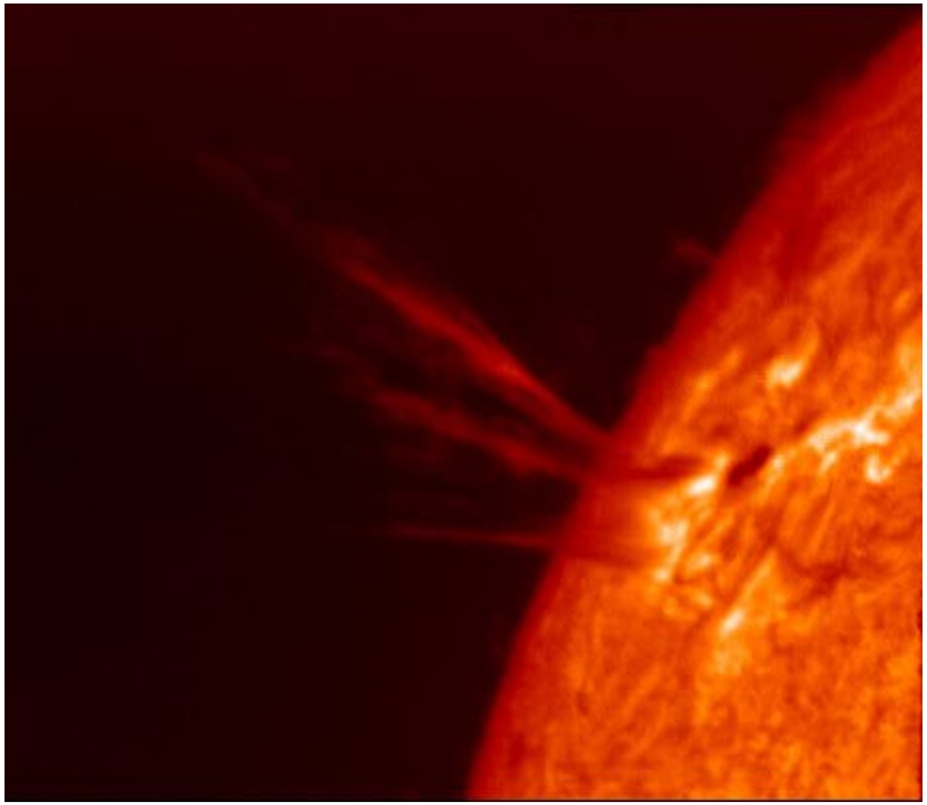

Solar Flares

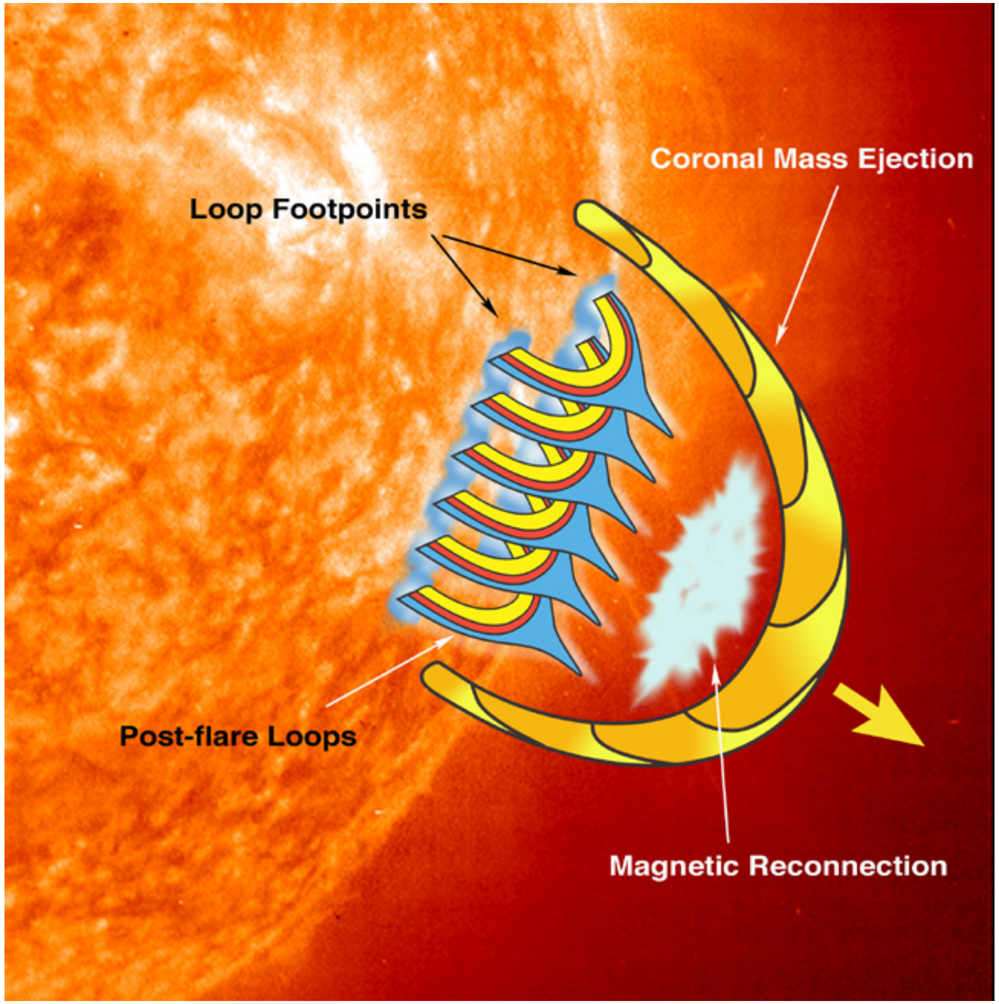

Challenge # 4

- Need arcminute positioning of gamma-ray sources (improving EGRET error box radii by a factor of 2-10).

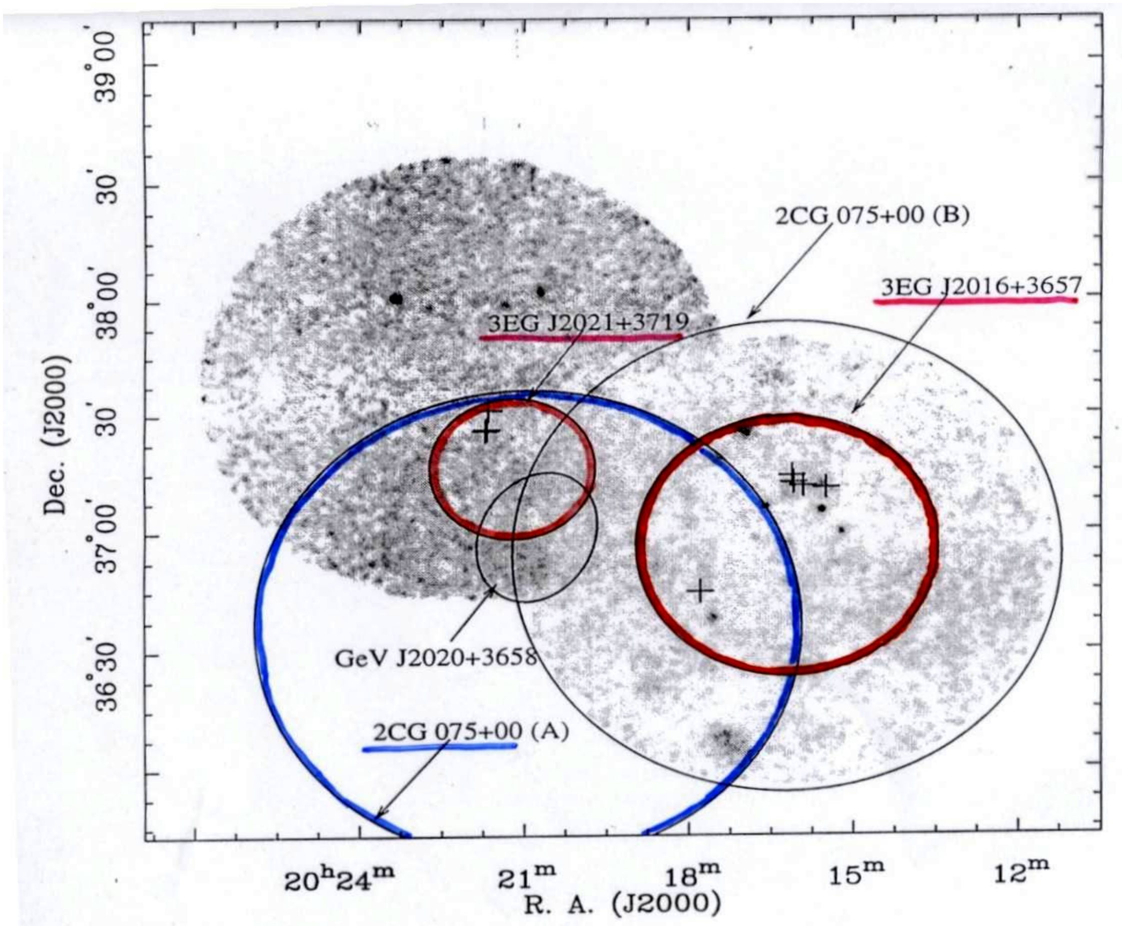

Supernova Remnants

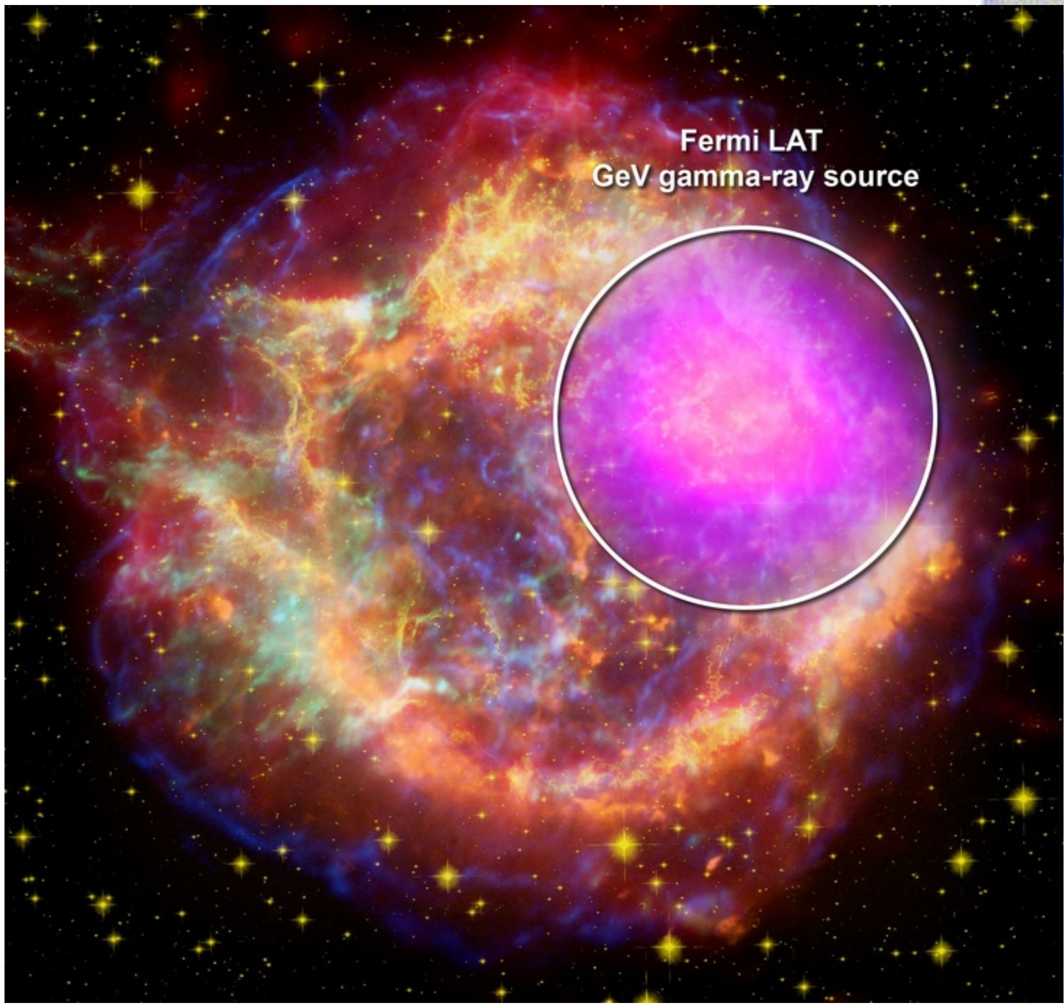

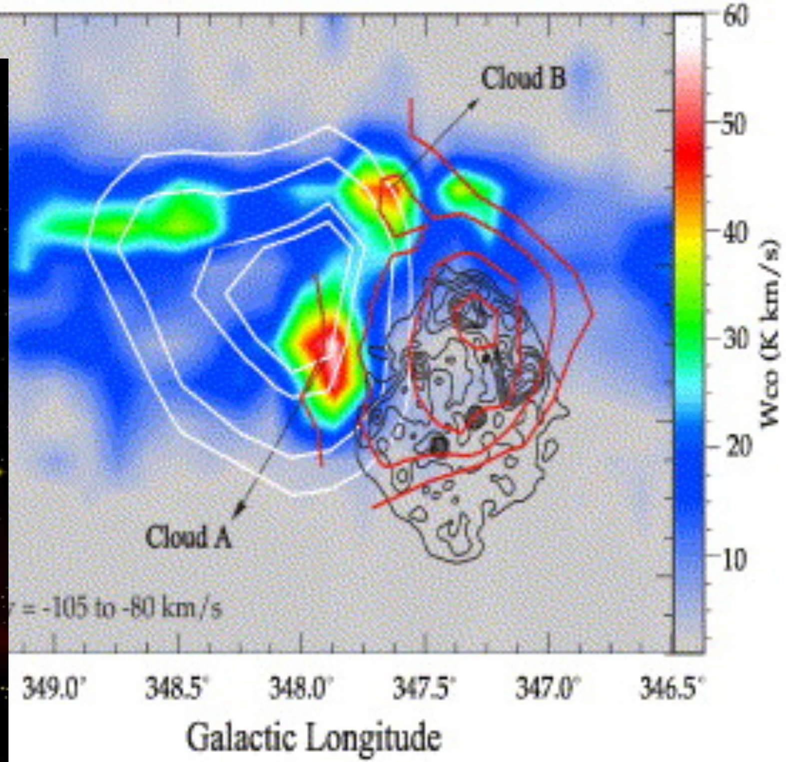

SNR

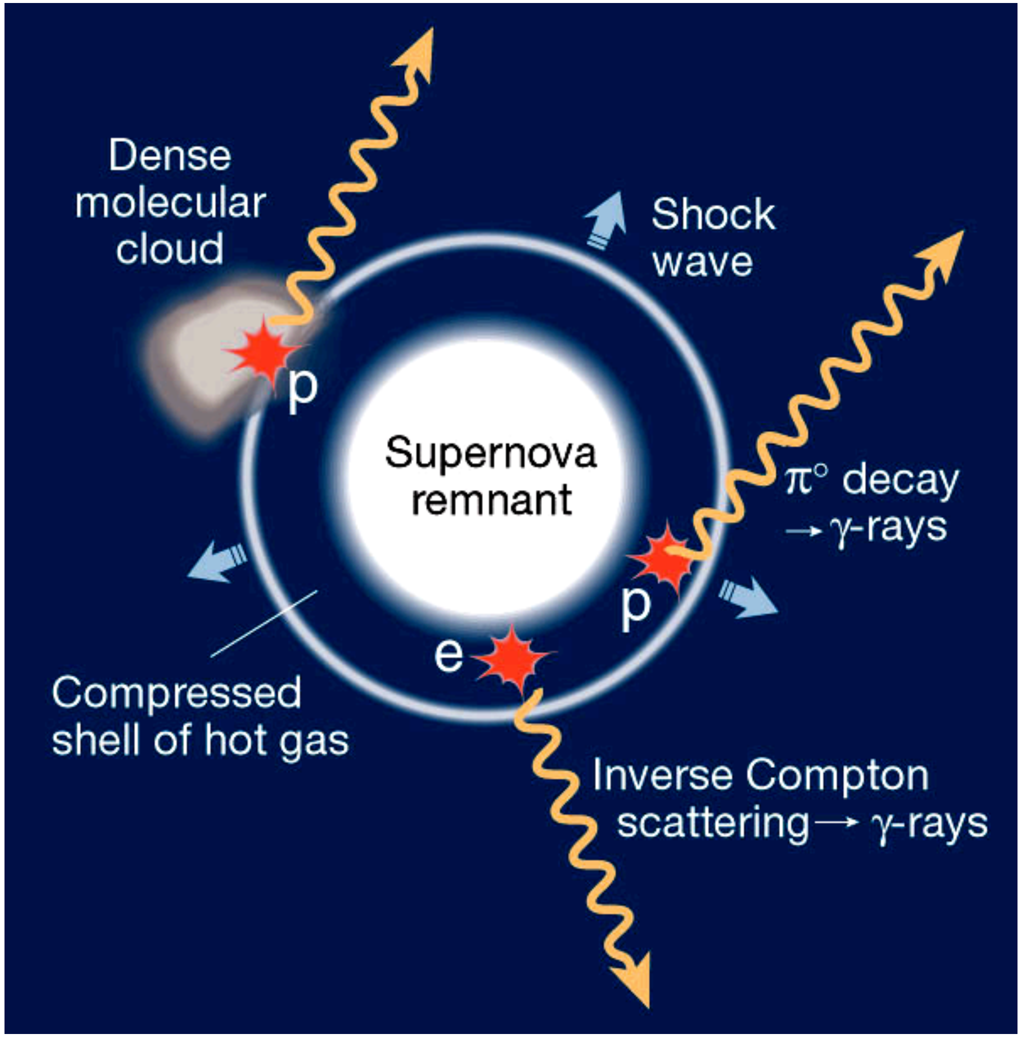
Dense
molecular
cloud
Shock
wave
p
Supernova
remnant
π° decay
→ γ-rays
p
e
Compressed
shell of hot gas
Inverse Compton
scattering → γ-rays

Challenge # 5

- Need improvements in Spectral Resolution fo check for DM signals

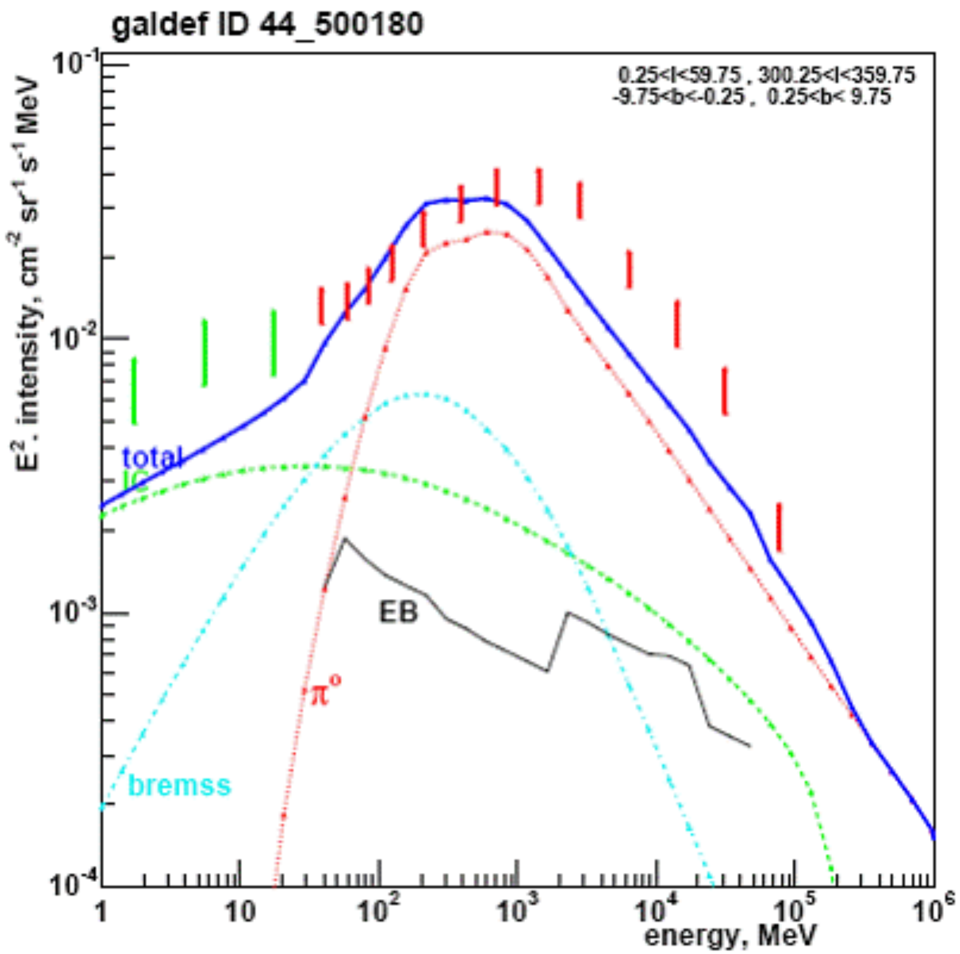

Dark Matter

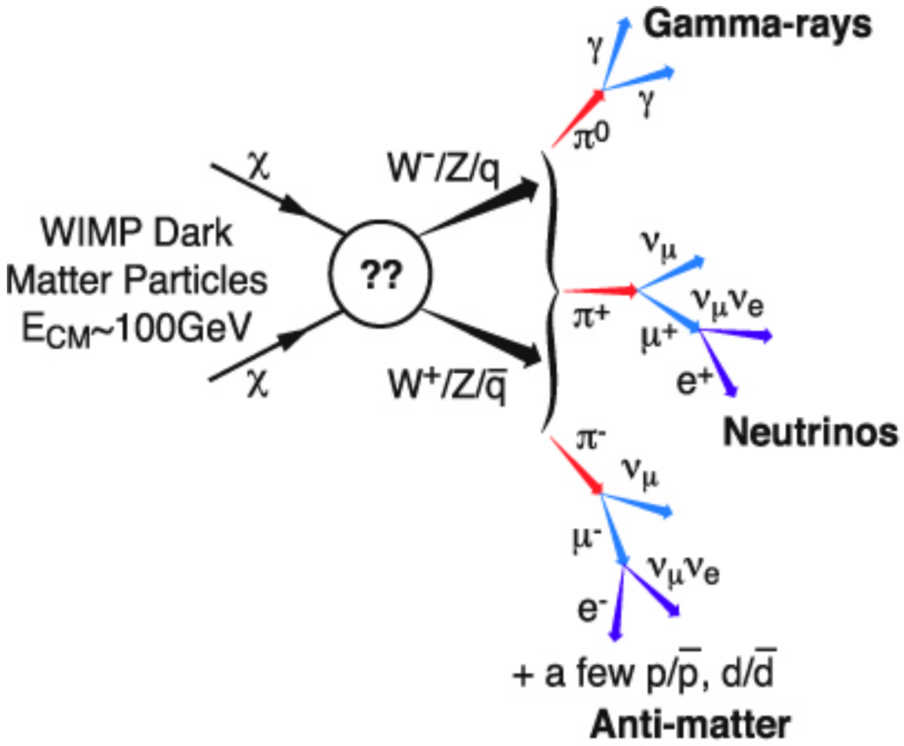
Gamma-rays
γ
γ
π0
χ
W-/Z/q
WIMP Dark
Matter Particles
ECM~100GeV
??
χ
W+/Z/q̄
νμ
π+
νμνe
μ+
e+
Neutrinos
π-
νμ
μ-
νμνe
e-
+ a few p/p̄, d/d̄
Anti-matter

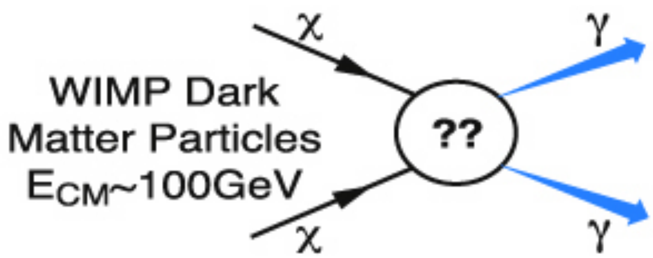
χ
γ
WIMP Dark
Matter Particles
ECM~100GeV
??
χ
γ

Detector Project

- Instrument must measure the direction, energy, and arrival time of high energy photons (from approximately 20 MeV to greater than 300 GeV):

- photon interactions with matter in GLAST energy range dominated by pair conversion:
  determine photon direction
  clear signature for background rejection

- limitations on angular resolution (PSF)
  low E: multiple scattering => many thin layers
  high E: hit precision & lever arm

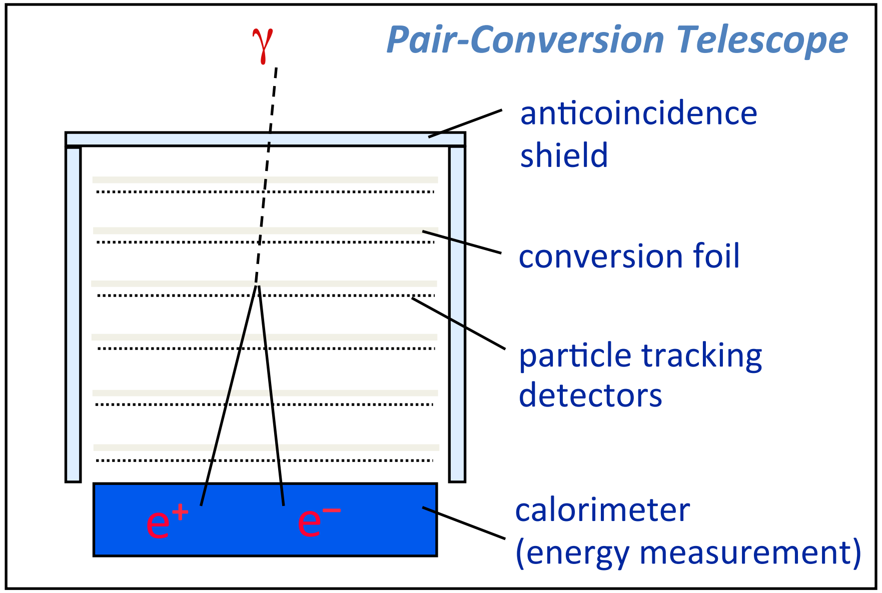

Energy loss mechanisms:

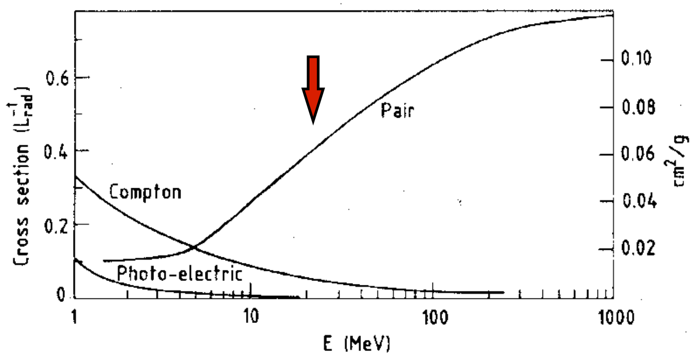

Fig. 2: Photon cross-section σ in lead as a function of photon energy. The intensity of photons can be expressed as $I = I_0 \exp(-\sigma x)$, where x is the path length in radiation lengths. (Review of Particle Properties, April 1980 edition).

- must detect γ-rays with high efficiency and reject the much larger (~10^4:1) flux of background cosmic-rays, etc.;
- energy resolution requires calorimeter of sufficient depth to measure buildup of the EM shower. Segmentation useful for resolution and background rejection.

Detector Project

The LAT design is based on detailed Monte Carlo simulations.
Integral part of the project from the start.

- **Background rejection**
- **Calculate effective area and resolutions (computer models now verified by beam tests). Current reconstruction algorithms are existence proofs -- many further improvements under development.**
- **Trigger design.**
- **Overall design optimization.**

Simulations and analyses are all C++, based on standard HEP packages.

Detailed detector model includes gaps, support material, thermal blanket, simple spacecraft, noise, sensor responses…

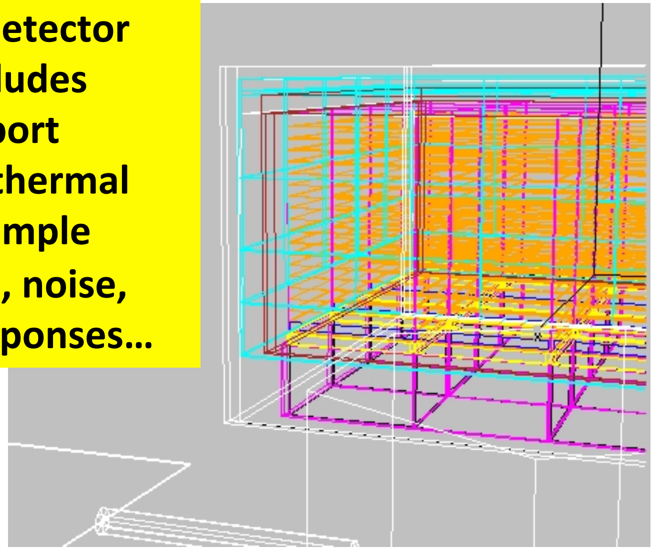

Instrument naturally distinguishes gammas from backgrounds, but details matter.

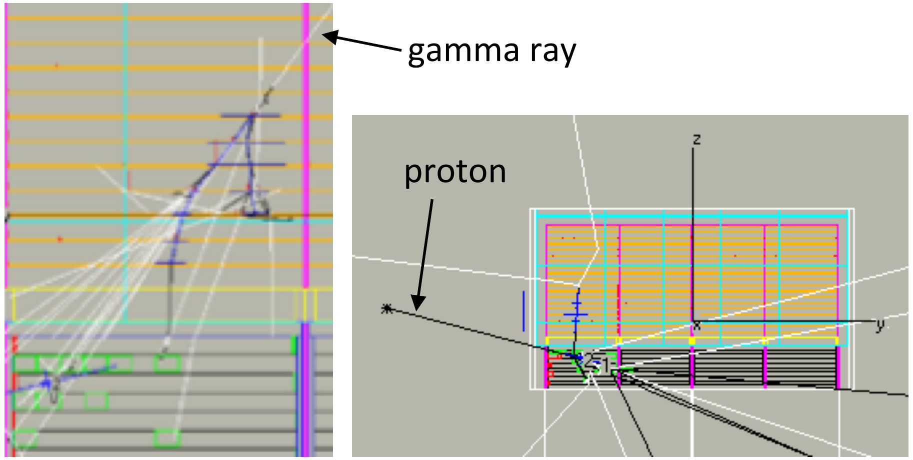

Beam test

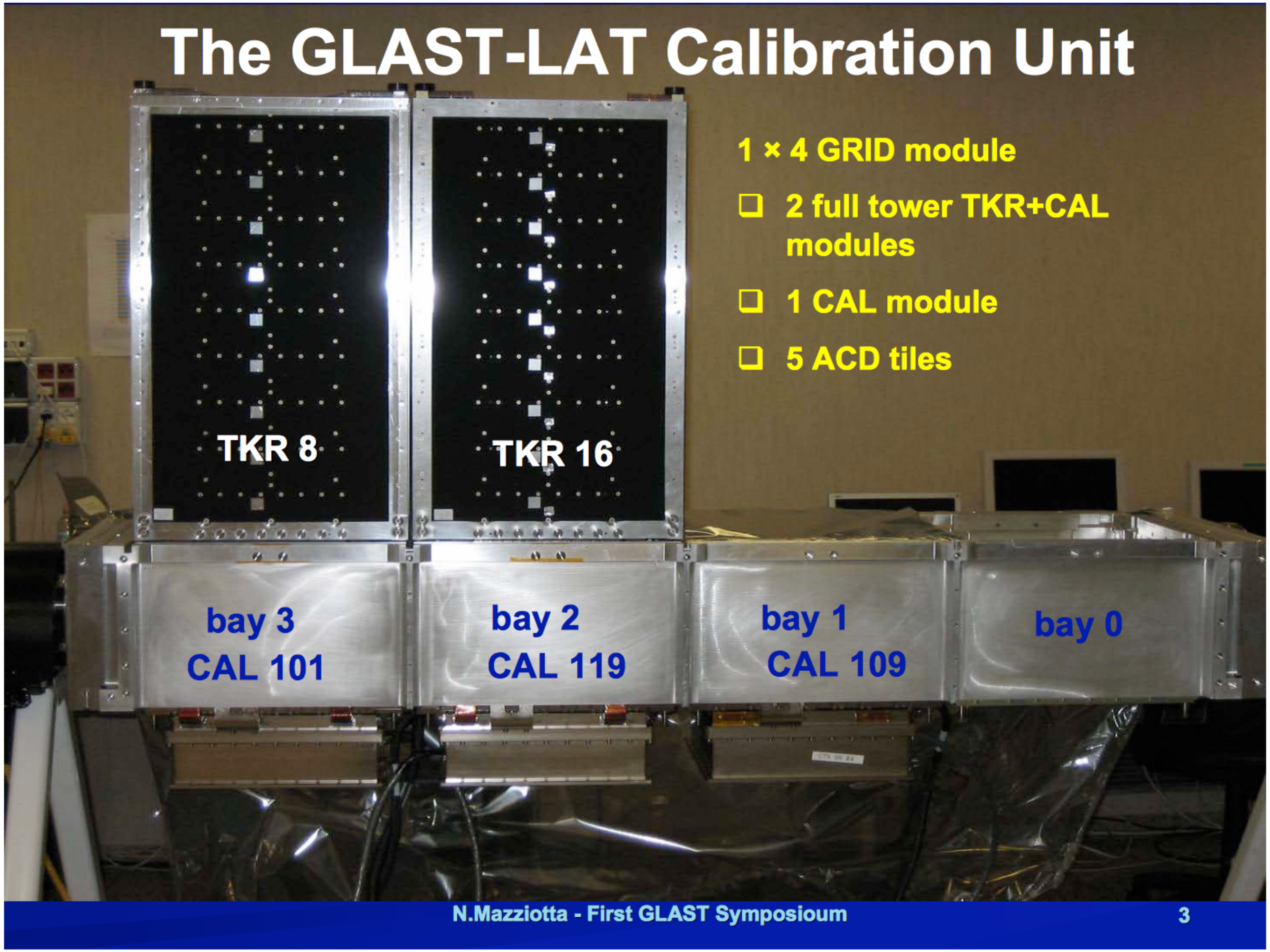

The GLAST-LAT Calibration Unit
1 × 4 GRID module
2 full tower TKR+CAL modules
1 CAL module
5 ACD tiles
TKR 8
TKR 16
bay 3
CAL 101
bay 2
CAL 119
bay 1
CAL 109
bay 0
N.Mazziotta - First GLAST Symposioum
3

Beam test

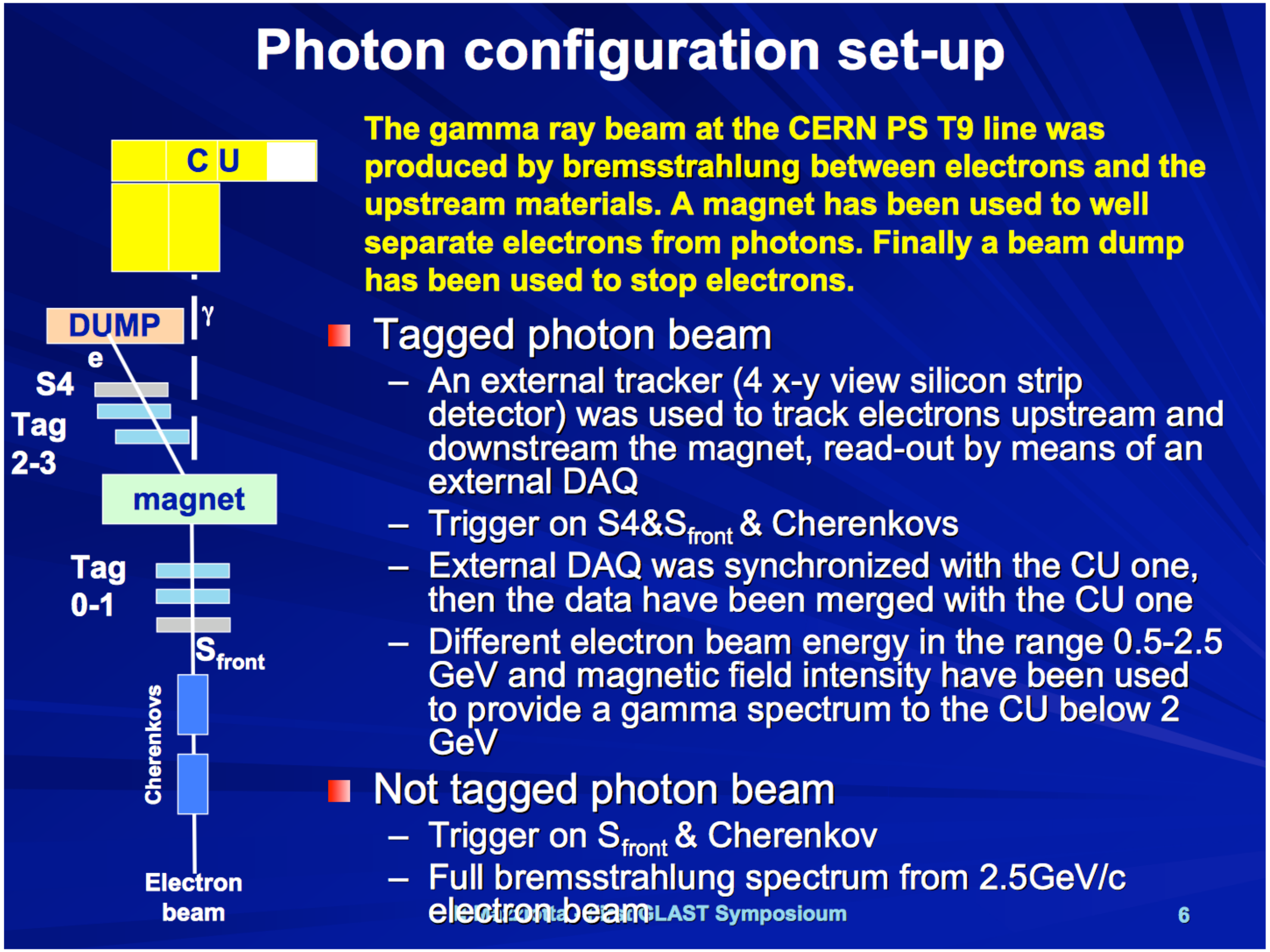
Photon configuration set-up
CU
DUMP
γ
e
S4
Tag 2-3
magnet
Tag 0-1
S_{front}
Cherenkovs
Electron beam
The gamma ray beam at the CERN PS T9 line was produced by bremsstrahlung between electrons and the upstream materials. A magnet has been used to well separate electrons from photons. Finally a beam dump has been used to stop electrons.
Tagged photon beam
– An external tracker (4 x-y view silicon strip detector) was used to track electrons upstream and downstream the magnet, read-out by means of an external DAQ
– Trigger on S4&S_{front} & Cherenkovs
– External DAQ was synchronized with the CU one, then the data have been merged with the CU one
– Different electron beam energy in the range 0.5-2.5 GeV and magnetic field intensity have been used to provide a gamma spectrum to the CU below 2 GeV
Not tagged photon beam
– Trigger on S_{front} & Cherenkov
– Full bremsstrahlung spectrum from 2.5GeV/c electron beam
GLAST Symposioum
6

Technology impact -- PSF

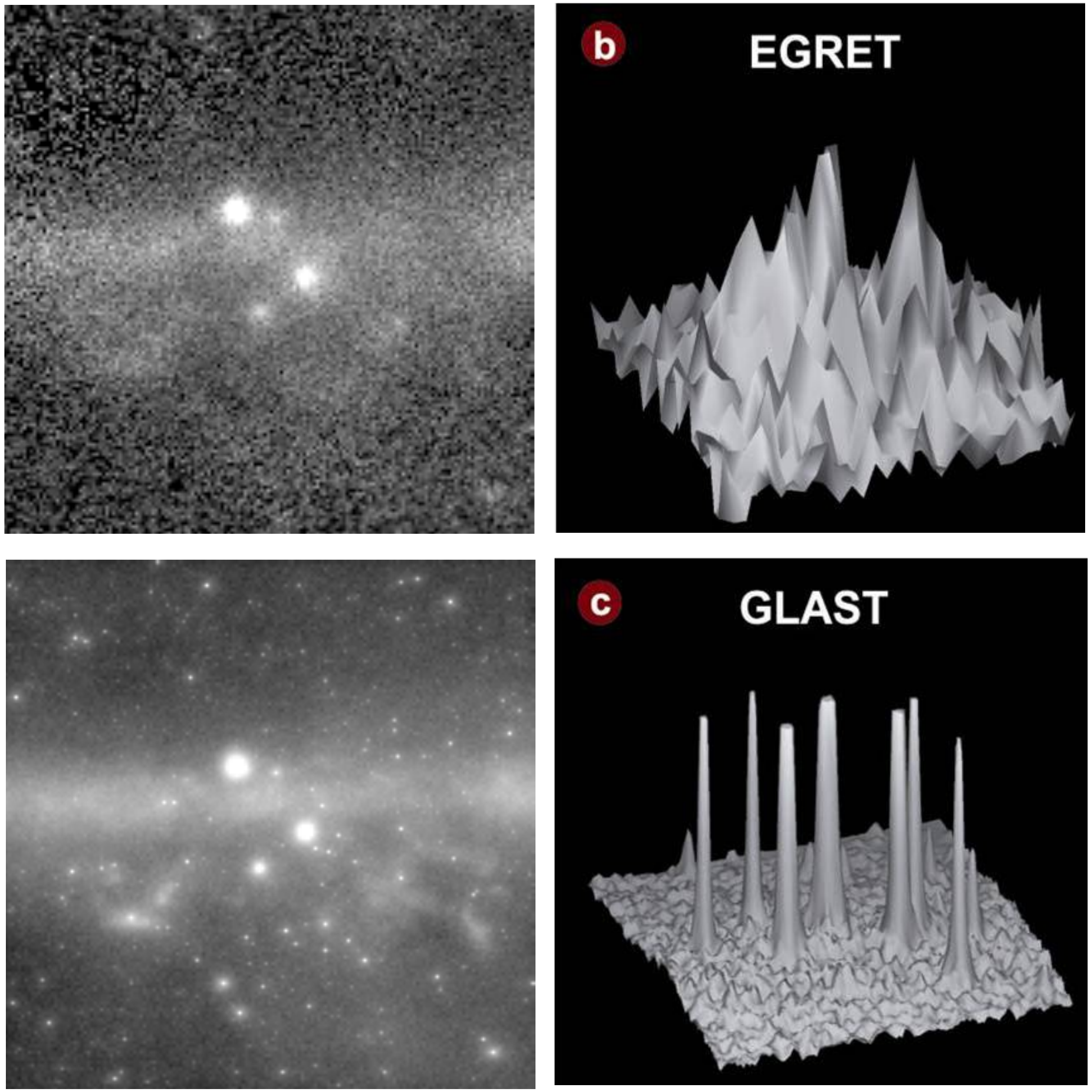

Cygnus region (15^0 x 15^0), $E\gamma$ > 1 GeV

EGRET
(1991-2000)
Phases 1-5

Spark chamber
- **sense electrode spacing ~mm**
- **sensitive layer depth ~cm**
  - ***up to 28 hit over >1m***

LAT
(2008- >2013)
1-yr simulation

Si-strip detectors
- **sense electrode spacing ~0.2mm**
  - ***better single hit resolution***
- **sensitive layer depth ~0.4mm**
  - ***up to 36 hit over 0.8m***
  - ***converter proximity to minimize MCS***

Technology impact - FoV

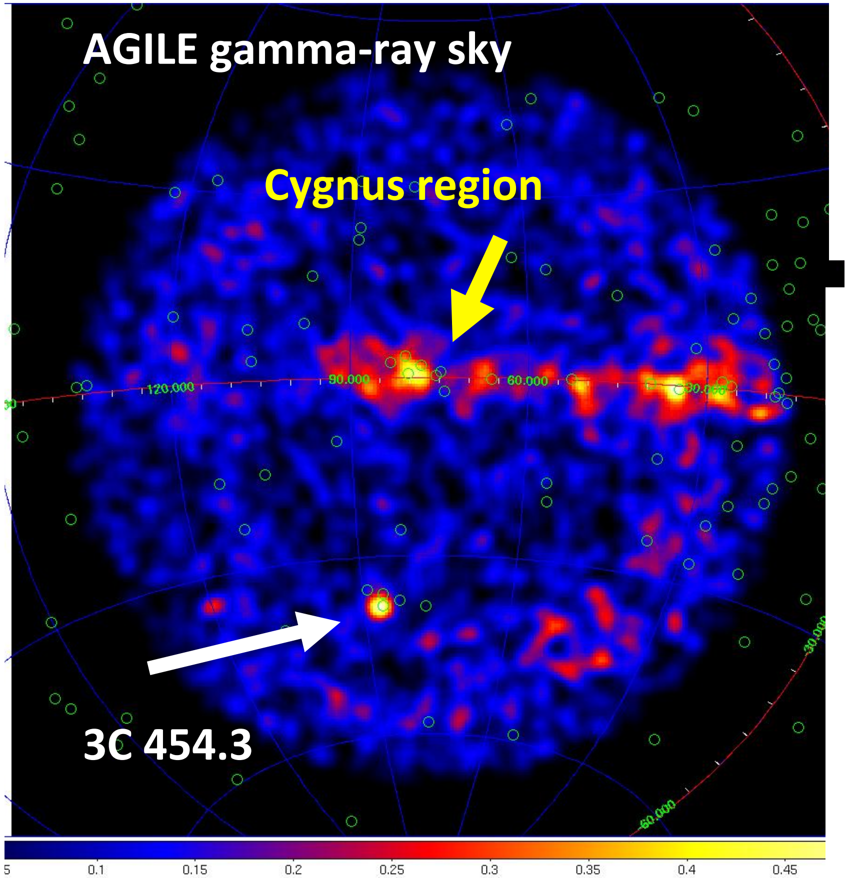

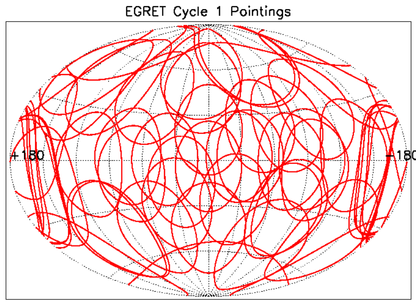

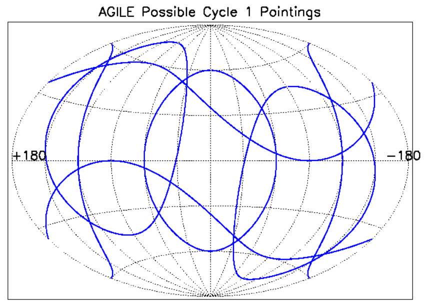

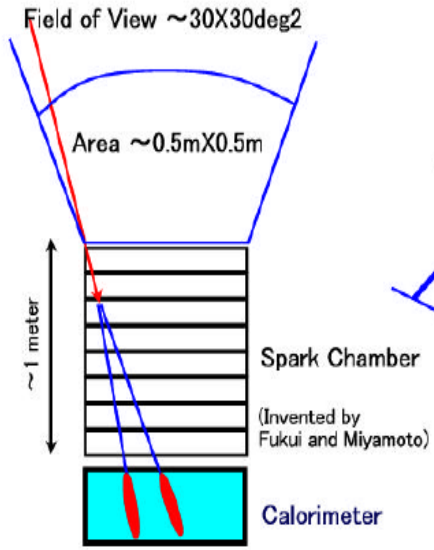

EGRET on Compton GRO

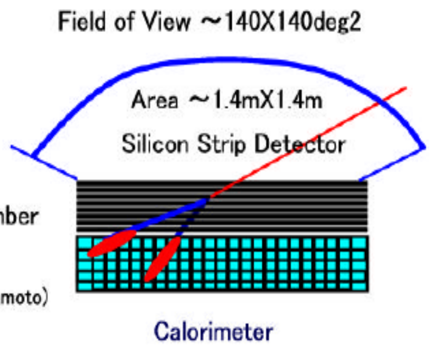

GLAST Large Area Telescope

AGILE

AGILE

agenzia spaziale italiana

INAF

INFN

CARLO GAVAZZI
Carlo Gavazzi Space SpA

OERLIKON CONTRAVES

ALCATEL ALENIA SPACE
An Alcatel/Finmeccanica company

telespazio
A Finmeccanica/Alcatel company

Galileo Avionica

MIPOT

ENEA

AGILE instrument

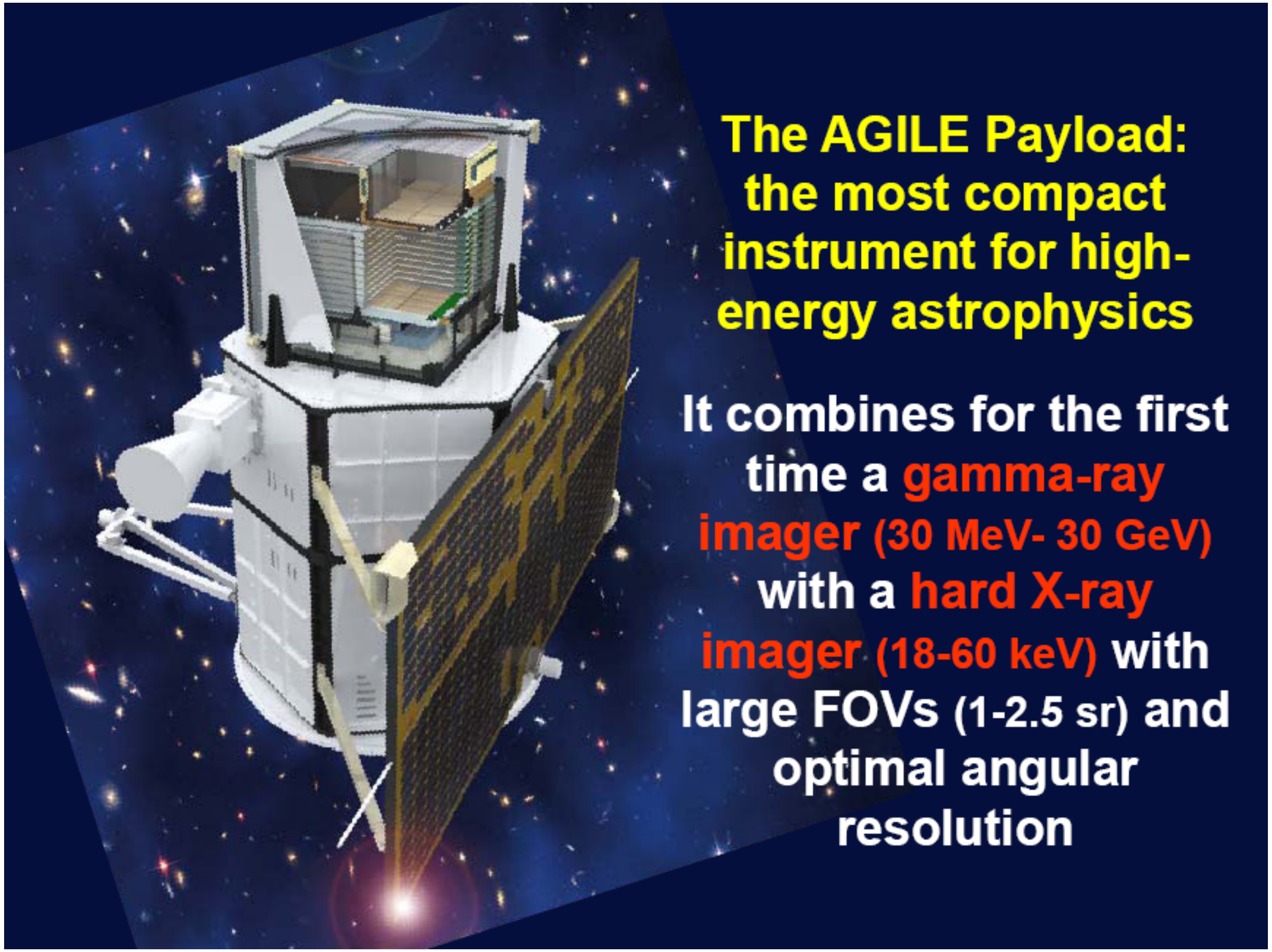


AGILE: inside the cube…
HARD X-RAY IMAGER
(SUPER-AGILE)
INAF-IASF-Rm (E.Costa, M. Feroci)
GAMMA-RAY IMAGER
SILICON TRACKER
INFN-Trieste
(G.Barbiellini, M. Prest)
ANTICOINCIDENCE
INAF-IASF-Mi (F.Perotti)
(MINI) CALORIMETER
INAF-IASF-Bo, Thales-Alenia Space (LABEN)
(G. Di Cocco, C. Labanti)

The Silicon Tracker

The AGILE silicon detectors

Detector specifications:

- dimension: 9.5x9.5 cm^2
- thickness: 410 μm (6 inch technology)
- readout pitch: 242 μm;
  physical pitch: 121 μm (one floating strip)
- number of strips/ladder: 384
- Single side and AC-coupled
- leakage current: 2 nA/cm^2 at Vbias=2.5*V_{FD} =200 V
- polarization resistor: 40 MΩ
- coupling capacitor: 55 pF/cm
- Al strip resistance: 4.3 Ω/cm
- max number of bad strips: <1%
- average number of bad strips: <0.5%

The AGILE frontend chip: TA1 → TAA1

- low noise, low power, SELF-TRIGGERING
- technology: 1.2 μ CMOS, double poly, double metal (final: 0.8 μ BiCMOS on epitaxial layer)
- features:
  - 128 channels
  - gain: 25 mV/fC; range: 18 fC
  - noise (e^- rms): 165+6.1/pF for T_{peak}=2 μs
  - power: <0.4 mW/channel
  - power rails: ±2 V
  - readout frequency: 5 Mhz
  - gain spread: <1.5%
  - threshold offset spread (TA1): 20% (in TAA1 will be implemented a 3 bit DAC per channel)

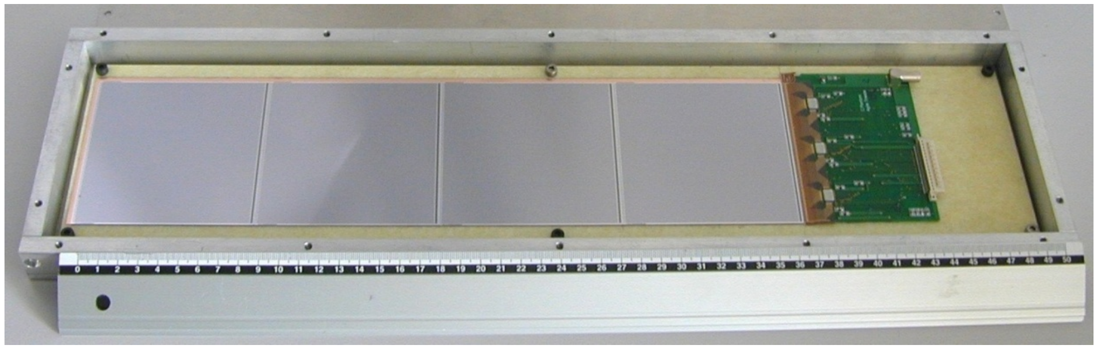

The AGILE TRK

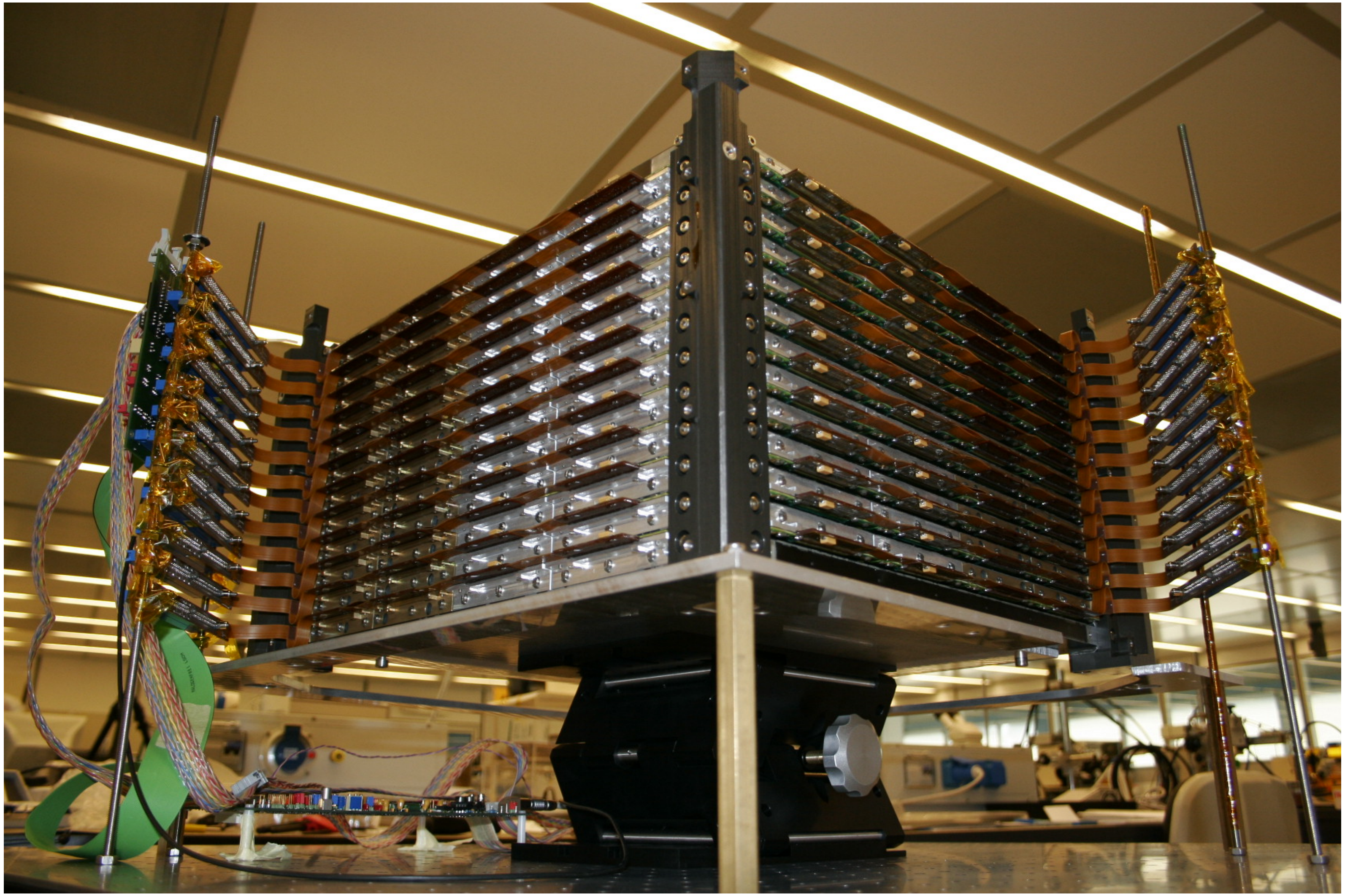

Performance

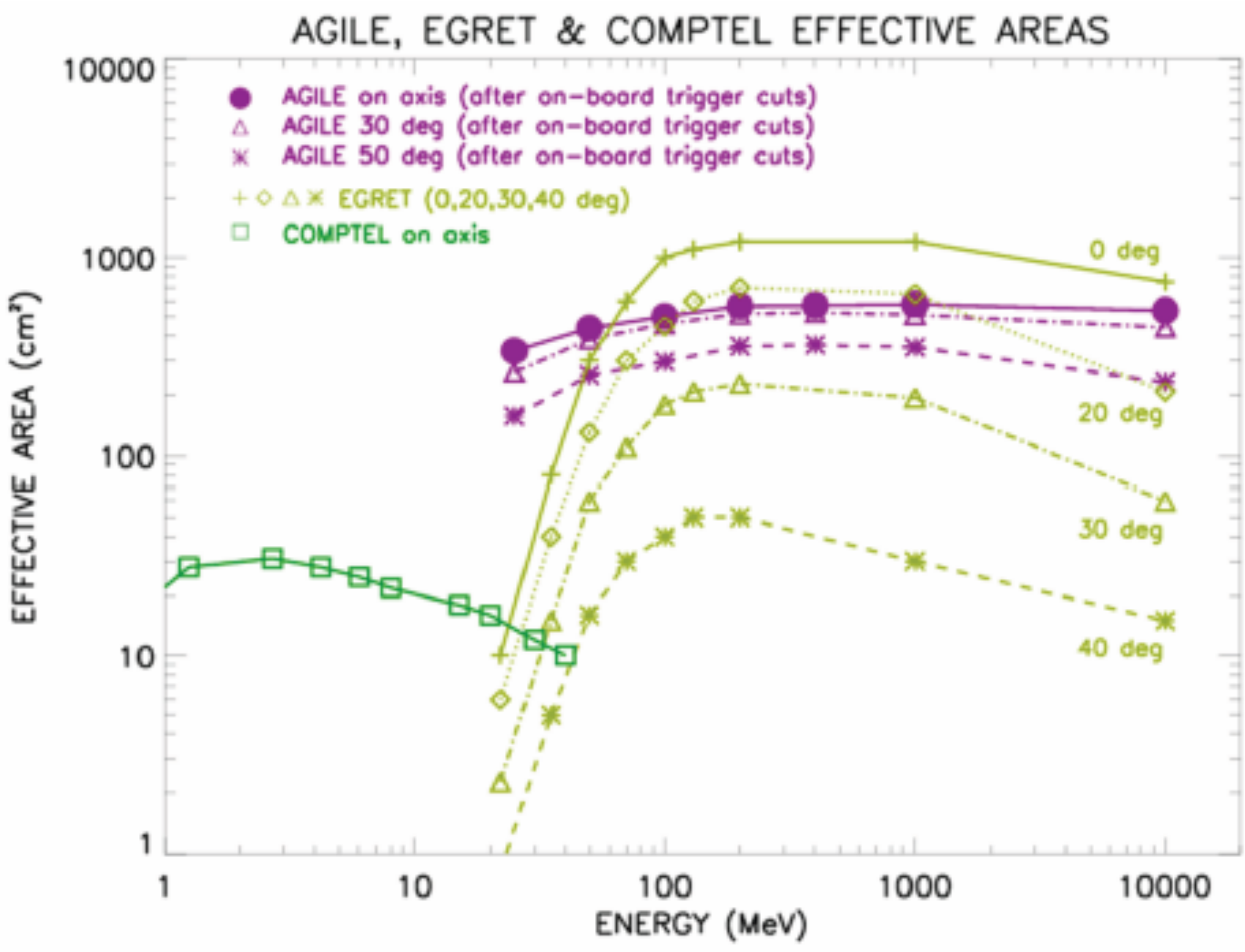

Si Self Trigger and FoV

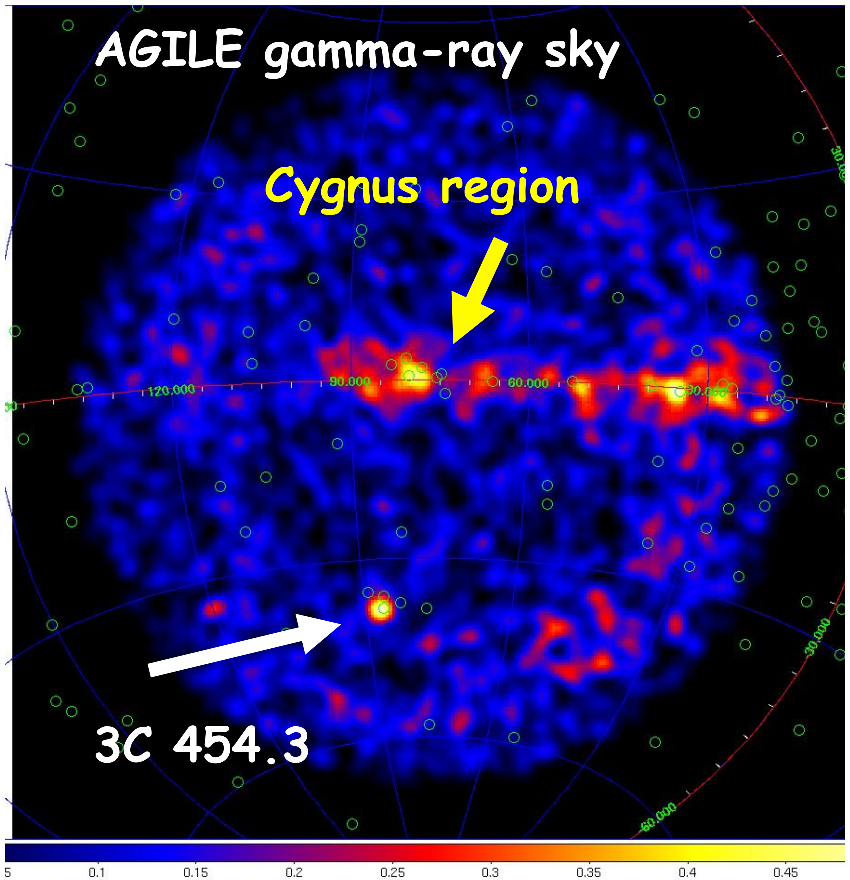

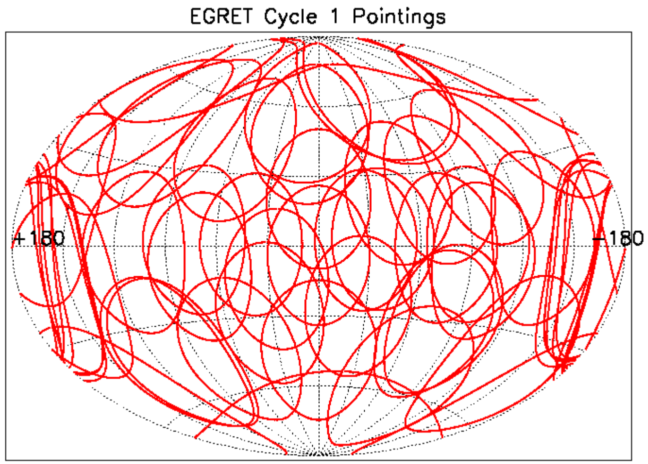

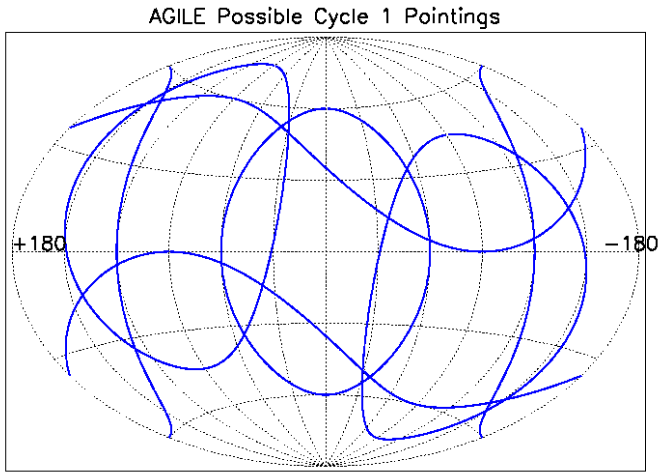

Analog readout and PSF

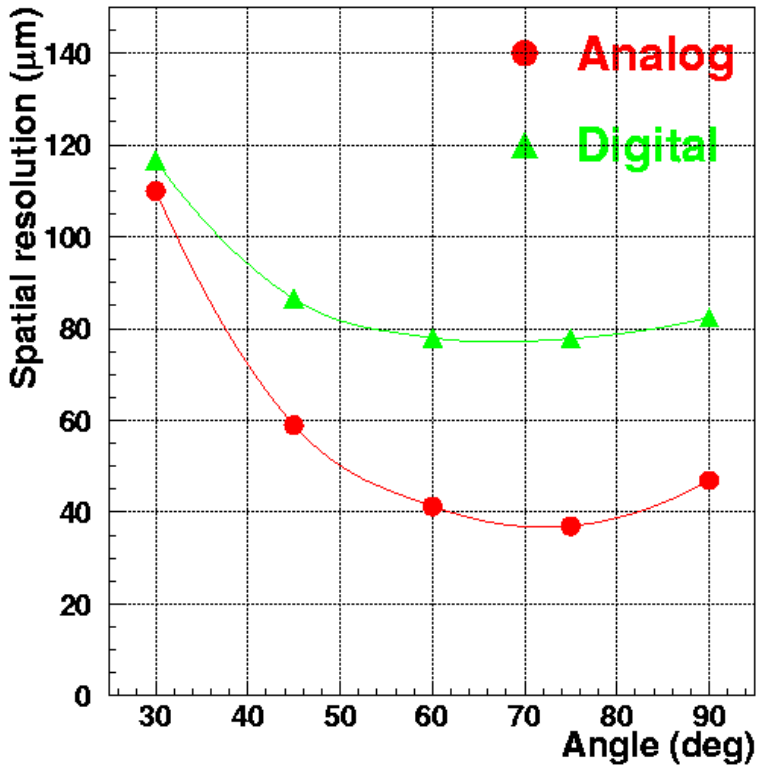

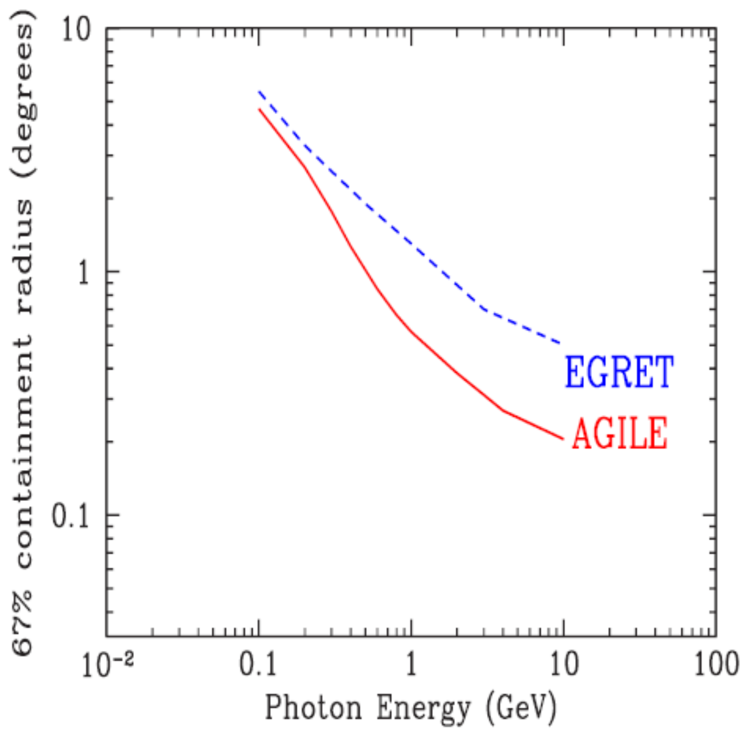

The AGILE launch

AGILE in orbit

First gamma-ray detected in orbit with the nominal GRID trigger configuration (May 10, 2007)

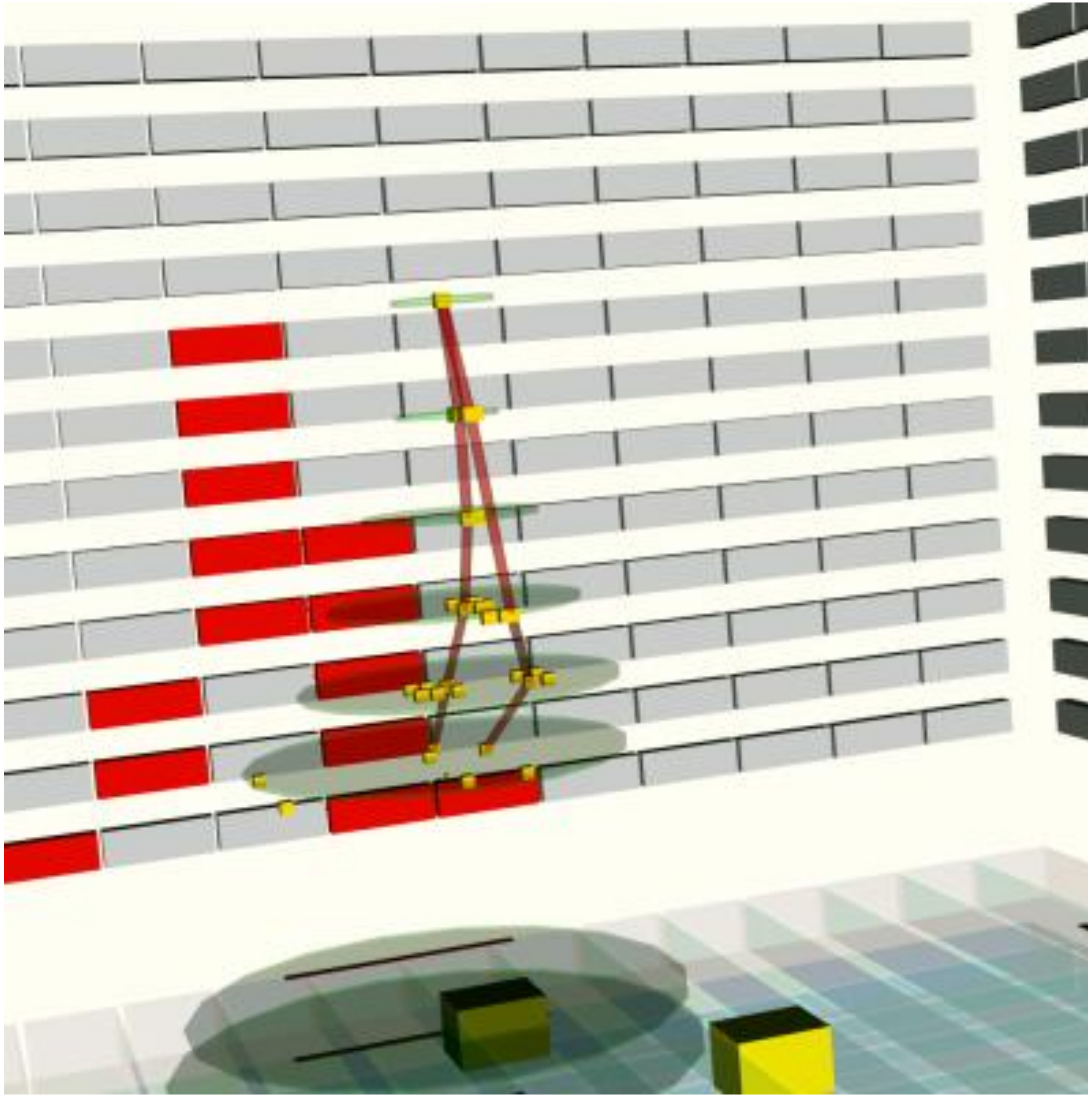

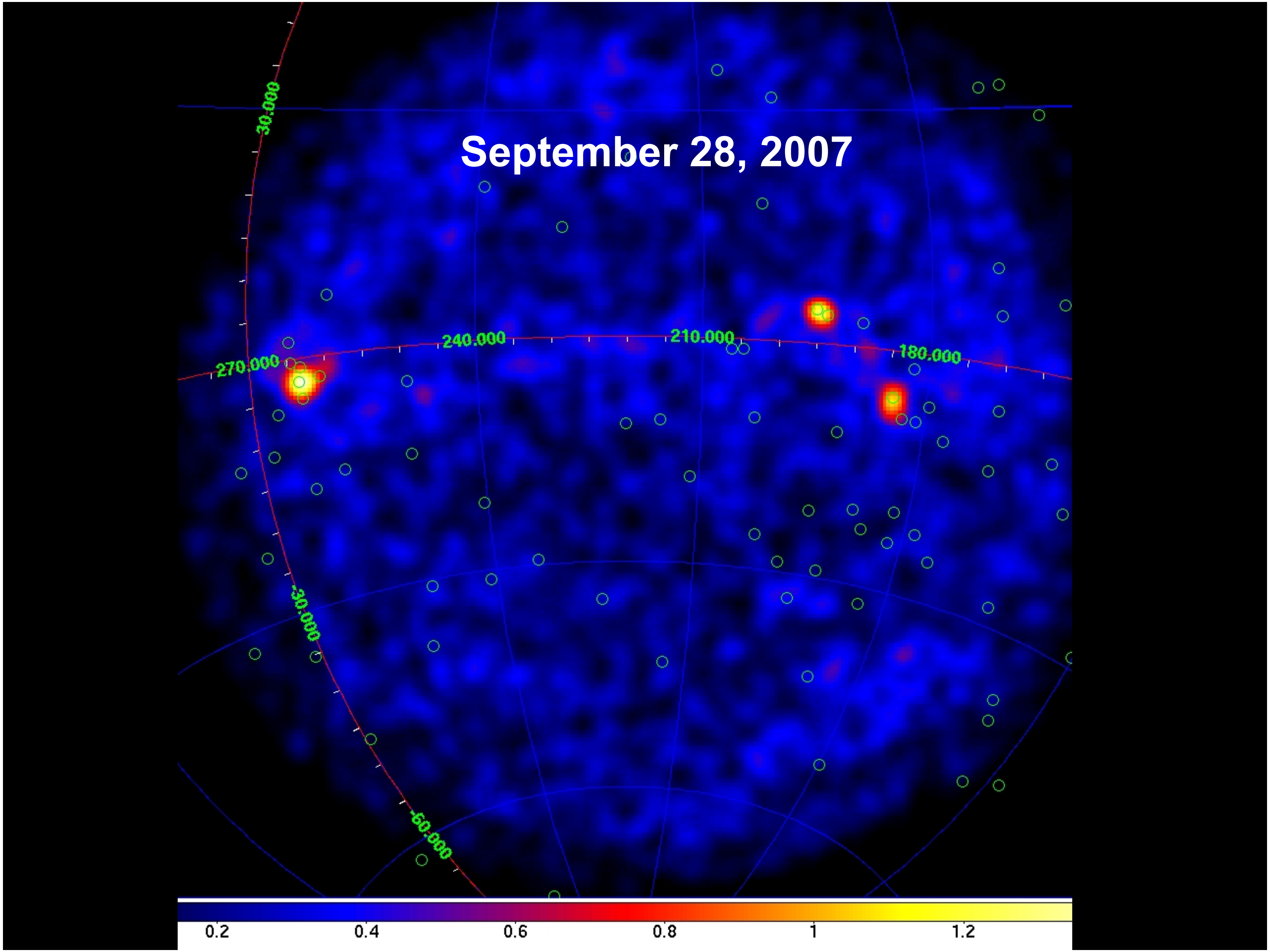
September 28, 2007
30.000
270.000
240.000
210.000
180.000
-30.000
-60.000
0.2
0.4
0.6
0.8
1
1.2

AGILE two lifes

	pointing-AGILE	spinning-AGILE
time period	Jul.07 – Oct.09	Nov. 2010 -
attitude	fixed	variable (spinning, 1°/sec)
sky coverage	1/5	~ 70%
source livetime fraction	~ 0.5	~ 0.2
1-day exposure (30 degree off-axis, 100 MeV)	~ 2 10^7 (cm^2 sec)	(0.5-1) 10^7 (cm^2 sec)

The AGILE sky

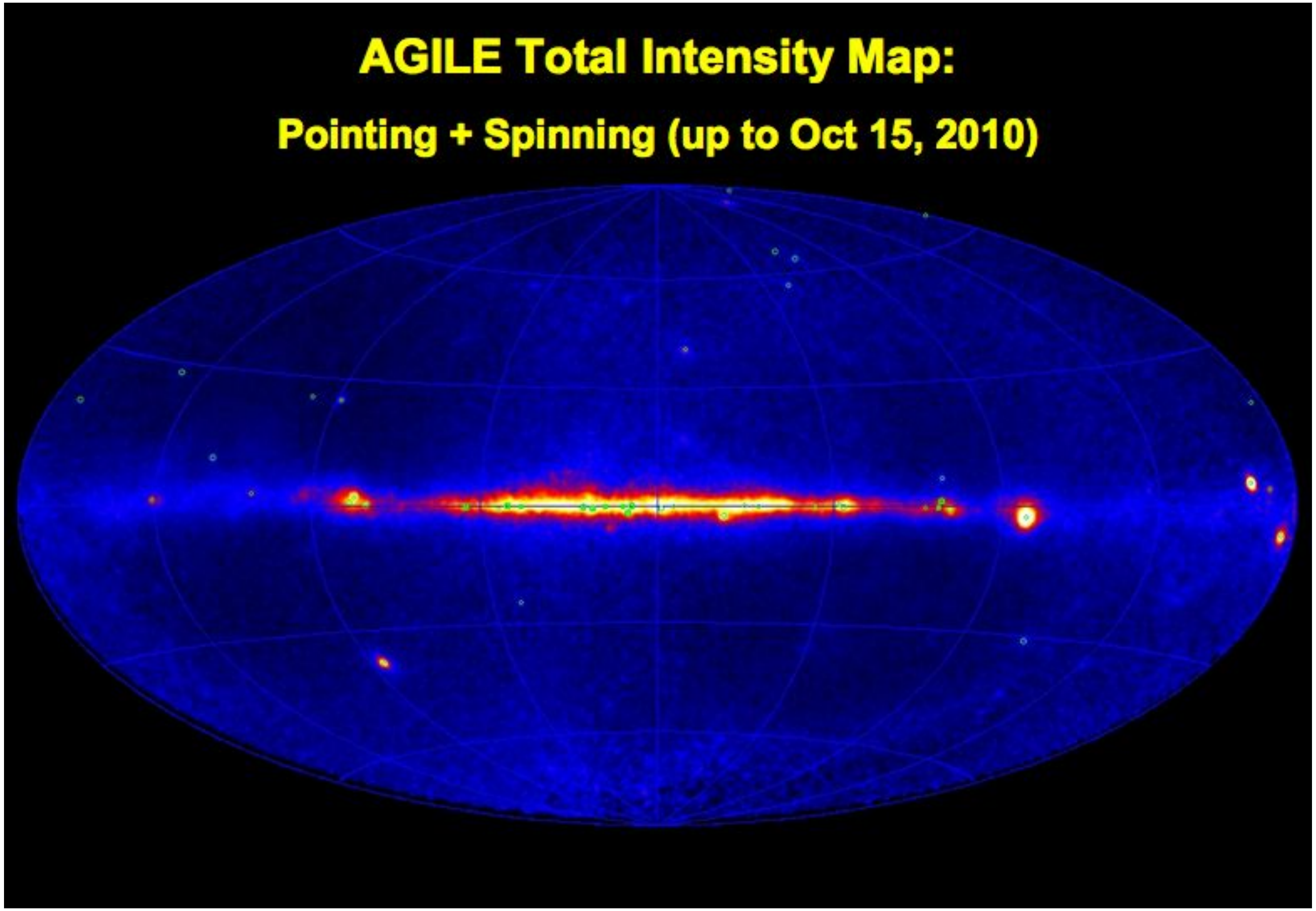

AGILE sources

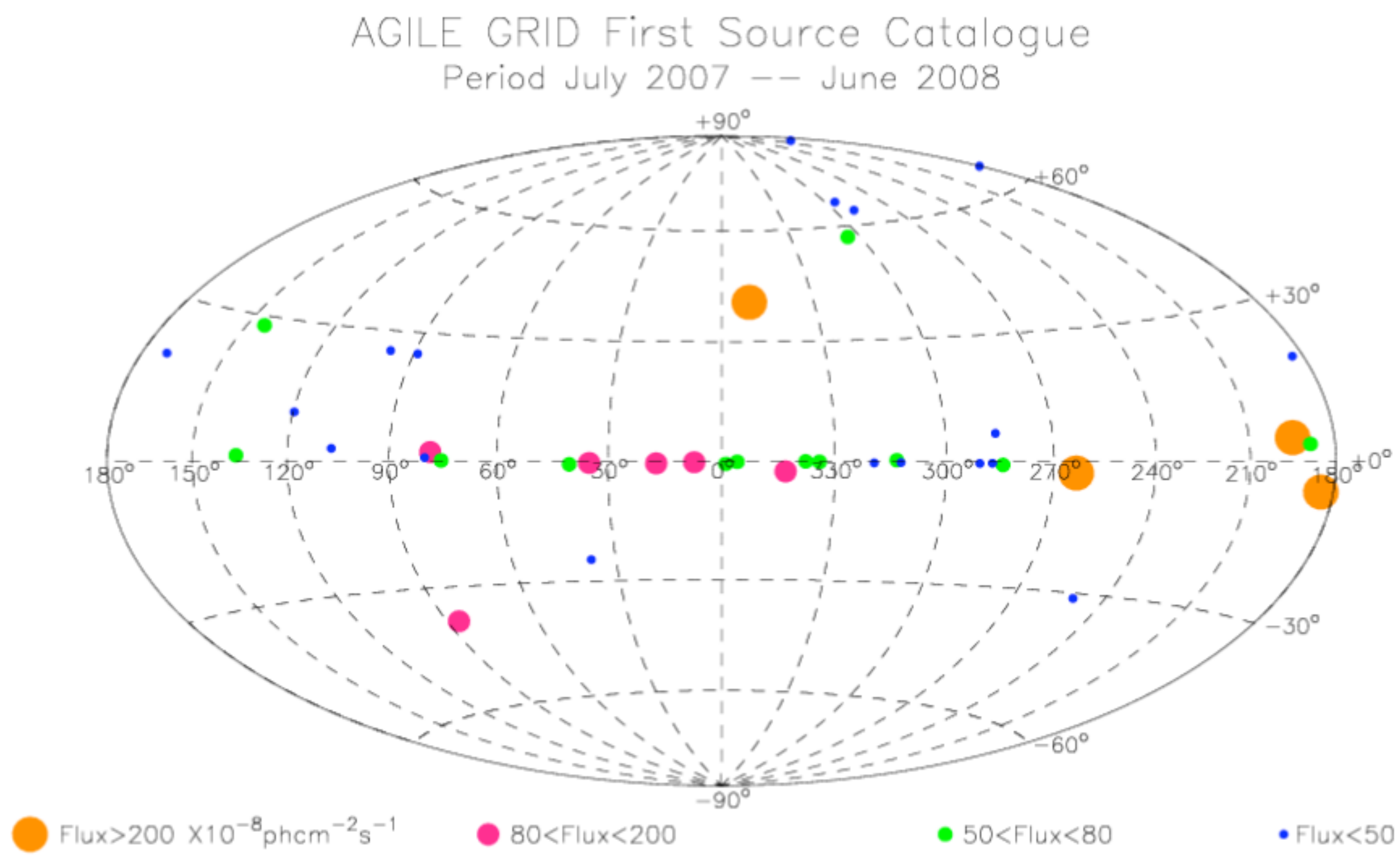

Pittori et al. 2009

2nd catalog of AGILE sources

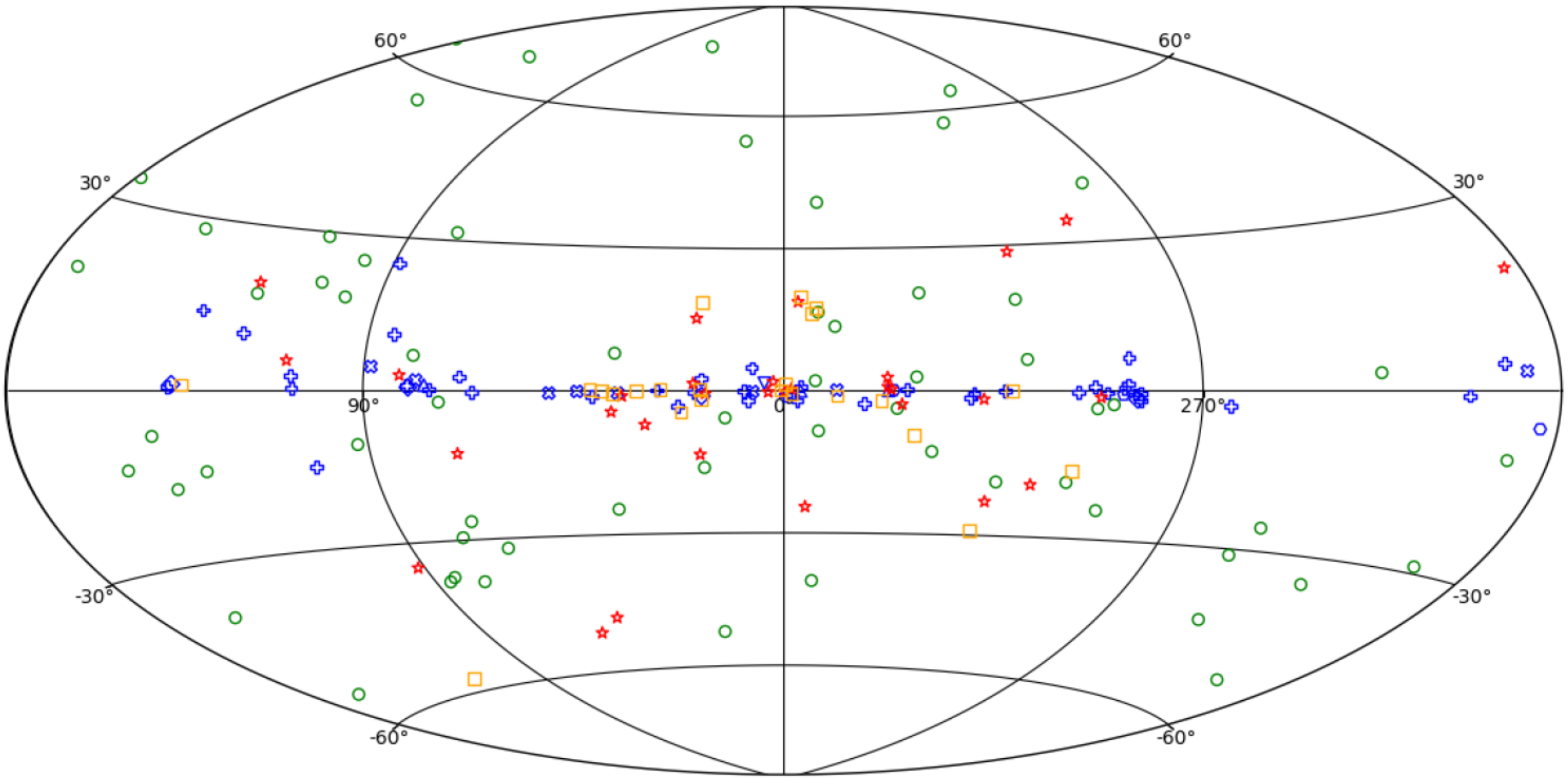

Bulgarelli et al. 2019

Challenge # 1 – AGN

Joint campaign with MAGIC and VERITAS on Mkn 421

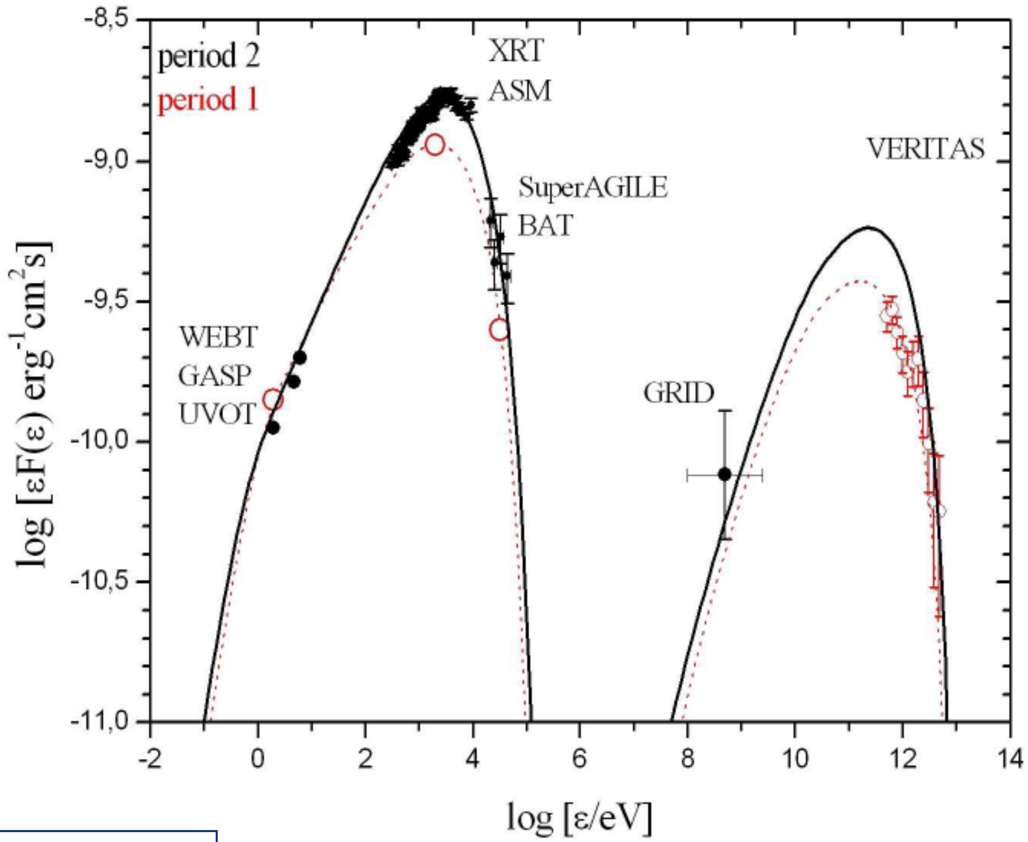

Donnarumma et al. 2009

Challenge # 2 – Pulsar

High Precision Timing (eg. Crab PSR)

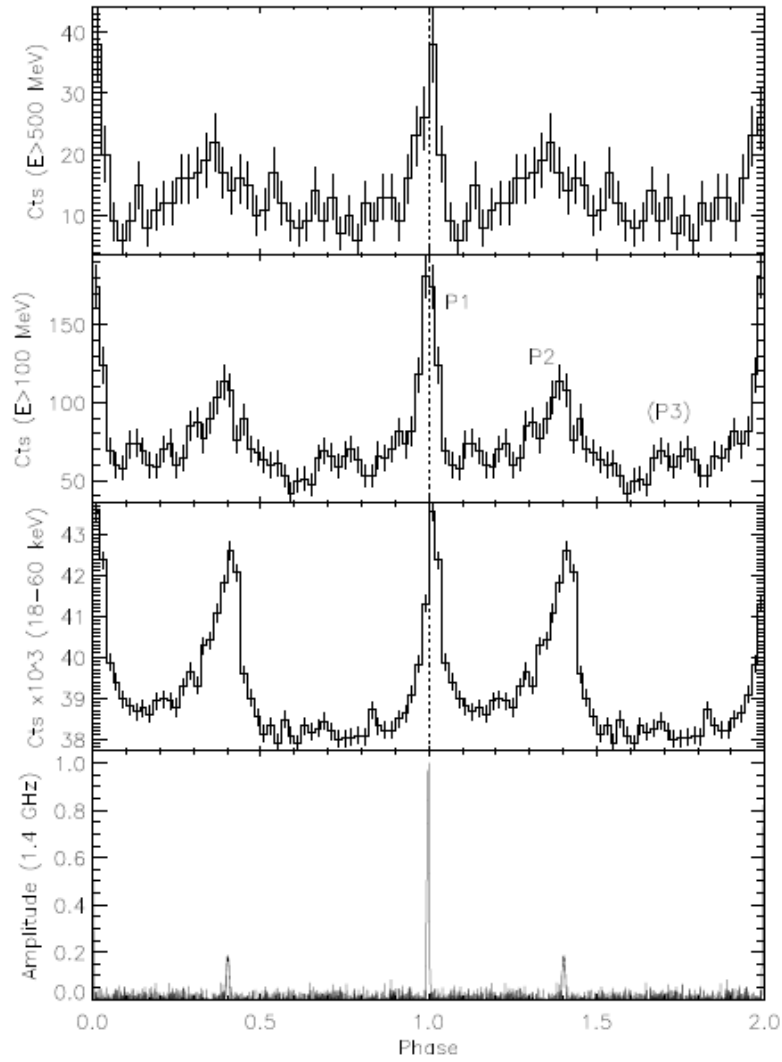

Pellizzoni et al. 2009

Challenge # 3 – GRB

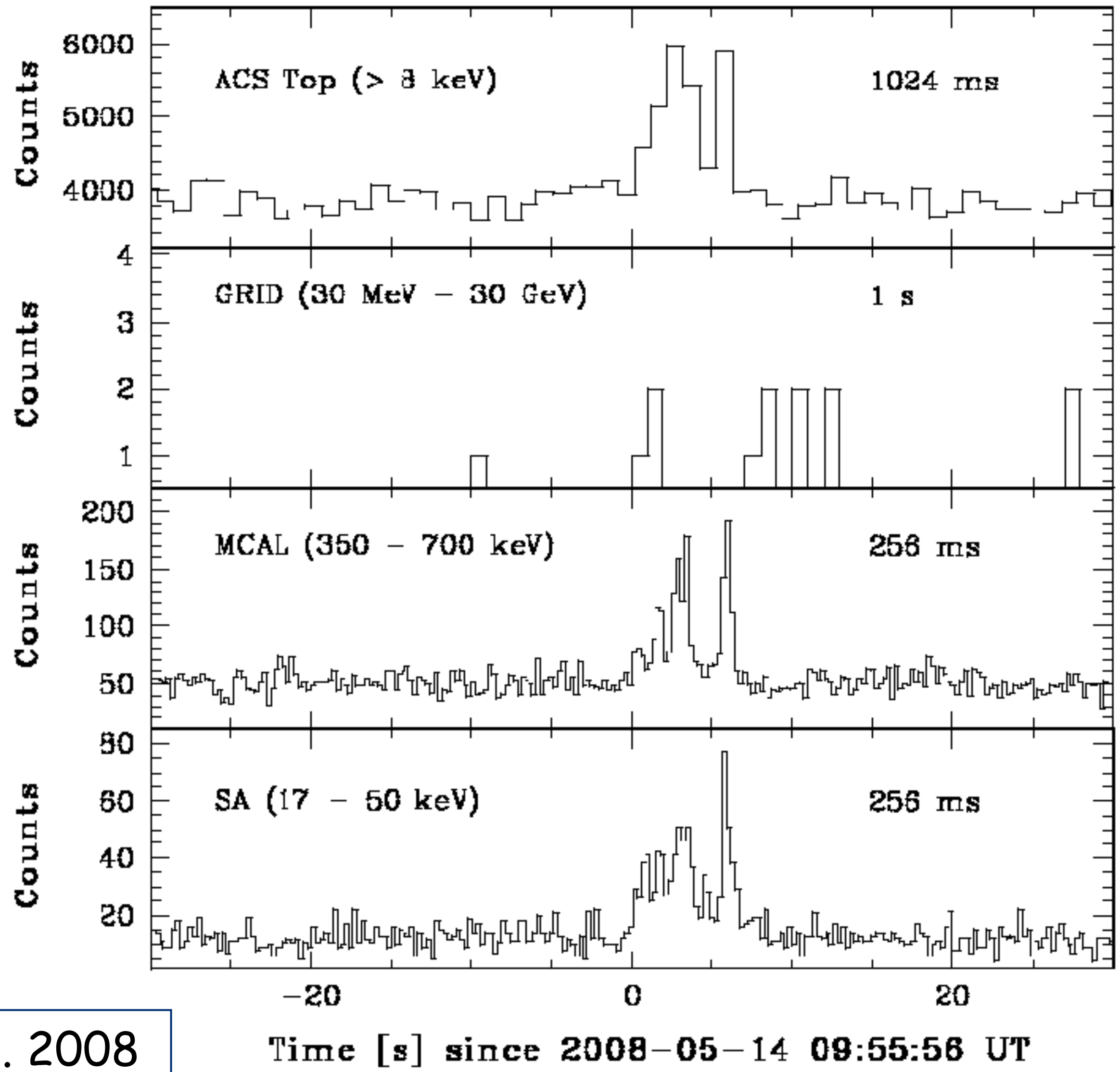

Giuliani et al. 2008

Challenge # 4 – Unidentified

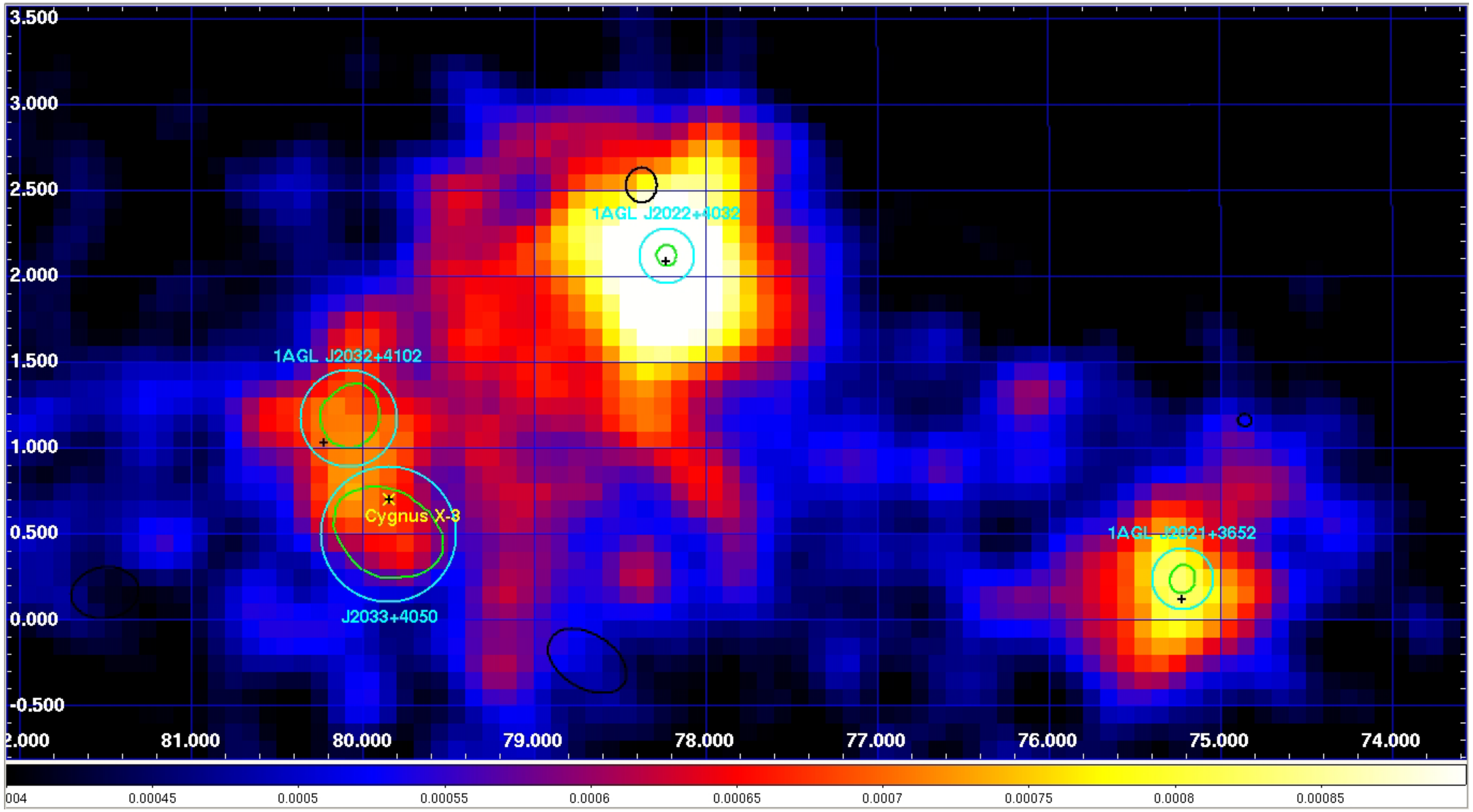

Chen et al. 2011

Challenge # 5 – Spectral resolution

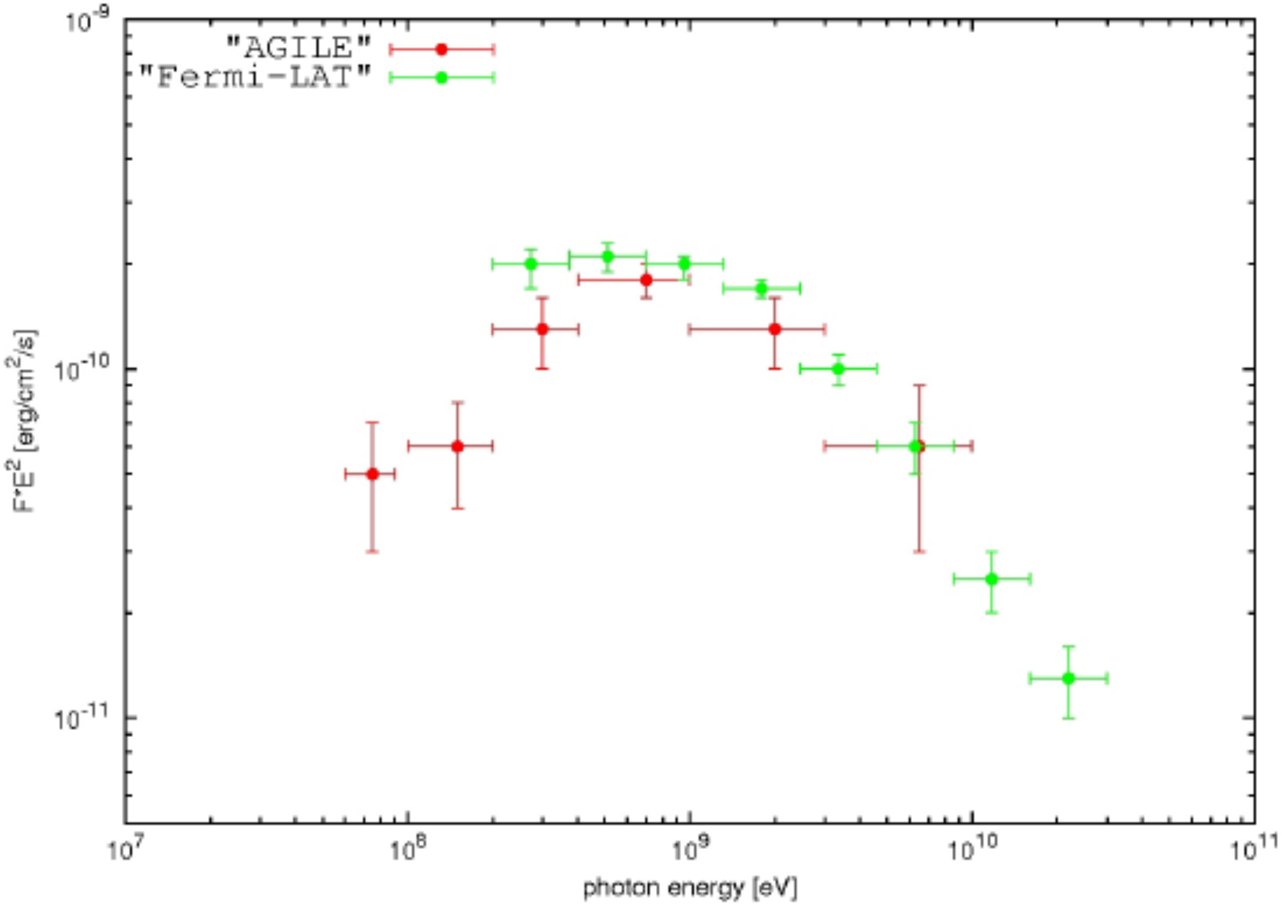

Giuliani et al. 2011

Key AGILE results

Terrestrial Gamma Ray Flashes

Marisaldi et al. 2010

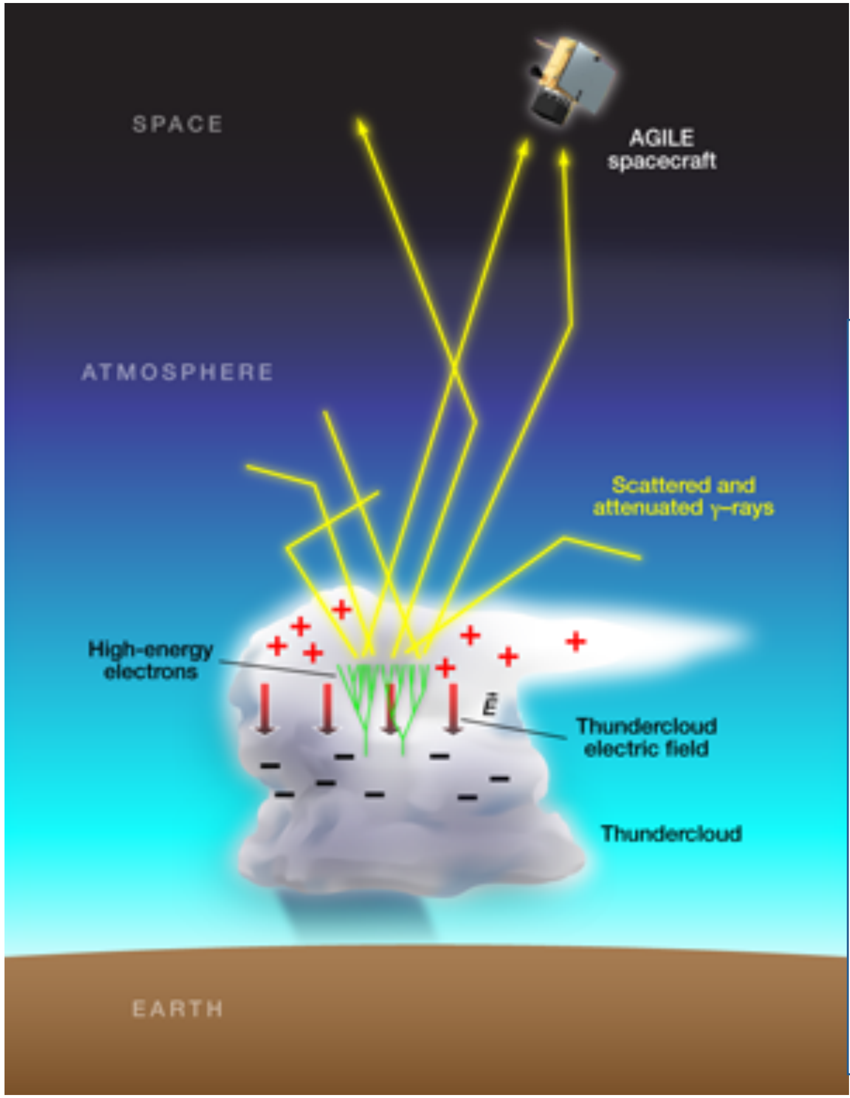

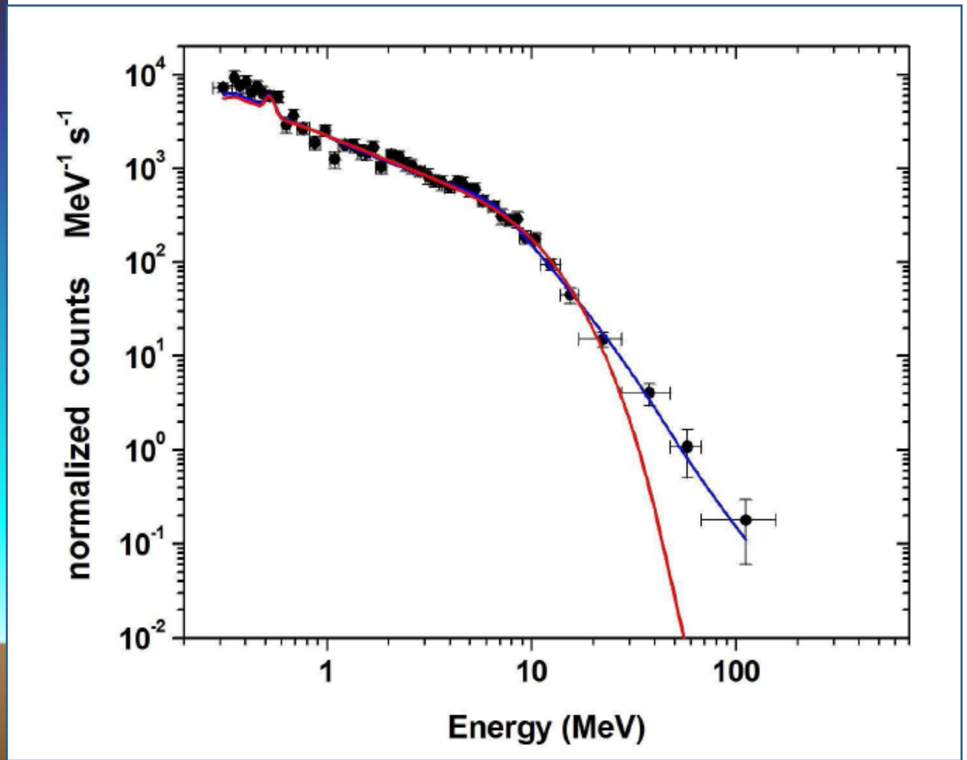

Galactic Transients: Cygnus X3

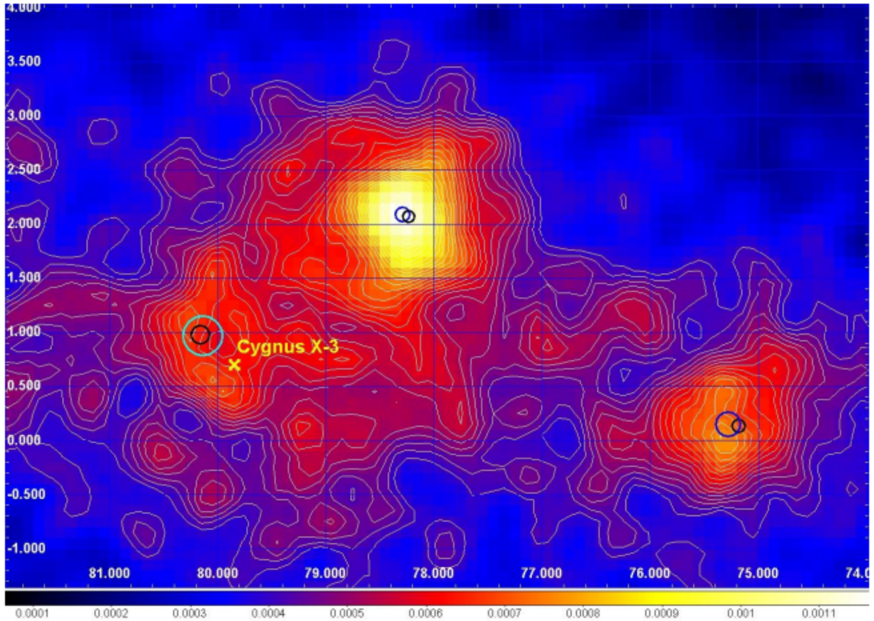

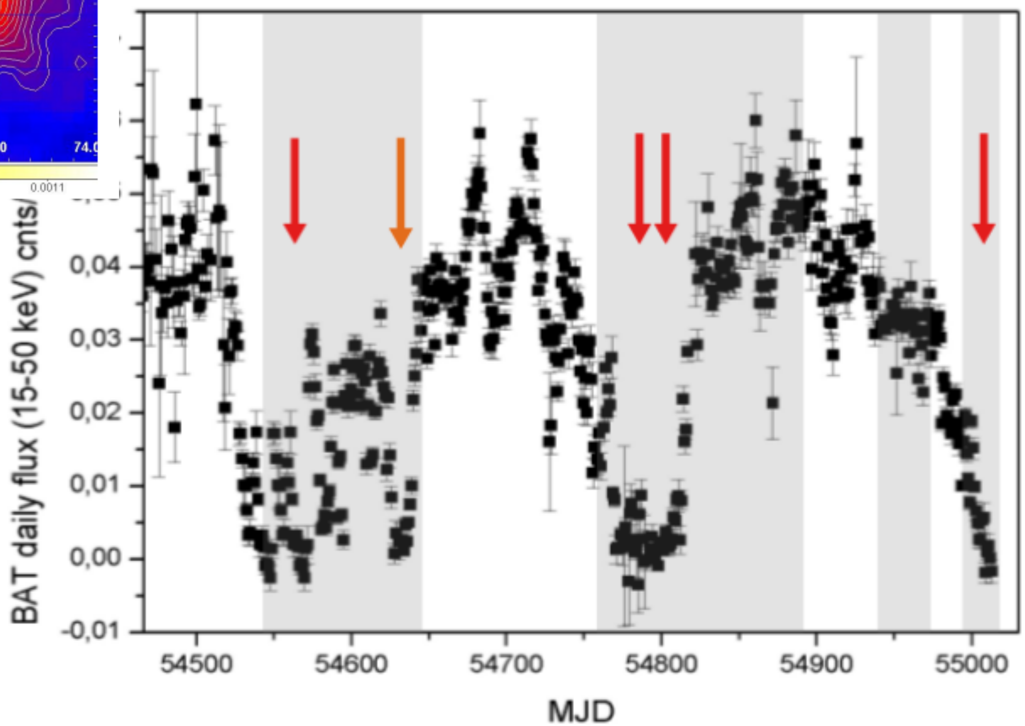

Tavani et al. 2009

Galactic Transients: The Flaring Crab

Tavani et al. 2011

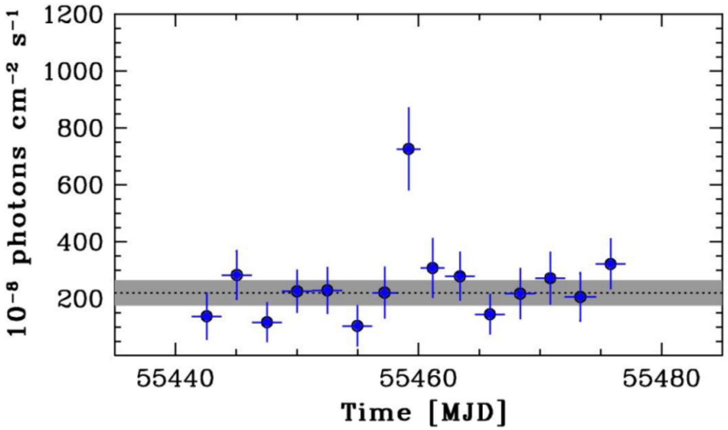

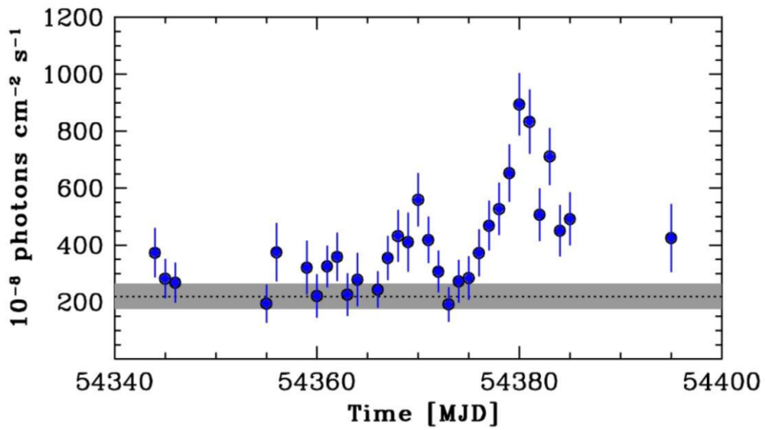

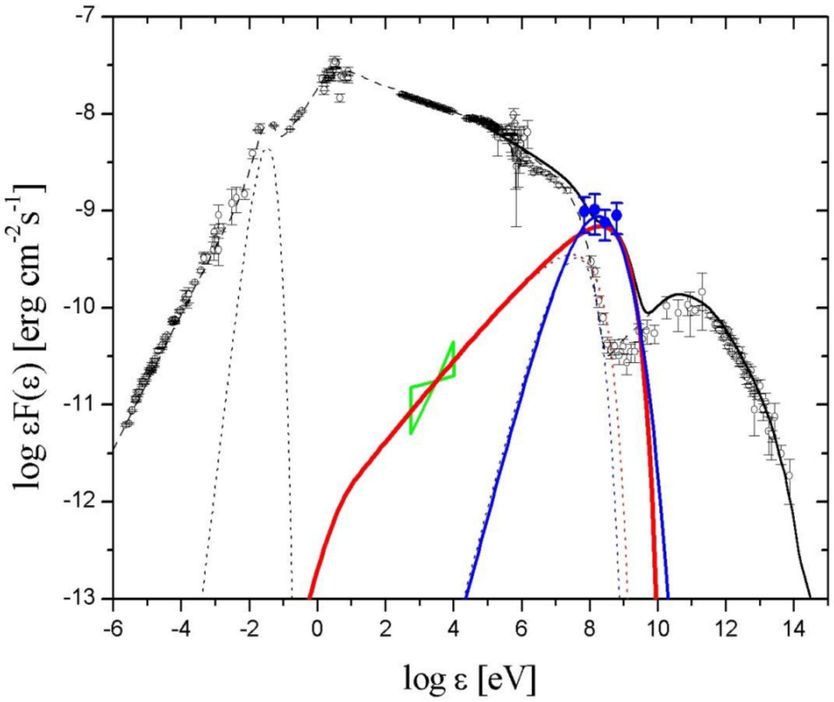

The Flaring Crab

AGILE detection of enhanced gamma-ray emission
from the Crab Nebula region

ATel #2855; M. Tavani (INAF/IASF Roma), E. Striani (Univ. Tor Vergata), A. Bulgarelli (INAF/IASF Bologna), F. Gianotti, M. Trifoglio (INAF/IASF Bologna), C. Pittori, F. Verrecchia (ASDC), A. Argan, A. Trois, G. De Paris, V. Vittorini, F. D'Ammando, S. Sabatini, G. Piano, E. Costa, I. Donnarumma, M. Feroci, L. Pacciani, E. Del Monte, F. Lazzarotto, P. Soffitta, Y. Evangelista, I. Lapshov (INAF-IASF-Rm), A. Chen, A. Giuliani(INAF-IASF-Milano), M. Marisaldi, G. Di Cocco, C. Labanti, F. Fuschino,M. Galli (INAF/IASF Bologna), P. Caraveo, S. Mereghetti, F. Perotti (INAF/IASF Milano), G. Pucella, M. Rapisarda (ENEA-Roma), S. Vercellone (IASF-Pa), A. Pellizzoni, M. Pilia (INAF/OA-Cagliari), G. Barbiellini, F. Longo (INFN Trieste), P. Picozza, A. Morselli (INFN and Univ. Tor Vergata), M. Prest (Universita` dell'Insubria), P. Lipari, D. Zanello (INFN Roma-1), P.W. Cattaneo, A. Rappoldi (INFN Pavia), P. Giommi, P. Santolamazza, F. Lucarelli, S. Colafrancesco (ASDC), L. Salotti (ASI)
on 22 Sep 2010; 14:45 UT
Distributed as an Instant Email Notice (Transients)
Password Certification: Marco Tavani (tavani@iasf-roma.inaf.it)

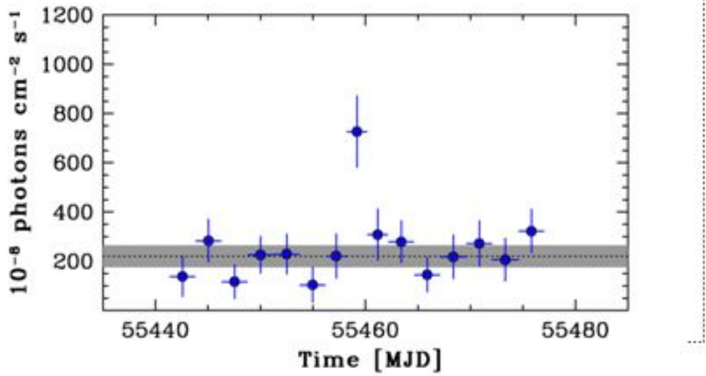

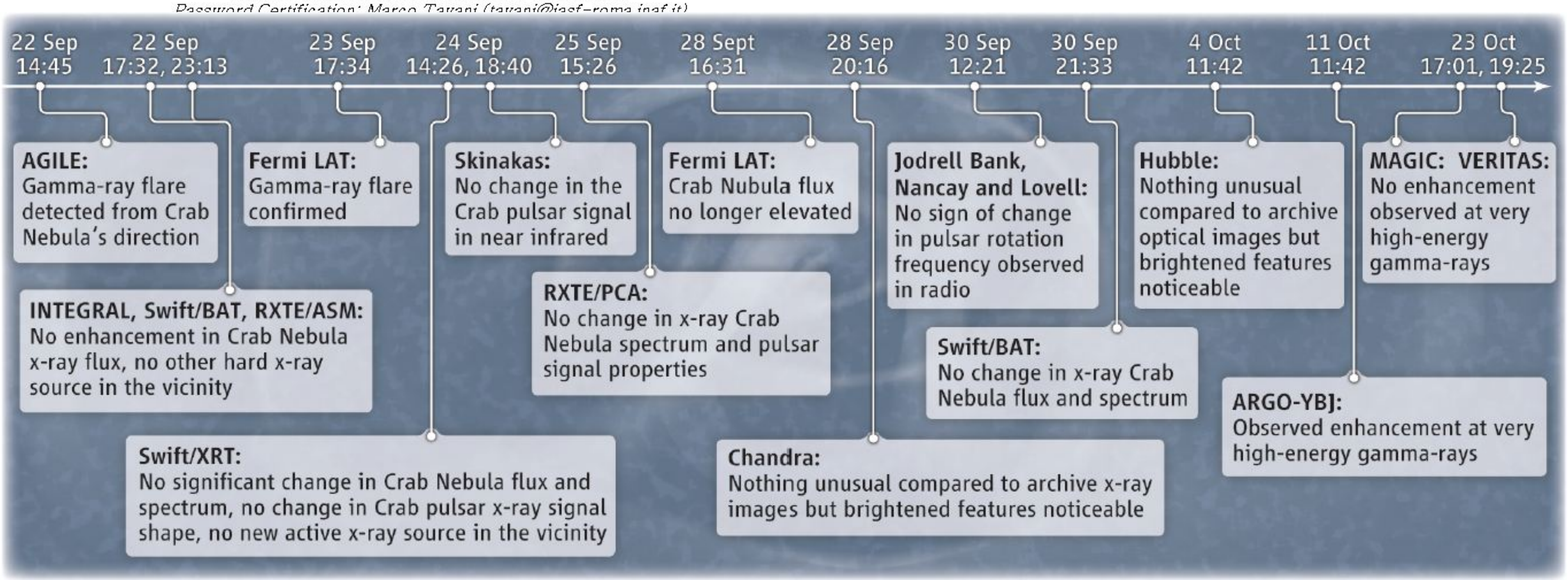

Fermi LAT

Overview of LAT

- Precision Si-strip Tracker (TKR) 18 XY tracking planes. Single-sided silicon strip detectors (228 μm pitch) Measure the photon direction; gamma ID.
- Hodoscopic CsI Calorimeter(CAL) Array of 1536 CsI(Tl) crystals in 8 layers. Measure the photon energy; image the shower.
- Segmented Anticoincidence Detector (ACD) 89 plastic scintillator tiles. Reject background of charged cosmic rays; segmentation removes self-veto effects at high energy.
- Electronics System Includes flexible, robust hardware trigger and software filters.

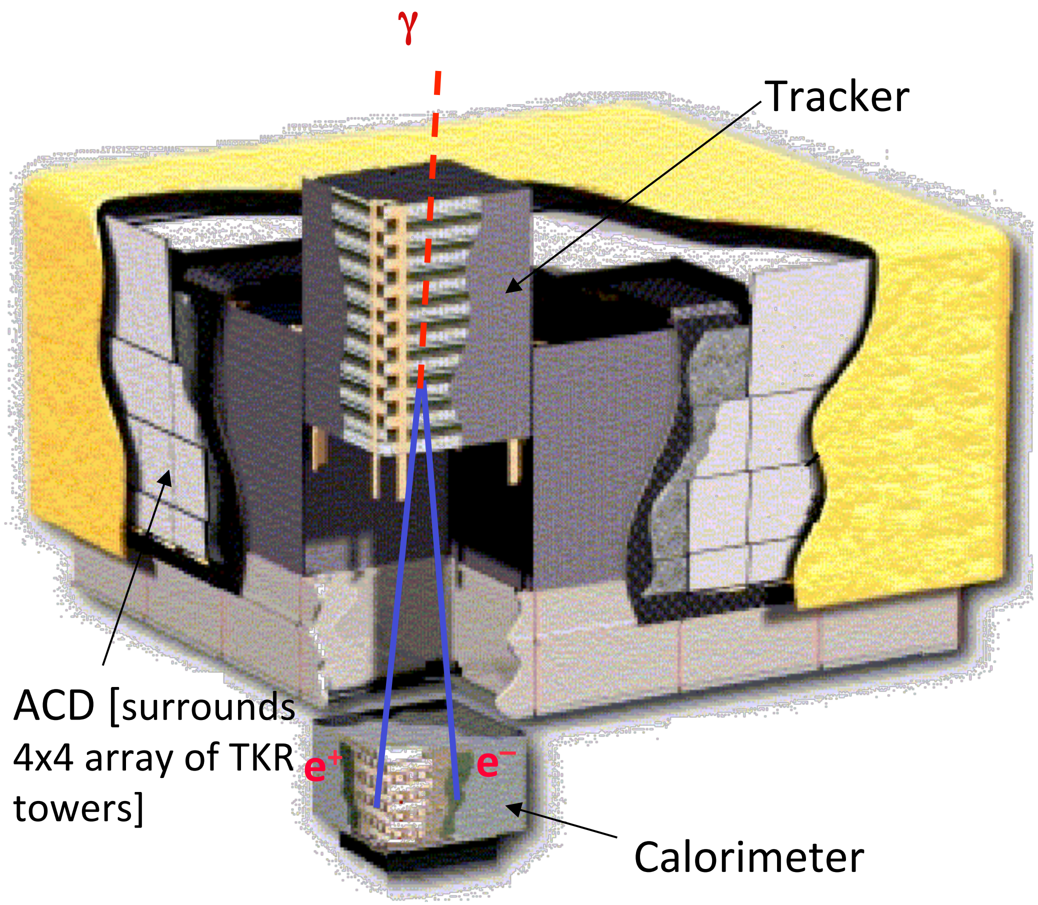

Systems work together to identify and measure the flux of cosmic gamma rays with energy 20 MeV - >300 GeV.

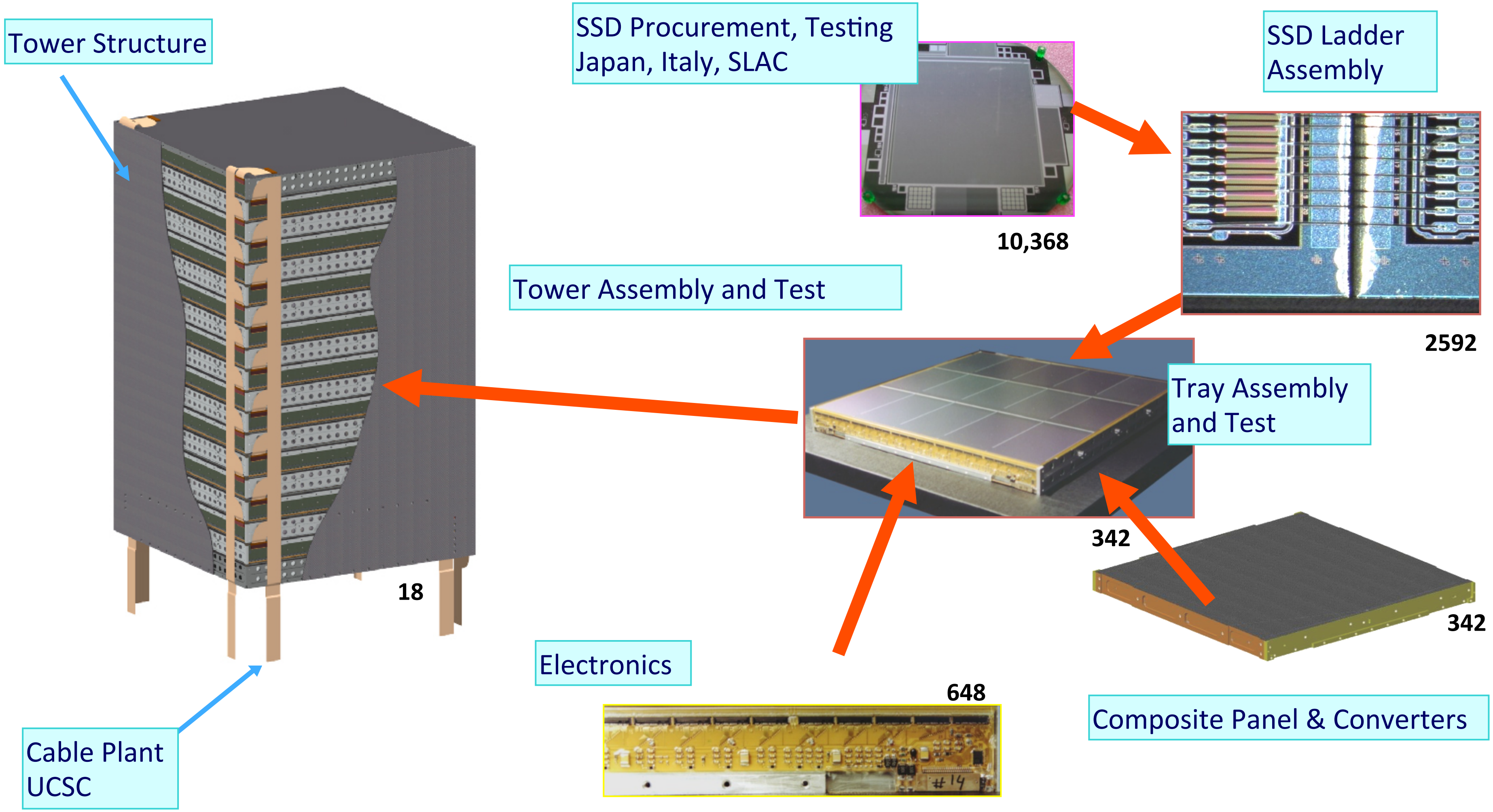

Tower Structure
SSD Procurement, Testing
Japan, Italy, SLAC
SSD Ladder
Assembly
10,368
Tower Assembly and Test
2592
Tray Assembly
and Test
342
18
342
Electronics
648
Composite Panel & Converters
Cable Plant
UCSC

Silicon Detectors

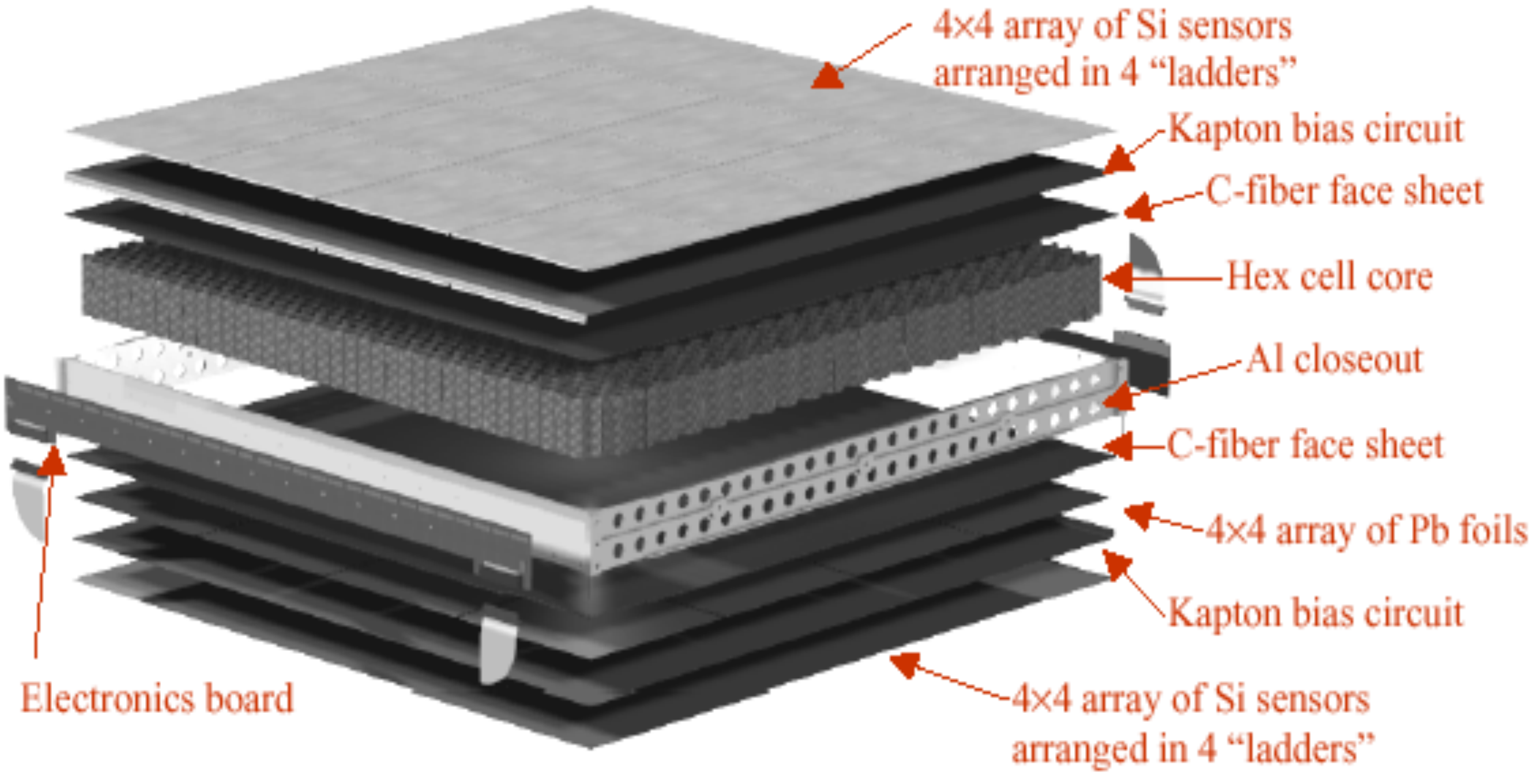

GLAST silicon tracker tray

Launch!

- Launch from Cape Canaveral Air Station 11 June 2008 at 12:05PM EDT
- Circular orbit, 565 km altitude (96 min period), 25.6 deg inclination.

Key Features

- Two instruments:
  - LAT:
    - high energy (20 MeV – >300 GeV)
  - GBM:
    - low energy (8 keV – 40 MeV)

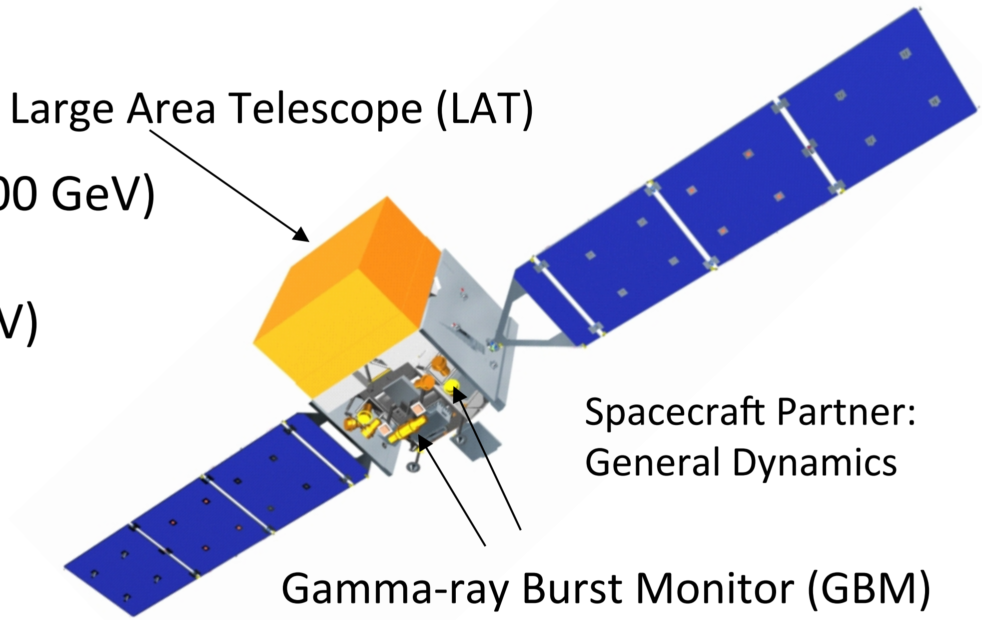

- Huge field of view
  - LAT: 20% of the sky at any instant; in sky survey mode, expose all parts of sky for ~30 minutes every 3 hours. GBM: whole unocculted sky at any time.
- Huge energy range, including largely unexplored band 10 GeV - 100 GeV
- Large leap in all key capabilities. Great discovery potential.

The Observatory

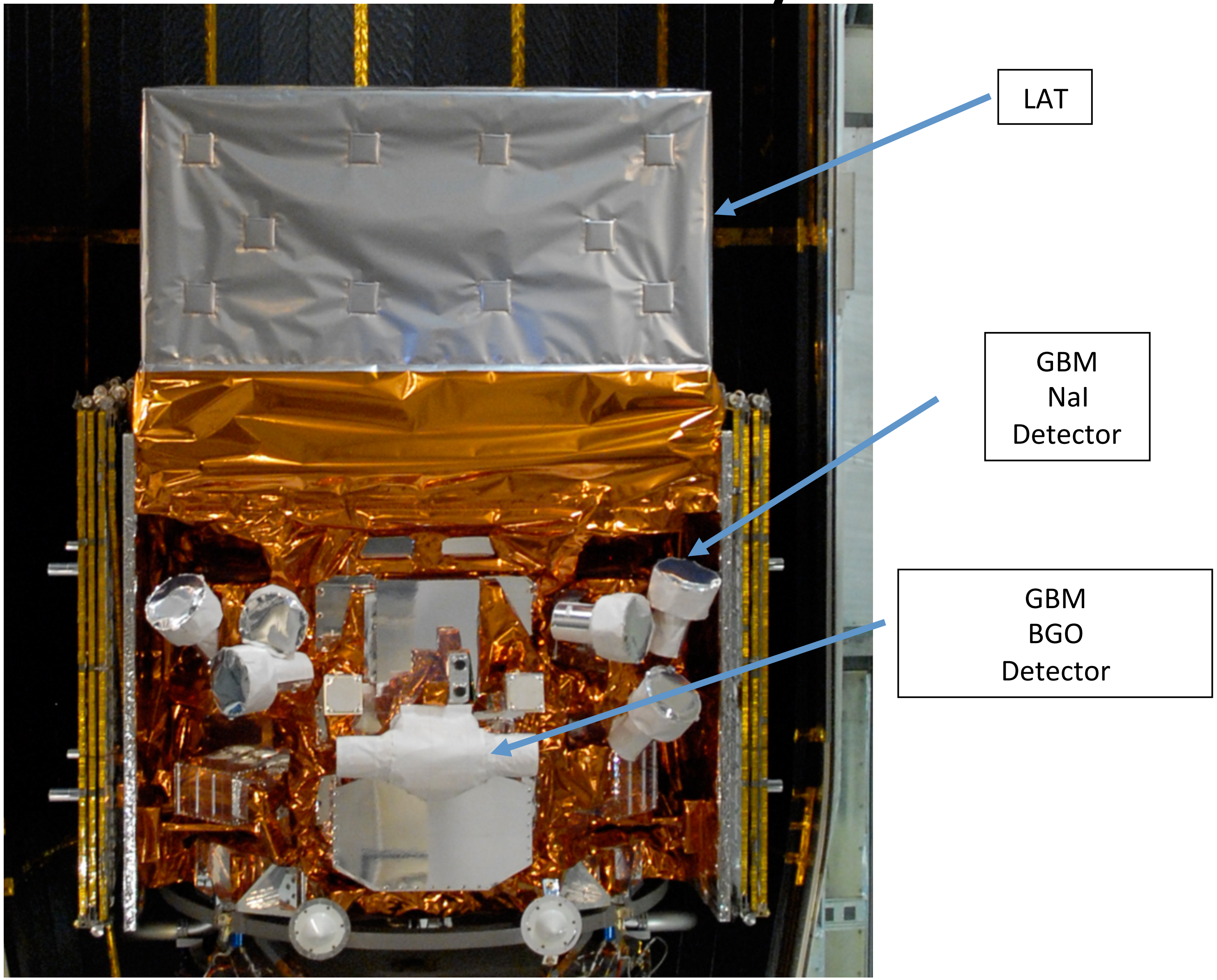

Effective Area (A_{eff})

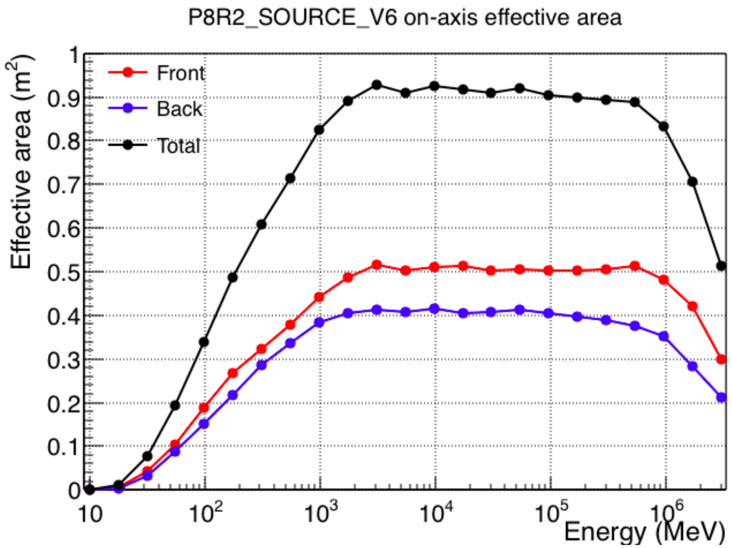

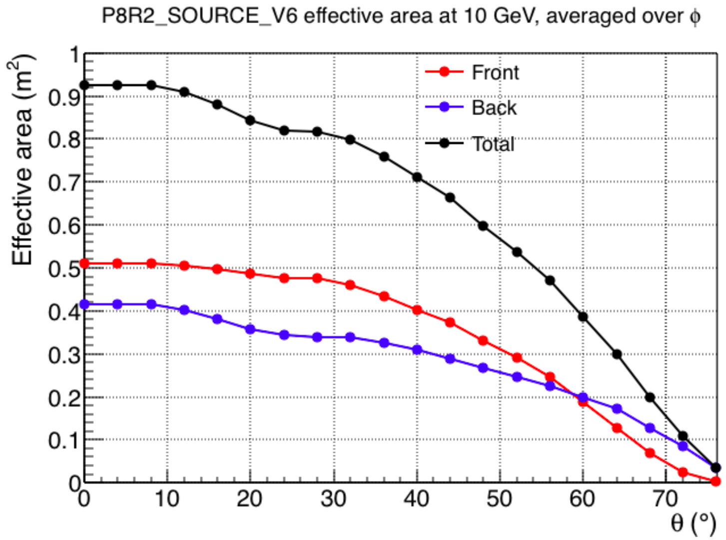

< 100 MeV limited by 3-in a row requirement

< 1 GeV limited discriminating information

> 100 GeV self-veto from backsplash

Off-axis: more material, less cross section

Shift from front/back events as we go off-axis

http://www.slac.stanford.edu/exp/glast/groups/canda/lat_Performance.htm

Point Spread Function (P)

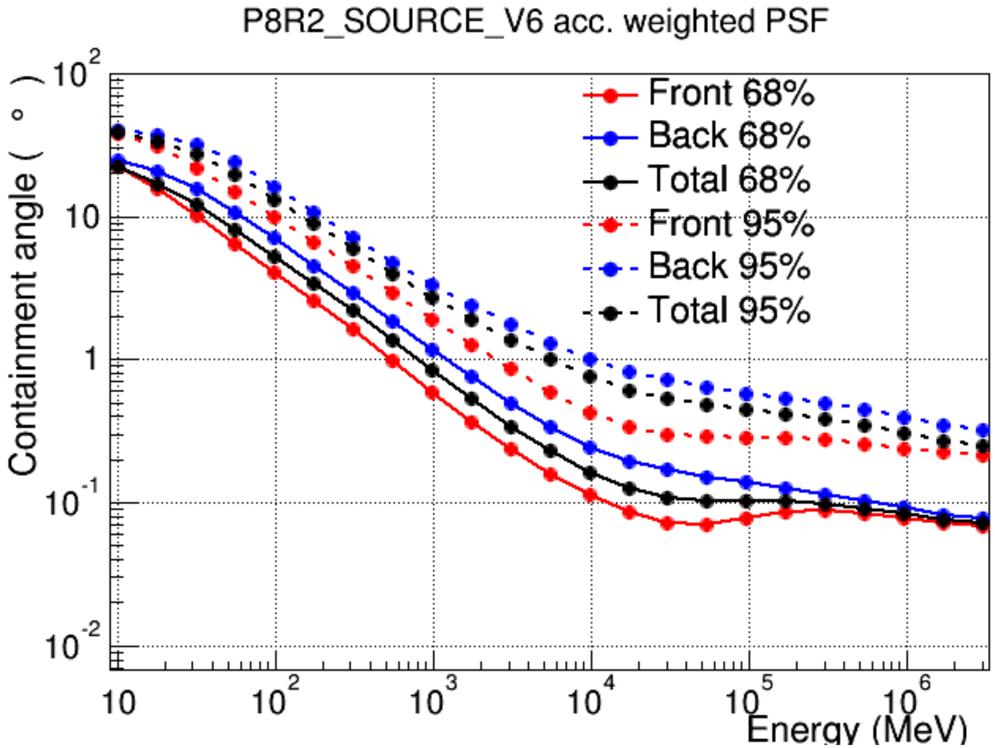

Low energy: dominated by MS

High energy: dominated by strip pitch

http://www.slac.stanford.edu/exp/glast/groups/canda/lat_Performance.htm

LAT first light

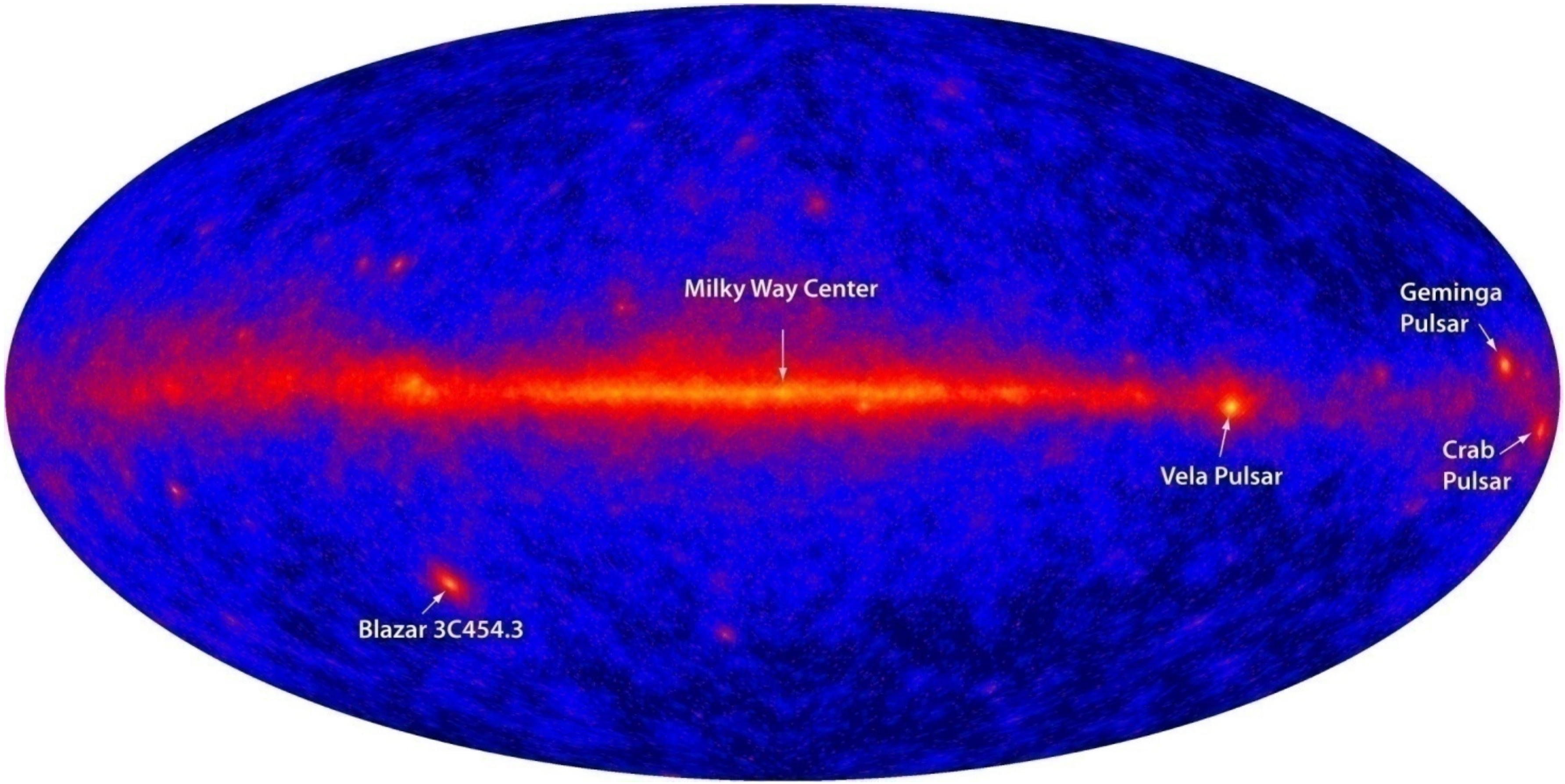

LAT discovers a radio-quiet pulsar!

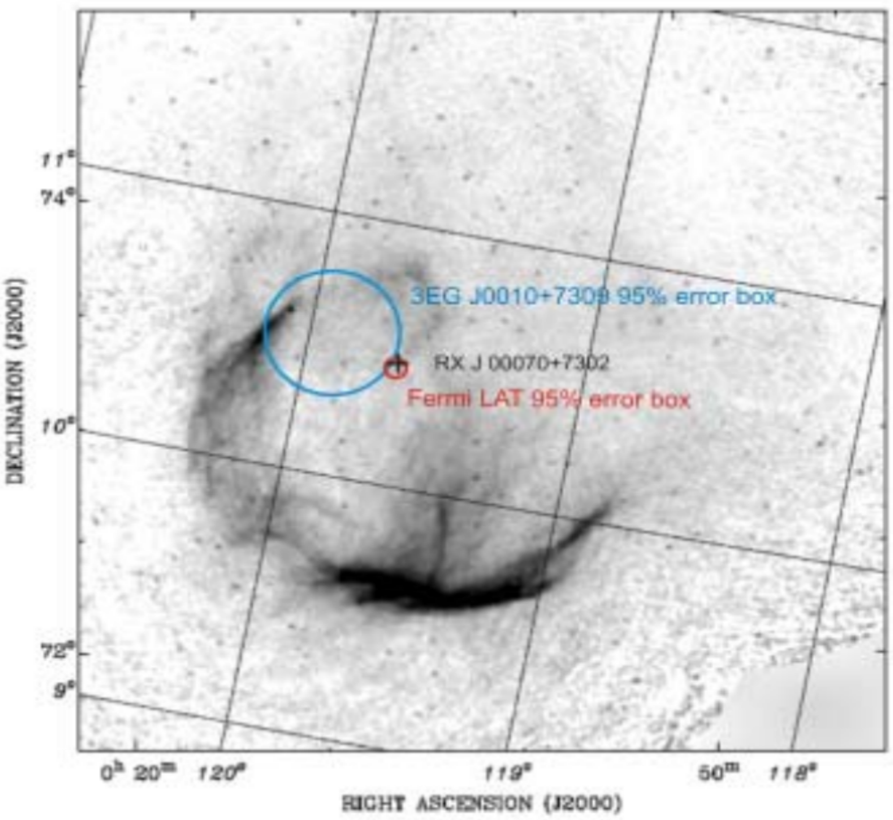

P ~ 317 ms
Pdot ~ 3.6E-13
Characteristic age ~ 10,000 yrs

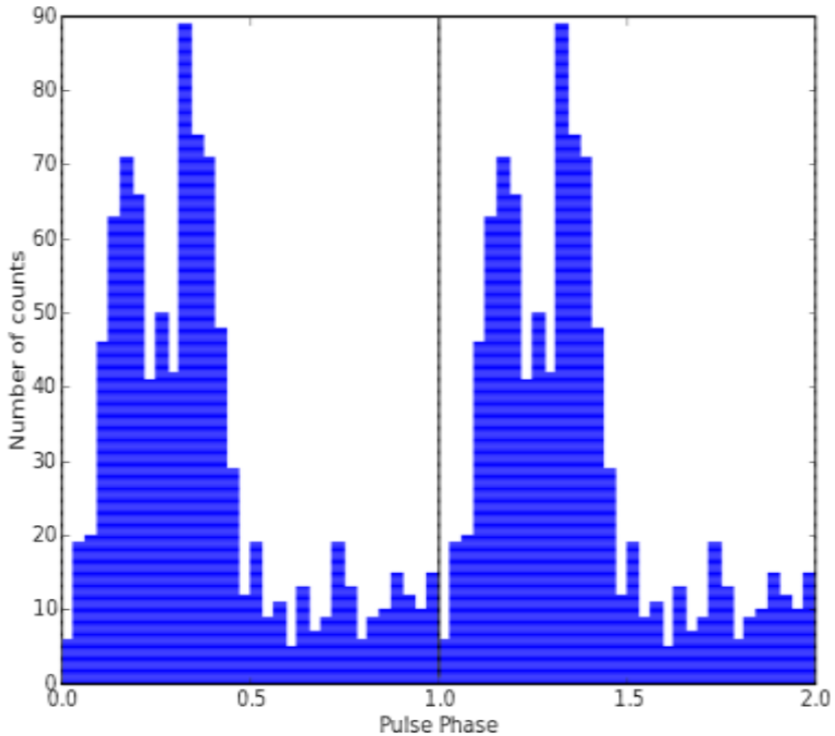

Location of EGRET source 3EG J0010+7309, the Fermi-LAT source, and the central X-ray source RX J0007.0+7303

Published in Science Express October 16, 2008

Fermi Gamma-ray Space Telescope

GLAST renamed *Fermi* by NASA on August 26, 2008

http://fermi.gsfc.nasa.gov/

“ Enrico Fermi (1901-1954) was an Italian physicist who immigrated to the United States. He was the first to suggest a viable mechanism for astrophysical particle acceleration. This work is the foundation for our understanding of many types of sources to be studied by NASA’s Fermi Gamma-ray Space Telescope, formerly known as GLAST. ”

Fermi LAT 3 months sky

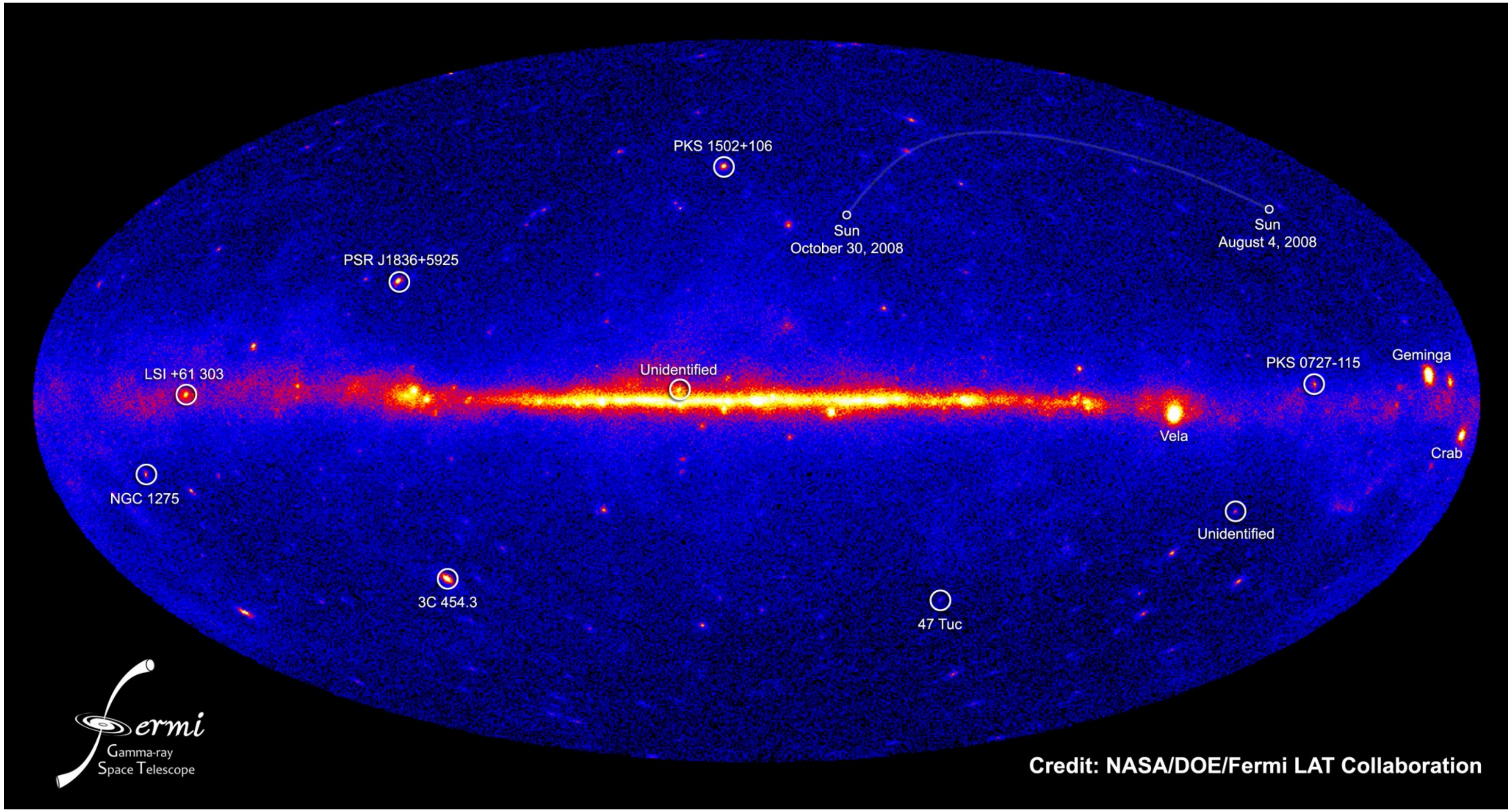

PKS 1502-106 and 3C454.3

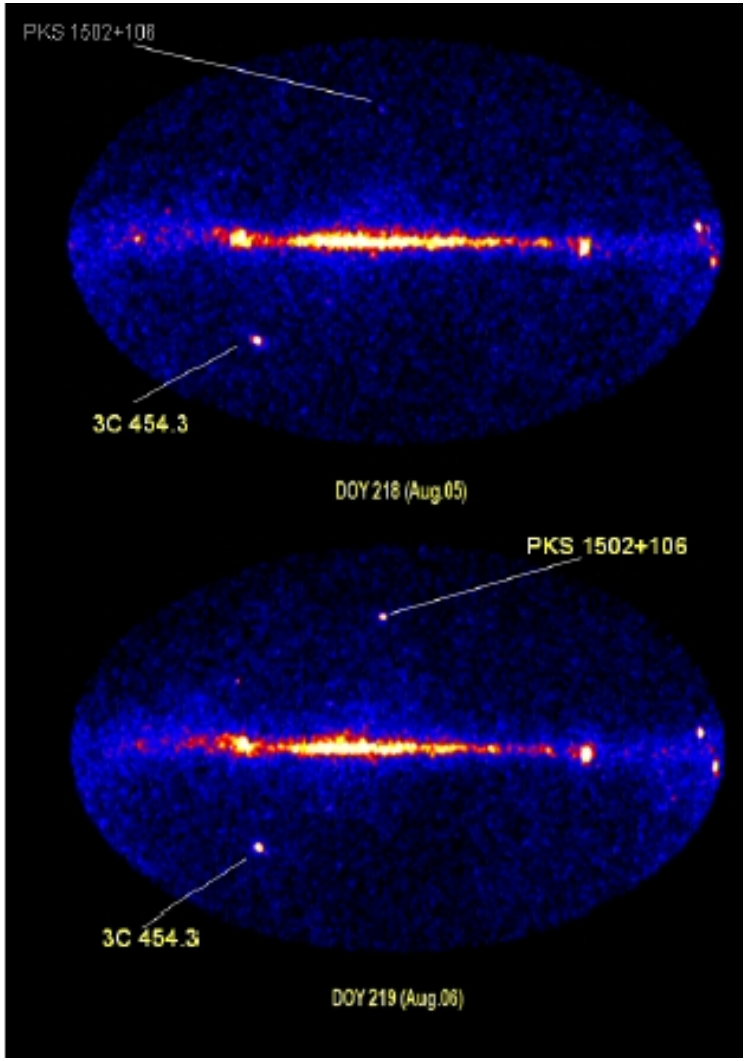

- The sky is dynamic, Fermi is monitoring the sky, catching flaring sources over different time scales.
- Atel #1628 (3C454.3) and #1650 (PKS 1502-106) issued to announce these flares.

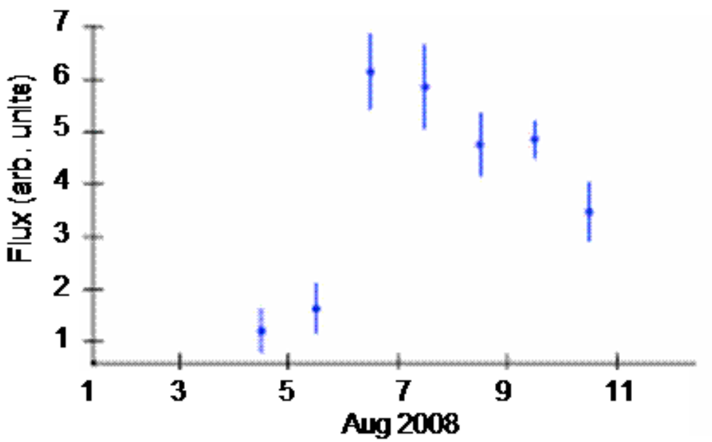

Fermi 1 yr sky

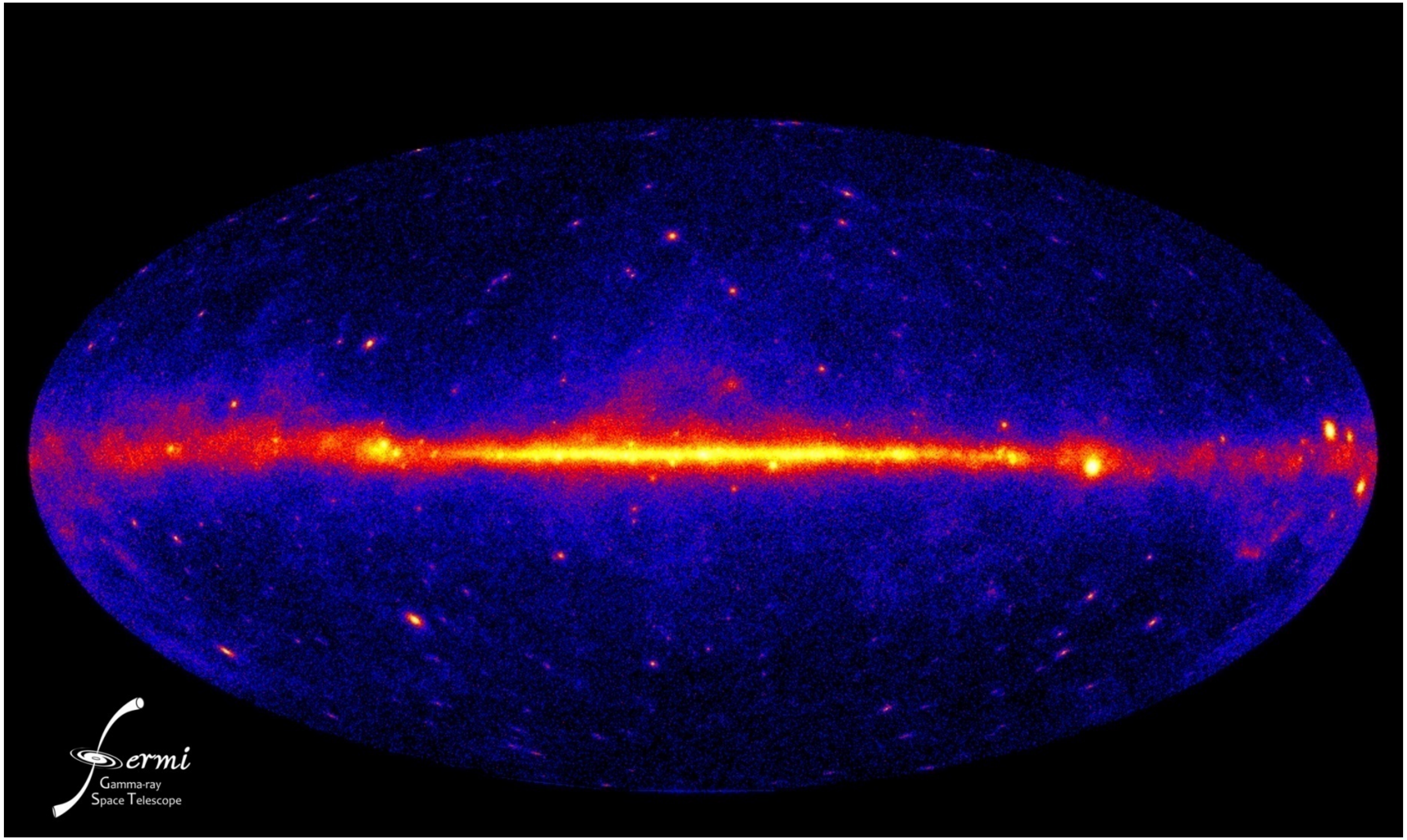

Fermi Year One Catalog

http://fermi.gsfc.nasa.gov/ssc/data/access/lat/1yr_catalog/

More than 1000 sources in year one catalog !

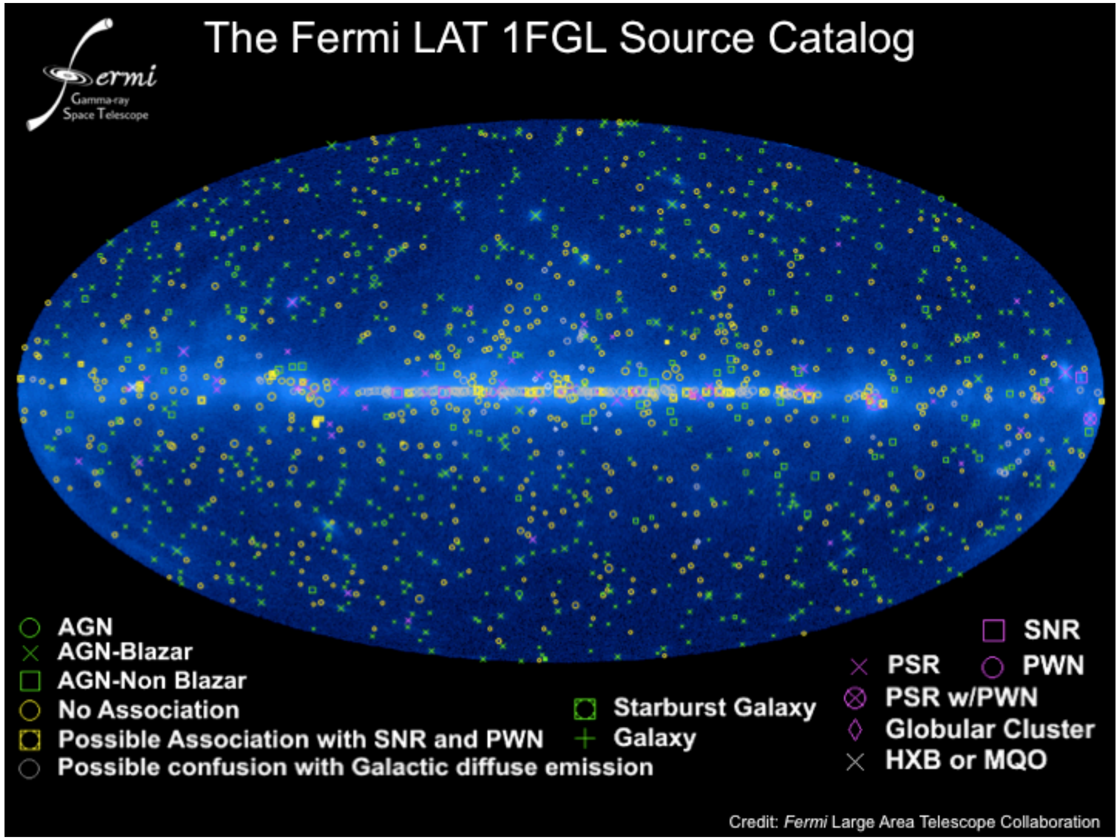

- About 250 sources show evidence of variability
- Half the sources are associated positionally, mostly blazars and PSRs
- Other classes of sources exist in small numbers (XRB, PWN, SNR, starbursts, globular clusters, radio galaxies, narrow-line Seyferts)
- Uncertainties due to the diffuse model, particularly in the Galactic ridge

2 year sky

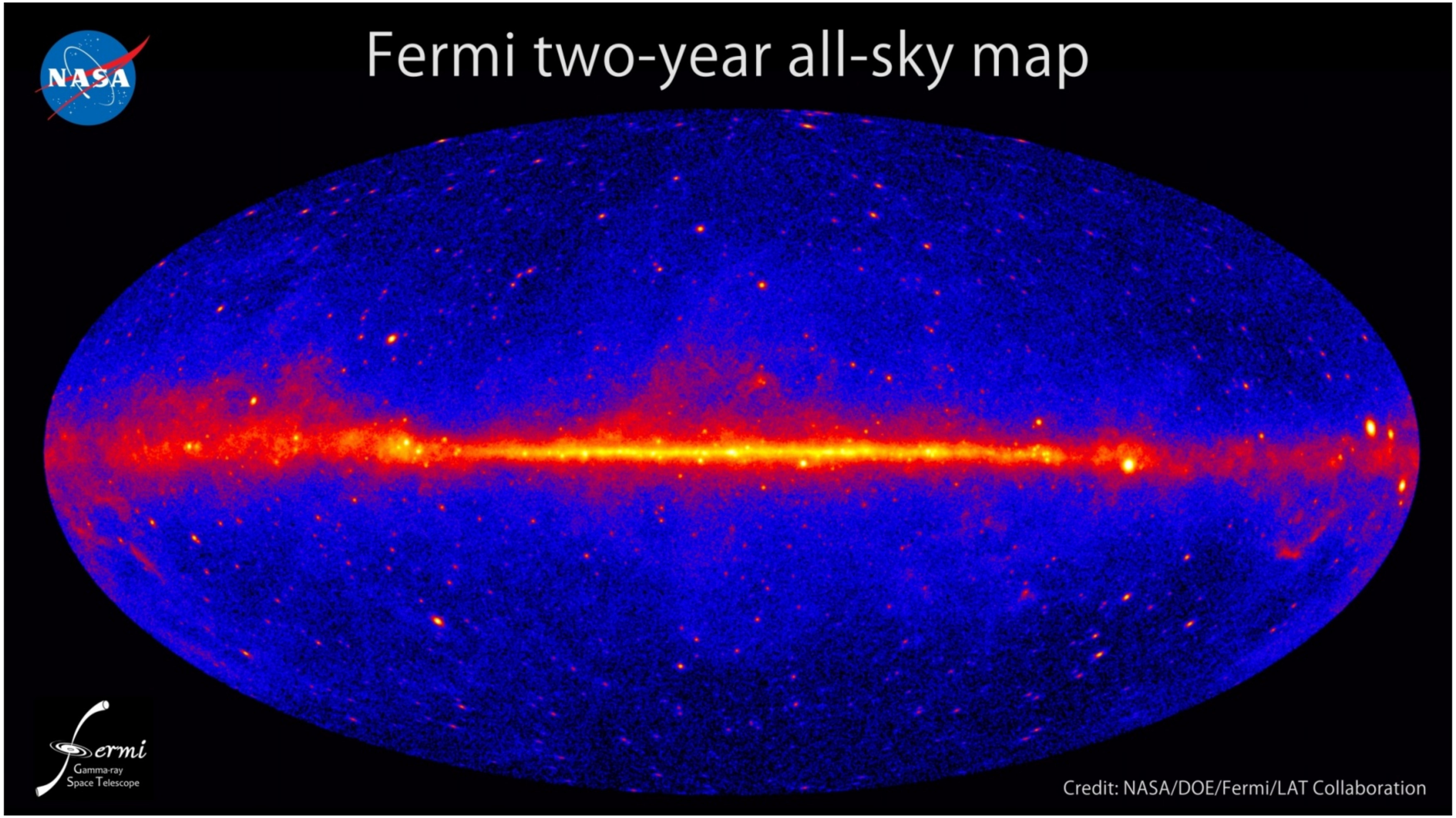
Fermi two-year all-sky map
NASA
Fermi
Gamma-ray
Space Telescope
Credit: NASA/DOE/Fermi/LAT Collaboration

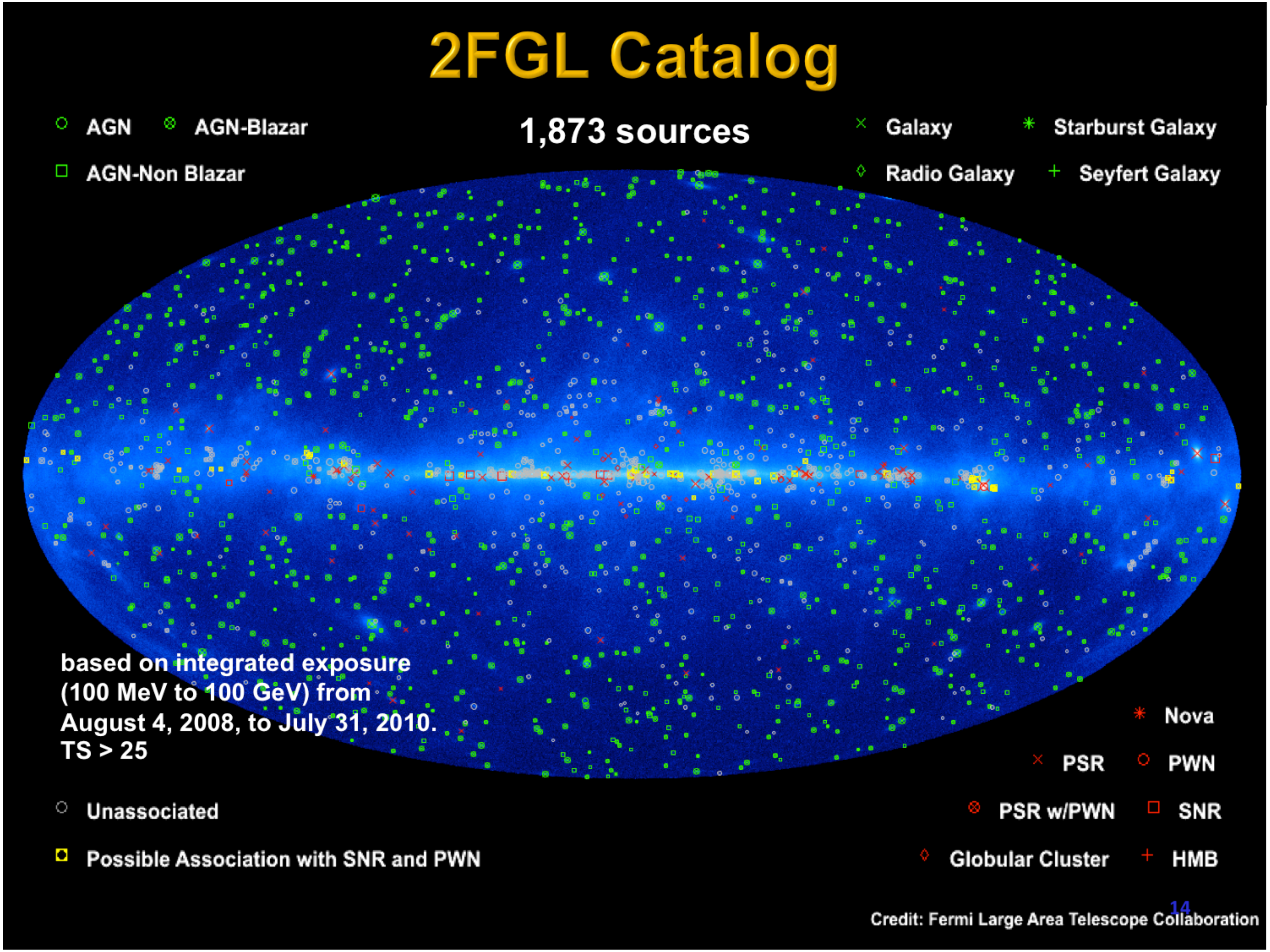
2FGL Catalog
1,873 sources
AGN
AGN-Blazar
AGN-Non Blazar
Galaxy
Starburst Galaxy
Radio Galaxy
Seyfert Galaxy
based on integrated exposure
(100 MeV to 100 GeV) from
August 4, 2008, to July 31, 2010.
TS > 25
Nova
PSR
PWN
PSR w/PWN
SNR
Globular Cluster
HMB
Unassociated
Possible Association with SNR and PWN
14
Credit: Fermi Large Area Telescope Collaboration

4 years sky

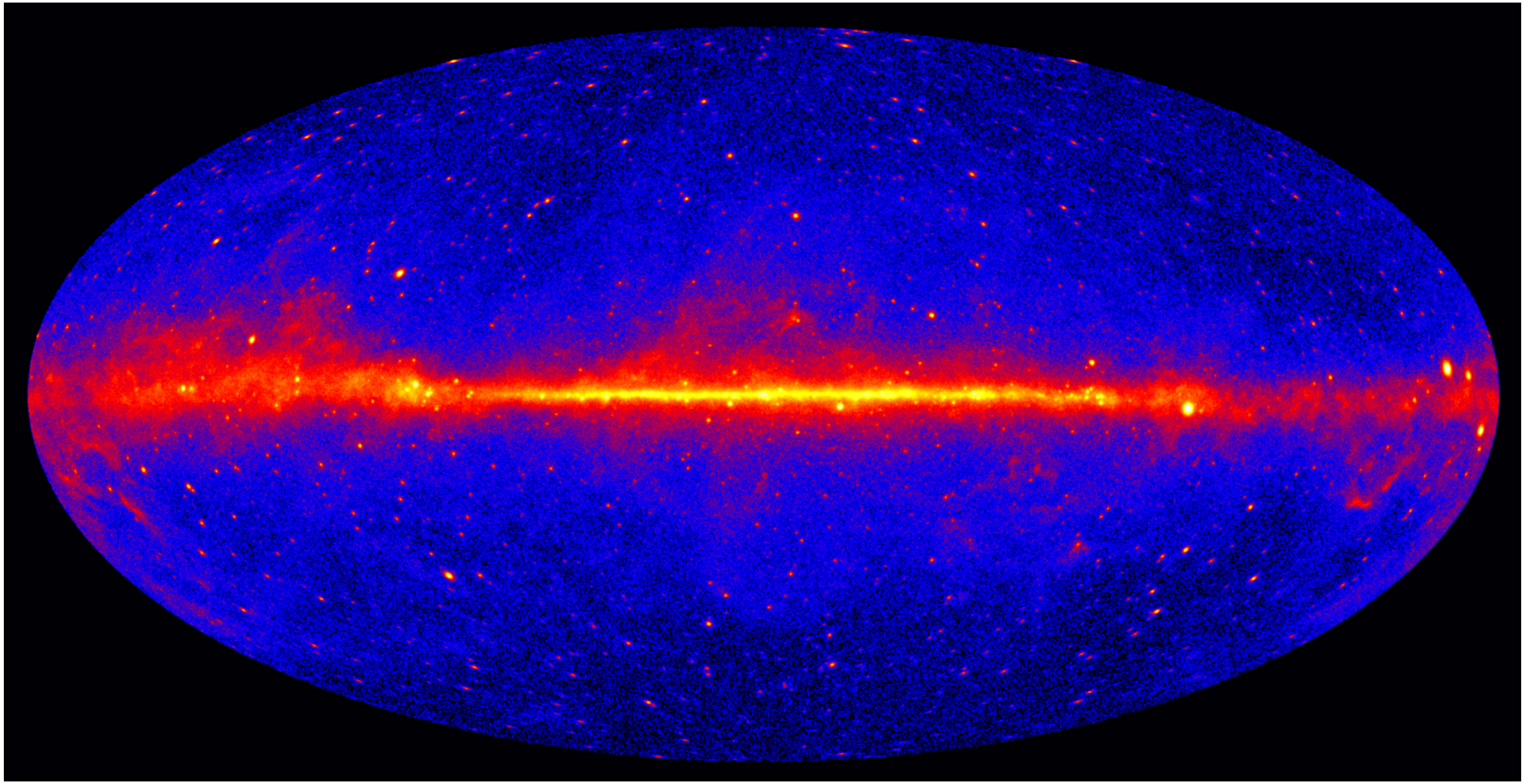

3FGL catalog – 3033 sources

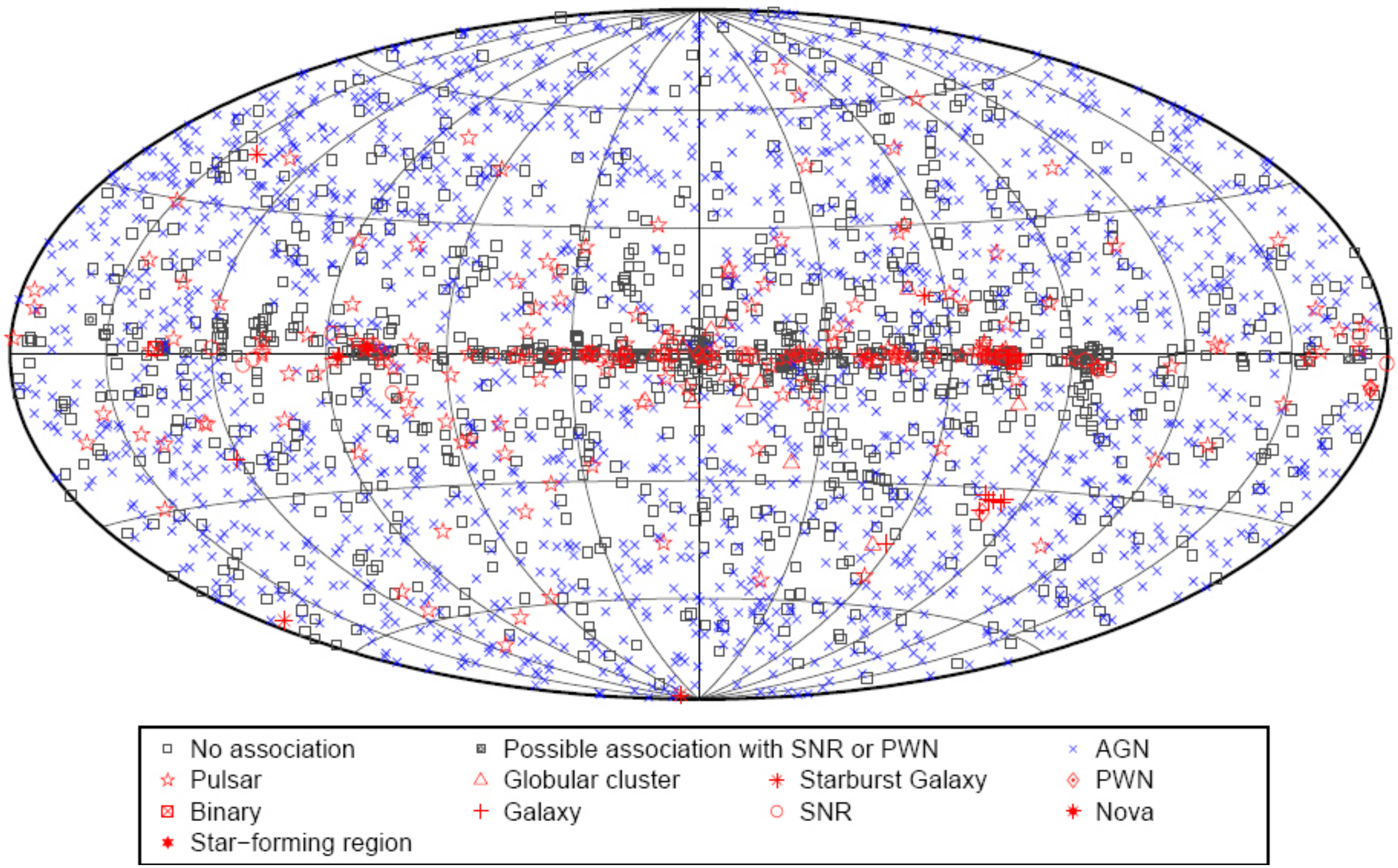

4FGL catalog

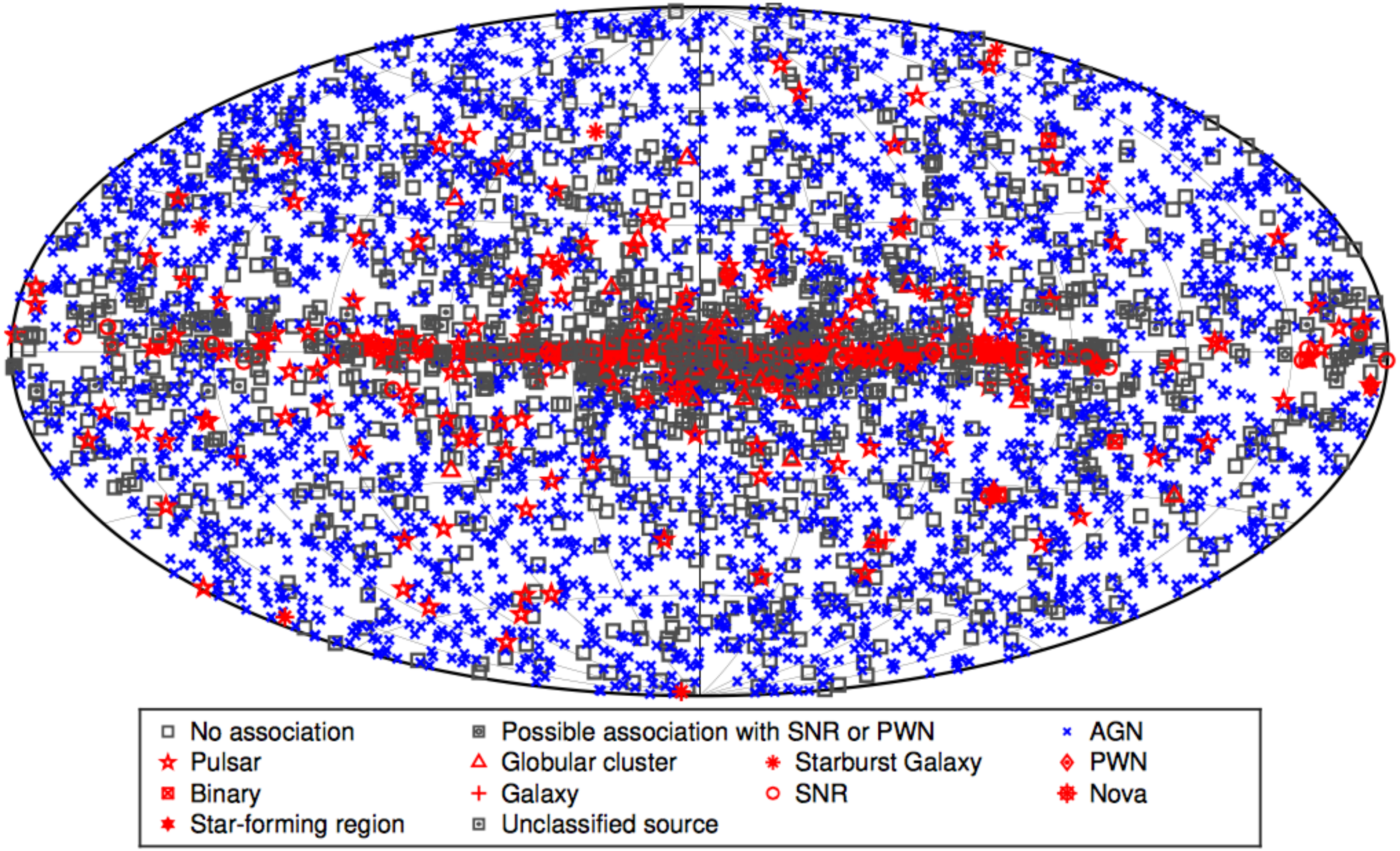

The LAT collaboration, in prep.

1 FHL (3 years, Pass7, E>10 GeV)

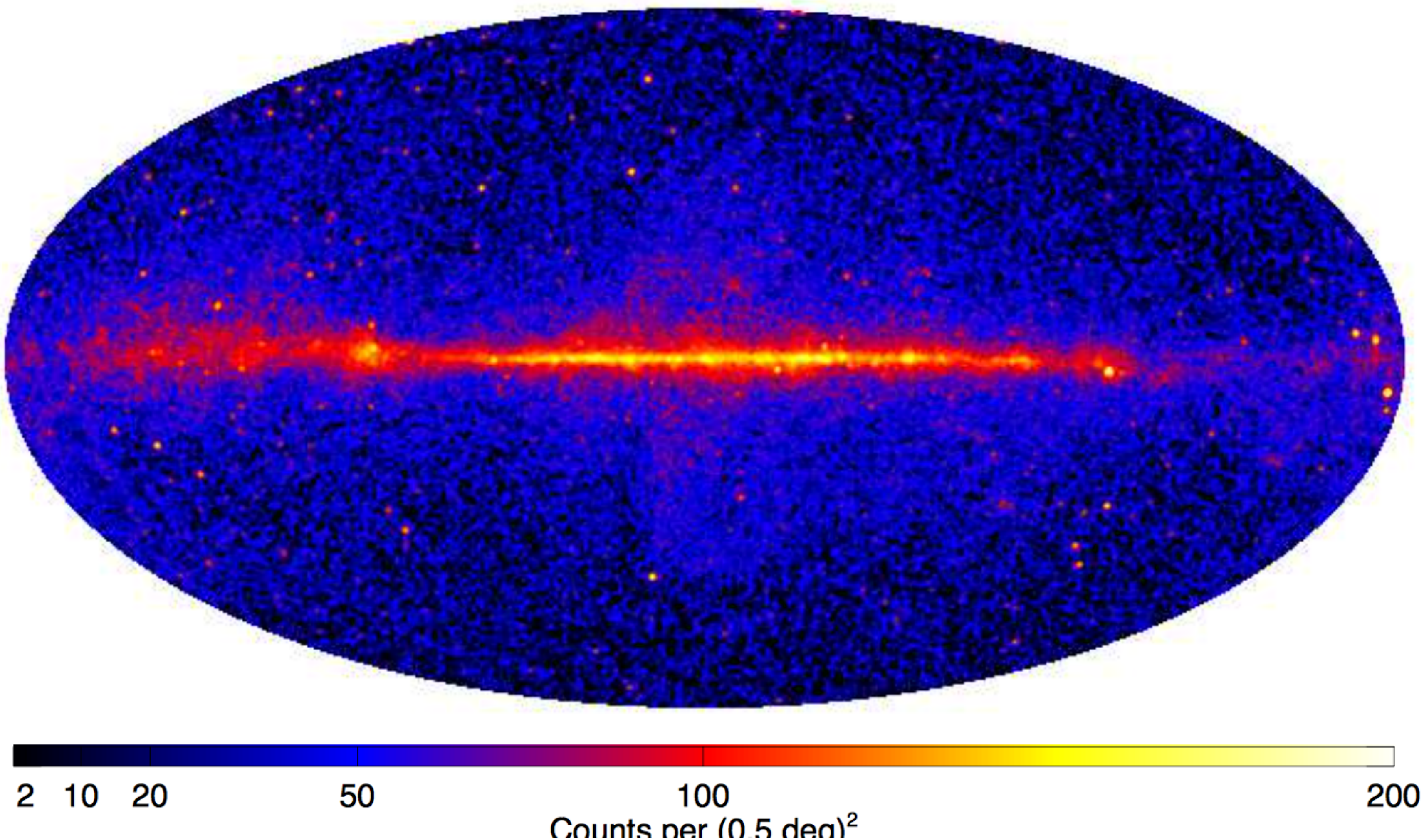

2FHL (P8 data >50 GeV) – 80 months

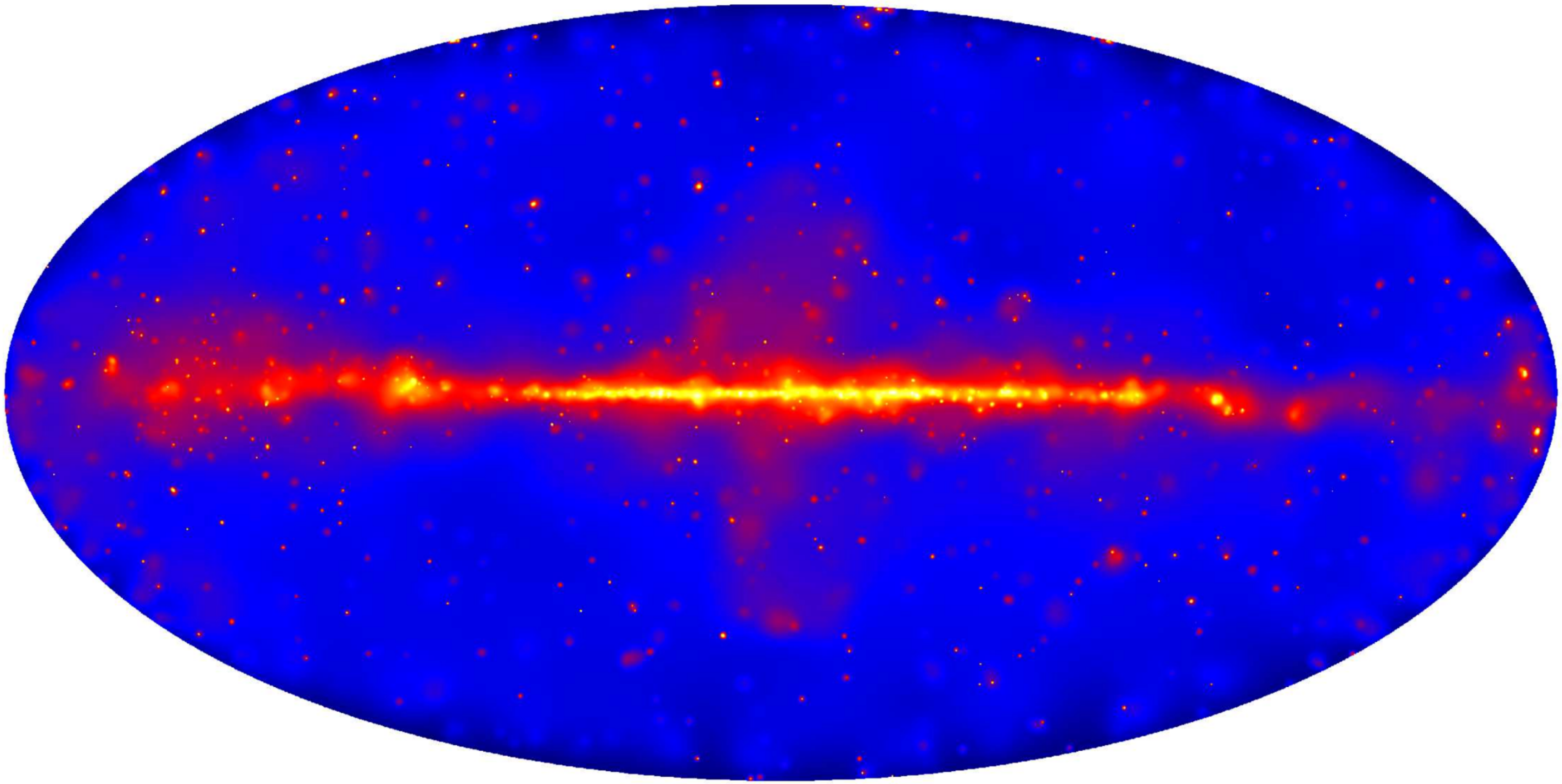

3FHL (E>10 GeV – P8)

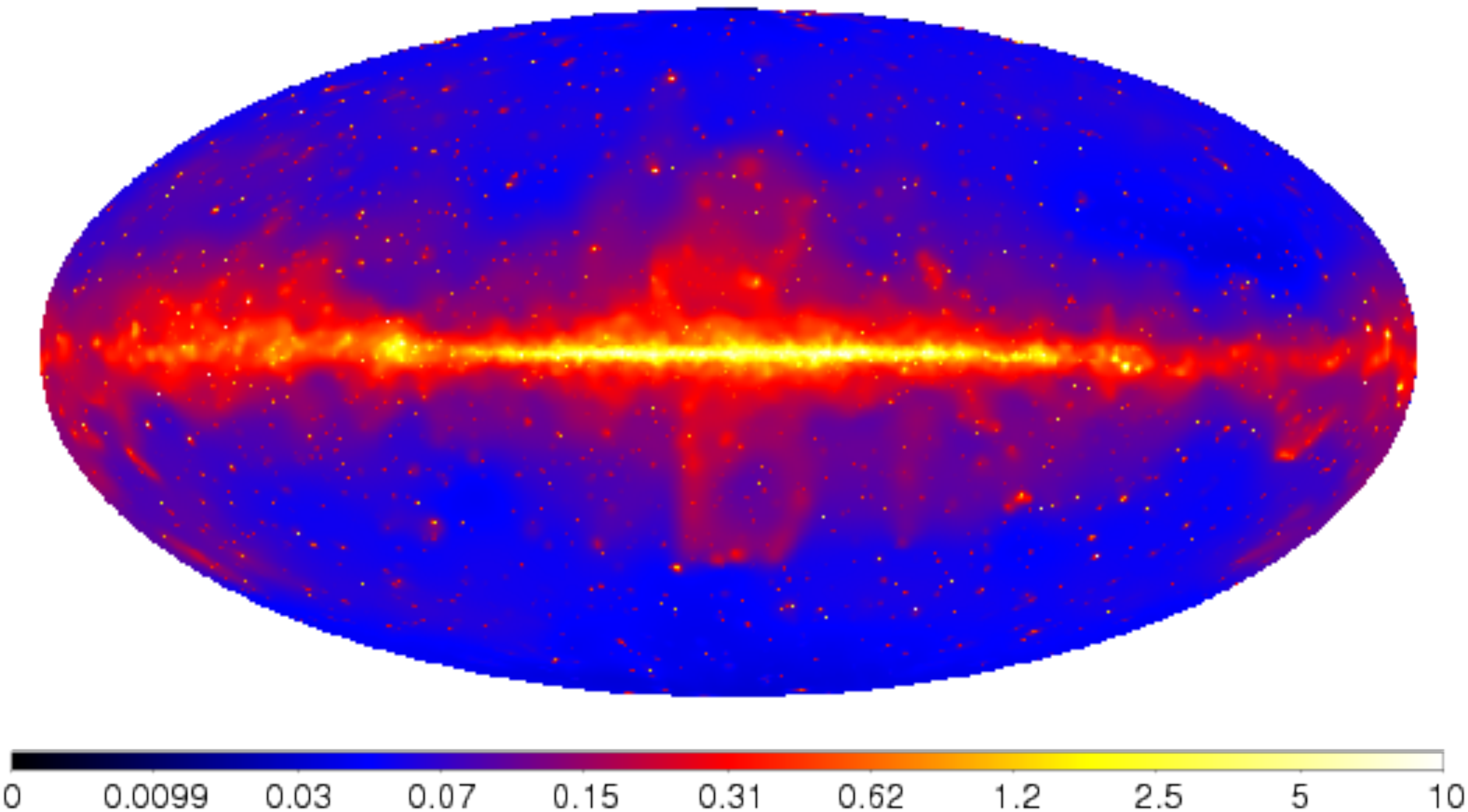

3 FHL

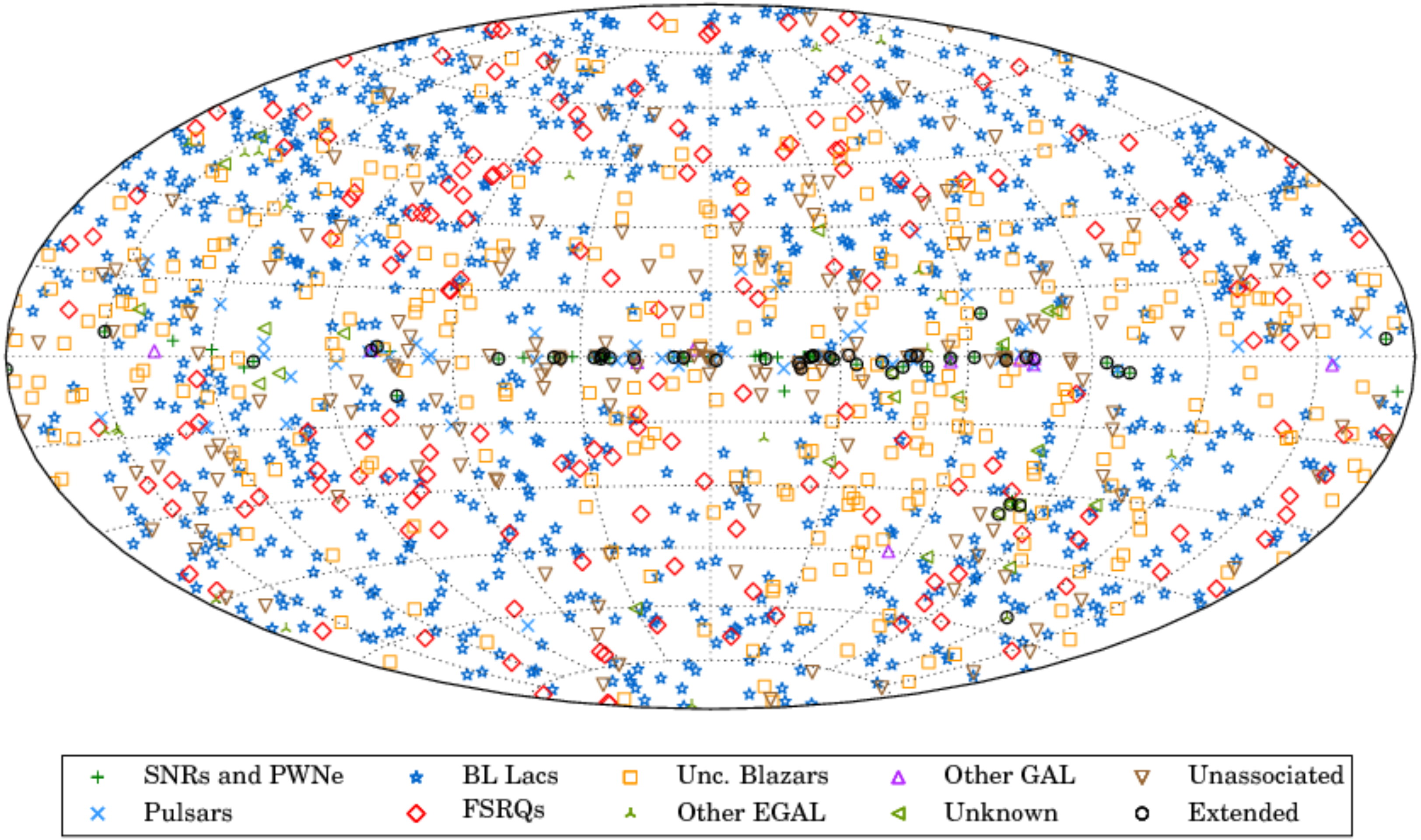

SNRs and PWNe
Pulsars
BL Lacs
FSRQs
Unc. Blazars
Other EGAL
Other GAL
Unknown
Unassociated
Extended

Challenge # 1 – AGN

Joint campaign on PKS 2155 with HESS

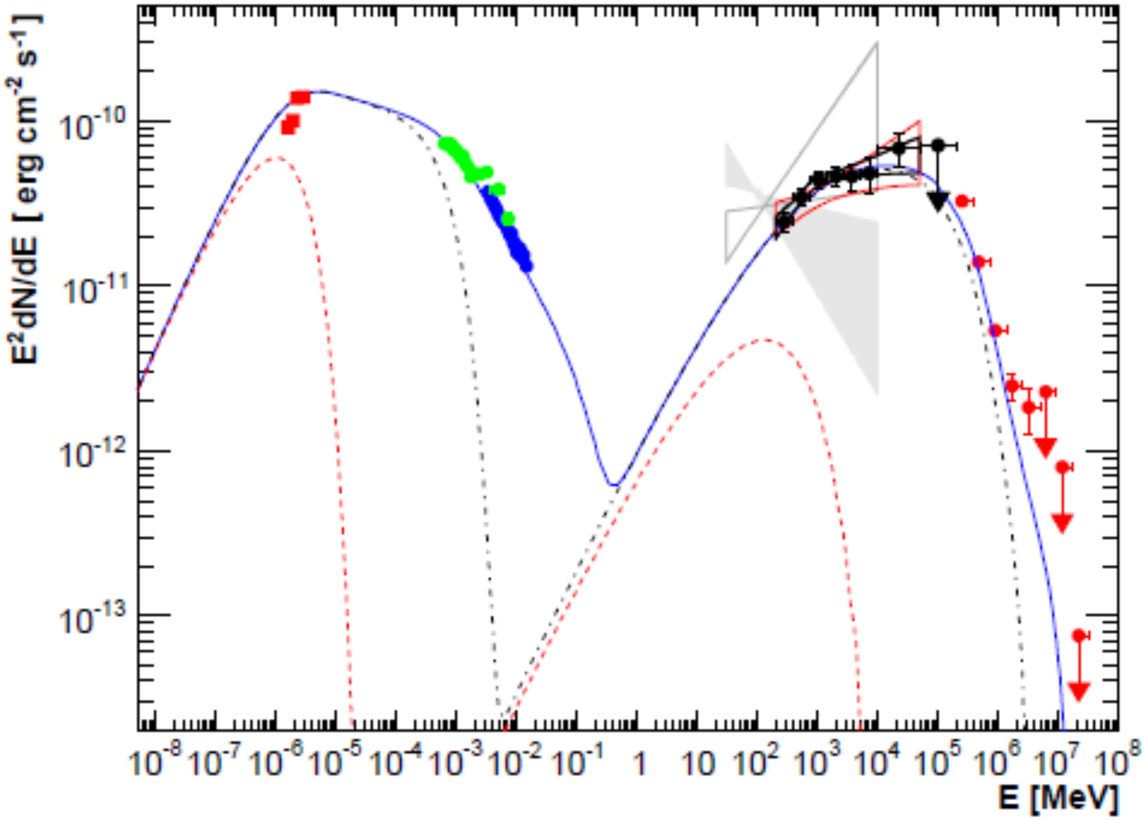

Aharonian et al. 2009

Challenge # 2 – Pulsars Blind Search

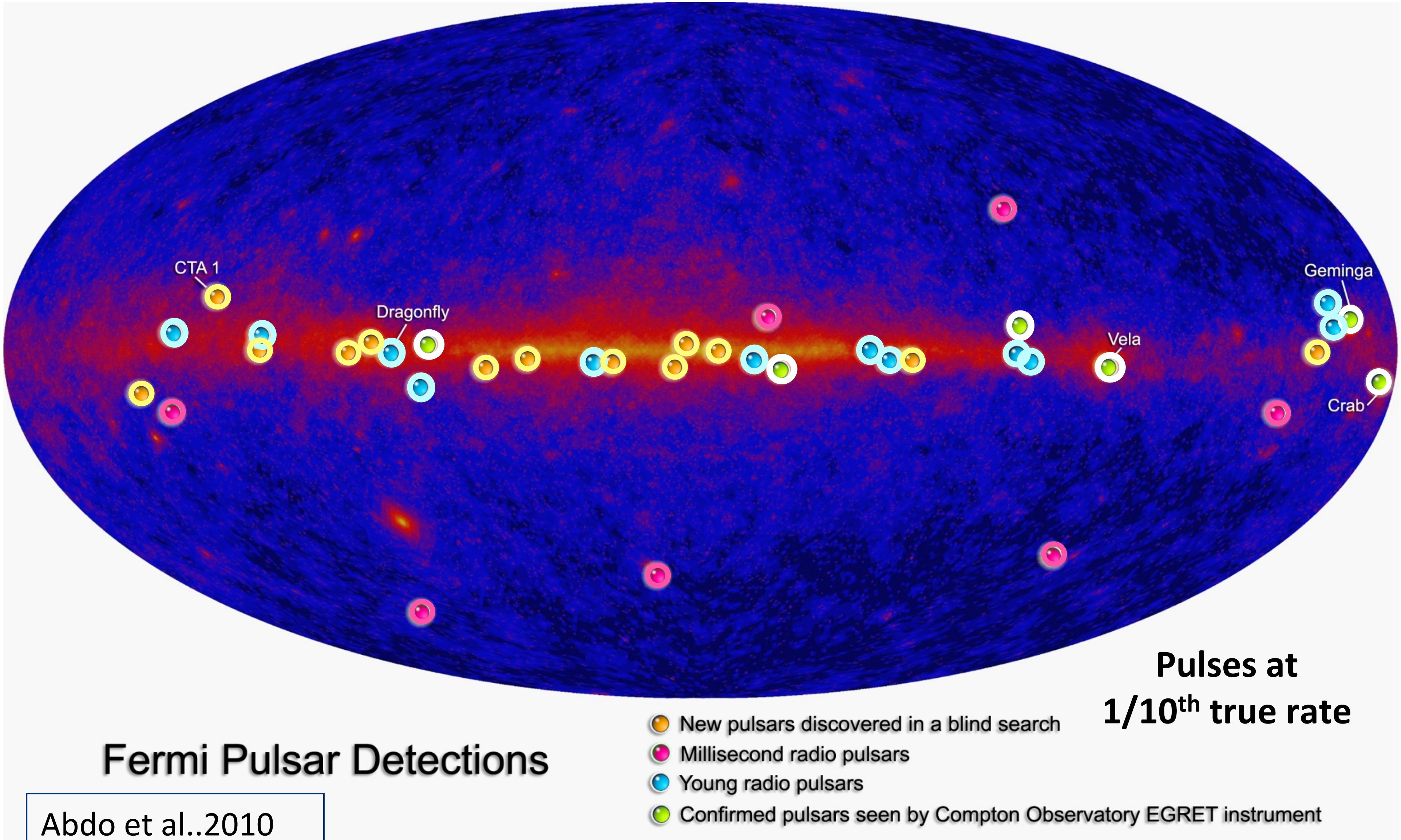

Pulses at $1/10^{th}$ true rate

Abdo et al..2010

The first blind ms Pulsar

The PSR J1311-3430 system (1/2)

- Following the discovery:
  → pulsar timing to precisely measure the system parameters ( )

Parameter	Value
Right ascension (J2000.0) (hh:mm:ss)	13:11:45.7242(2)
Declination (J2000.0) (dd:mm:ss)	−34:30:30.350(4)
Spin frequency, f (Hz)	390.56839326407(4)
Frequency derivative, $\dot{f}$ (Hz s^{-1})	$-3.198(2) \times 10^{-15}$
Reference time scale	TDB
Reference time (MJD)	55266.90789575858
Orbital period P_{orb} (d)	0.0651157335(7)
Projected pulsar semi-major axis x (lt-s)	0.010581(4)
Time of ascending node T_{asc} (MJD)	56009.129454(7)
Eccentricity e	< 0.001
Data span (MJD)	54682 - 56119
Weighted RMS residual (μs)	17
Derived Quantities	
Companion mass m_c ($M_\odot$)	> 0.0082
Spin-down luminosity $\dot{E}$ (erg s^{-1})	4.9×10^{34}
Characteristic age τ_c (yr)	1.9×10^9
Surface magnetic field B_S (G)	2.3×10^8
Gamma-Ray Spectral Parameters	
Photon index, Γ	1.8 ± 0.1
Cutoff energy, E_c (GeV)	3.2 ± 0.4
Photon flux above 0.1 GeV, F (10^{-8} photons cm^{-2} s^{-1})	9.2 ± 0.5
Energy flux above 0.1 GeV, G (10^{-11} erg cm^{-2} s^{-1})	6.2 ± 0.2

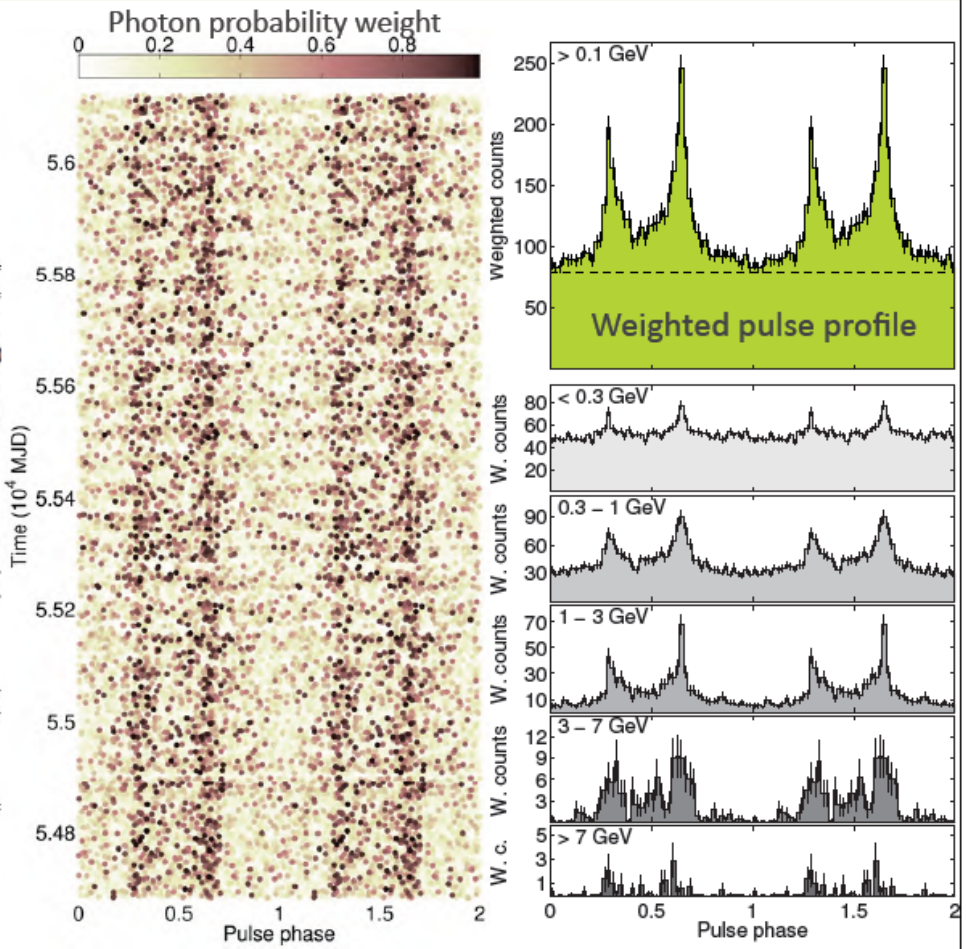

New MSP and GW detection

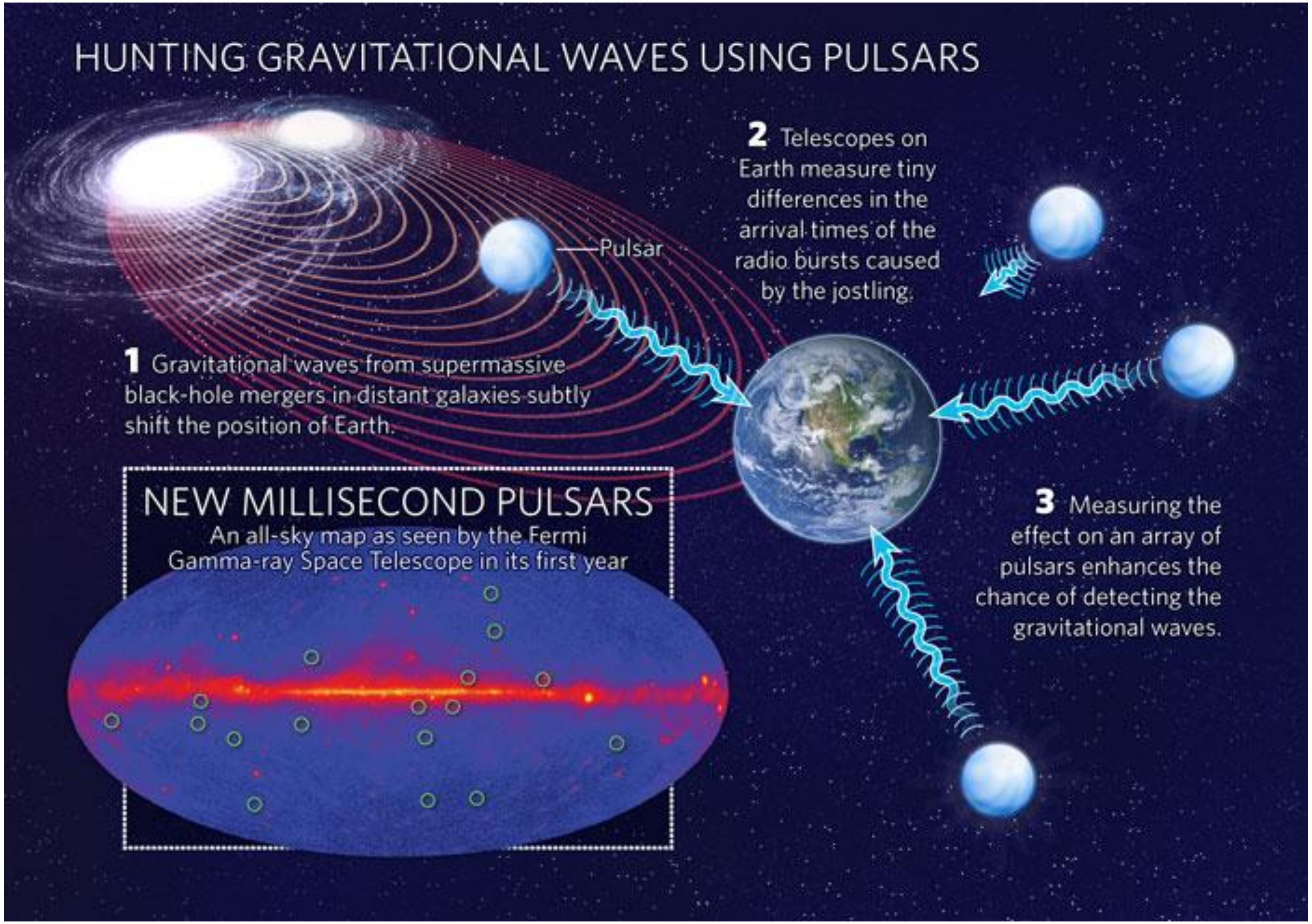

Challenge # 3 – GRB

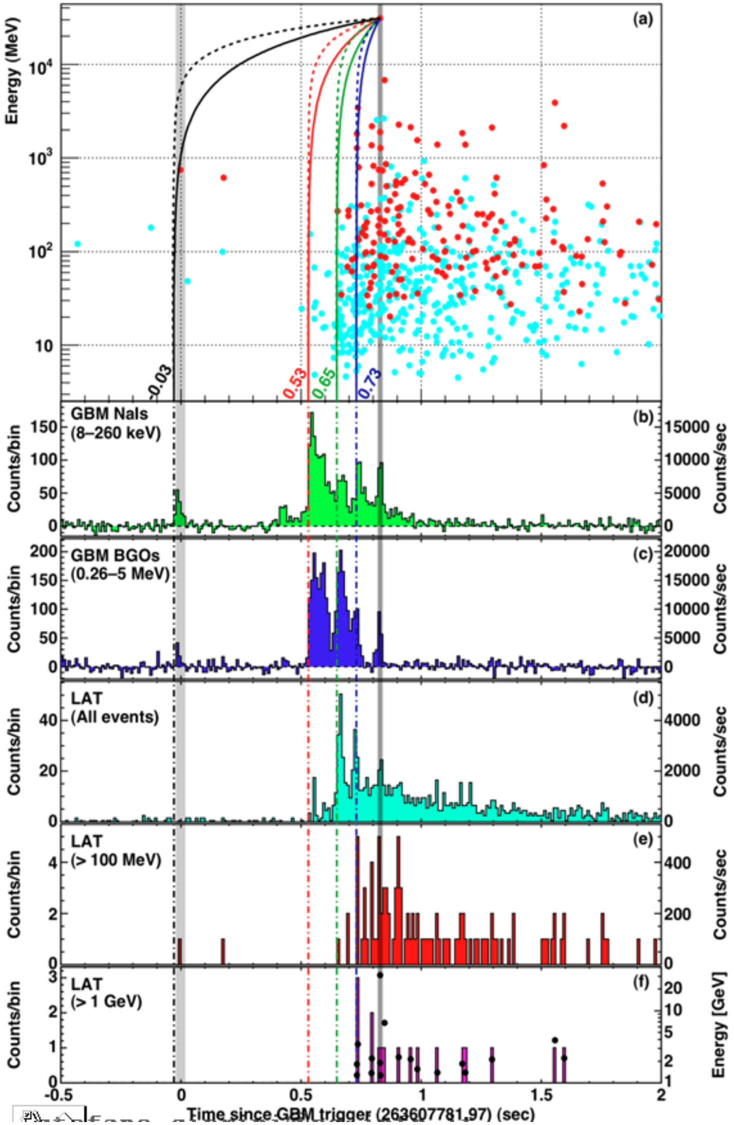

- This GRB is a perfect case for studying Lorentz Invariance Violation
  - z = 0.9 (5.381 Gyr)
  - Emission of 31 GeV photon after 859 ms since the trigger
- Only conservative assumption!
  - the HE photon is not emitted *before* the LE photons, at different events.

Table 2 | Limits on Lorentz Invariance Violation

#	$t_{start} - T_0$ (ms)	Limit on $\|\Delta t\|$ (ms)	Reasoning for choice of t_{start} or limit on Δt or $\|\Delta t/\Delta E\|$	E_l † (MeV)	Valid for s_n *	Lower limit on $M_{QG,1}/M_{Planck}$
(a)✧	−30	< 859	start of any < 1 MeV emission	0.1	1	> 1.19
(b)✧	530	< 299	start of main < 1 MeV emission	0.1	1	> 3.42
(c)✧	*648*	< 181	start of main > 0.1 GeV emission	100	1	> 5.63
(d)✧	730	< 99	start of > 1 GeV emission	1000	1	> 10.0
(e)♦	—	< 10	association with < 1 MeV spike	0.1	±1	> 102
(f)♦	—	< 19	If 0.75 GeV‡ γ-ray from 1st spike	0.1	−1	> 1.33
(g)♠	$\|\Delta t/\Delta E\|$ < 30 ms/GeV		lag analysis of > 1 GeV spikes	—	±1	> 1.22

GRB080916C - Multiple detector light curve

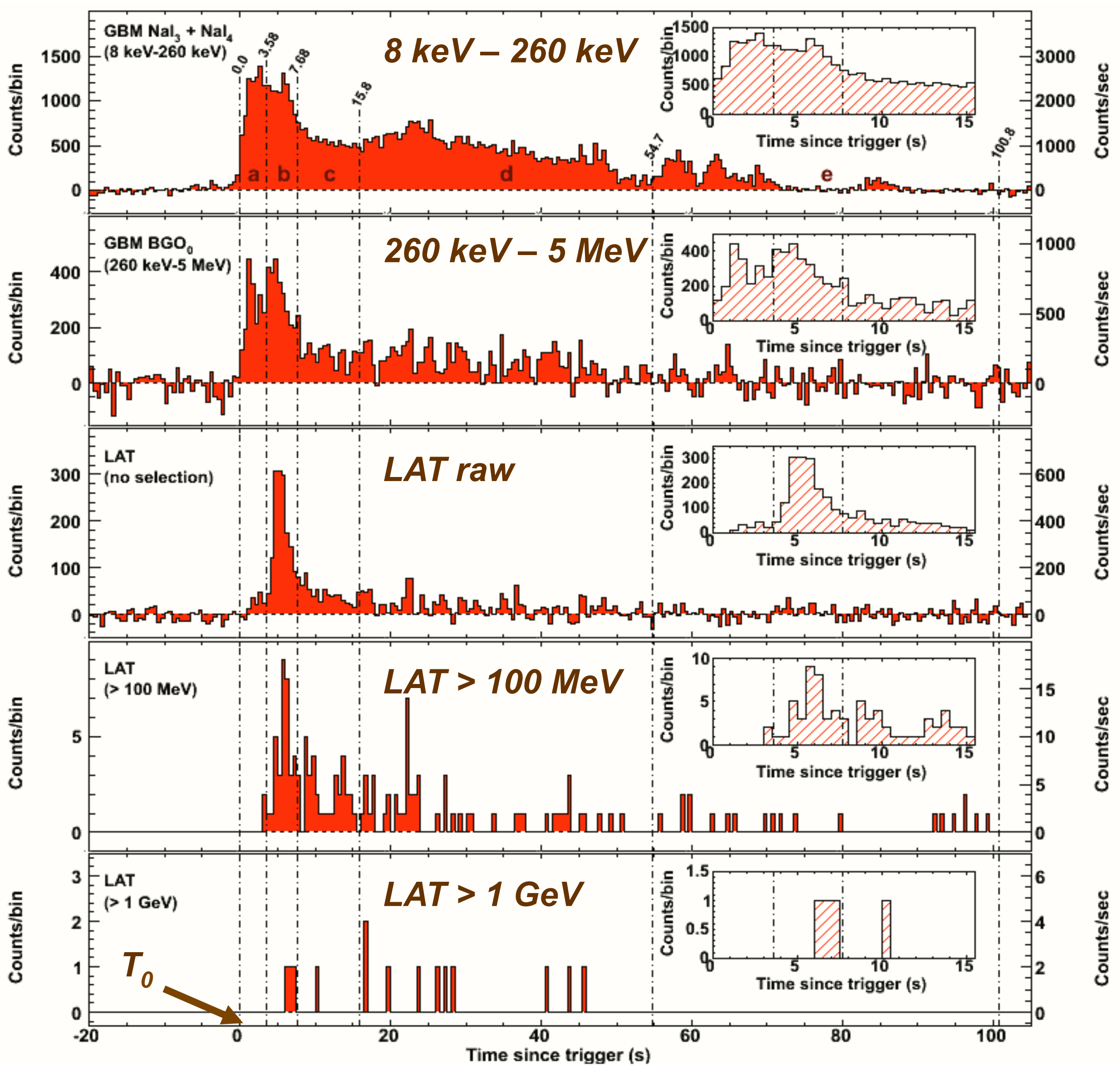

First 3 light curves are background subtracted

The LAT can be used as a counter to maximize the rate and to study time structures above tens of MeV

- **The first low-energy peak is not observed at LAT energies**

Spectroscopy needs LAT event selection (>100 MeV)

- **14 events above 1 GeV**

Multiple detector light curve

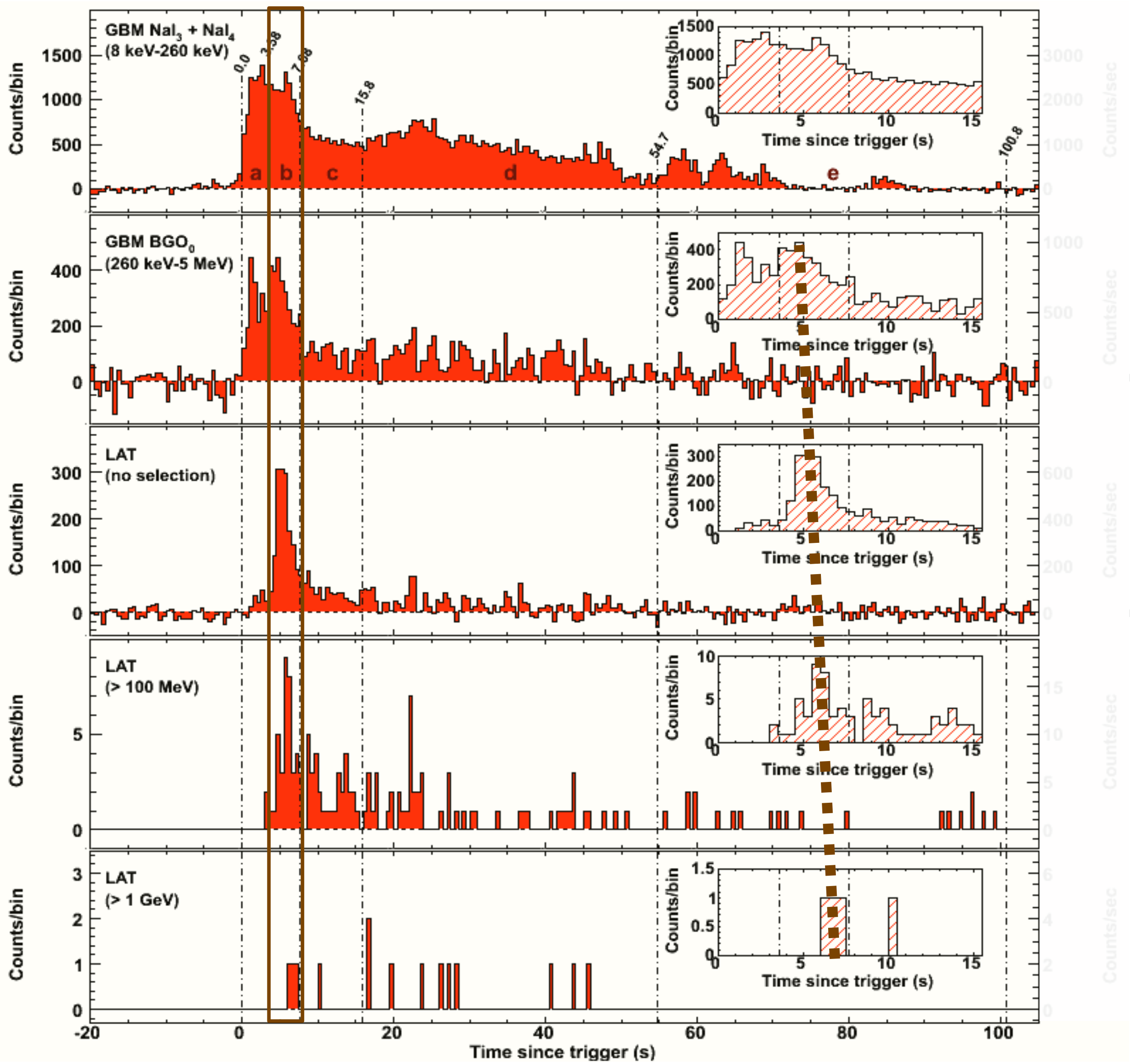

- The bulk of the emission of the 2nd peak is moving **toward later times as the energy increases**
- Clear signature of **spectral evolution**

GRB 130427A

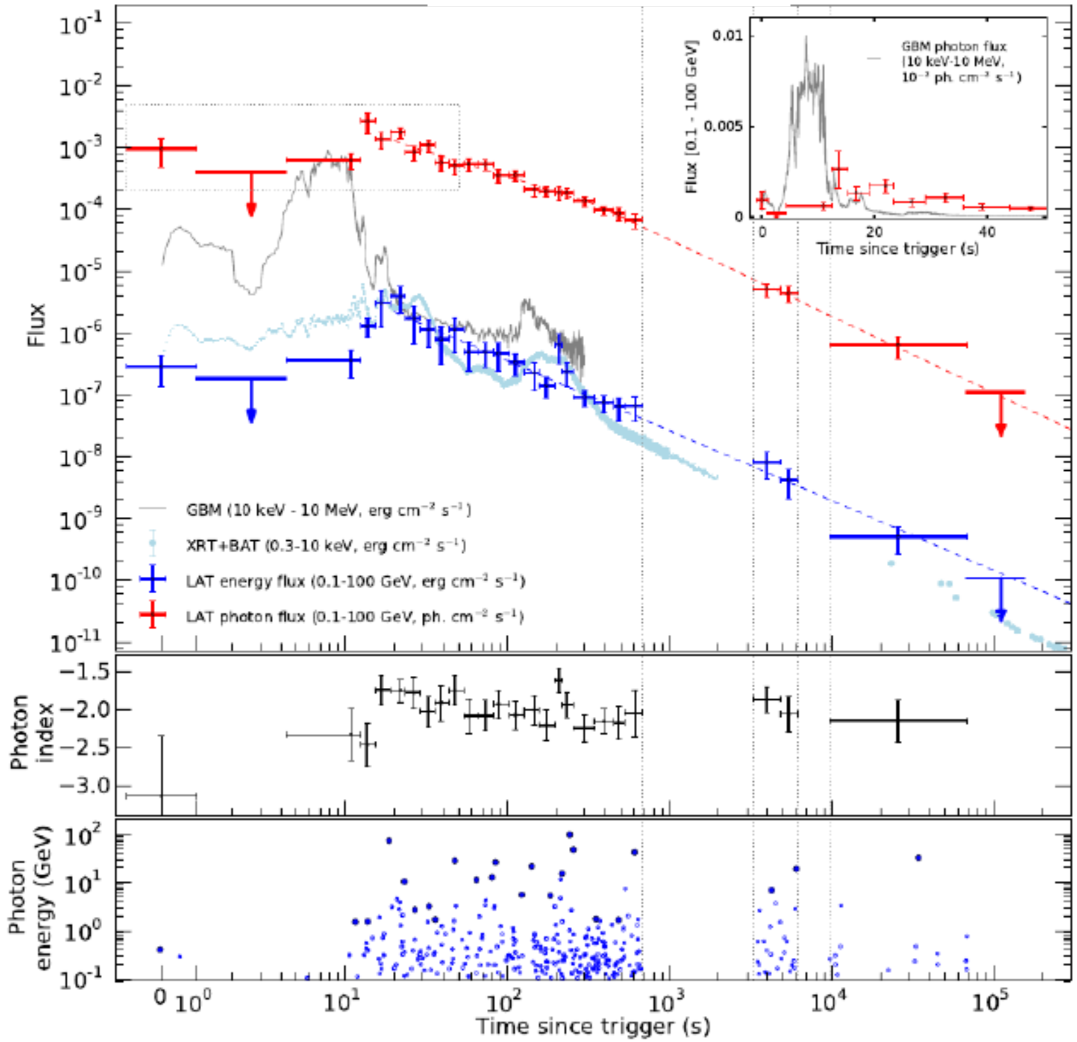

(Ackermann et al., Science, Vol. 343 no. 6166 pp. 42-47)

GRB 130427A

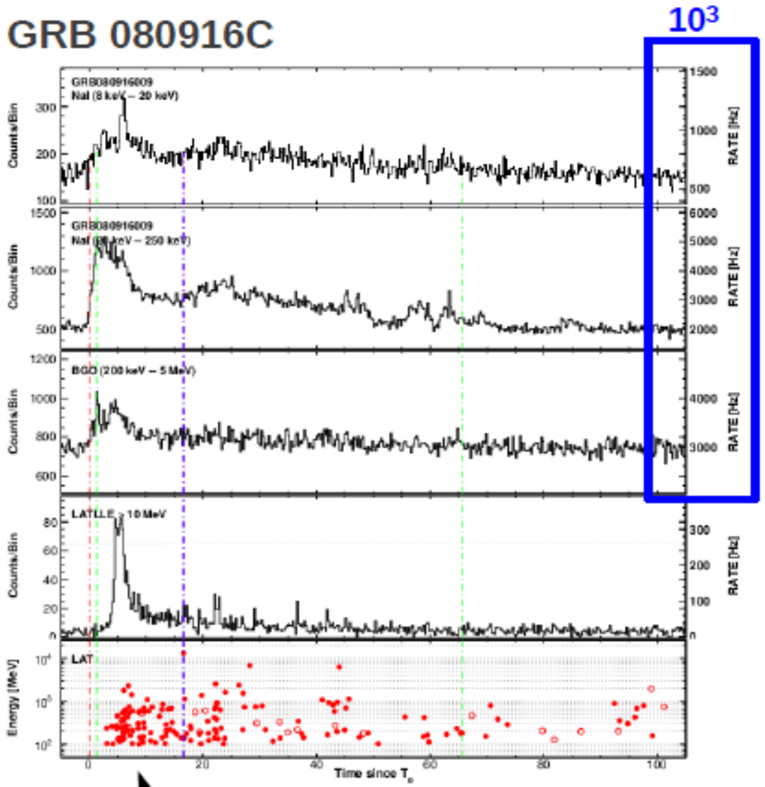

LAT emission dying down

LAT and GBM are bright at the same time

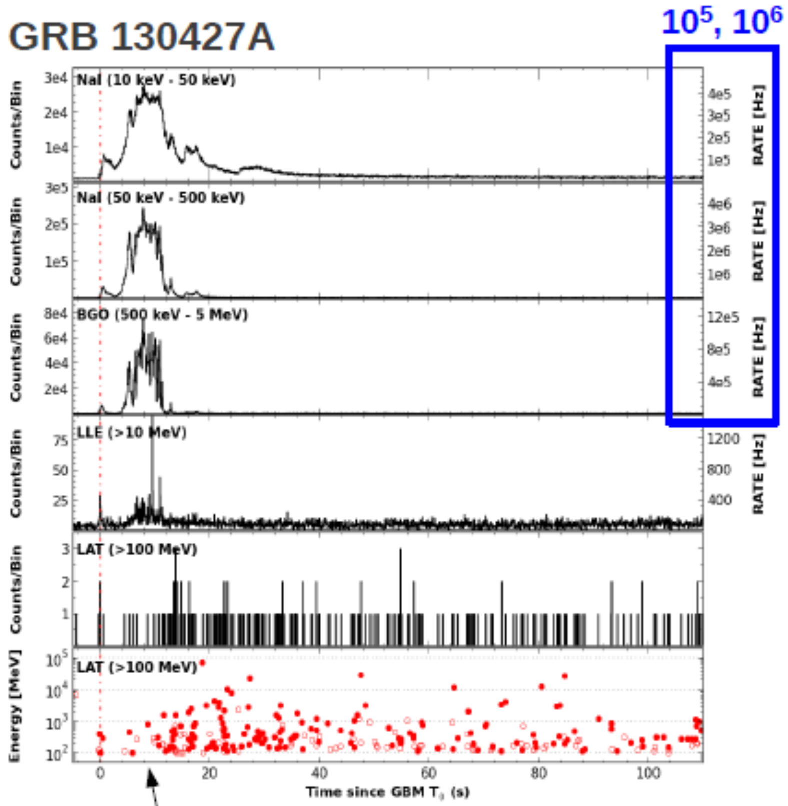

LAT emission still going

Very little LAT emission when GBM emission is bright

Challenge # 4 – Unidentified

CTA 1 Discovery

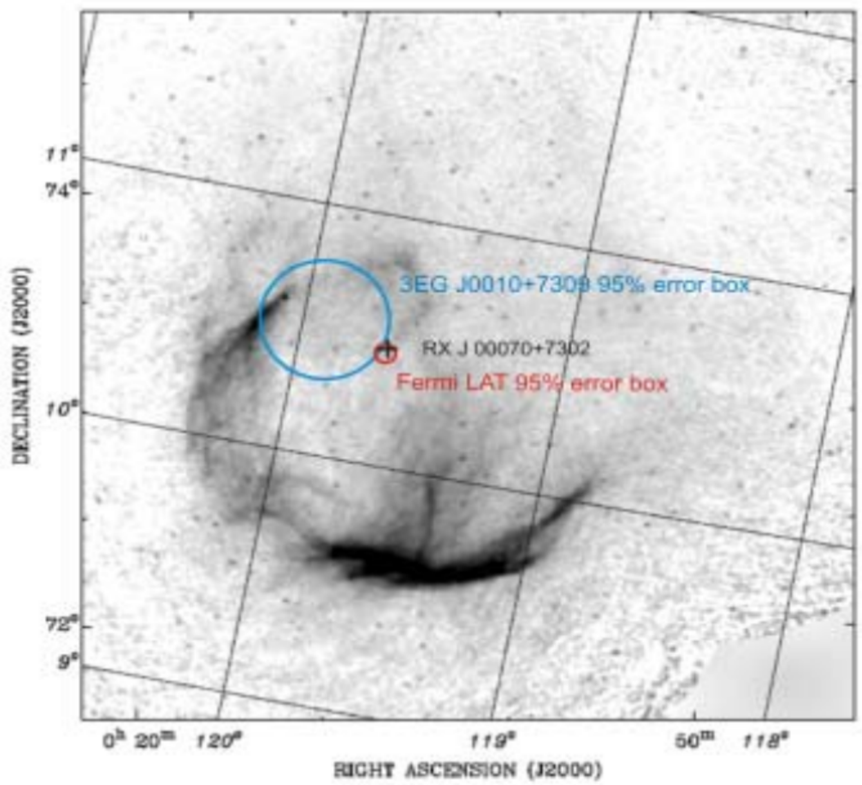

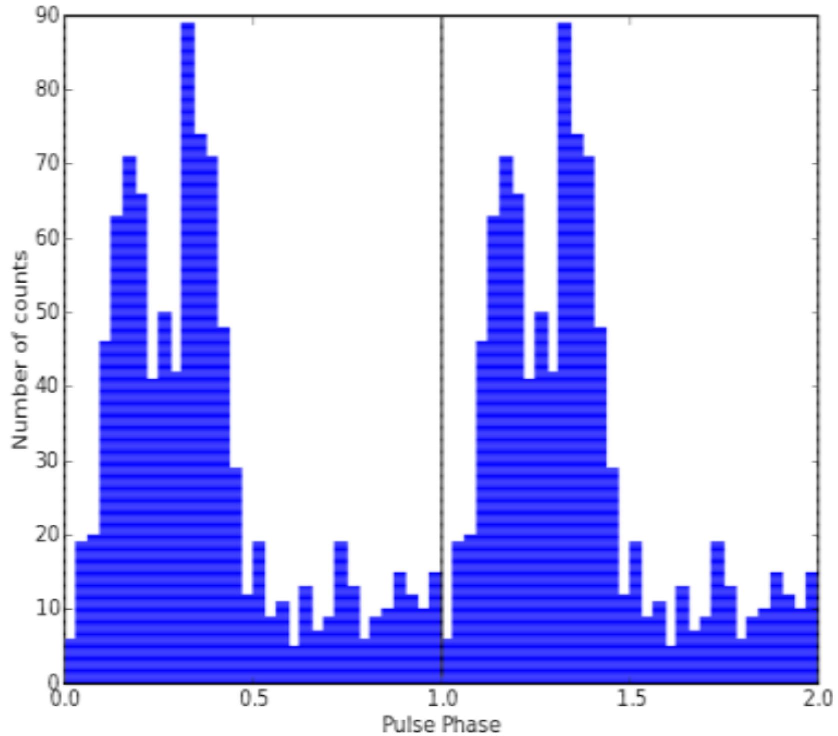

Abdo et al. 2008

Challenge # 4
Location of Gamma-ray emission

Observations of the Large Magellanic Cloud with *Fermi*

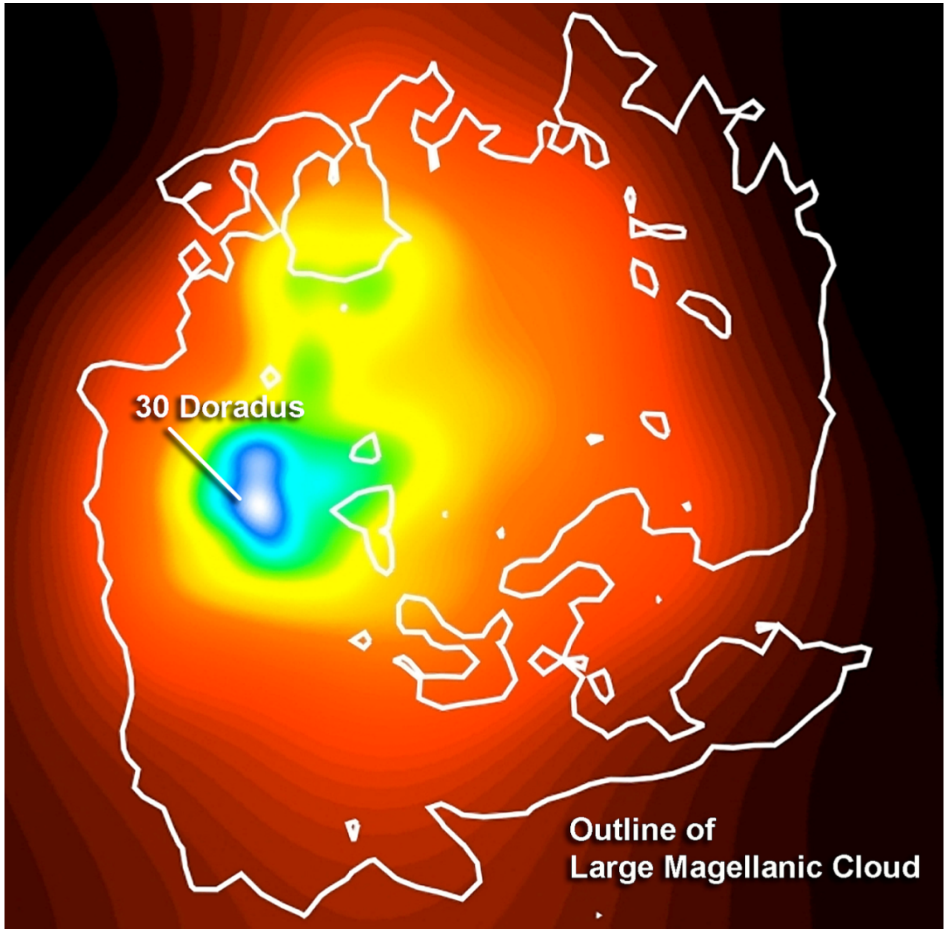

Abdo, A. A. et al. 2010

Challenge # 4
Location of Gamma-ray emission

Gamma-Ray Emission from the Shell of Supernova Remnant W44 Revealed by the Fermi LAT

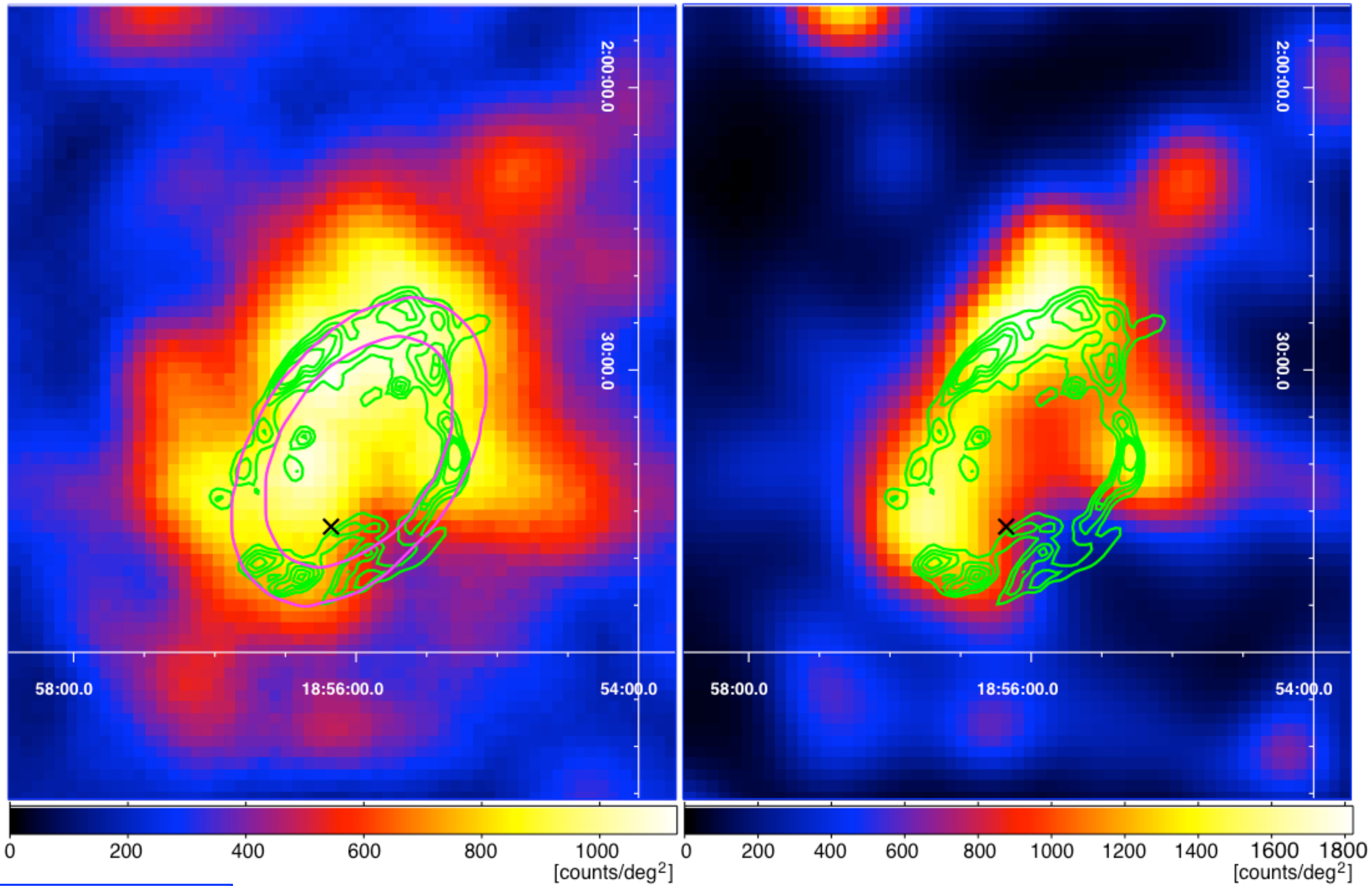

Abdo, A. A. et al. 2010

Challenge # 5 – Spectral Resolution

Fermi Large Area Telescope Measurements of the Diffuse Gamma-Ray Emission at Intermediate Galactic Latitudes

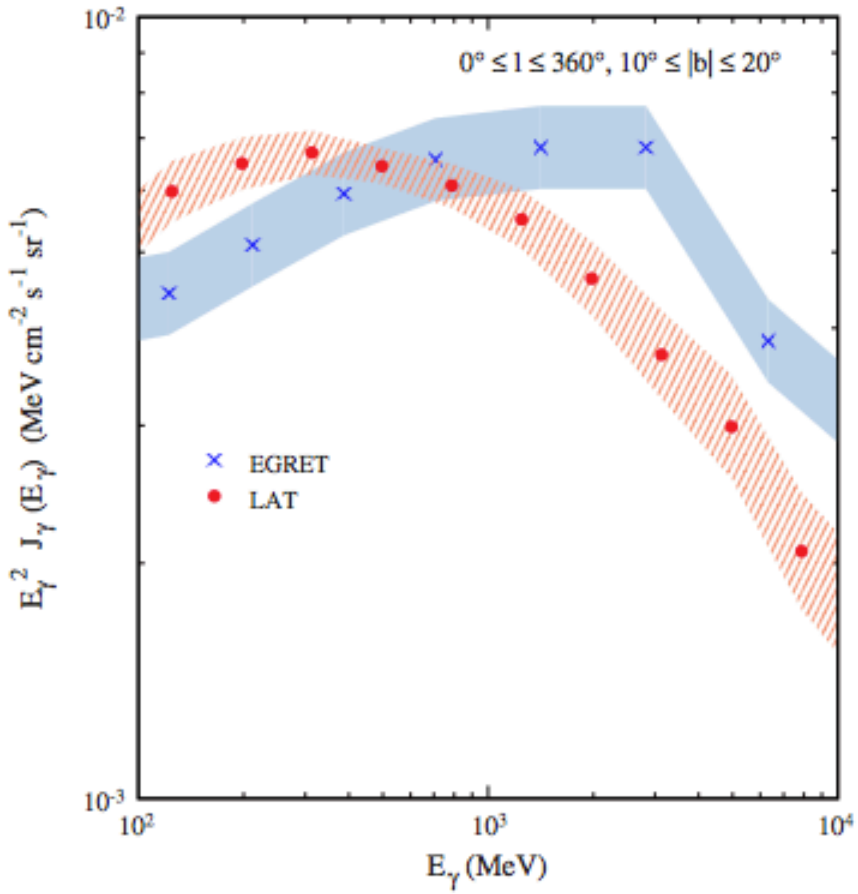

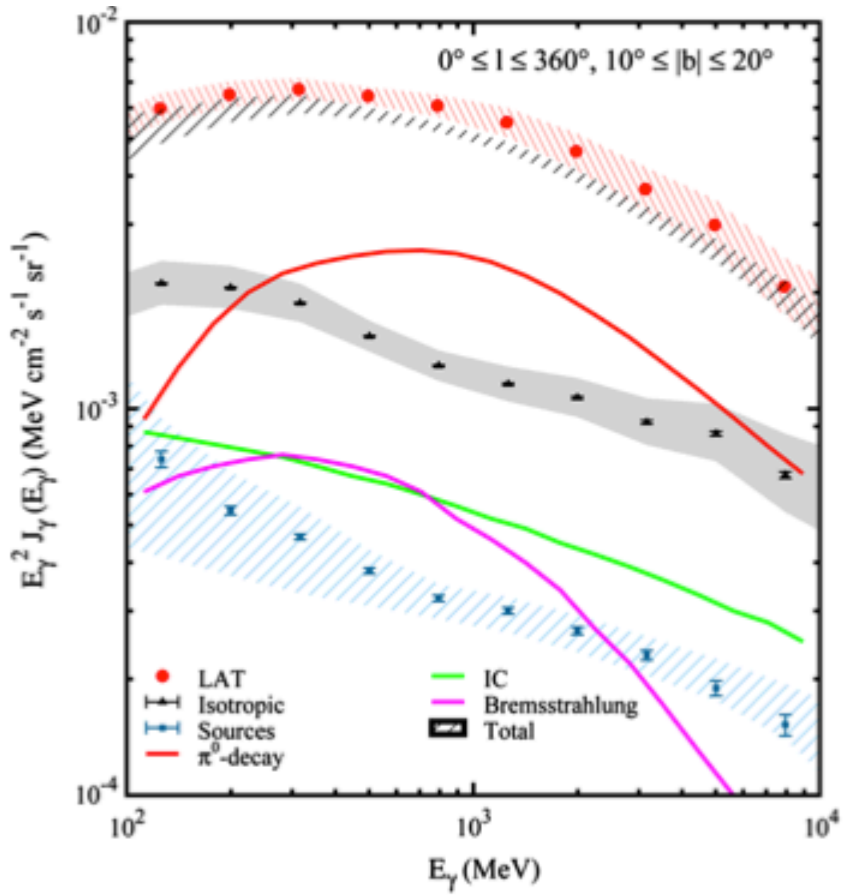

Abdo, A. A. et al. 2009

Cosmic Rays – Gamma-rays connection

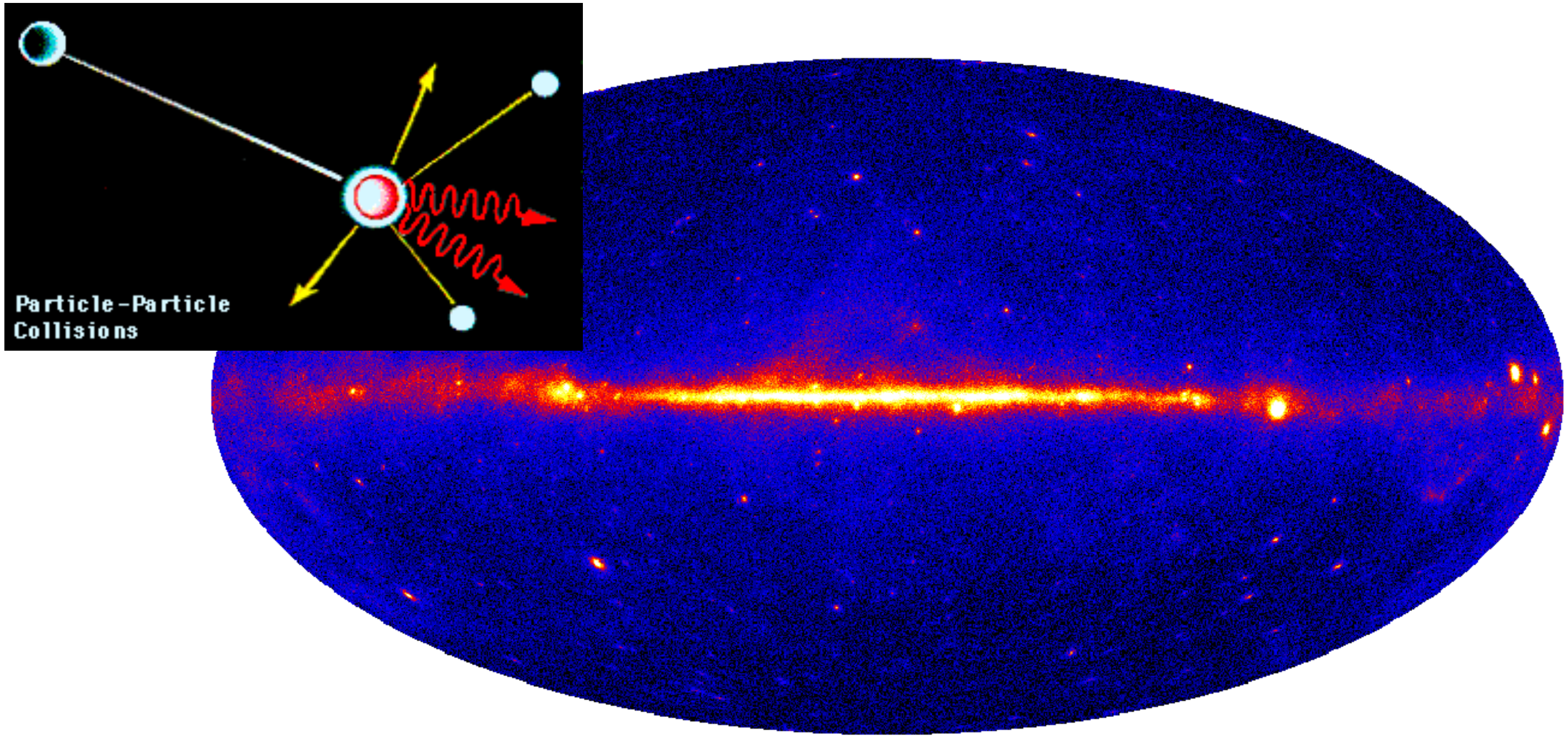

- **Galactic gamma rays trace cosmic-ray proton interactions (cosmic-ray acceleration sites & propagation)**
- **Observations of nearby galaxies provide an outside view**
- **Primary targets: galactic plane, starburst galaxies, LMC, SNR**
- **Direct CR observations**

Supernova Remnants

Ackermann et al. 2013

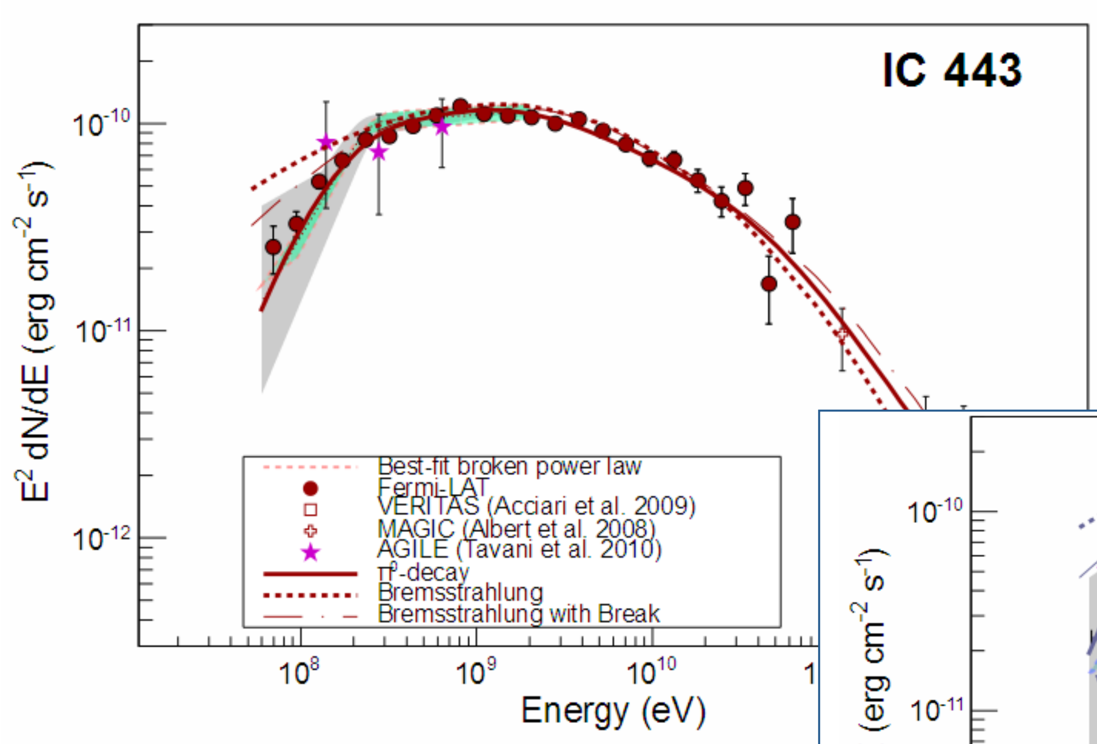

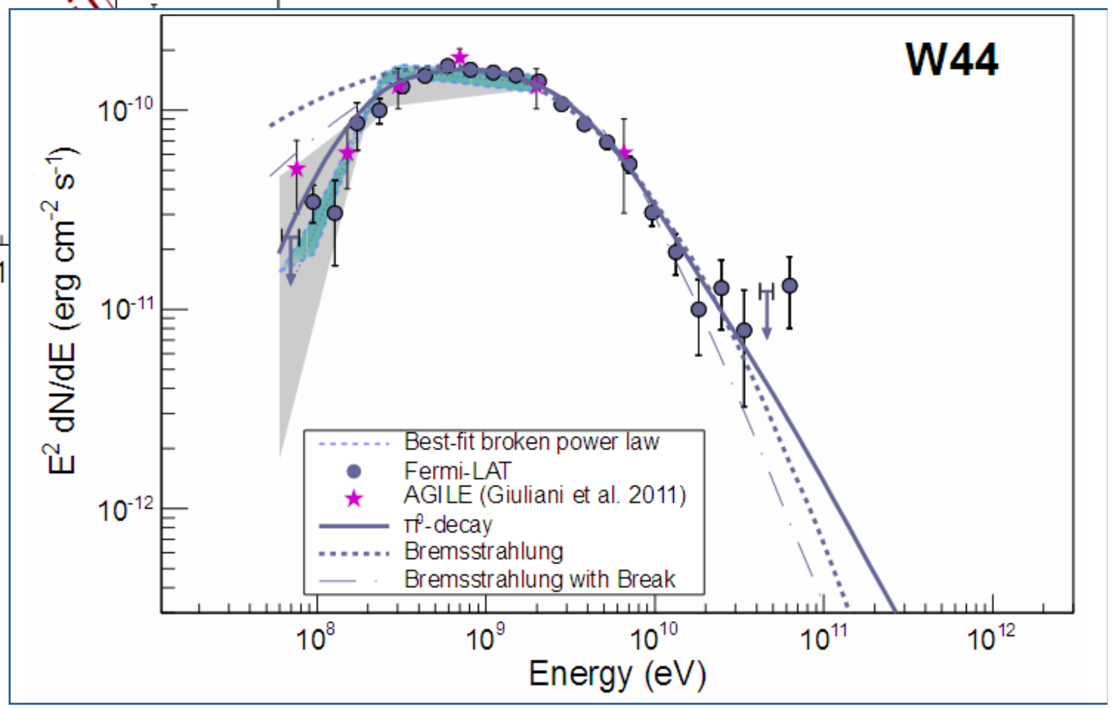

Science Perspectives

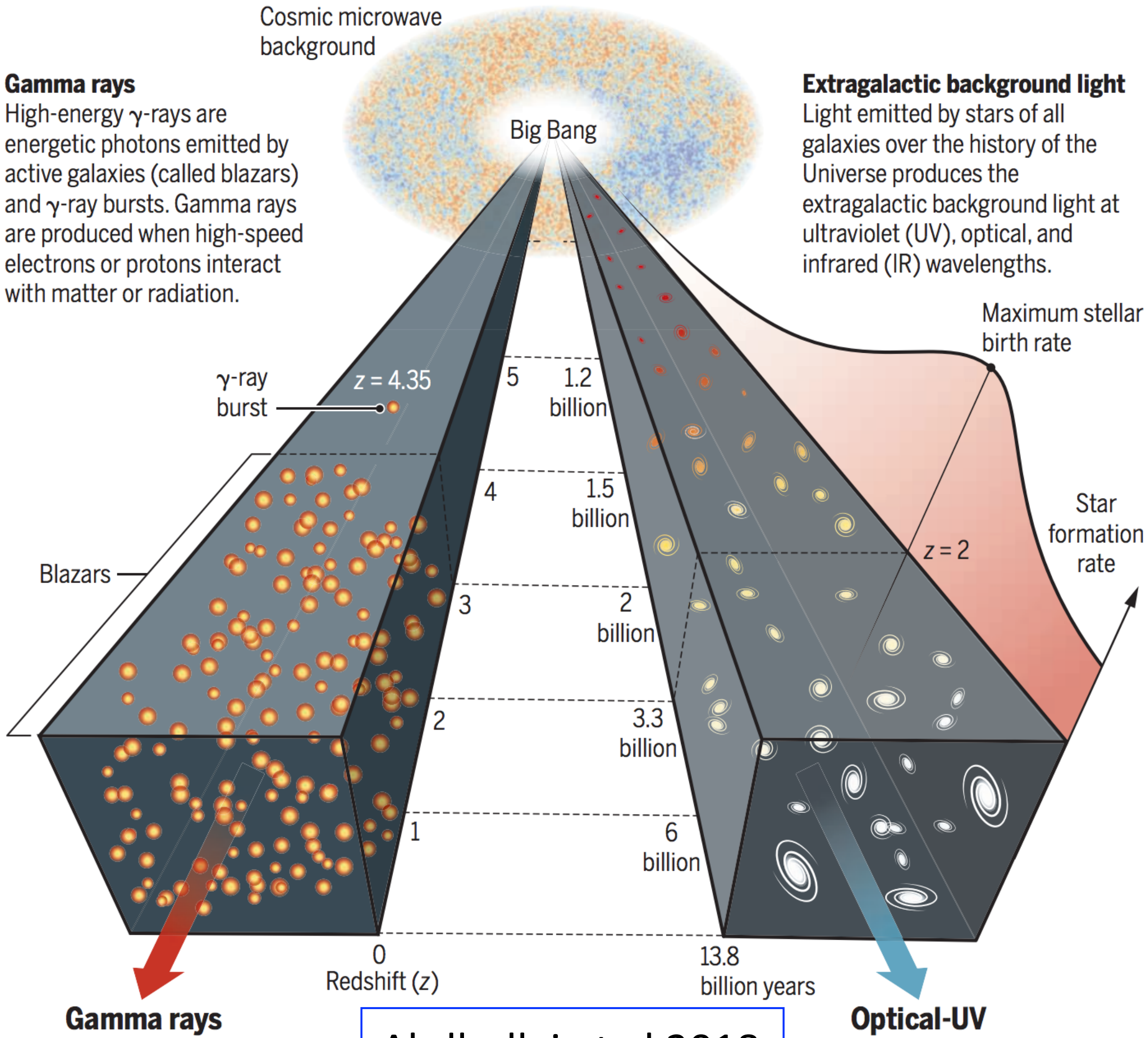

Abdhollai et al 2018

The Extragalactic Background Light

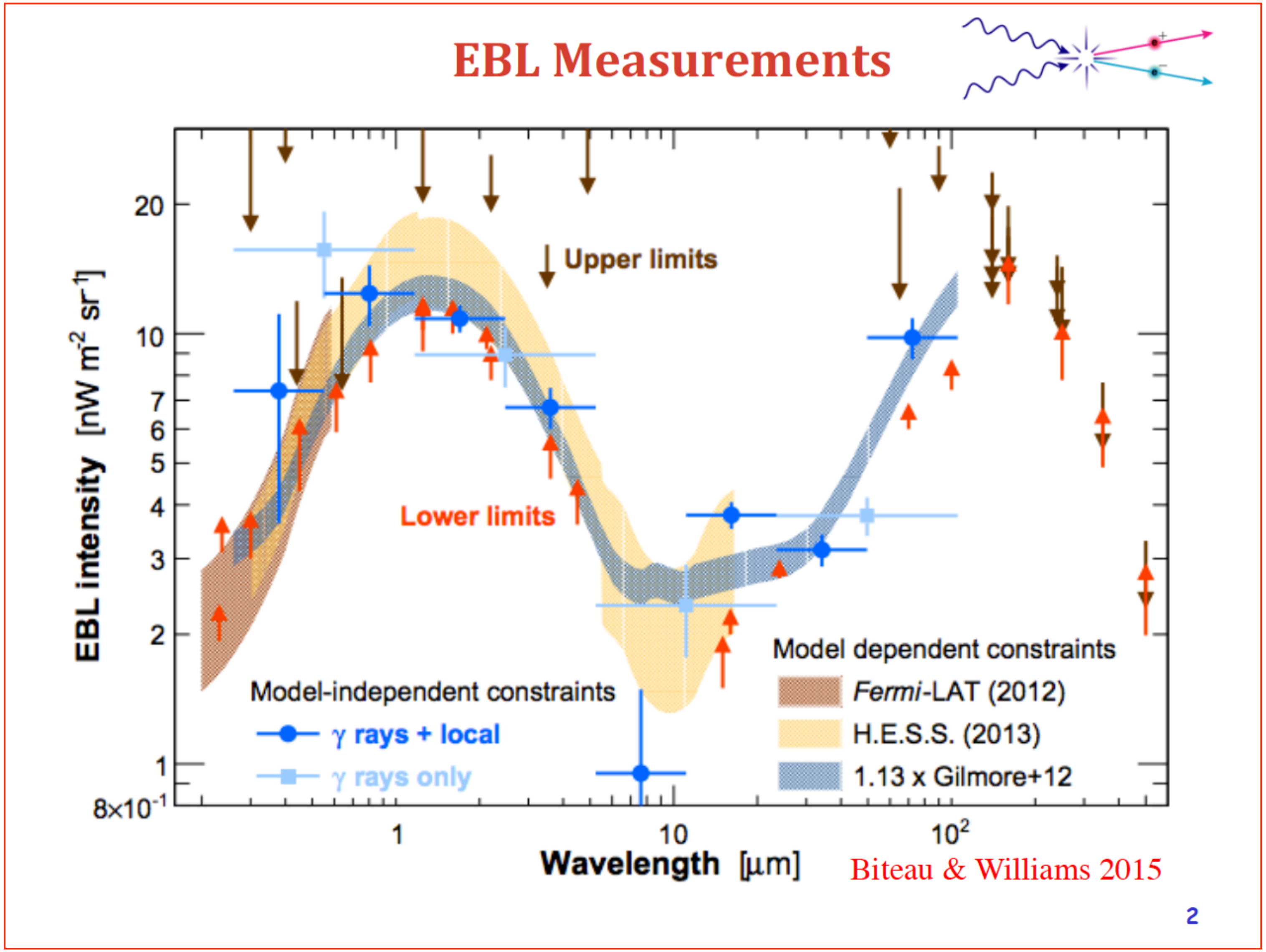

Dark Matter Searches

Gamma-ray indirect emission

Satellites
Low background and good source id, but low statistics, astrophysical background

Galactic Center
Good Statistics but source confusion/diffuse background

Milky Way Halo
Large statistics but diffuse background

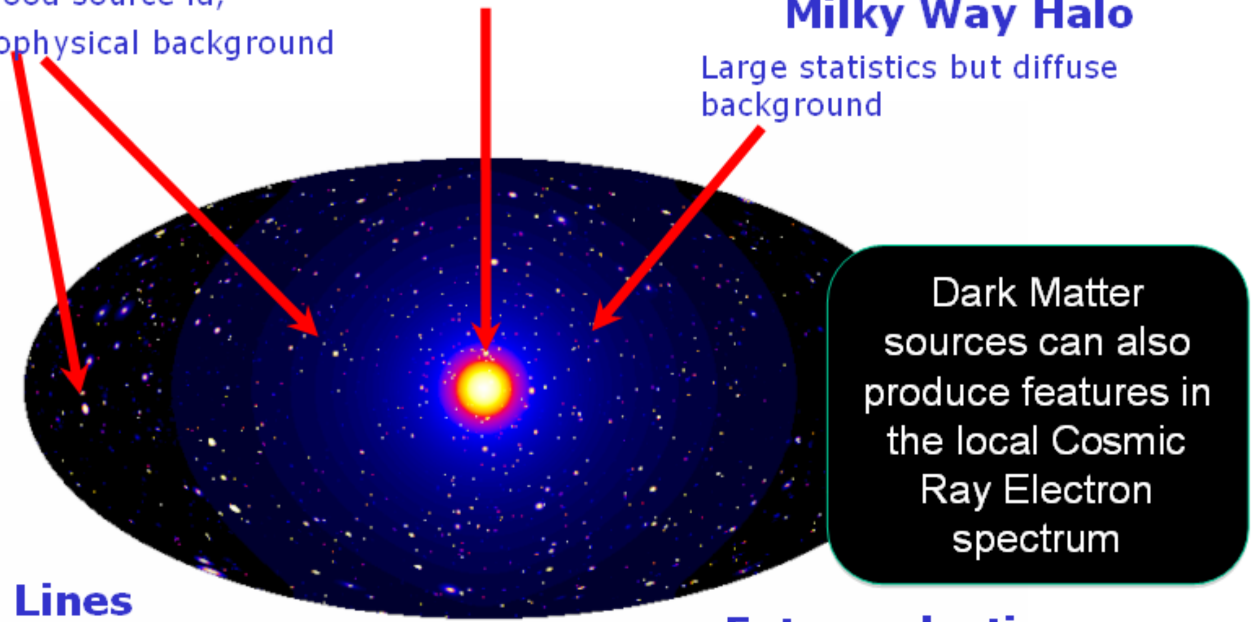

All-sky map of simulated gamma ray signal from DM annihilation (Baltz 2006)

Spectral Lines
No astrophysical uncertainties, good source id, but low sensitivity because of expected small BR

Extra-galactic
Large statistics, but astrophysics, galactic diffuse background

Narrow Spectral Feature at 130

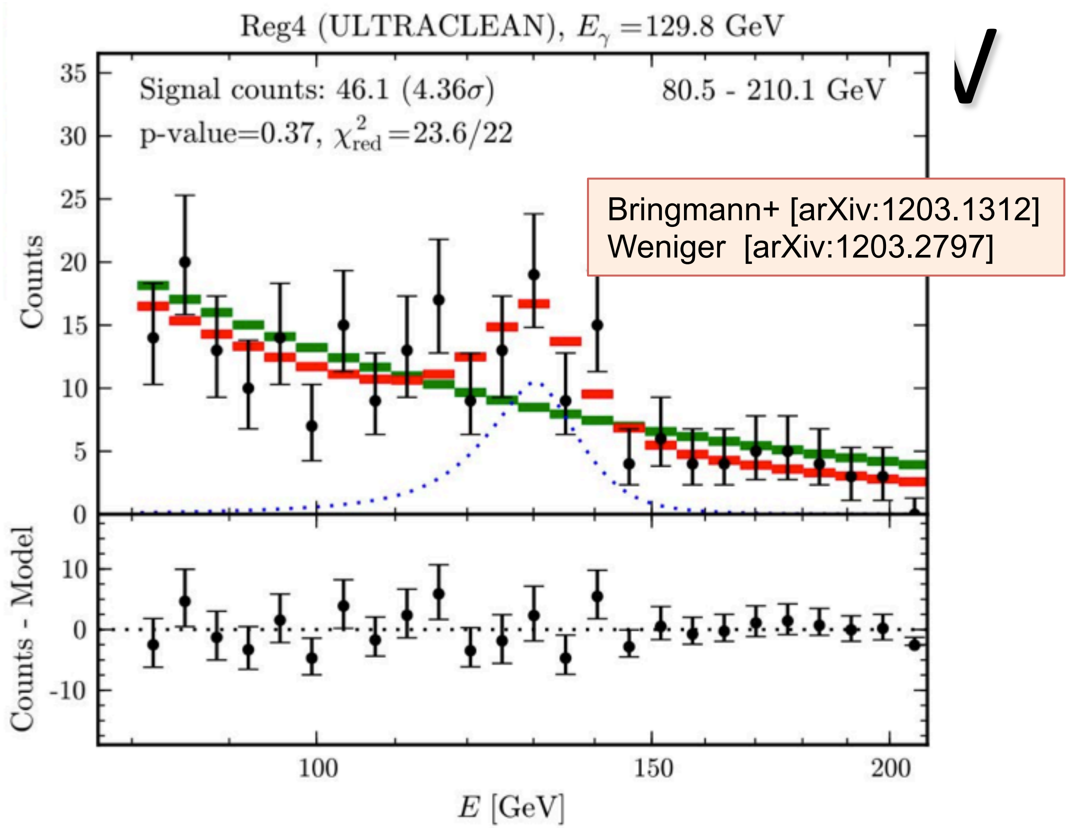

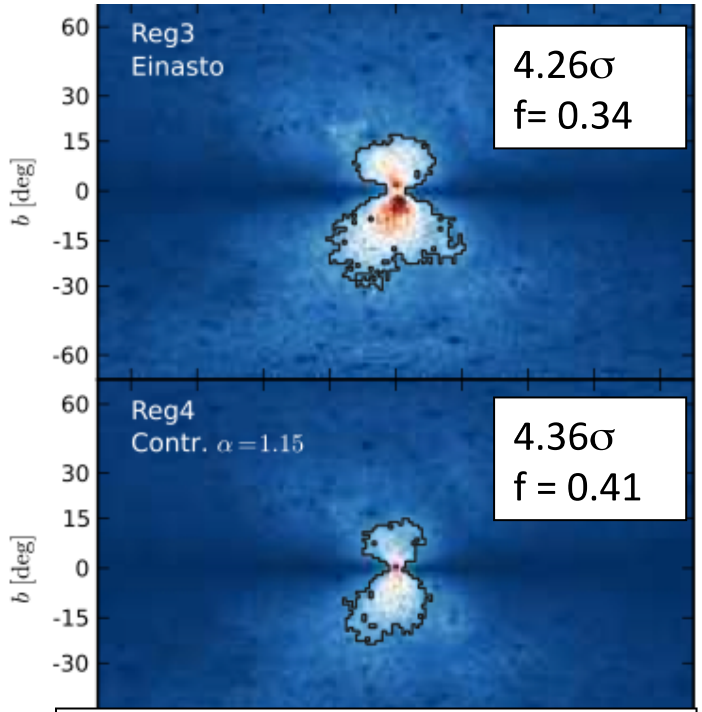

Fractional Residual (i.e., S/N):
$f = s^2 / n_s$

Bringmann et al. and Weniger showed evidence for a narrow spectral feature near 130 GeV near the Galactic center (GC) in the LAT data.

- Signal is particularly strong in 2 out of 5 test regions, shown above.
- Over 4σ local significance with S/N > 30%, up to ~60% in optimized ROI.
- Some indication of double line (111 &130 GeV).

Dark Matter searches – Galactic Center

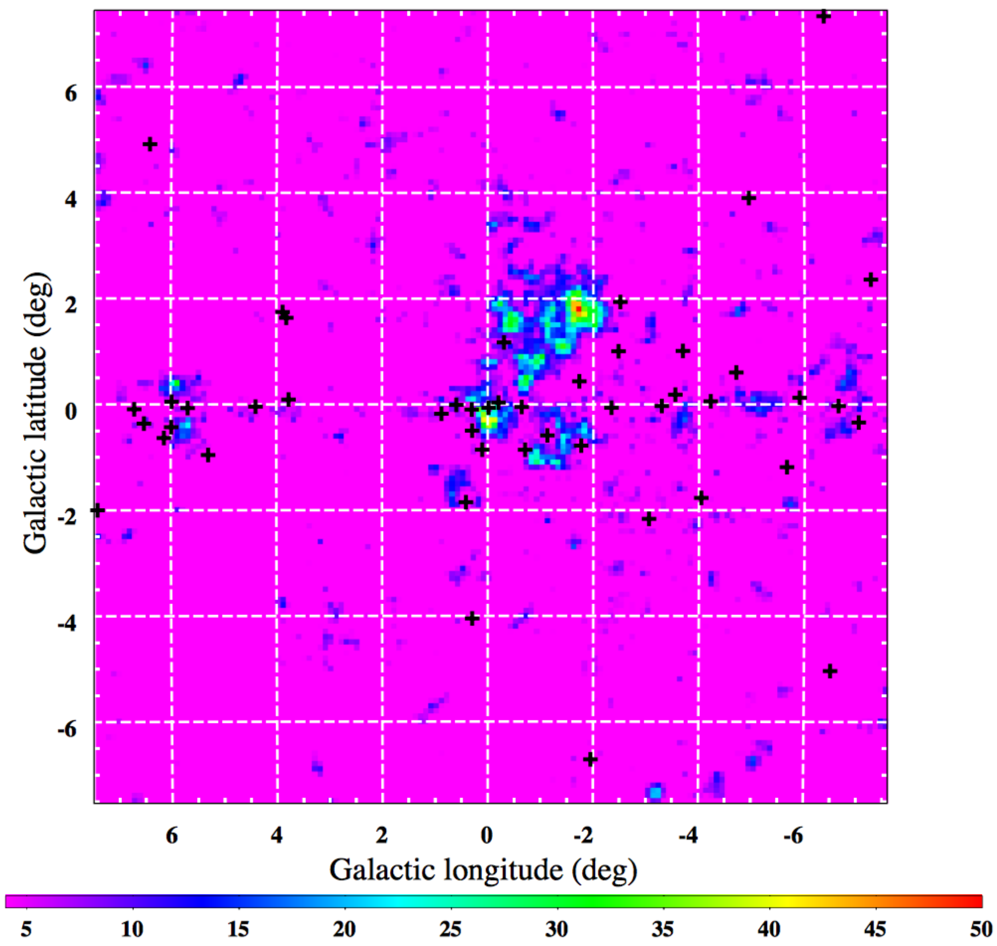

Ackermann, M. et al. 2017

Dark Matter searches – GC

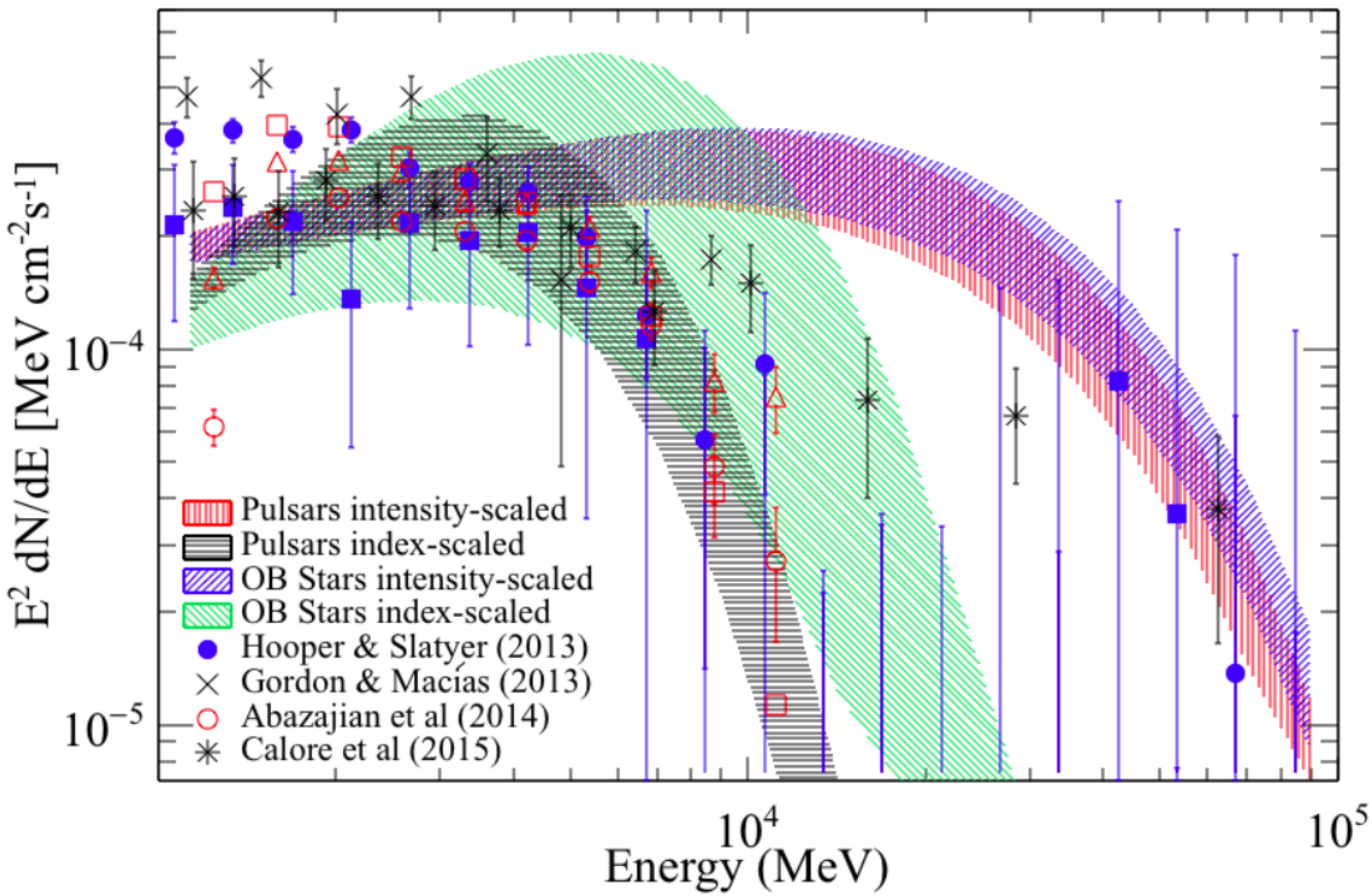

Ackermann, M. et al. 2017

Dark Matter searches – Dwarfs Galaxies

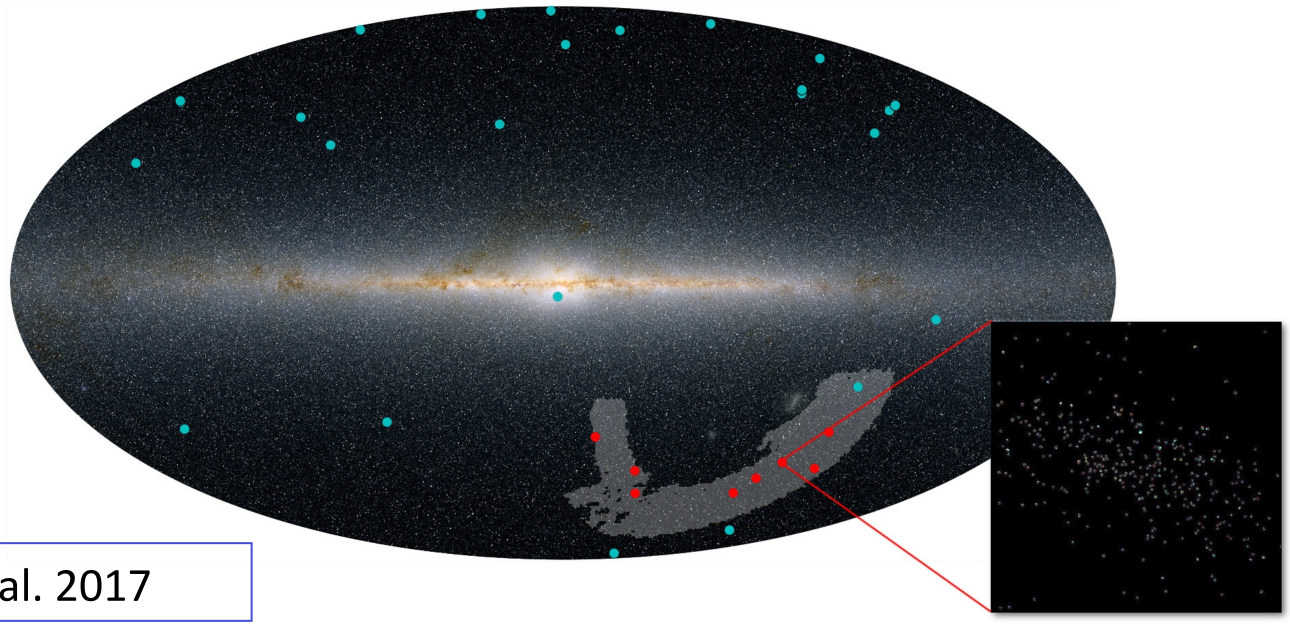

Albert, A. et al. 2017

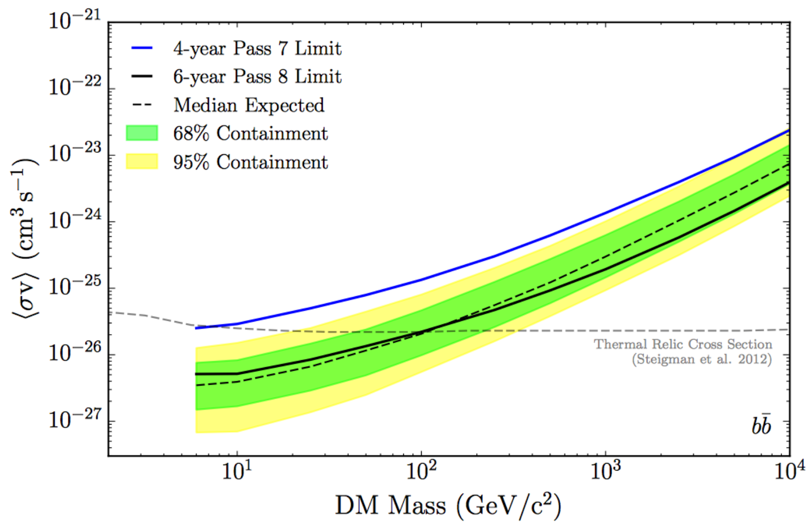

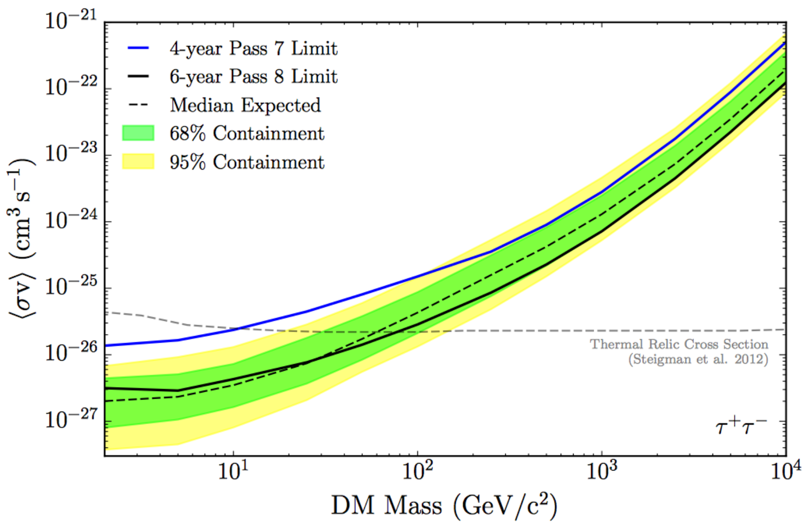

How the LAT detects electrons

Trigger and downlink

Very versatile and configurable
- Triggering on ~ all particles that cross the LAT
  - Including electrons (8M/yr)

On board filtering to fit bandwidth
- Remove many charged particles
- Keeps all events with more than 20 GeV in the CAL (HE)
- Prescaled (1:250) sample of unfiltered triggers (LE)

Electron identification

The challenge is identifying the good electrons among the proton background
- Rejection power of $10^3 - 10^4$ required
- Can not separate electrons from positrons
- → Dedicated high energy electron event selection

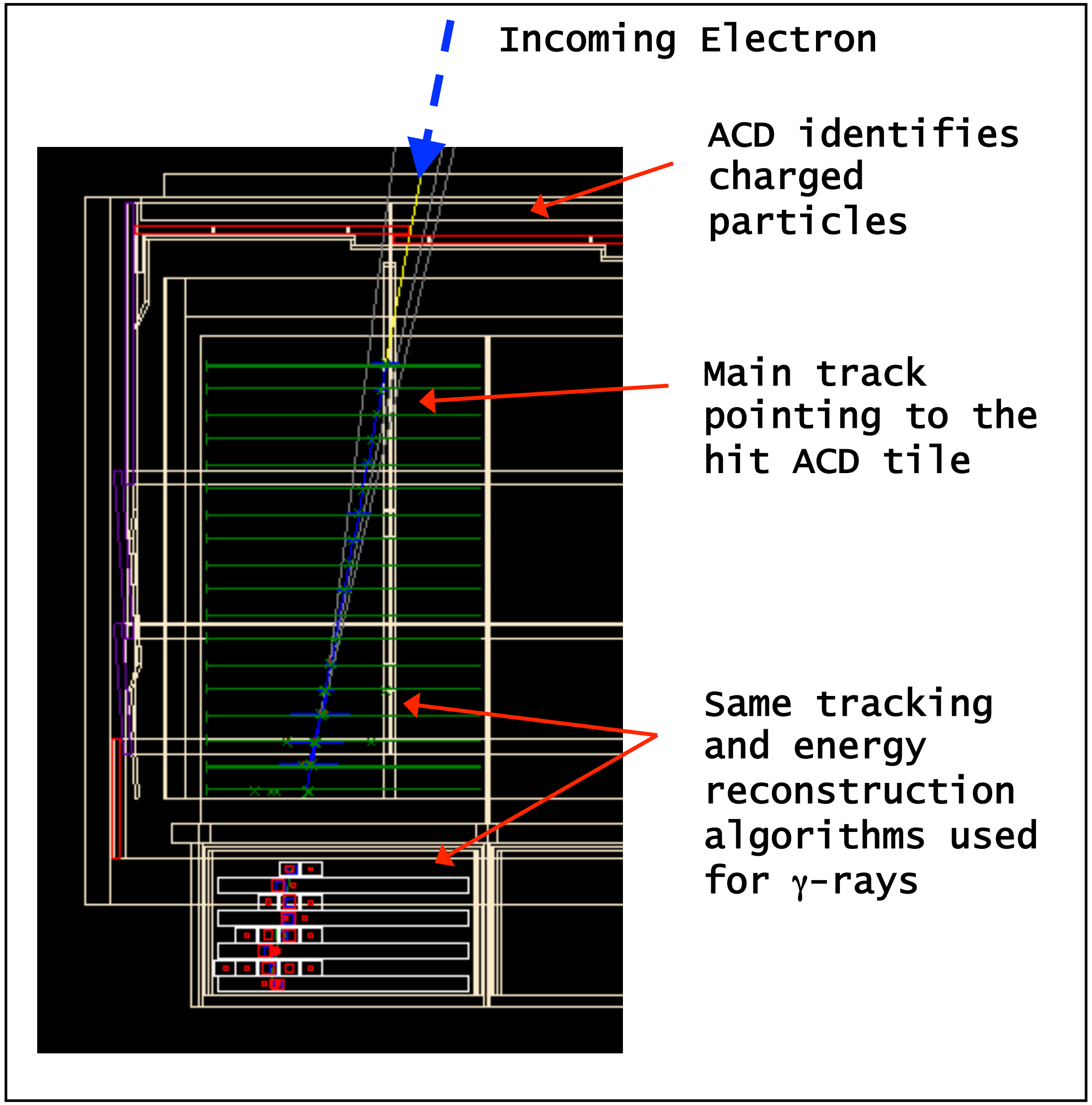

Importance of a direct CRE measurement

- Probe CR models
  - Sources (including DM), interactions, propagation, diffusion
- Probe CR targets (ISM, ISRF)
  - Propagation and diffusion
  - Strong connection with diffuse gamma-ray radiation
- Probe possible nearby sources
  - limited electron lifetime within Galaxy
- Answers to long-standing questions and vast literature

THE ASTROPHYSICAL JOURNAL, 162:L181–L186, December 1970

PULSARS AND VERY HIGH-ENERGY COSMIC-RAY ELECTRONS

C. S. SHEN*
Department of Physics, Purdue University, Lafayette, Indiana 47907
Received 1970 June 8; revised 1970 September 19

PRL 102, 181101 (2009)
Selected for a Viewpoint in *Physics*
PHYSICAL REVIEW LETTERS
week ending
8 MAY 2009

Measurement of the Cosmic Ray $e^+ + e^-$ Spectrum from 20 GeV to 1 TeV with the Fermi Large Area Telescope

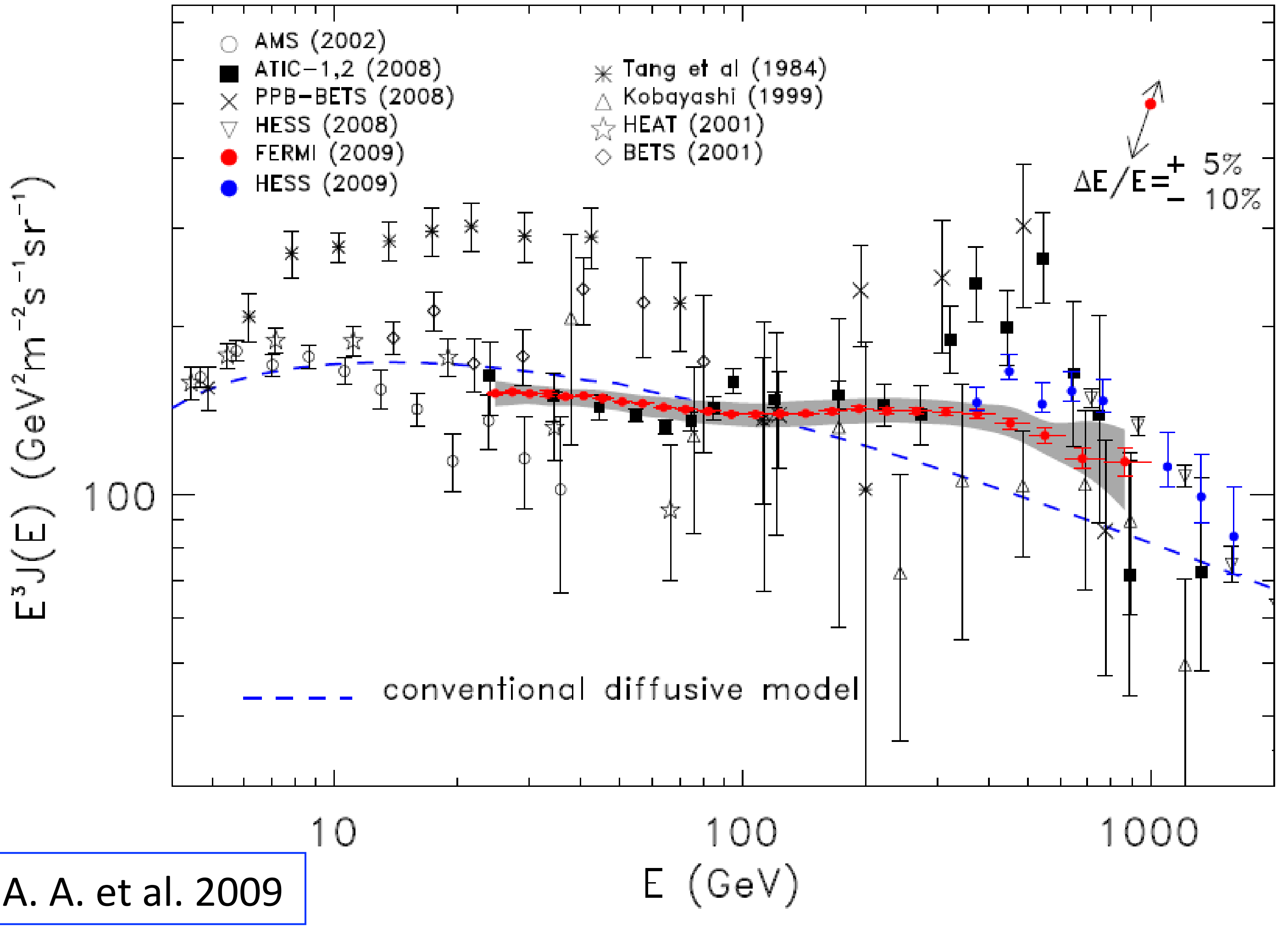

Abdo, A. A. et al. 2009

Positron Fraction Measurements

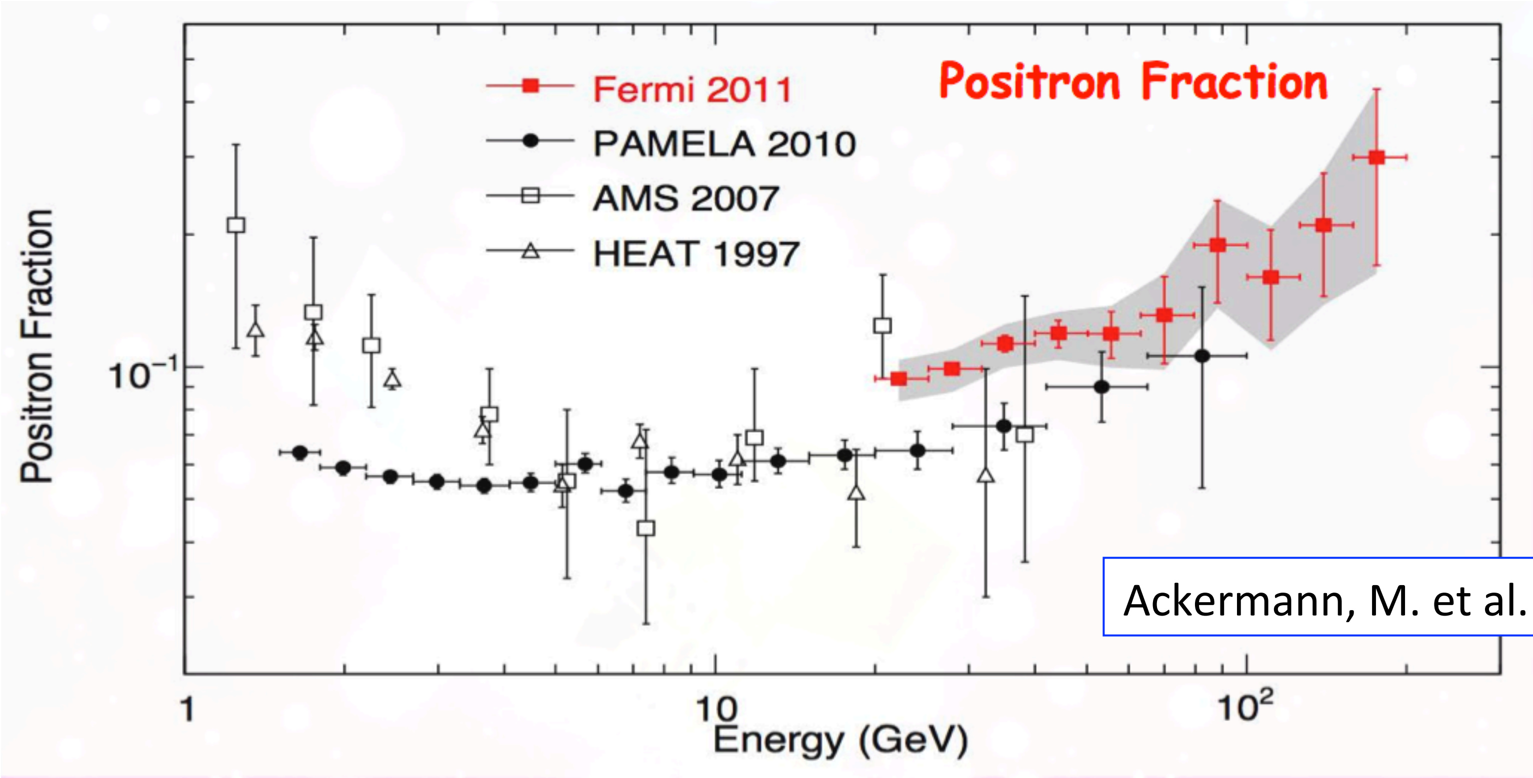

Ackermann, M. et al. 2012

•PAMELA and Fermi-LAT observe a rise in local e^+ fraction above ~10 GeV
•This disagrees with conventional models (e.g., GALPROP) for cosmic rays (secondary e^+ production only)
•No similar rise is seen in anti-proton fraction

The Quiet Sun

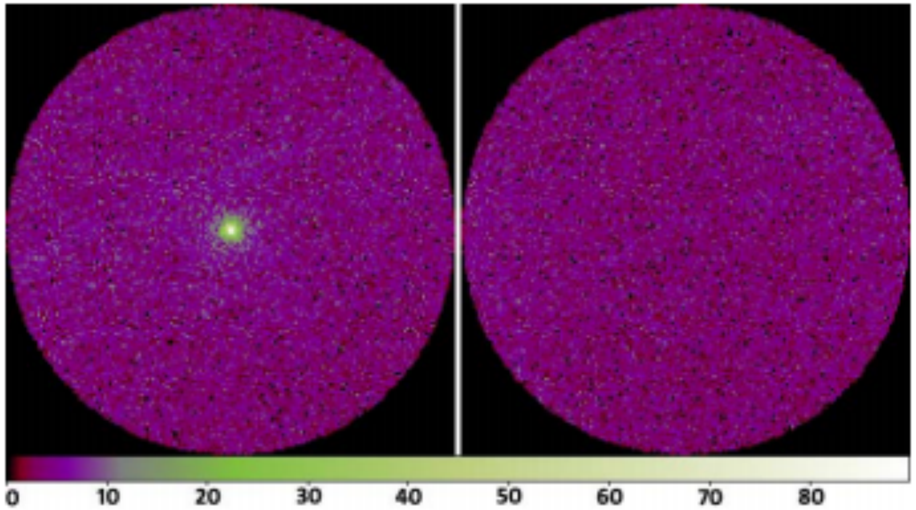

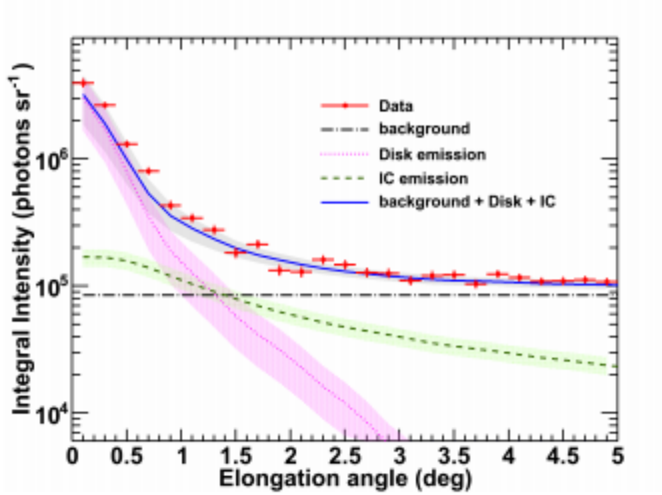

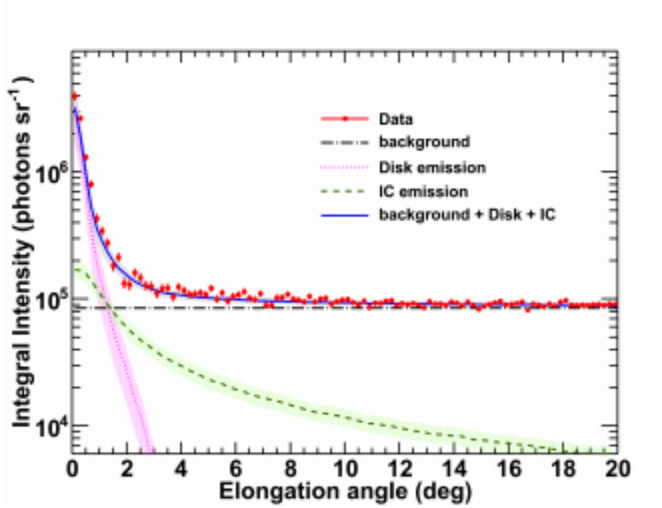

Abdo, A. A. et al. 2011

Challenge #5: Flaring Sun

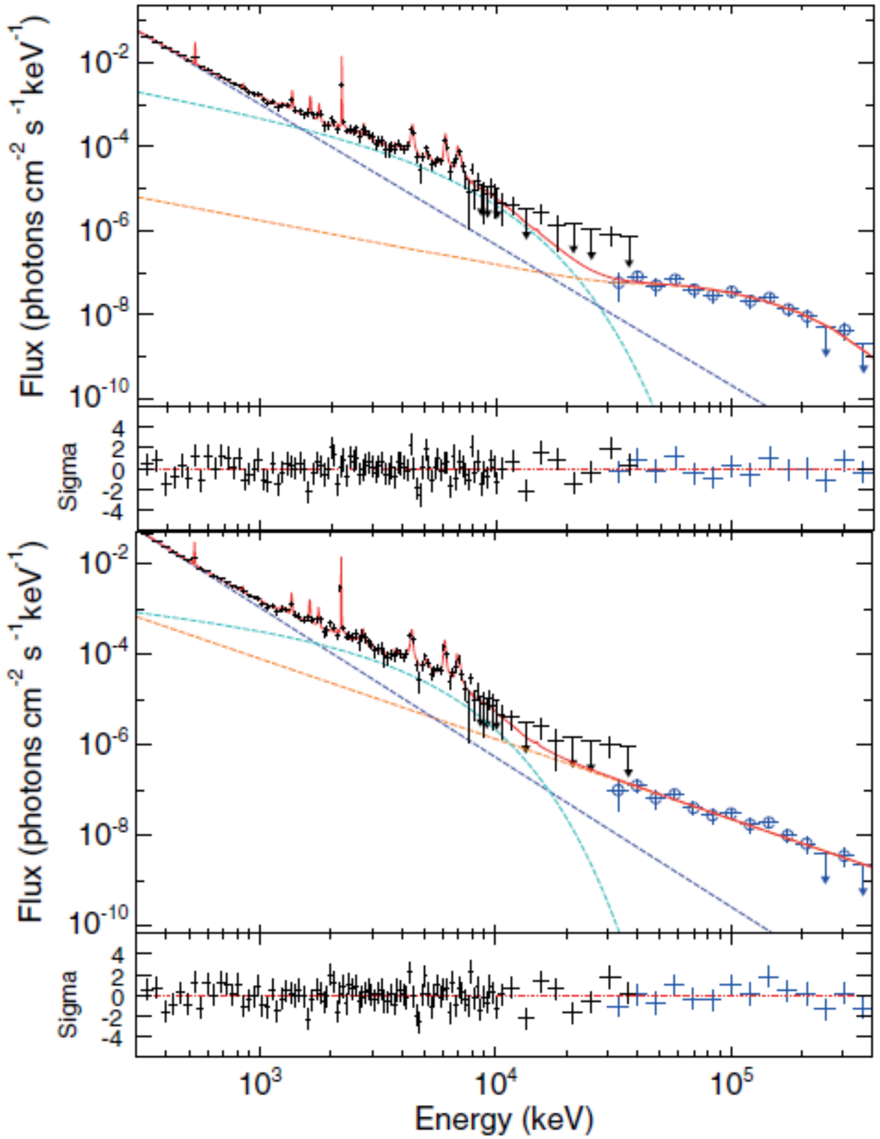

Ackermann, M. et al 2012

Solar Flares

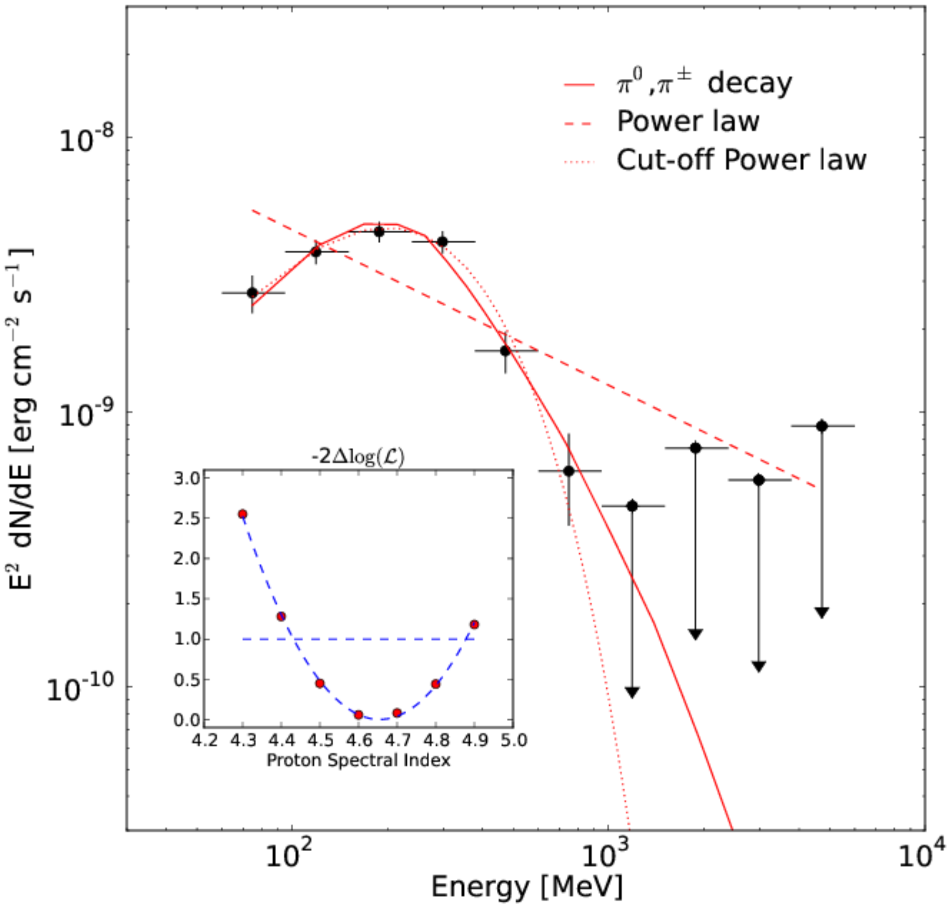

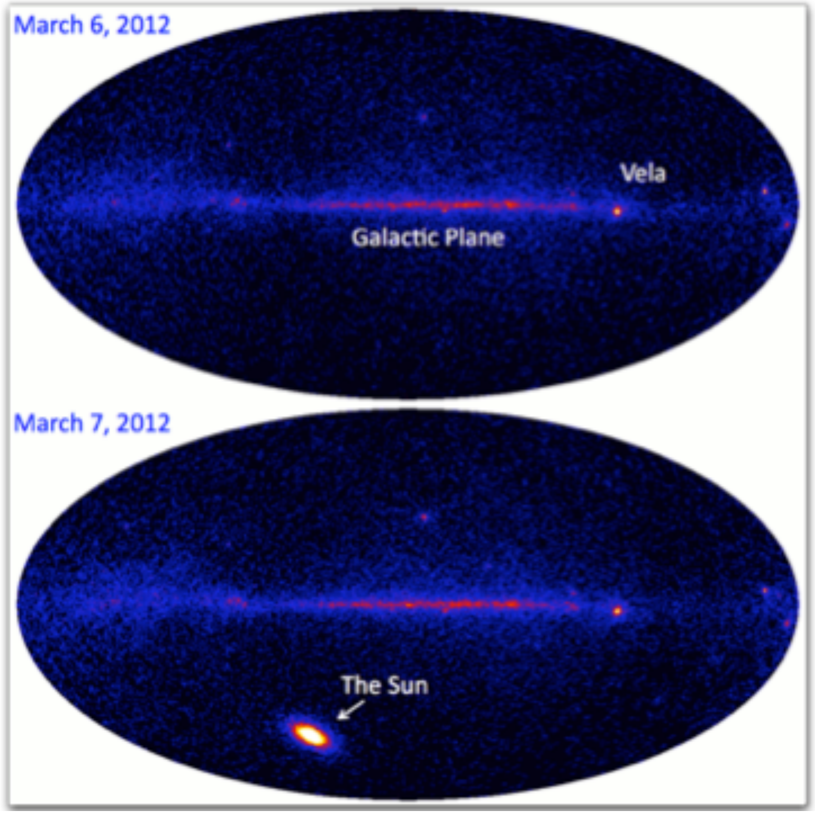

Ajello, M. et al. 2014

Surprise! Nova emitting in Gamma Rays!

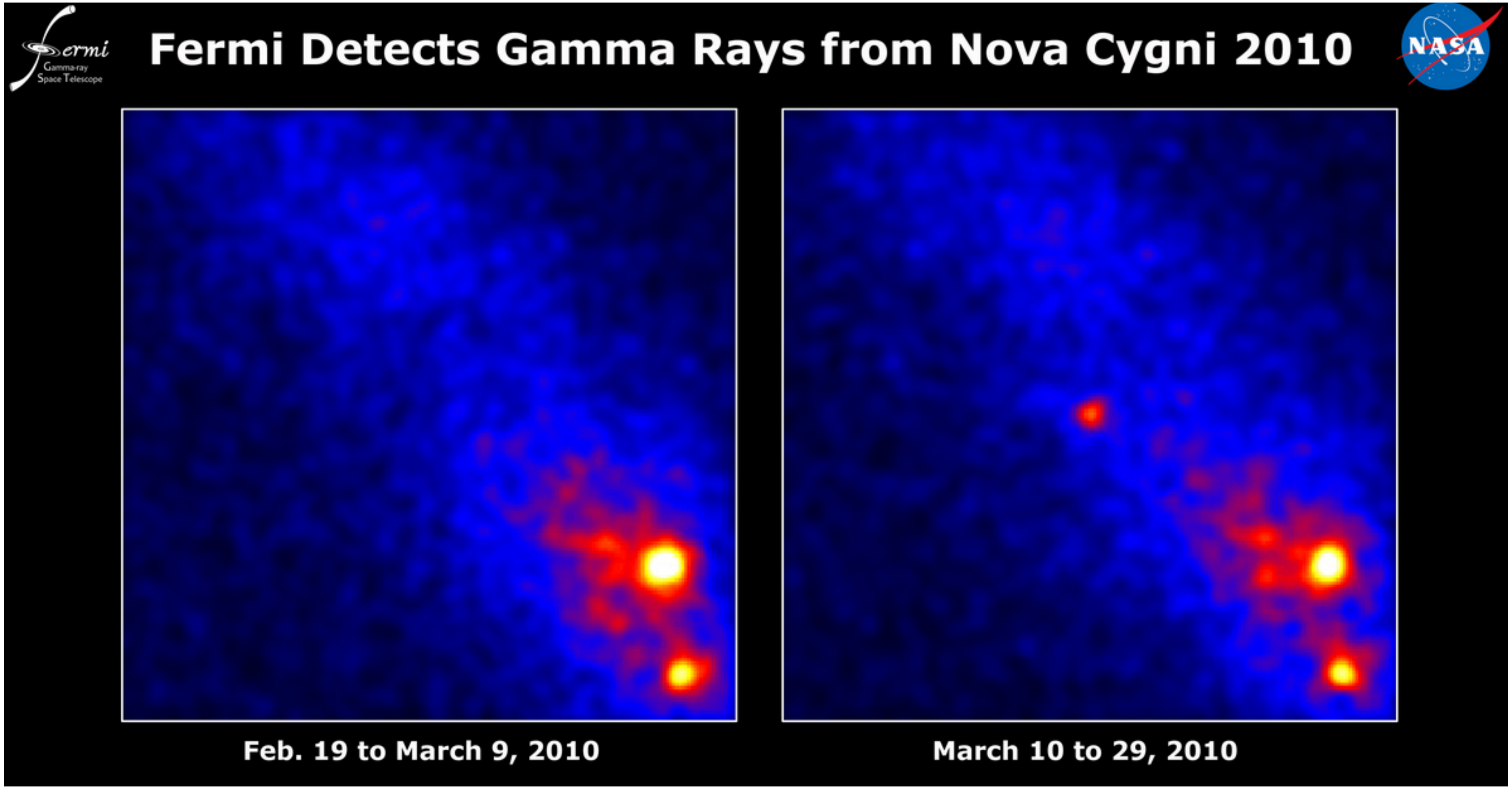

Abdo, A. A. et al. 2010

Gamma Ray Novae

Surprise! The Fermi Bubbles

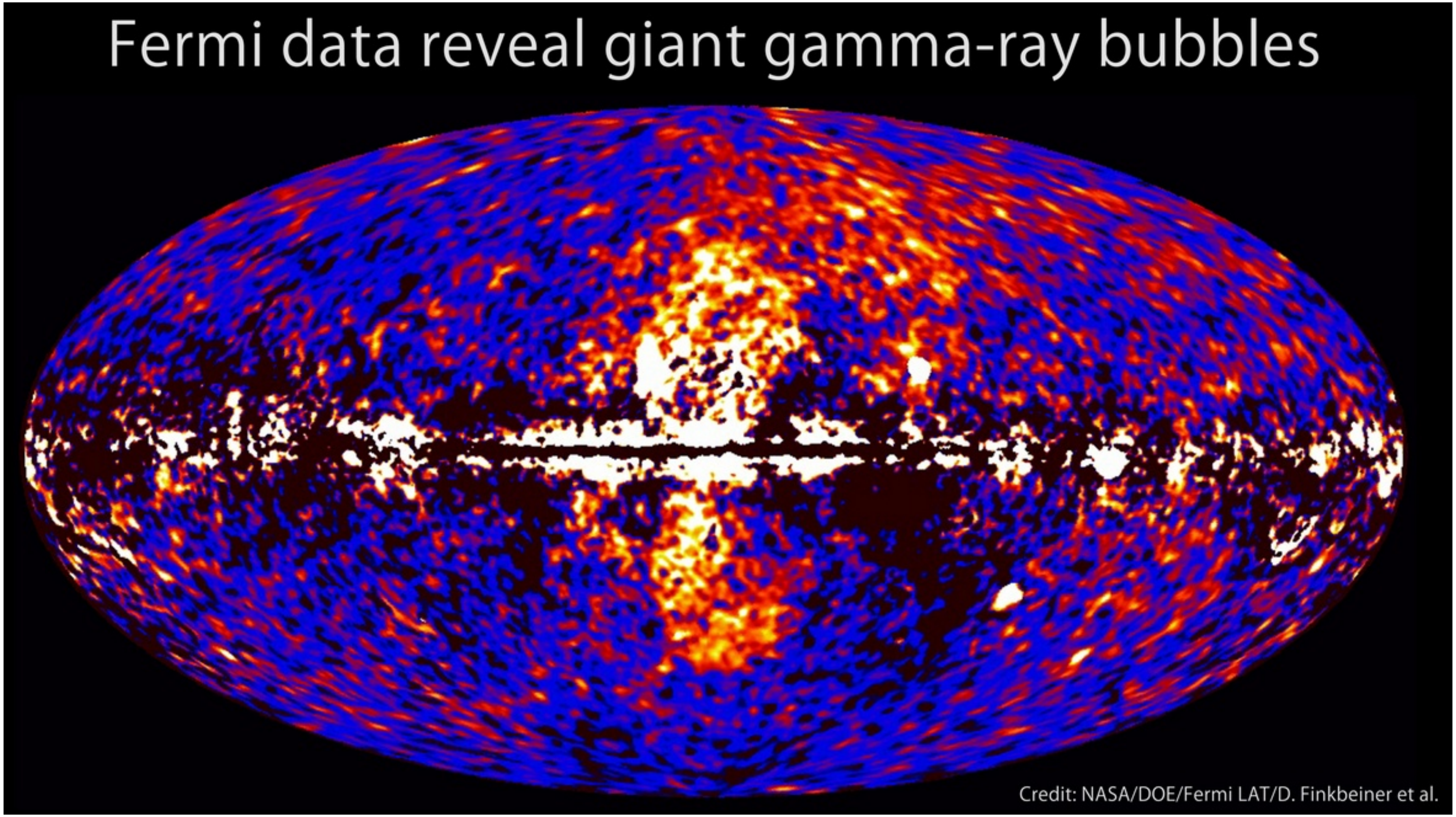

Fermi bubbles

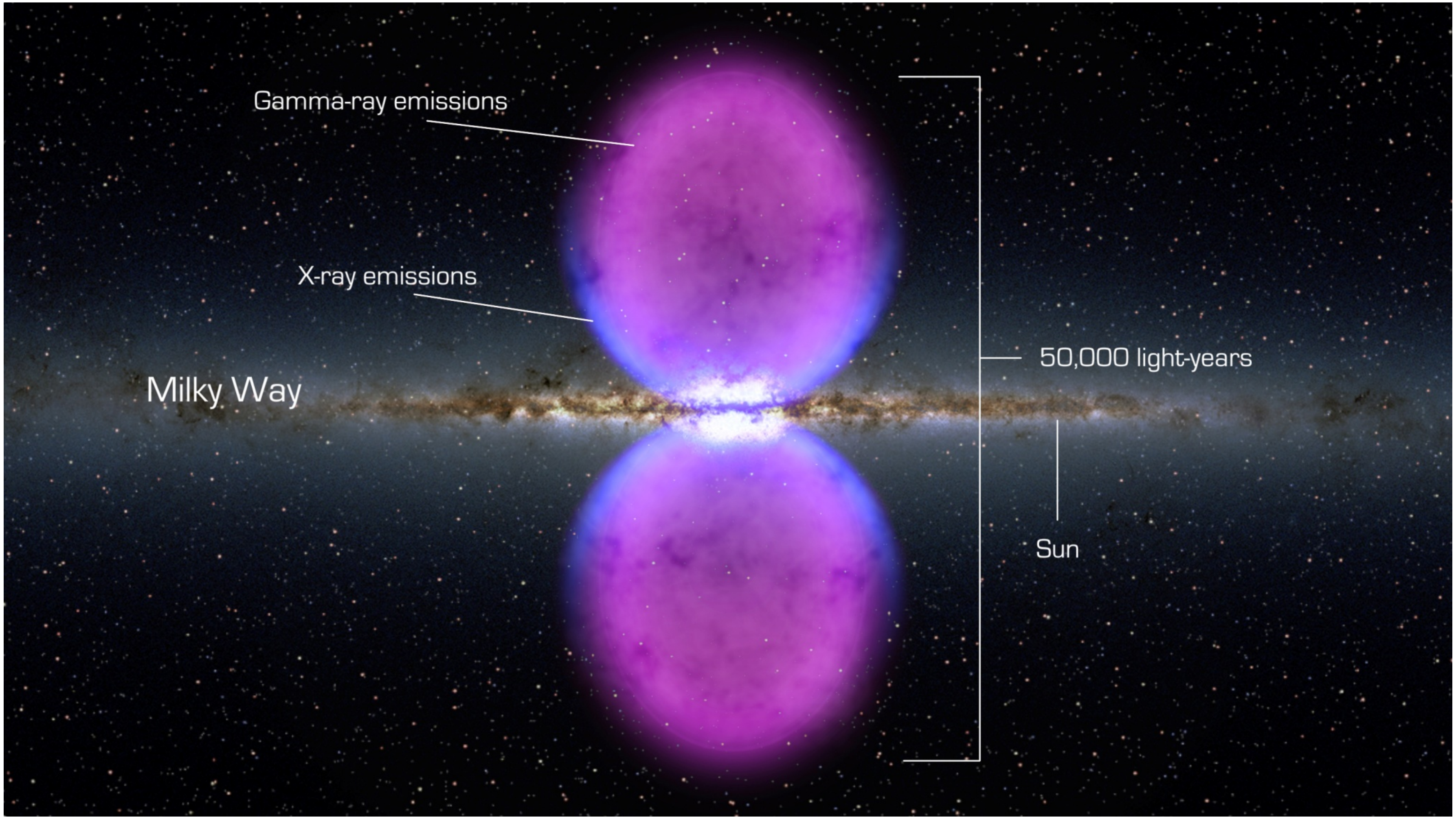

LAT team analysis: Ackermann, M. et al. 2017

CALET?

CALorimetric Electron Telescope (CALET)

P. S. Marrocchesi for the CALET Collaboration – RICAP11 – 2011 May 26

- **Instrument:**
  High Energy Electron and Gamma-Ray Telescope
- **Carrier:**
  HTV: H-IIA Transfer Vehicle
- **Attach Point on the JEM-EF: #9**
  for heavy (< 2000 kg) payloads
- **Nominal Orbit:**
  407 km, 51.6º inclination
- **Launch plan:**
  FY 2013
- **Life Time:**
  ≥ 5 years

Firenze
Pisa
Siena
Roma Tor Vergata

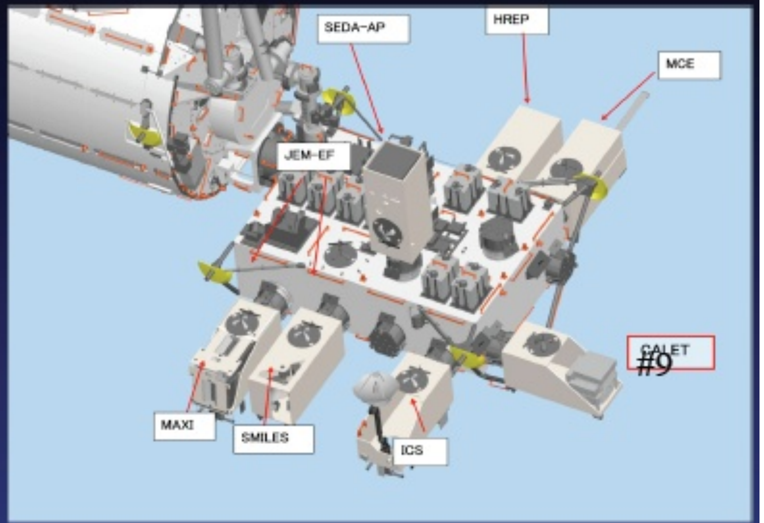

1 GeV ~ 20 TeV for electrons

20 MeV ~ TeV for gamma-rays

Weight: 500 kg

GF (fiducial volume): ~ 0.12 m^2sr

Power Consumption: 640 W

Data Rate: 300 kbps

CALET?

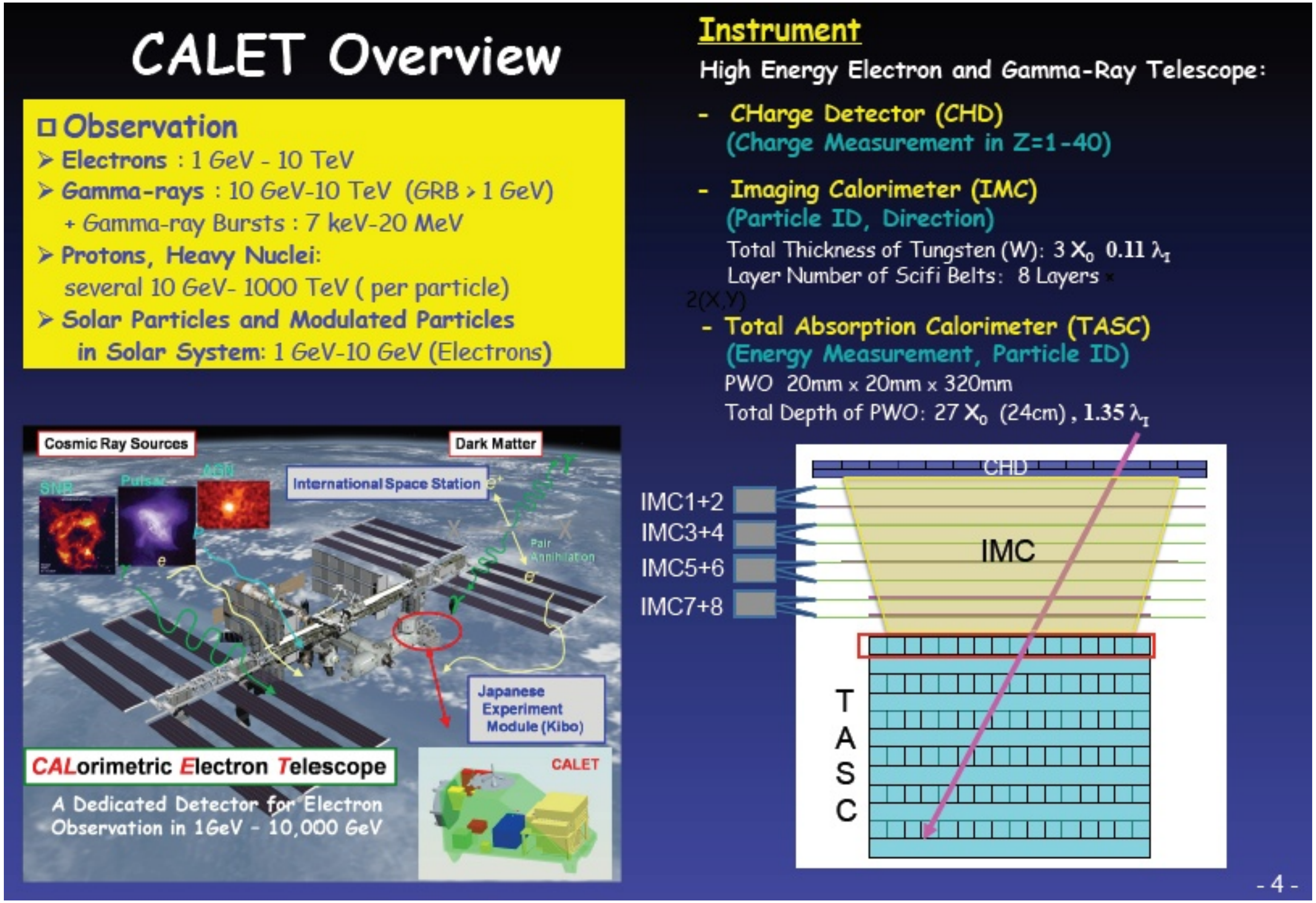
CALET Overview
Observation
Electrons : 1 GeV - 10 TeV
Gamma-rays : 10 GeV-10 TeV (GRB > 1 GeV)
+ Gamma-ray Bursts : 7 keV-20 MeV
Protons, Heavy Nuclei:
several 10 GeV- 1000 TeV (per particle)
Solar Particles and Modulated Particles
in Solar System: 1 GeV-10 GeV (Electrons)
Cosmic Ray Sources
Dark Matter
International Space Station
Pair Annihilation
Japanese Experiment Module (Kibo)
CALorimetric Electron Telescope
A Dedicated Detector for Electron Observation in 1GeV - 10,000 GeV
CALET
Instrument
High Energy Electron and Gamma-Ray Telescope:
- CHarge Detector (CHD)
(Charge Measurement in Z=1-40)
- Imaging Calorimeter (IMC)
(Particle ID, Direction)
Total Thickness of Tungsten (W): 3 X_0 0.11 λ_I
Layer Number of Scifi Belts: 8 Layers × 2(X,Y)
- Total Absorption Calorimeter (TASC)
(Energy Measurement, Particle ID)
PWO 20mm x 20mm x 320mm
Total Depth of PWO: 27 X_0 (24cm), 1.35 λ_I
CHD
IMC1+2
IMC3+4
IMC5+6
IMC7+8
IMC
TASC
- 4 -

CALET

CALET/CAL Shower Imaging Capability (Simulation)

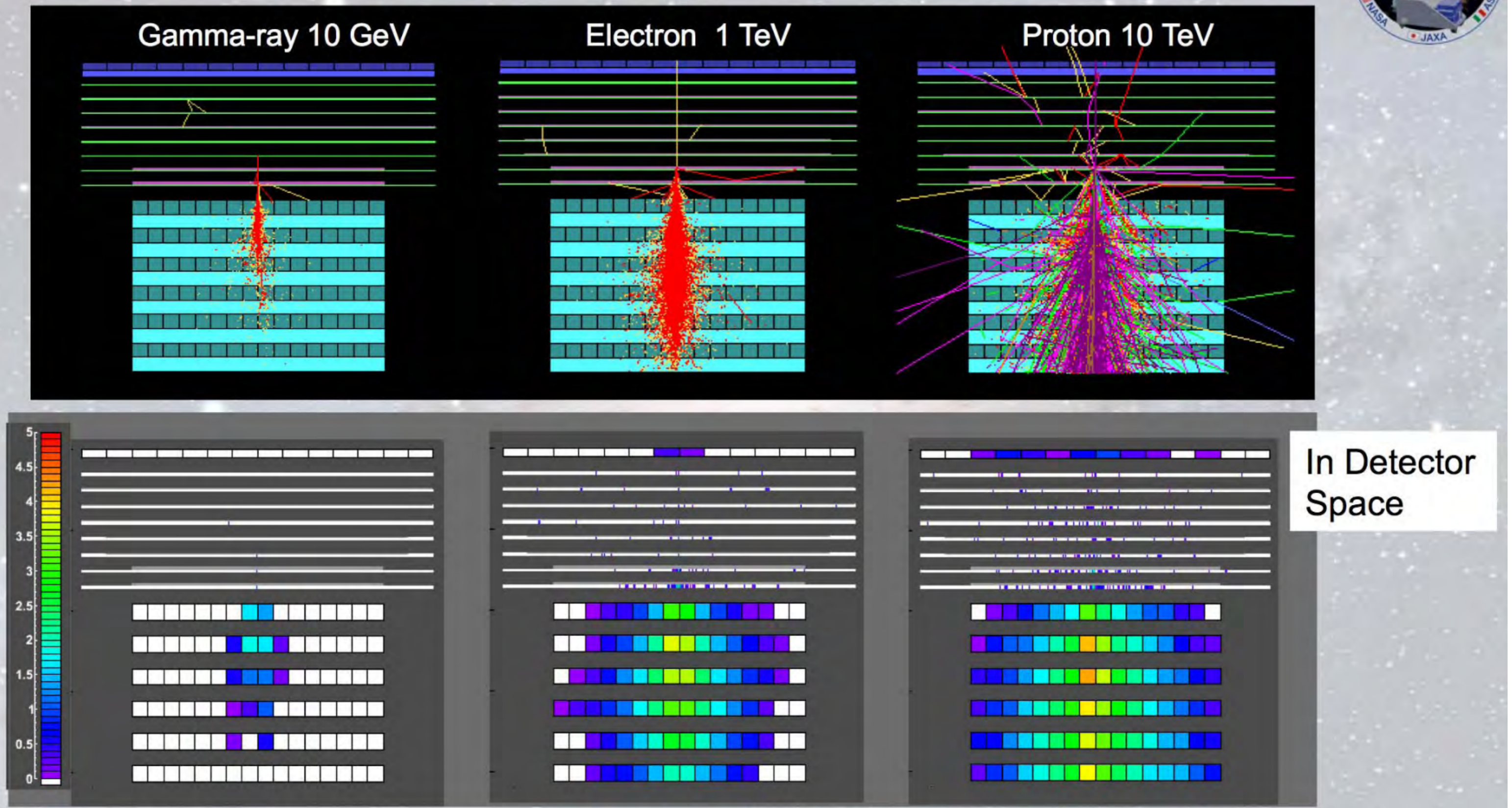

- Proton rejection power > 10^5 can be achieved with the IMC and TASC shower imaging capability.
- Charge of incident particle is determined to $\Delta Z = 0.15 – 0.3$ with the CHD.

CALET gamma-sky

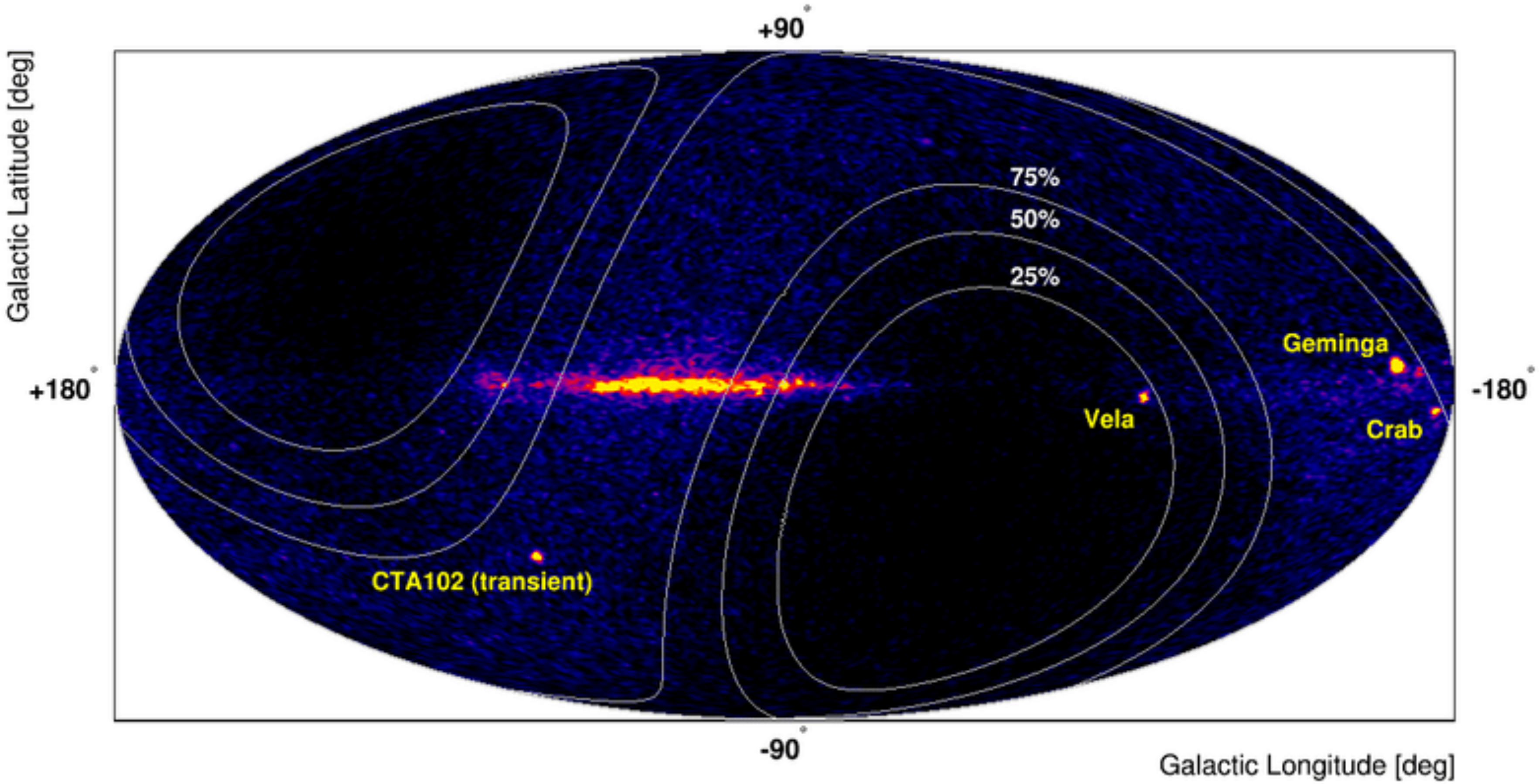

Gamma-400?

AC - anticoincidence detectors

C - multilayer converter

C1- C6 6 x 0,14Xo W

CD1 - CD6 6 x Si (x,y) strip detectors (pitch 0.1 mm)

CD7 - CD8 Si (x,y) strip detectors (pitch 0.1 mm)

S1, S2 - TOF detectors

TRD - transition radiation detectors

CC1 - imaging calorimeter (9Xo) 10 layers BGO + Si (x, y) strip detectors (pitch 0.5 mm)

CC2 - BGO imaging calorimeter (21.5Xo)

S3, S4 - scintillator detectors

ND - neutron detectors

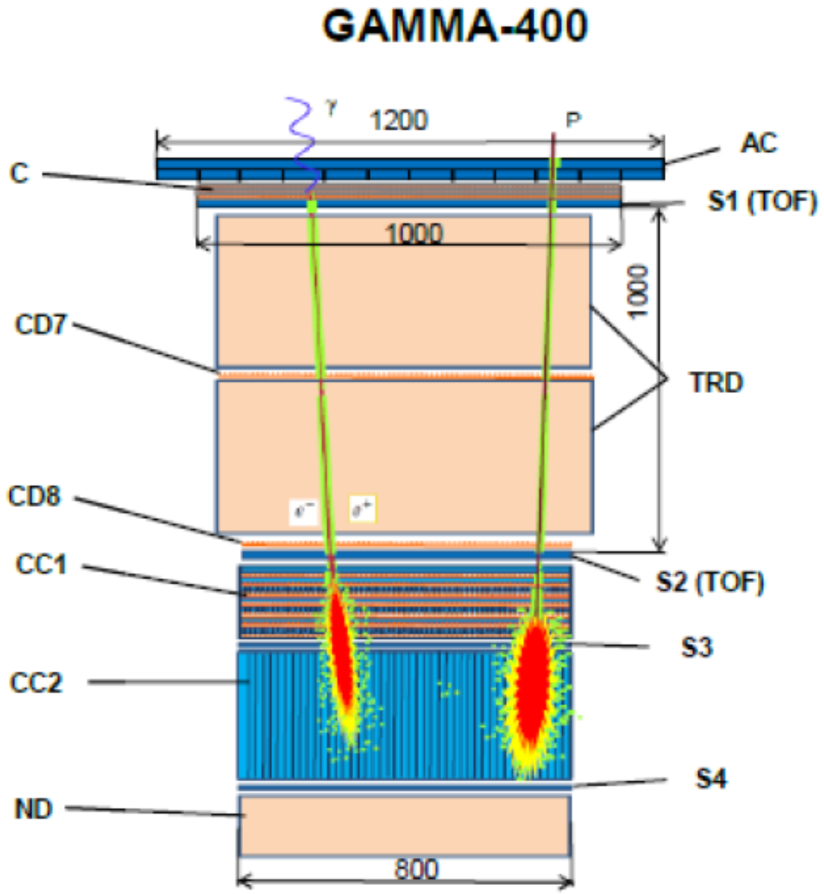

Gamma400

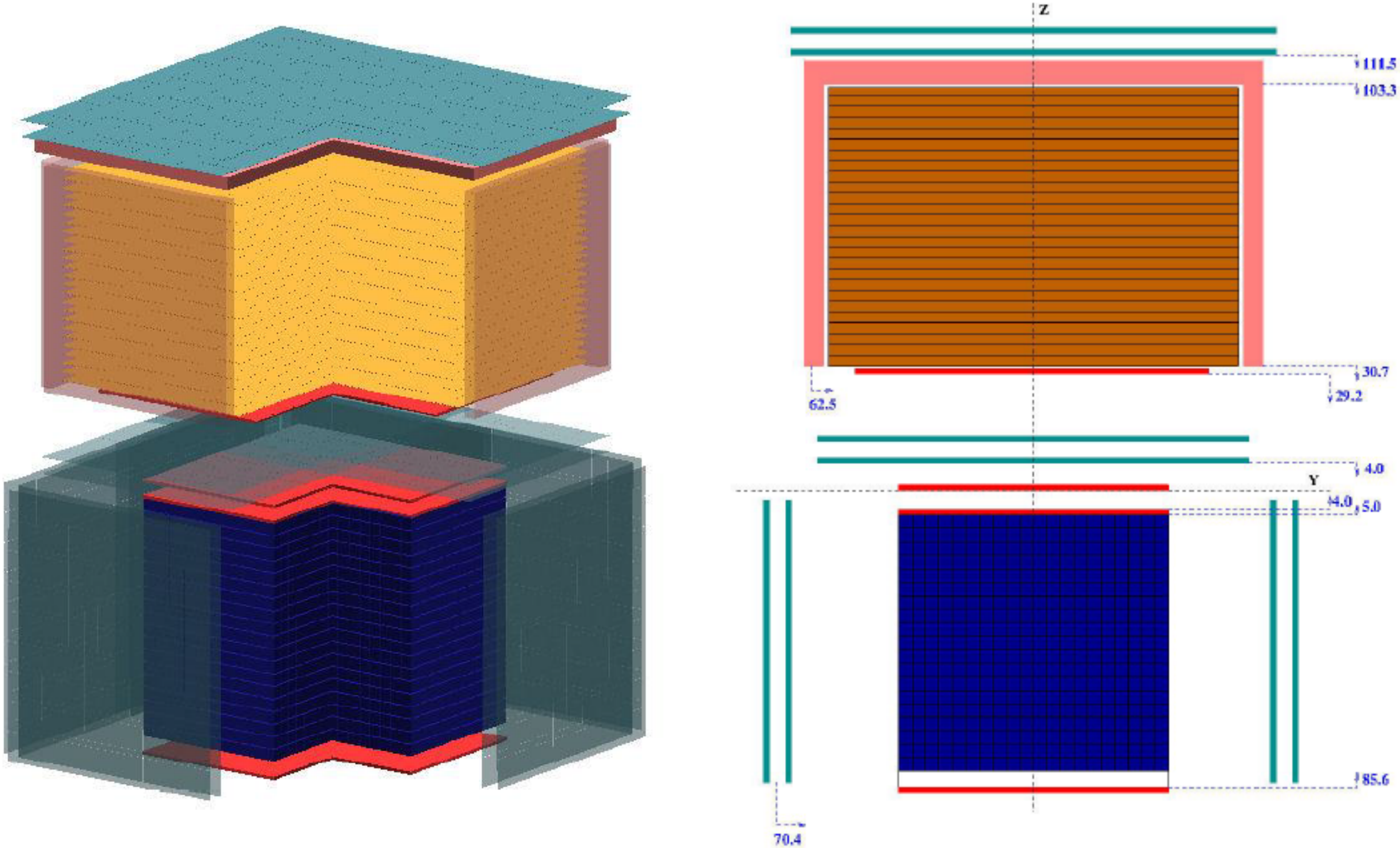

DAMPE

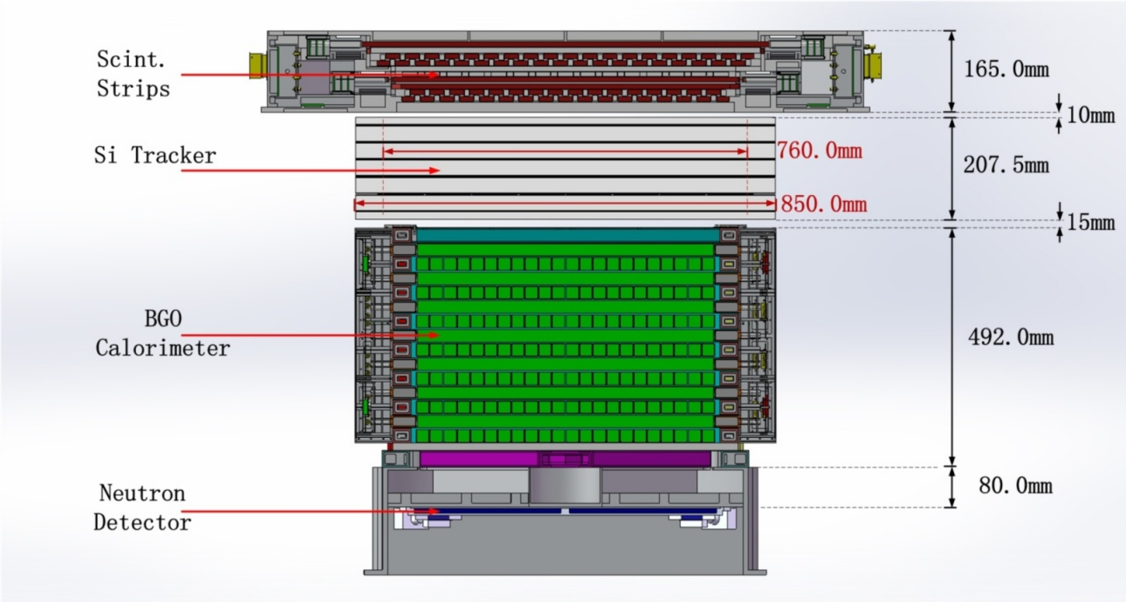

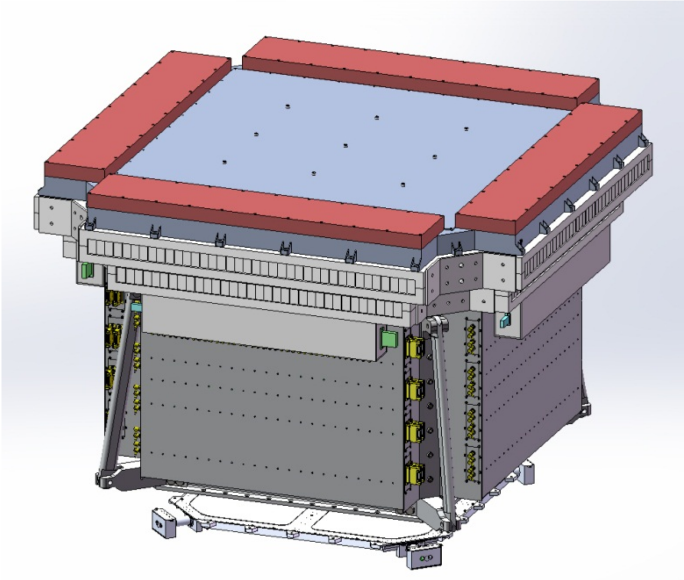

The detector is consisted of 4 parts:
Top scintillators (charge measurement)
Si tracker (5 layers)
BGO calorimeter
Neutron detector

DAMPE Gamma results

DAMPE γ-ray Selection: Different Events

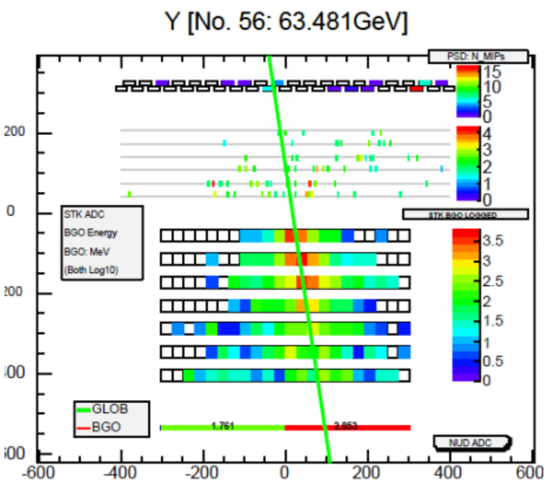

Proton

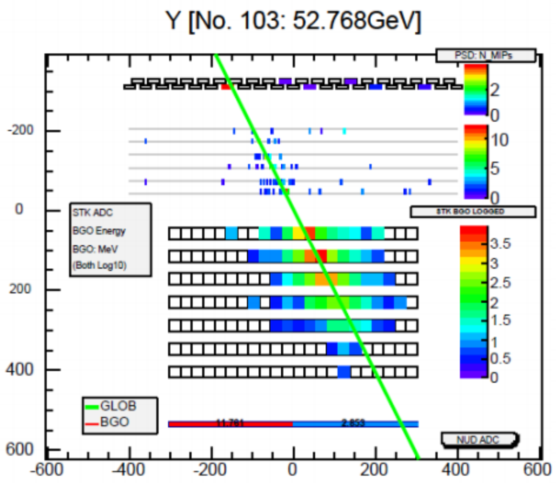

Electron

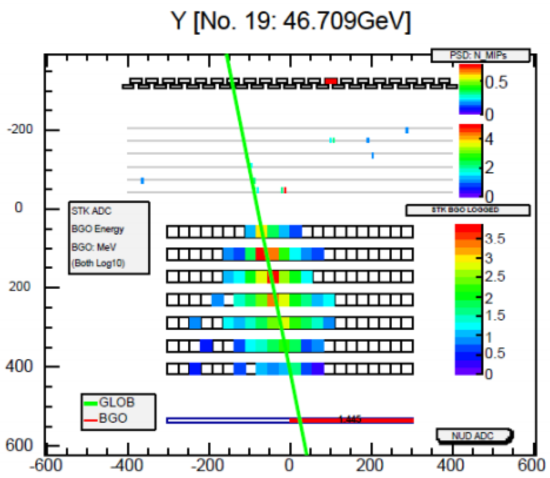

Gamma-ray

- e(γ)/p separation: BGO shower pattern
- e/γ separation: PSD and STK charge measurement

DAMPE Gamma results

DAMPE γ-ray Sky Map (Counts)

- 510 days
- E>2 GeV
- 90,000 events
- 0.5°×0.5° pexel
- Mollweide projection

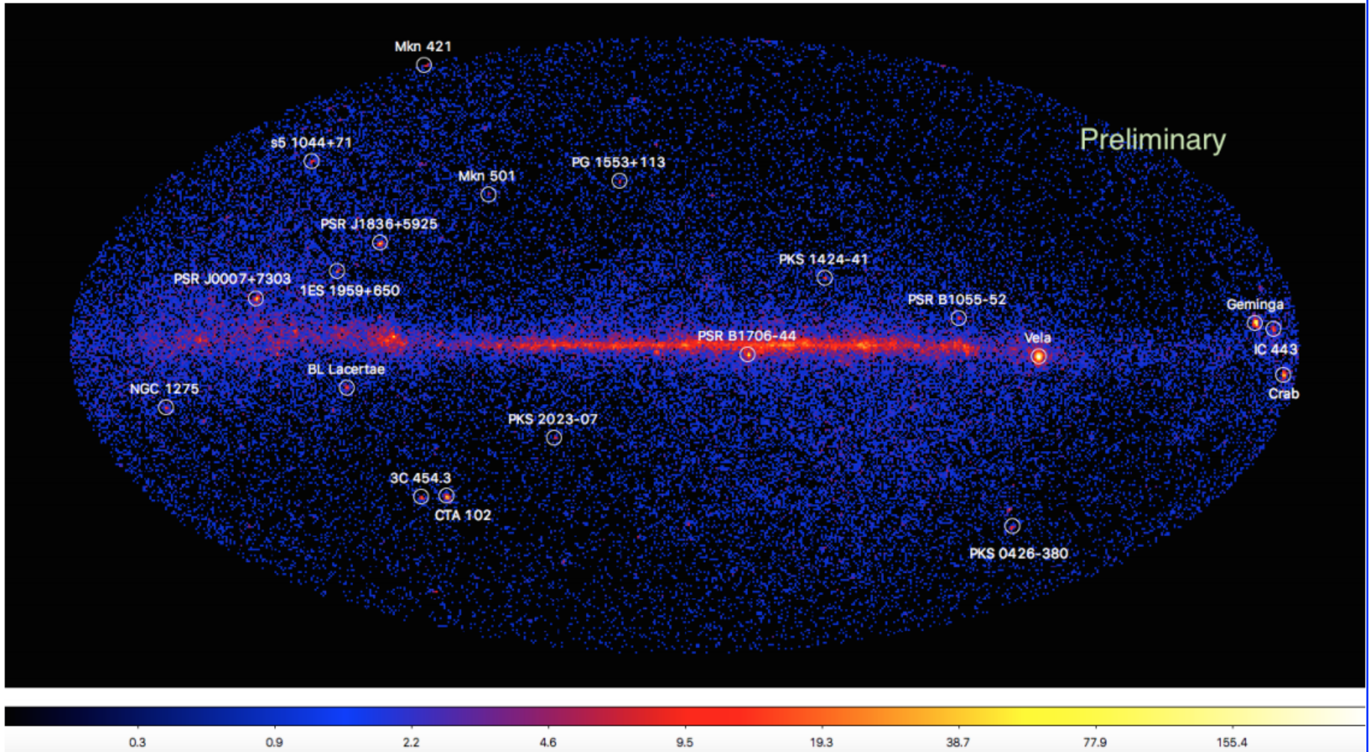

HERD

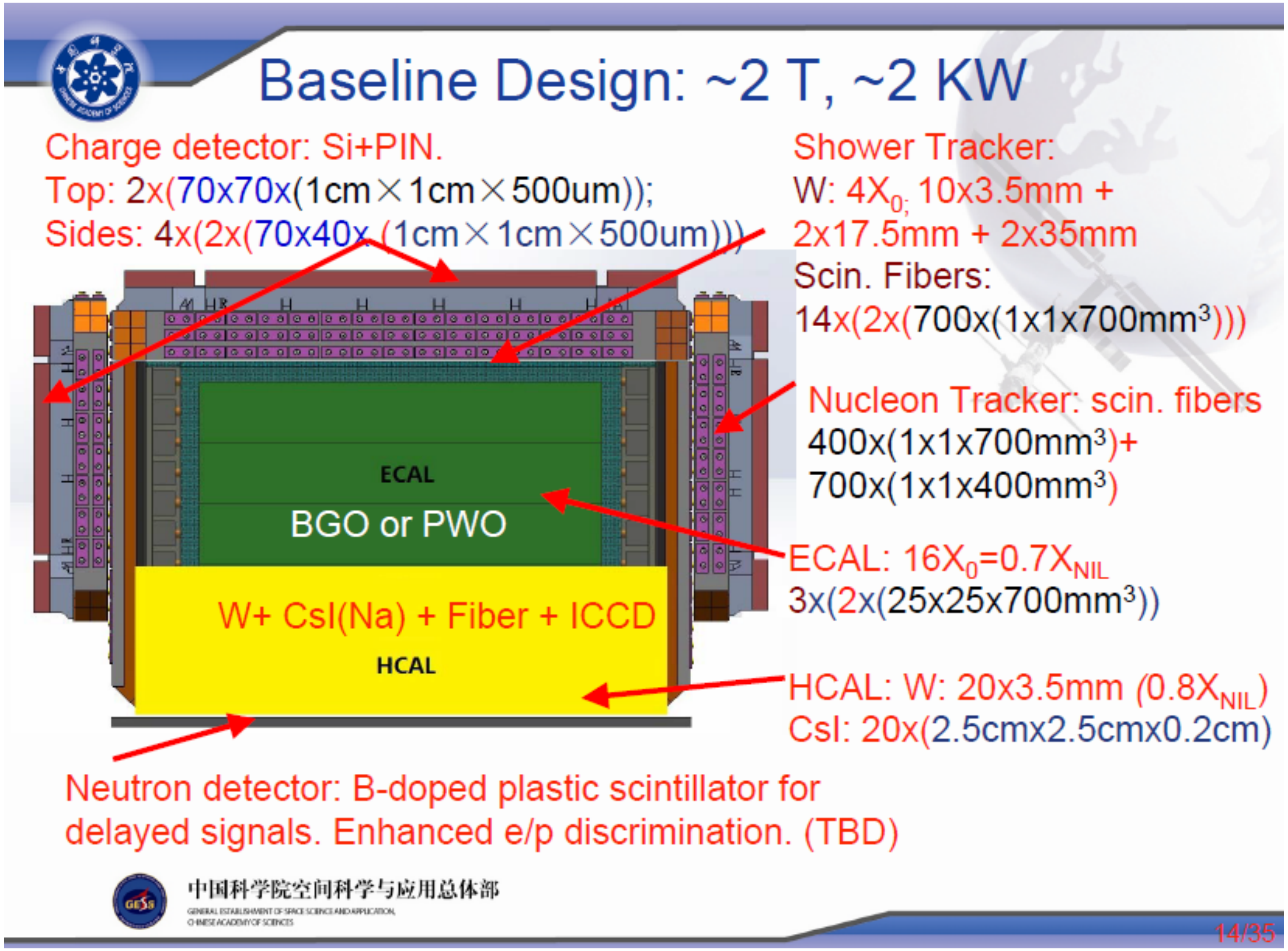
Baseline Design: ~2 T, ~2 KW
Charge detector: Si+PIN.
Top: 2x(70x70x(1cm×1cm×500um));
Sides: 4x(2x(70x40x (1cm×1cm×500um)))
Shower Tracker:
W: 4X0; 10x3.5mm +
2x17.5mm + 2x35mm
Scin. Fibers:
14x(2x(700x(1x1x700mm3)))
Nucleon Tracker: scin. fibers
400x(1x1x700mm3)+
700x(1x1x400mm3)
ECAL
BGO or PWO
ECAL: 16X0=0.7XNIL
3x(2x(25x25x700mm3))
W+ CsI(Na) + Fiber + ICCD
HCAL
HCAL: W: 20x3.5mm (0.8XNIL)
CsI: 20x(2.5cmx2.5cmx0.2cm)
Neutron detector: B-doped plastic scintillator for
delayed signals. Enhanced e/p discrimination. (TBD)
中国科学院空间科学与应用总体部
GENERAL ESTABLISHMENT OF SPACE SCIENCE AND APPLICATION, CHINESE ACADEMY OF SCIENCES
14/35